

A Thesis Submitted for the Degree of PhD at the University of Warwick

Permanent WRAP URL:

<http://wrap.warwick.ac.uk/88012>

Copyright and reuse:

This thesis is made available online and is protected by original copyright.

Please scroll down to view the document itself.

Please refer to the repository record for this item for information to help you to cite it.

Our policy information is available from the repository home page.

For more information, please contact the WRAP Team at: wrap@warwick.ac.uk

Functionalised Azamacrocycles

Andrew. C. Benniston BSc (Hons)

**A thesis submitted for
the degree of
Doctor of Philosophy**

**Department of Chemistry
University of Warwick**

August 1990

**To my Mom and Dad,
brother Mike,
and sister Jo**

In the last analysis magic, religion and science
are nothing but theories of thought; and as science
has supplanted its predecessors, so it may hereafter
be itself superseded by some more perfect hypothesis
perhaps by some totally different way of looking at the
phenomina- of registering the shadows on the screen- of
which we in this generation can form no idea

Sir James Frazer, O.M

The Golden Bough

Table of Contents

	page
Table of contents	i
List of Tables	v
Acknowledgements	vii
Declaration	viii
Summary	ix
Macrocycles discussed in this thesis	x
Abbreviations	xii
Chapter 1-Introduction	
<i>Section 1.1</i> Macrocycles(General)	1
<i>Section 2.1</i> Cation Selectivity and Complex Stability(General)	3
<i>Section 3.1</i> Macrocyclic Compounds(Thermodynamics)	6
<i>Section 4.1</i> Macrocyclic Effect	15
<i>Section 5.1</i> Synthesis of Macrocycles(General)	17
<i>Section 6.1</i> Functionalised Macrocycles	26
<i>Section 7.1</i> Redox Active Macrocycles	29
<i>Section 8.1</i> Cyclic Voltammetry	32
Chapter 2-The synthesis and study of redox active macrocycles based on 1,4,8,11-tetraazacyclotetradecane(cyclam).	
<i>Section 1.2</i> Introduction	36
<i>Section 2.2</i> Synthesis and Electrochemistry of L ¹	37
<i>Section 3.2</i> Electrochemistry of L ¹	41
<i>Section 4.2</i> Synthesis and Electrochemistry of L ²	45
<i>Section 5.2</i> Crystal structure of L ²	49
<i>Section 6.2</i> Electrochemistry of L ²	54
<i>Section 7.2</i> Synthesis and Electrochemistry of L ³ .HCl and L ³	56
<i>Section 8.2</i> Synthesis of L ³ .HCl and L ₃	56
<i>Section 9.2</i> Crystal structure of L ³ .HCl	60

<i>Section 10.2</i>	Conclusions to Syntheses	64
<i>Section 11.2</i>	Crystal structure of $2.L^b.Fe_2OCl_6$	64
<i>Section 12.2</i>	Electrochemistry of $L^3.HCl$ and L^3	67
<i>Section 13.2</i>	Conclusions	72
<i>Section 14.2</i>	Experimental	79
<i>Section 15.2</i>	Crystallography	84
Chapter 3-The synthesis and electrochemistry of further redox active macrocycles		
<i>Section 1.3</i>	Introduction	86
<i>Section 2.3</i>	Synthesis of L^4	87
<i>Section 3.3</i>	Metal complexes of L^4	90
<i>Section 4.3</i>	Electrochemistry of L^4	96
<i>Section 5.3</i>	Electrochemistry of metal complexes of L^4	98
<i>Section 6.3</i>	The synthesis of L^5	100
<i>Section 7.3</i>	Electrochemistry of L^5	101
<i>Section 8.3</i>	Conclusions	108
<i>Section 9.3</i>	Experimental	114
Chapter 4-The synthesis and study of two pyrrolidinyl pendant arm triazamacrocycles		
<i>Section 1.4</i>	Introduction	119
<i>Section 2.4</i>	The synthesis of L^6 and L^7	121
<i>Section 3.4</i>	Metal complexes of L^6 and L^7 (General)	123
<i>Section 4.4</i>	Synthesis of zinc(II) and copper(II) complexes of L^6	123
<i>Section 5.4</i>	Synthesis of nickel(II) and cobalt(III) complexes of L^6	124
<i>Section 6.4</i>	Synthesis of zinc(II), copper(II), cobalt(II) and cobalt(III) complexes of L^7	127

	page
<i>Section 7.4</i> Attempted synthesis of a nickel(II) complex of L ⁷	130
<i>Section 8.4</i> Crystal structures of [Zn(L ⁶)(OCIO ₃)] ⁺ and [Zn(L ⁷)] ²⁺	132
<i>Section 9.4</i> Attempted functionalisation of L ⁶	140
<i>Section 10.4</i> Conclusions	141
<i>Section 11.4</i> Experimental	148
<i>Section 12.4</i> Synthesis of metal complexes of L ⁶ and L ⁷	153
<i>Section 13.4</i> Crystallography	156
Chapter 5 The synthesis of two tetra-N-substituted derivatives of 1,4,8,11-tetraazacyclotetradecane(cyclam), and their nickel(II) complexes.	
<i>Section 1.5</i> Introduction	158
<i>Section 2.5</i> Synthesis of L ⁸ and L ⁹ .	160
<i>Section 3.5</i> Nickel(II) complexes of L ⁸	164
<i>Section 4.5</i> Crystal structure of [Ni(L ⁸)(NCS) ₂]	171
<i>Section 5.5</i> Thermodynamic and Kinetic studies of [Ni(L ⁸)] ²⁺ in acetonitrile.	178
<i>Section 6.5</i> Nickel(II) complexes of L ⁹ .	180
<i>Section 7.5</i> Conclusions	186
<i>Section 8.5</i> Experimental	192
<i>Section 9.5</i> Crystallography	195
Chapter 6 Future work and Conclusions	
<i>Section 1.6</i> Redox active macrocycles	196
<i>Section 2.6</i> Functionalised Triazamacrocycles	199
<i>Section 3.6</i> Tetra-N-alkylated macrocycles	200
Chapter 7 Experimental	
<i>Section 1.7</i> Experimental techniques and instrumentation	201
<i>Section 2.7</i> Electrochemical Techniques	202
<i>Section 3.7</i> Conductivity experiments	203

	page
<i>Section 4.7</i> Magnetic Susceptibility measurements	203
<i>Section 5.7</i> Atomic Absorption Spectrophotometry.	204
<i>Section 6.7</i> Solvent exchange by n.m.r line broadening	204
References	206
Appendix I Atomic co-ordinates, Bond lengths and angles	215
Appendix II Coulometric Titration for L ²	229

List of Tables

Chapter 1

Table 1.1- Thermodynamics of complex formation	5
Table 2.1- Strain energy of some macrocycles	8
Table 3.1- Thermodynamic data for some macrocycles	16
Table 4.1- Diagnostic tests for reversible electrochemistry	33
Table 5.1- Diagnostic tests for quasi reversible electrochemistry	34
Table 6.1- Diagnostic tests for irreversible electrochemistry	34

Chapter 2

Table 6.2- Selected bond lengths and angles for L^2	53
Table 7.2- Selected bond lengths and angles of $L^3.HCl$	63
Table 8.2- Bond lengths and angles of $2L^b.Fe_2OCl_6$	66
Table 1.2- 1H n.m.r data in $CDCl_3$ (ref $Me_4Si \delta = 0$)	73
Table 2.2- 1H decoupled ^{13}C n.m.r data in $CDCl_3$ (ref $Me_4Si \delta = 0$)	74
Table 3.2- Combustion analysis results	76
Table 4.2- Crystal data for L^2 , $L^3.HCl$ and $2L^b.Fe_2OCl_6$	77
Table 5.2- Mass spectral data	78

Chapter 3

Table 1.3- 1H decoupled ^{13}C n.m.r data	110
Table 2.3- Combustion analysis results	111
Table 3.3- Mass Spectral data	112
Table 4.3- Spectroscopic data	113

Chapter 4

Table 6.4- Bond lengths and angles for $[Zn(L^6)(OCLO_3)](ClO_4)$	137
Table 7.4- Bond lengths and angles for $[Zn(L^7)](ClO_4)_2$	138
Table 1.4- 1H decoupled ^{13}C n.m.r data in $CDCl_3$ (ref $Me_4Si \delta = 0$)	142
Table 2.4- Spectroscopic data	143
Table 3.4- Combustion analysis results	144
Table 4.4- Mass spectral data.	145

Table 5.4- Crystal data for $[\text{Zn}(\text{L}^6)(\text{OCLO}_3)](\text{ClO}_4)$ and $[\text{Zn}(\text{L}^7)](\text{ClO}_4)_2$	146
Chapter 5	
Table 6.5- Selected crystal data for $[\text{Ni}(\text{TMC})]^{2+}$ and $[\text{Ni}(\text{L}^8)(\text{NCS})_2]$	172
Table 8.5- Bond lengths and angles for $[\text{Ni}(\text{L}^8)(\text{NCS})_2]$	177
Table 7.5- Thermodynamic and Kinetic data for $[\text{Ni}(\text{L}^8)(\text{NCS})_2]$ in acetonitrile	178
Table 1.5- ^1H decoupled ^{13}C n.m.r data in CDCl_3 (ref $\text{Me}_4\text{Si } \delta = 0$)	187
Table 2.5- Combustion analysis results	188
Table 3.5- Spectroscopic data	189
Table 4.5- Mass spectral data	190
Table 5.5- Crystal data for $[\text{Ni}(\text{L}^8)(\text{NCS})_2]$	191

Acknowledgments

This page should be as long as my whole thesis, as I have come in contact with so many people over my six years at Warwick, both as an undergraduate and a postgraduate. However I would like to personally thank all of the following people:-

Dr Peter Moore for all his academic help, and also allowing me to use his laser printer to obtain this thesis.

All the macrocyclic group over the past four years- Dr.H.A.A.Omar, Dr.C.J."Jimbo" Reader, Dr.S.C.Rawle, Dr.F.McLaren, Dr.A.Wynn, and Simon Grant, Dr.N.S.Gosal, and Dr.L.Chung

Peter Wong for some excellent n.m.r work in his 3rd year project.

The X-ray crystallography department- especially Dr.N.W.Alcock for allowing me to have a "bash" on the diffractometer, and Dr.M.Roe for a excellent piece of crystal cutting on some twinned samples.

The electrochemistry group- Dr.P.N.Bartlett for his expertise. The following of whom I'm grateful for the use of their equipment; Dr.R.G.Whitaker, Jon "Gladstone" Farrington, Vanessa "Ness" Eastwick-Field.

The department- Inder Katal for all the mass spectra. Dr O.W.Howarth, Jeremy and Jag for 400MHz spectra. Eric Burgess for his humour, and the mending of broken glassware.

My old chemistry teacher Dr.J.Perrott, and his excellent teaching, of which I am eternally grateful.

All the postgraduates and undergraduates whom I've known over the past six years, which are far to many to mention, but not forgotten.

Dr Alicia Dachs for endless discussions on synthesis, and "friendship".
Phillipa Cross for checking the English and spelling in this thesis.

Dr.A.F.Hill for the use of his computer for the drawing of diagrams.

Jag for proof reading this thesis.

This thesis is brought to you by the letter M.

Declaration

The work submitted in this thesis is my own work and was carried out in the University of Warwick's Chemistry Department. The kinetic and thermodynamic data obtained in Chapter 5 (Table 7.5) was obtained by a joint collaboration with Mr.P.Wong, whilst under my supervision on his 3rd year project.

A.C.Benniston (BSc)

Summary

Potential uses of functionalised azamacrocycles have been investigated. Nine new azamacrocyclic ligands have been synthesised and characterised, some containing redox active centres, and these are identified on the following page.

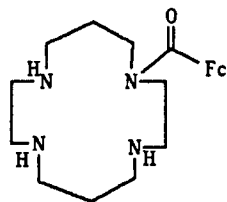
In Chapter 2 a series of redox active macrocycles L^1 , L^2 and L^3 , incorporating ferrocene as the redox active centre have been synthesised, based on the parent macrocycle 1,4,8,11-tetraazacyclotetradecane (cyclam), and been investigated. Their potential as transition metal ion sensors has been studied. The ligand L^1 shows irreversible electrochemistry in acetonitrile solution, with no reverse peak being observed in the cyclic voltammogram. However, on addition of Zn^{2+} the system becomes reversible as shown by the reappearance of the reverse peak. The crystal structure of L^2 reveals that the nitrogen atoms are not in suitable positions for chelation, in line with the observation that no metal complexes could be made of this macrocycle. The electrochemistry of L^2 shows a single four electron cyclic voltammogram and there is no change on addition of transition metal ions. The ligand L^3 does show a significant shift in the $E_{1/2}$ value for the ferrocene/ferrocenium couple on addition of transition metal ions.

In Chapter 3 studies of two macrocycles (L^4 and L^5) containing the redox active centre as part of the macrocyclic ring itself are described. In the case of L^4 ferrocene was used, but owing to problems with the electrochemistry, it was not a good transition metal ion sensor. Metal complexes of this macrocycle were synthesised and are of the general formula $[ML^4](CH_3COO)_2 \cdot xH_2O$, $\{M = Zn^{2+}, x=2.5, Ni^{2+}, x=4, Cu^{2+}, x=3\}$. A more promising metal ion sensor was the cobalticenium macrocycle L^5 and this shows very large shifts in the half wave potential, on the addition of transition metal ions like Zn^{2+} and Ni^{2+} . Problems with obtaining very pure samples at the moment hinder its useful application as a transition metal ion sensor.

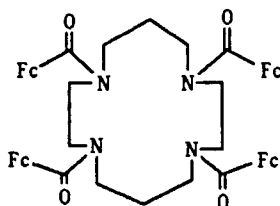
In Chapter 4, two pyrrolidinyl pendant arm triazamacrocycles are discussed L^6 and L^7 , together with some of their transition metal complexes. Two crystal structures have been undertaken of the zinc(II) complexes of L^6 and L^7 . A change in geometry from a trigonal bipyramid to a tetrahedron is brought about by an increase in length of the pendant arm in going from L^6 to L^7 .

In Chapter 5, a general route to N-alkylated macrocycles is described. Two new tetra-N-alkylated derivatives of cyclam (L^8 and L^9) have been synthesised, and their nickel(II) complexes studied. These metal complexes have been compared to the nickel(II) complexes of 1,4,8,11-tetramethyl,1,4,8,11-tetraazacyclotetradecane (TMC). The complex $[Ni(L^8)]^{2+}$ was obtained as two isomers in nitromethane solution, these are tentatively assigned to the Trans-I and Trans-III conformations. The crystal structure of $[Ni(L^8)(NCS)_2]$ is six co-ordinate and unusually the macrocycle adopts the Trans-I geometry. The nickel(II) complexes of L^9 have the general formula $[Ni(L^9)(X)]^{2+}$ where $X = DMSO$ or H_2O . Only one isomer exists in solution as shown by ^{13}C n.m.r., and is assigned to the Trans-I conformation.

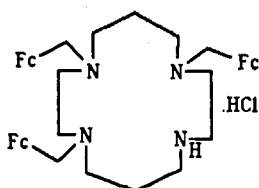
Macrocycles discussed in this thesis



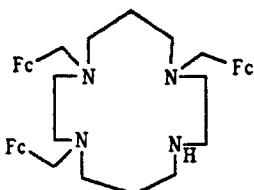
L^1



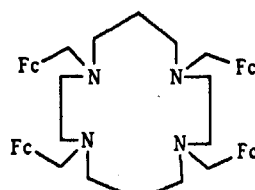
L^2



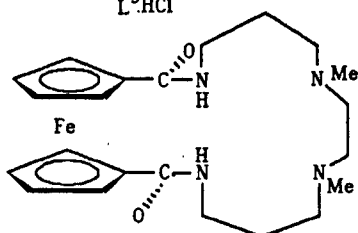
$L^3 \cdot HCl$



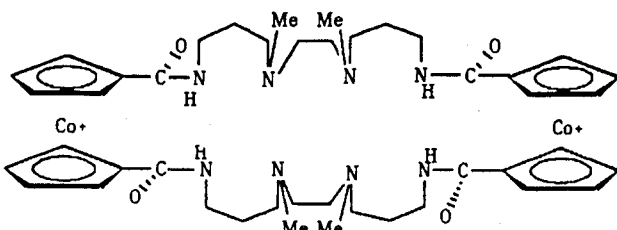
L^3



L^c

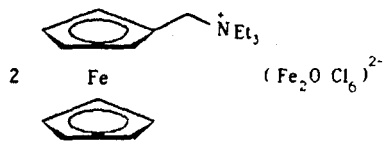
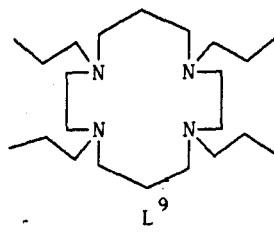
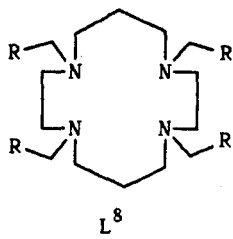
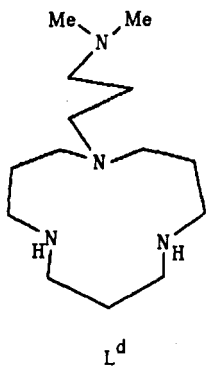
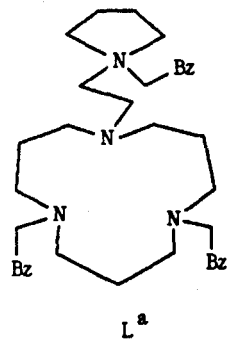
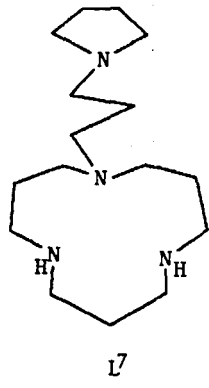
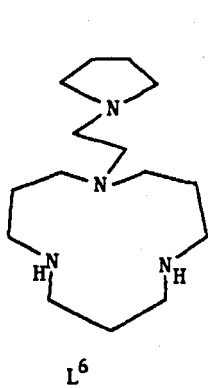


L^4



L^5

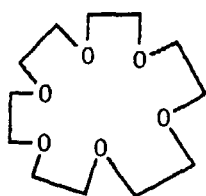
$(PF_6)_2$



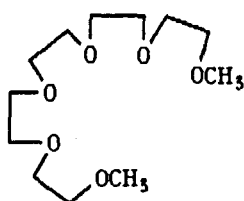
Abbreviations

ATP: Adenosine triphosphate
A.R: Analytical reagent
br: Broad
c.p: Cyclopentadiene
C.I: Chemical ionisation
 ^{13}C : Carbon 13 n.m.r
C: Coulombs
DMSO: Dimethylsulphoxide
DMF: Dimethylformamide
d: Doublet
E.I: Electron impact ionisation
 $E_{1/2}$: Half wave potential
F.A.B: Fast atom bombardment
Fc: Ferrocene
F.T: Fourier transform
 ^1H : Proton n.m.r
i: Current
I.r: Infrared
lit: Literature value
mer: Meridional
n.m.r: Nuclear magnetic resonance
mV: Millivolts
mV/s: Millivolts per second
Me, Si: Tetramethylsilane
M: Molar
mmol: Millimoles
m.p: Melting point
phen: Phenanthroline
ppm: Parts per million
q: Quartet
S.C.E: Standard calomel electrode
s: Singlet
THF: Tetrahydrofuran
t: Triplet
Tosyl: p-Toluenesulphonyl chloride
TEATFB: Tetraethylammonium Tetrafluoroborate
TBAHFP: Tetrabutylammonium Hexafluorophosphate
TBATFB: Tetrabutylammonium Tetrafluoroborate
U.V: Ultraviolet
V: Volts
 μA : Microamps
 λ : Wavelength
 ϵ : Extinction Coefficient
 ν : Frequency
 δ : Chemical shift

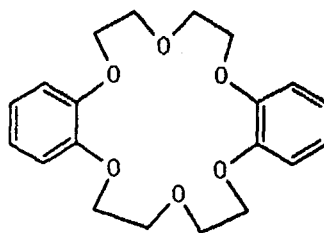
Ligand Abbreviations



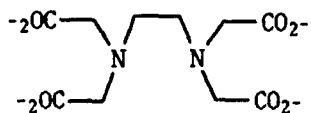
18-crown-6



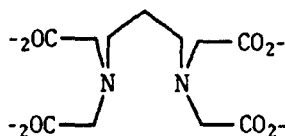
Pentaglyme



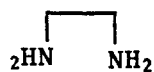
Dicyclohexyl-18-crown-6



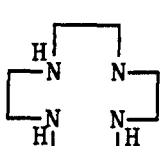
EDTA



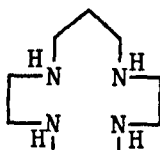
TMDTA



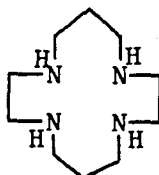
En



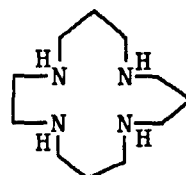
[12]aneN



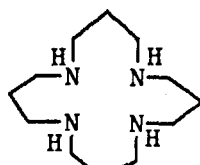
[13]aneN



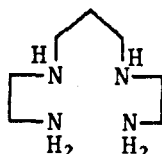
[14]aneN



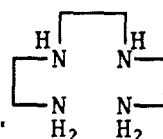
[15]aneN



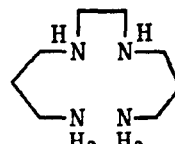
[16]aneN



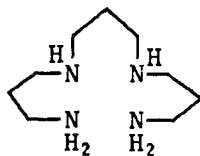
2.3.2. tet



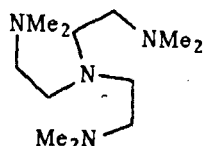
2.2.2. tet



3.2.3. tet



3.2.3. tet



TrenMe

CHAPTER 1

Introduction

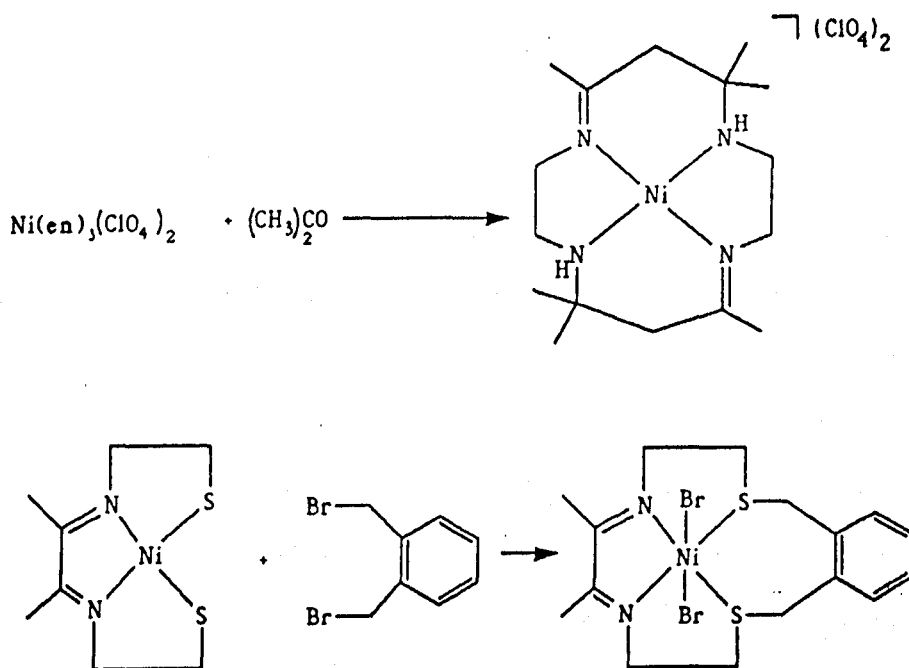
Section 1.1

Macrocycles (General)

The field of macrocyclic ligand chemistry has grown over the past thirty years to a point where it is now an integral part of inorganic chemistry, the crowning glory being the award of the Nobel prize in 1987, to Cram, Pedersen, and Lehn.¹

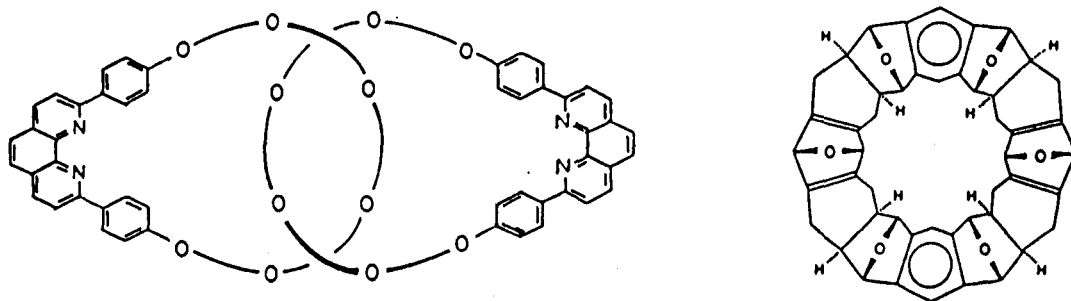
This thesis will show some of the different areas in which macrocycles can be utilised, especially in the field of co-ordination chemistry and chemical sensors. There have been a number of excellent review articles on the early work on macrocycles,² so only a brief summary will be given here.

Two early syntheses of a macrocycle were carried out in the early 1960s by Curtis,³ and independently by Busch and Thompson⁴ (Scheme 1.1).



Scheme 1.1

The birth of this new field of inorganic chemistry led to a rapid growth in the 1960s, which has continued up until the present day with the synthesis of more elaborate macrocycles such as the catenands by Sauvage⁵ and kohnkene by Stoddart⁶ (Figure 1.1).



A Catenand

Kohnkene

Figure 1.1

With this growth in macrocyclic chemistry, there came a series of interesting questions. Why were the macrocycles more stable than their open chain analogues? Could these macrocycles be selective towards metal ions, and if so what factors were the most important (*e.g.* ring size, type of donor atom, solvent effects)?

These questions have been partially answered, but uncertainties remain. The observed properties of macrocycles have led to a number of applications. For example, recently Lehn⁷ has used a polyammonium macrocycle as a supramolecular catalyst in the phosphoryl transfer in ATP hydrolysis. Beer *et al.* have used the selective binding of crown ethers in the sensing of alkali and alkaline earth metals⁸, as well as cobalticinium macrocycles for the detection of anions.⁹ Parker,¹⁰ has also been using functionalised macrocycles in anti-body labelling, for possible tumour imaging and radioimmotherapy.

Section 2.1

Cation selectivity and complex stability

There are a number of factors which influence the stability of macrocyclic complexes,^{1 1} these are :-

- 1: Type of binding sites in the ring.
- 2: Number of binding sites.
- 3: Relative size of ion and macrocyclic cavity.
- 4: Physical placement of the binding sites.
- 5: Steric hindrance in the ring.
- 6: Solvent, and the extent of solvation of the ion binding sites.
- 7: Charge of the ion.

Probably the most studied relationship has been that between the macrocyclic ring size (hole) and the size of the cation. This has been carried out for donor atom systems and varying ring size. Recently molecular mechanics has played an important part in gaining insights into such aspects as metal ion selectivity, and macrocyclic ligand design. The use of molecular mechanics has recently been reviewed by Hancock,^{1 2} and so will only be summarised briefly.

Molecular Mechanics Calculations

A bond is assumed to have an ideal length (r^0) which is distorted by strain to its observed length (r). The strain produced (U_B) is given by Hooke's law (1).

$$U_B = 1/2.K_B.(r^0-r)^2 \rightarrow (1).$$

K_B = the force constant for a particular bond.

The strain induced by angle deformation (U_θ) is also given by Hooke's law, Equation(2).

$$U_\theta = 1/2.K_\theta.(\theta^0-\theta)^2 \rightarrow (2).$$

θ^0 = ideal bond angle, θ = observed angle

Another form of strain energy is torsional strain (U_ϕ), given by the expression (3).

$$U_\phi = V/2.[1 + \cos(n.\phi)] \rightarrow (3).$$

ϕ = torsional angle, V = constant for particular atoms.

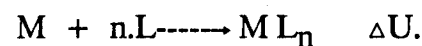
The most important strain energy contribution is that of the forces between atoms that are not bonded to each other (U_{NB}). Equation (4).

$$U_{NB} = A.e^{-(B.r)} - C/r^6 \rightarrow (4).$$

A, B, C are constants, r = internuclear separation.

The order of importance of these forces are: non-bonded repulsive forces > bond length deformation forces > bond angle deformation \geq torsional forces > non-bonded attractive forces.

To analyse the role of strain energy in complex formation, the increase in strain energy that occurs when a free ligand is complexed is considered.



$$U_M \quad U_L \quad U_{MLn}$$

$$\Delta U = U_{MLn} - U_M - n.U_L$$

Metal Chelates

The use of molecular mechanics has revealed a number of properties for metal chelates.

1: Small metal ions with M-N bond lengths close to 1.6 Å will co-ordinate with the least steric strain to six membered chelates.

2: Large metal ions will co-ordinate with least steric strain to five membered rings.

The true test of such convictions is to compare thermodynamic parameters relating complex stability to chelate ring size (Table 1.1).^{1 2}

Thermodynamics of Complex Formation of edta (Five Membered Chelate Ring)
Compared to tmdta (Six Membered Chelate Ring)

Metal Ion	Ionic Radius	Edta			tmdta		
		log K_1	ΔH	ΔS	log K_1	ΔH	ΔS
Cu ²⁺	0.57	18.70	-8.2	58	18.82	-7.7	60
Ni ²⁺	0.69	18.52	-7.6	59	18.07	-6.7	60
Zn ²⁺	0.74	16.44	-4.9	59	15.23	-2.3	62
Cd ²⁺	0.95	16.36	-9.1	44	13.83	-5.4	45
Ca ²⁺	1.00	10.61	-6.6	26	7.26	-1.7	27
La ³⁺	1.03	15.46	-2.9	61	11.28	+3.8	64
Pb ²⁺	1.18	17.88	-13.2	38	13.70	-6.4	41

¹Units are angstroms (Å) for ionic radii, kilocalories per mole (kcal · mol⁻¹) for ΔH , and calories per degree per mole (cal · deg⁻¹ · mol⁻¹) for ΔS .

Table 1.1

These results show that large metal ions are destabilised more than small metal ions by an increase in chelate ring size.

Section 3.1

Macrocyclic compounds (Thermodynamics)

The most important concept in macrocyclic ligands is that the most stable complexes are formed by a metal which fits perfectly the cavity of the ligand. This is known as size match selectivity. If a macrocycle is already orientated to accept a metal ion then very little reorganisation energy is required, and so complex stability will be high. These macrocycles have been termed "preorganised" by Cram,^{1 3} and are observed in the spherands. Recently the question of what happens when a metal is too large for the macrocyclic cavity has been studied. Busch *et al.*^{1 4} when studying a series of Co(III) tetraaza macrocycles proposed that the metal ion is compressed, and so explained the large ligand field splitting. However, Hancock^{1 5} has attributed this high ligand field to the greater inductive effect of the secondary nitrogen donors of the macrocycle.

Tetra-aza macrocycles

The complication of working with tetra-aza macrocycles is that they can adopt a number of conformations depending on the orientation of the hydrogens on the nitrogen. For example, the possibilities for 1,4,8,11-tetraazacyclotetradecane (cyclam) are shown in Figure 2.1.^{3 6}

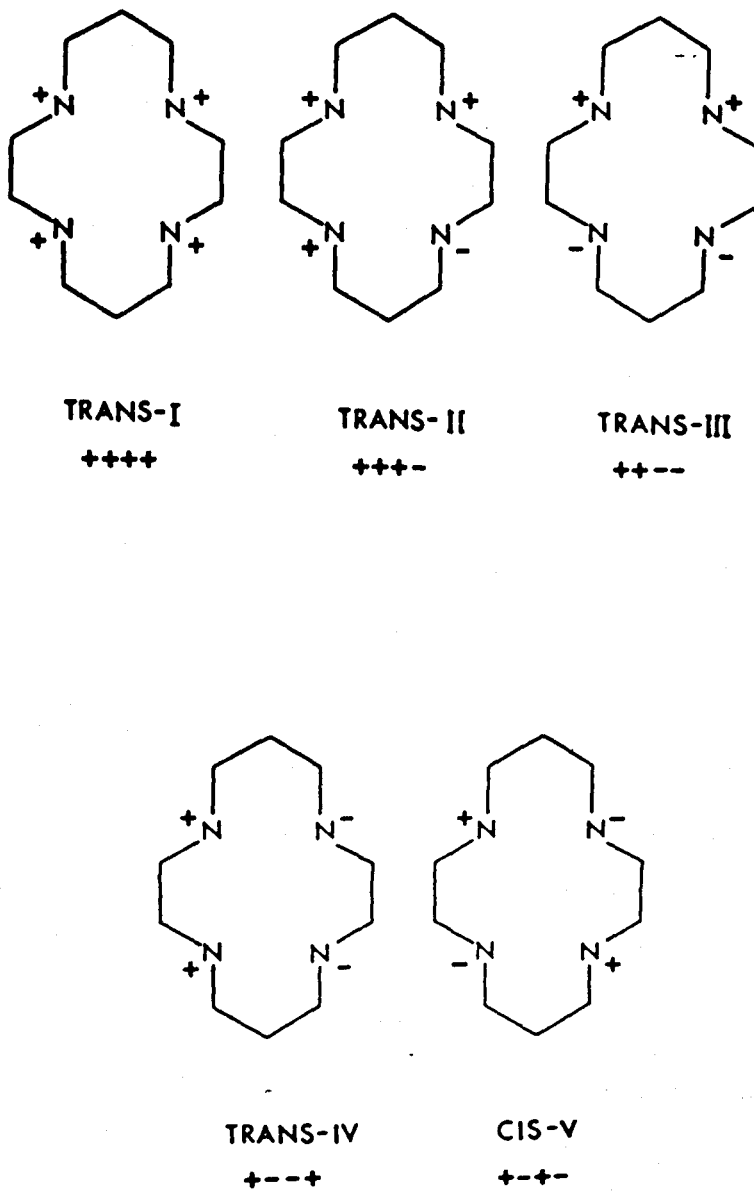


Figure 2.1

The possible conformations of 1,4,8,11-Tetraazacyclotetradecane(cyclam). The + and - signs indicate whether hydrogens are above or below the plane of the macrocyclic ring.

Busch *et al*¹⁴ studied a series of tetra-azamacrocycles [12]aneN₄ to [16]aneN₄ with Co(III) and calculated the corresponding strain energy (Table 2.1).

Table 2.1

	Strain energy/kcal mol ⁻¹
[13]aneN ₄	19.74
[14]aneN ₄	11.53
[15]aneN ₄	21.33
[16]aneN ₄	35.56

Thus the co-ordination of a metal ion, which is either larger or smaller than the ideal size, results in an increase in strain energy of the ligand. However, these fits correspond to the metal lying in the plane of the four nitrogen donors. Hancock¹⁶ has furthered this work by looking at the dependence of strain energy on metal ion size for the Trans-I and Trans-III conformers of [12]aneN₄ → [14]aneN₄. He predicted that the small macrocycle [12]aneN₄ would have a preference for larger metal ions when compared to [14]aneN₄. The importance of the "hole" becomes meaningless as the metal lies above the plane of the macrocycle. Other work (Figure 3.1)¹⁶ shows how a large metal such as Pb (II) undergoes a decrease in stability with increasing ring size. This is contrary to what is expected for a Trans-III conformer, but entirely fitting with a Trans-I geometry. The main conclusion to be drawn is that a large metal ion will prefer to co-ordinate in a Trans-I geometry, and that increasing ring size will decrease complex stability. However, a smaller metal ion adopts the Trans-III conformation and so stability follows the course of "best fit".

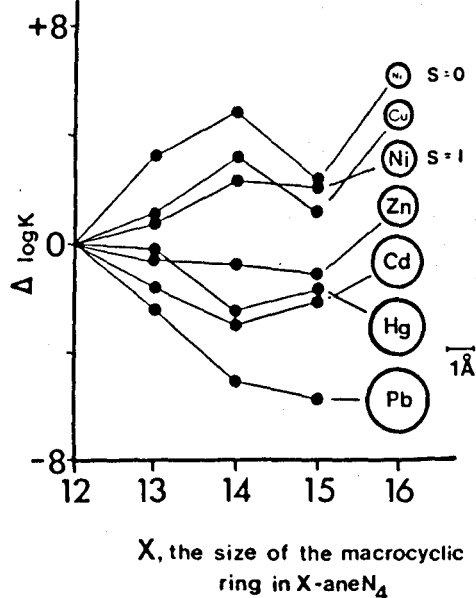


Figure 3.1

Continuing work of Hancock^{17,21} using molecular mechanics and thermodynamic data has shown that the size selectivity of tetra-azamacrocycles is mainly controlled by the size of the chelate rings, rather than that of the macrocyclic ring (Figure 4.1).

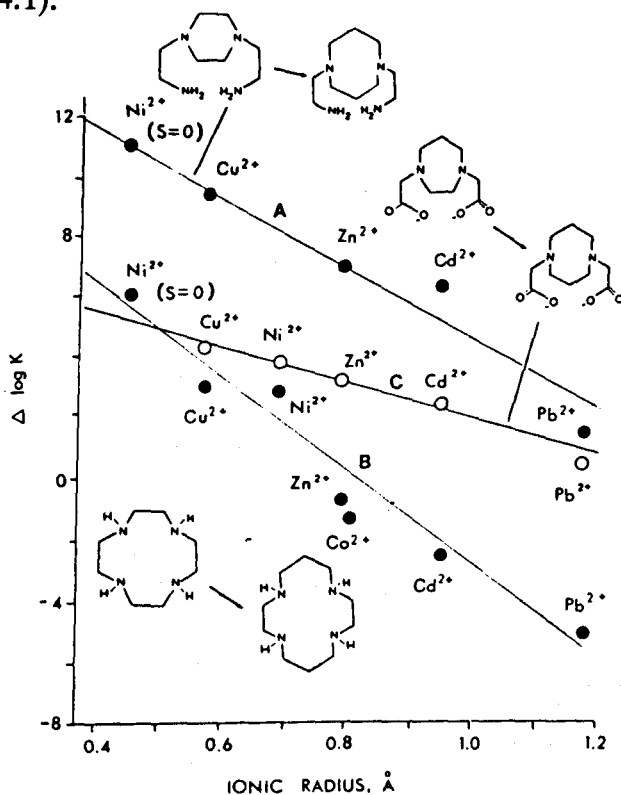


Figure 4.1

Relationship between the change in complex stability on increasing the size of the chelate ring from five membered to six membered, $\Delta \log K$, and the ionic radius of metal ions, for the ligands shown. The similarity of steepness of slope A to that for B supports the idea that metal ion selectivity of tetra-azamacrocycles is controlled by chelate ring size.

Another complication of tetra-azamacrocycles is that of folding to form the Cis-V conformer (Figure 2.1). This is observed when larger metal ions are introduced and compression of the Trans-III geometry is relieved by folding.

The compression of metals in macrocycles is of current interest, as this seems to account for the high ligand field strengths. However, Fabbrizzi^{2 2} has shown, with a series of macrocycles [12]aneN₄ → [16]aneN₄, for low spin Ni(II), that the maximum ligand field occurs with the best fit around the metal ion. A possible explanation is that of donor basicity. The ligand baetbc^{2 3} has a high ligand field strength with Ni(II) even though its Ni-N bond length is similar to that of Ni(en)₂^{2 +}, the main difference being the introduction of a tertiary nitrogen (Figure 5.1).^{1 2}

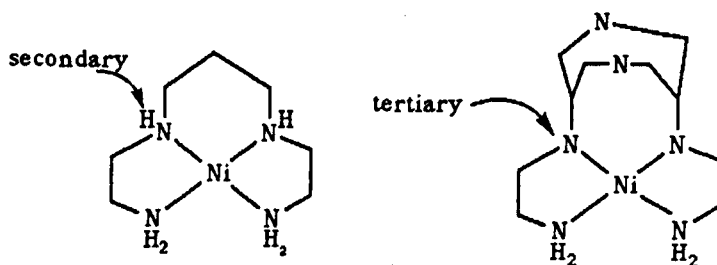
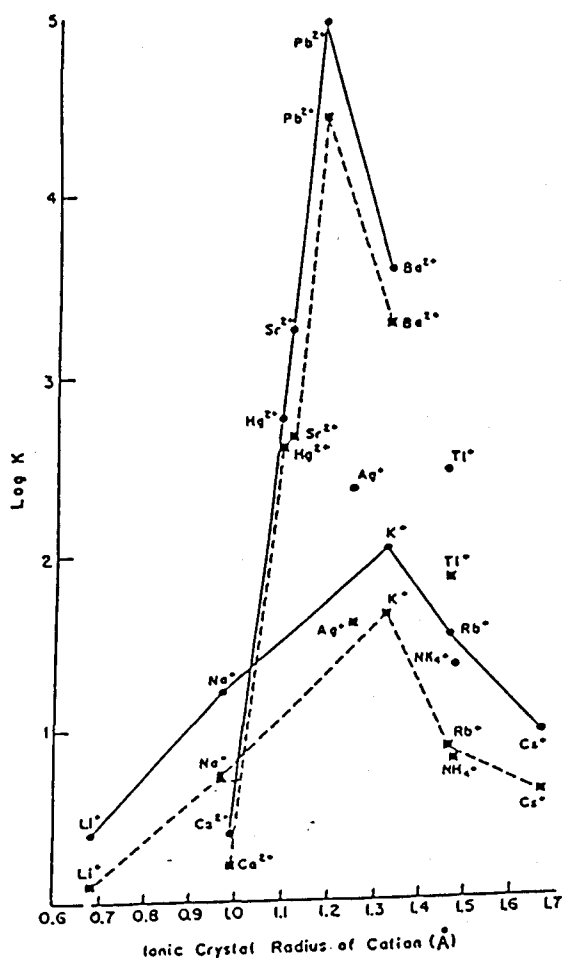


Figure 5.1

Crown ethers

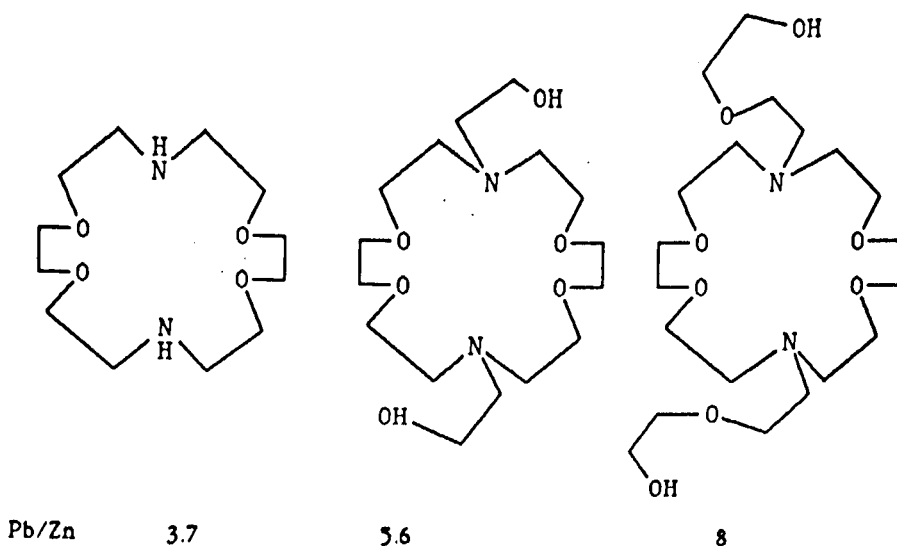
The cyclic polyethers have been found to form a number of 1:1 complexes with a number of metal ions.^{24,25} An interesting property of polyethers is their ability to selectively bind various cations. Studies have shown that a difference in stability of 10^5 , for Pb^{2+}/Ca^{2+} , was achieved for dicyclohexyl-18-crown-6. (Figure 6.1)^{9,8}



Plot of $\log K$ vs cation radius for the reaction in aqueous solution, $M^{n+} + L = ML^{n+}$ where L = dicyclohexyl-18-crown-6, Isomer A (●), dicyclohexyl-18-crown-6 Isomer B (■). $T = 25^{\circ}$.

Figure 6.1

The size match selectivity has been challenged by Hancock,^{26,20} and he concludes that perhaps it is not just closest fit of cation to "hole", but the presence of neutral oxygen donors which determines selectivity. Results have demonstrated that large metal ions form complexes with an increased stability when groups containing neutral oxygen atoms are added to existing crowns, whereas small ions tend to show a decrease in complex stability (Scheme 2.1).



Scheme 2.1

The theory of preorganisation^{1 2} is predominant in the work on polyethers. Crystallographically 18-crown-6 has been shown to adopt a conformation different to that in its complexes. This ligand in its free state has a C_1 symmetry with the lone pairs of the oxygens orientated out of the macrocyclic cavity. The C_1 conformer has been shown to be 5 kcal mol^{-1} lower in energy than the complexed D_{3d} conformer²⁷. Interestingly, Kollman²⁸ has shown that K^+ prefers the D_{3d} conformer, whilst Na^+ prefers the C_1 structure (Figure 7.1).^{1 2}

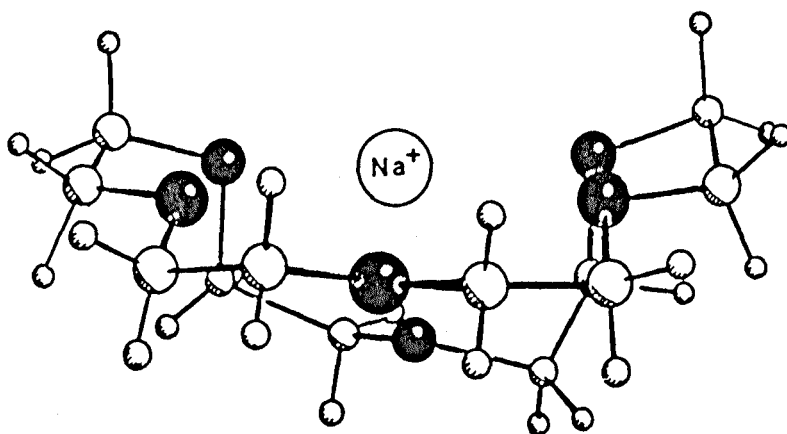


Figure 7.1

The structure of Na [18-crown-6], taken from reference 12.

The change for Na^+ is attributed to the conformer C_1 allowing shorter Na-O bonds.

Mixed donor macrocycles.

Lindoy and co-workers have worked extensively on mixed nitrogen, oxygen and nitrogen, sulphur macrocycles.^{29,30,34,35} The term "goodness of fit" was coined to explain the selectivity of metals to these macrocycles. The "goodness of fit"³¹ is defined as the ratio of the bonding cavity radius (R_A) to the Pauling covalent radius (R_P) of the metal involved. Thus the ratio $R_A/R_P = 1$ represents the perfect match of a metal to the binding cavity. This has been demonstrated for the nickel (II) complexes of an O_2N_2 macrocycle (Figure 8.1), where n and m are varied to produce 14→17 membered rings.^{32,33} As shown, Figure 8.1, the highest stability occurs at the 16 membered ring where $R_A/R_P = 1.01$.

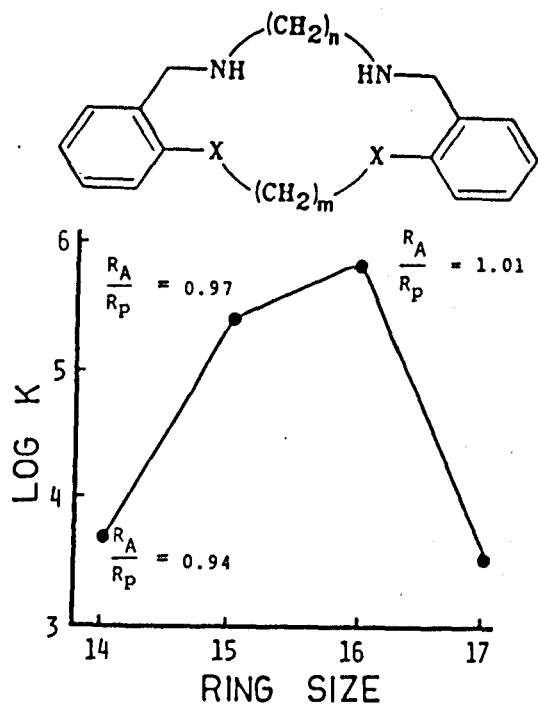


Figure 8.1

A further theory is that of "dislocations".^{3 4} This is where a small change in a ligand can cause a marked change in geometry, and thus a decrease in complex stability. For example, the pentadentate ($N_3 O_2$) macrocycle (Figure 9.1) shows a change in geometry with Ni (II) by substitution of a methyl for a hydrogen at R. The selectivity between Cu(II)/Ni(II) has been greatly increased by the methyl substitution.^{3 5}

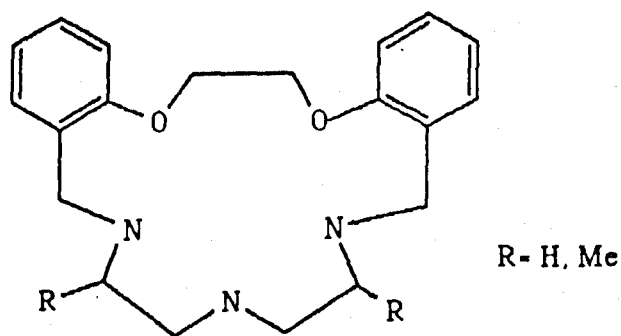
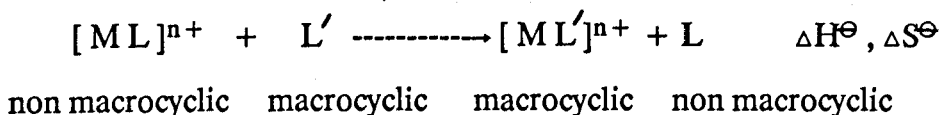


Figure 9.1

The Macrocyclic Effect

The macrocyclic effect can be related to a Gibbs energy term below.



The macrocyclic effect was a term coined by Cabbiness and Margerum^{3 7} to account for the greater stability of macrocycles over their open chain analogues. It was shown that the macrocyclic effect is approximately ten times greater than the chelate effect for Cu^{2+} , with multidentate amine complexes. Margerum^{3 7} attributed the macrocyclic effect to the difference in configurational solvation of "free" macrocyclic ligands, compared to non cyclic analogues. However, this has been contested by other workers, such as Kimura^{3 8} and Paoletti^{3 9}.

The driving force of the macrocyclic effect (entropy or enthalpy) has been a long contested problem. Logically the entropy term should be the dominant factor, because before co-ordination a macrocyclic ligand should "lose" less entropy after co-ordination, when compared to an open chain analogue.

Tetra-azamacrocycles

Margerum^{4 0} studied the enhanced stability of $Ni[14]aneN_4$ over $Ni(2,3,2,tet)$, and showed that there was an increase of 14 kcal mol^{-1} in ΔH^\ominus , whilst a decrease of $16 \text{ cal deg}^{-1} \text{ mol}^{-1}$ in ΔS^\ominus was observed for the macrocycle. Other work^{4 1, 4 2} supported the theory that the macrocyclic effect was due to solvation effects. Paoletti,^{3 9} using a series of aza macrocycles $[12]aneN_4 \rightarrow [15]aneN_4$ with $Cu(II)$ and $Zn(II)$, showed that entropy contributions were more dominant (Table 3.1).^{3 9}

Ligand	Cu(II) Complexes		Zn(II) Complexes	
	ΔH° kcal mol ⁻¹	ΔS° cal K ⁻¹ mol ⁻¹	ΔH° kcal mol ⁻¹	ΔS° cal K ⁻¹ mol ⁻¹
[12]ane N ₄	-22.7	+36.2	-14.5	
[13]ane N ₄	-29.2	+33.7		
[14]ane N ₄	-32.4		-14.8	
[15]ane N ₄	-26.5	+22.7	-16.5	
2,2,2 tet	-21.6	+19.5	- 8.9	+25.0
2,3,2 tet	-27.7	+16.5	-11.9	+18.8
3,2,3 tet	-25.9	+13.1	-10.6	+15.9
3,3,3 tet	-19.5	+12.8	- 7.4	+18.0

Table 3.1

Kimura,⁴⁴ using polarographic studies calculated $\Delta S = 51.4$ cal K⁻¹ mol⁻¹ in good agreement with Paoletti,⁴⁵ showing an entropic driving force to the macrocyclic effect. However, Paoletti,⁴³ studying the relationship between enthalpy of formation and frequency maxima in electronic absorption spectra of Cu(II) tetra-amine complexes, concluded that the macrocyclic effect was not just an enhanced chelate effect. Even though the chelate effect is mainly an entropy effect, this work showed that the macrocyclic effect was both enthalpy and entropy driven.

Crown Ethers

The macrocyclic effect is observed in cyclic ethers, and the same uncertainties in the origins exist. Frensdorff⁴⁶ showed how 18-crown-6 had a greater stability for Na⁺ and K⁺ over pentaglyme. Kodama and Kimura⁴⁷ attributed the macrocyclic effect to a favourable entropy contribution. But Christensen⁴⁸ showed that for a series of metals (Na⁺, K⁺, Ba²⁺) with 18-crown-6, in water methanol mixtures, the macrocyclic effect was enthalpic.

The apparent ambiguities in the origins of the macrocyclic effect can only lead to the conclusion that entropy and enthalpy make varying contributions to the macrocyclic effect.

Synthesis of Macrocycles (General)

There have been a number of excellent reviews covering the synthesis of macrocycles, including nitrogen, oxygen, sulphur and other donor groups such as phosphorous, and arsenic.^{1 1, 4 9-5 3}

In the synthesis of any donor macrocycle the underlying goal is to produce a cyclic system in good yield with few or no unwanted side products (*e.g.* polymers). Most commonly there are three kinds of cyclisation steps used:

1: Richman-Atkins.^{5 4}

2: Template Synthesis⁴

3: High Dilution.^{7 0}

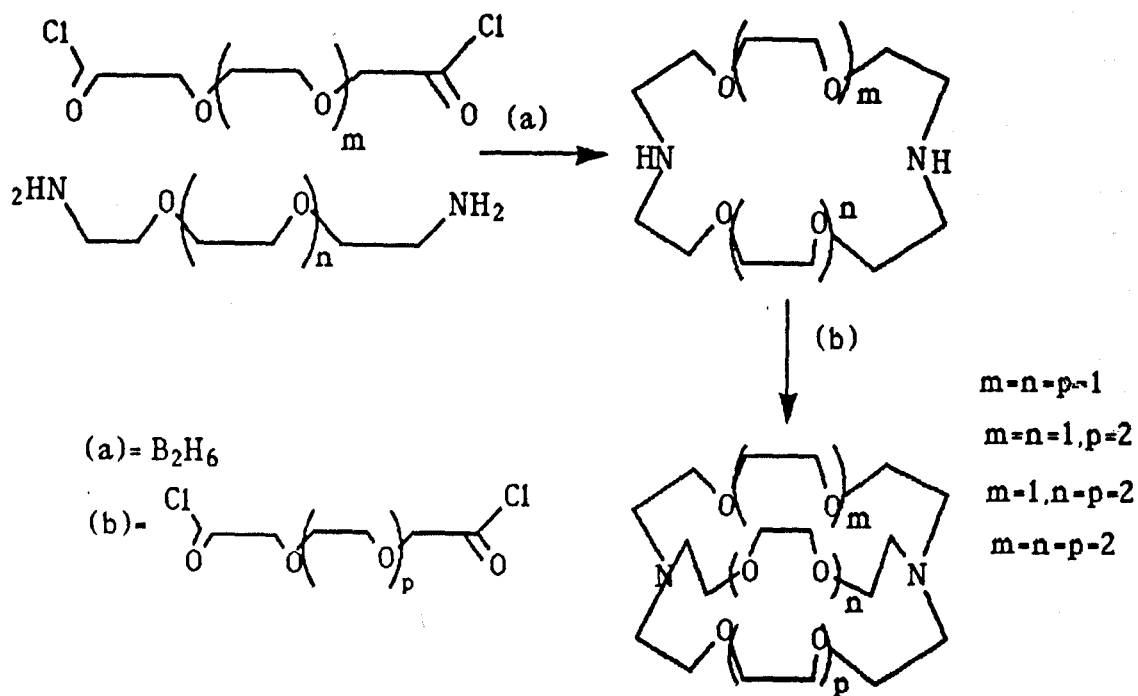
Each method has its own advantages and disadvantages, and these will be discussed in the following sections.

Crown ethers

The macrocyclic polyethers, especially derivatives of 18-crown-6, have received notable interest since they have rich chemistry with metal ions.^{5 5} The polyethers have been applied in a number of areas, such as the selective transport of metals across liquid membranes, chiral recognition,^{5 6} and phase transfer catalysis.^{5 7}

The synthesis of crown ethers is usually carried out under high dilution conditions (~ 0.05 M).^{5 8} However, Pedersen,^{5 9} in the synthesis of dibenzo-18-crown-6 achieved high yields (39-48%) with concentrations of ~ 0.75 M. This high yield was attributed to a template effect. Greene,^{6 0} working on the synthesis of 18-crown-6 postulated that potassium ions acted as a template, because of the increased yields with potassium present.

A three dimensional class of crown ethers are the cryptands produced by Lehn and co-workers,^{6 1} and synthesised as in Scheme 3.1.

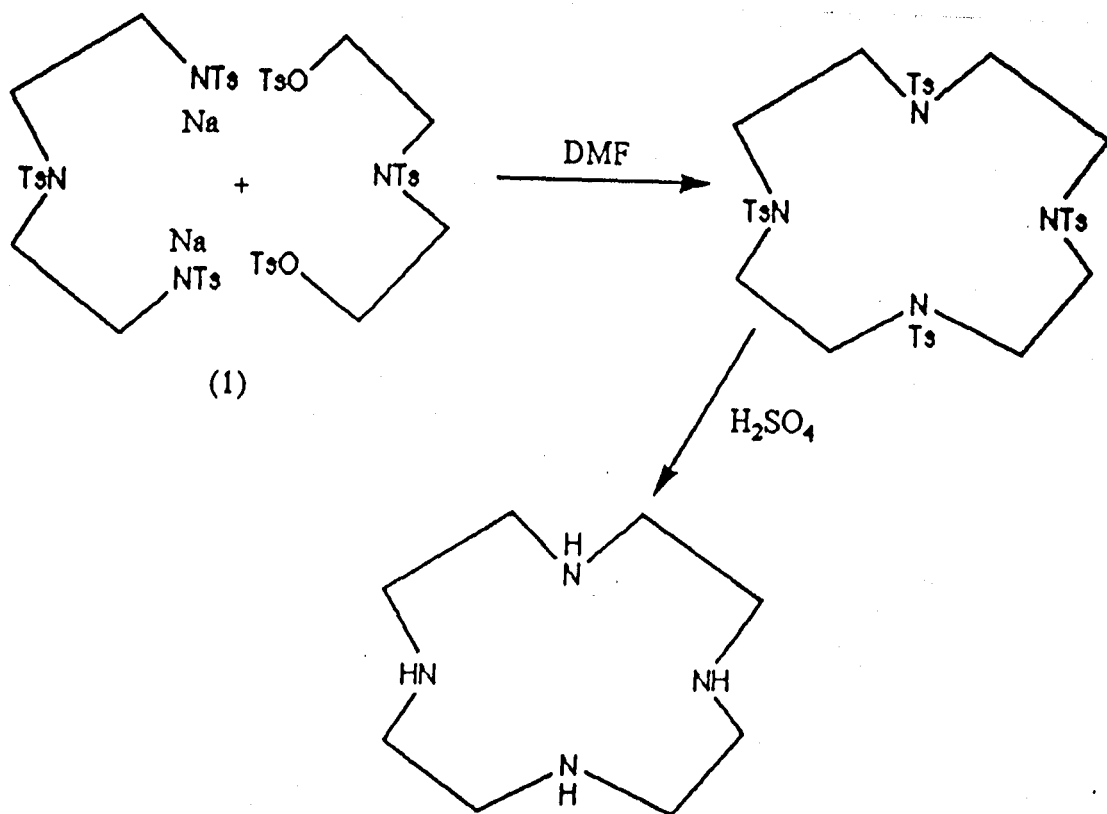


Scheme 3.1

The overall yield is 25%, which is good given that high dilution methods were employed. The three dimensional nature of the ligand means that greater discrimination for cations is achieved.^{6 2}

Azamacrocycles

The use of Richman-Atkins^{5 4} synthesis is probably the most widely used method in azamacrocycle ligand design. The method involves the condensation of two moieties in a dipolar aprotic solvent (*e.g* DMF) (Scheme 4.1).^{5 0}

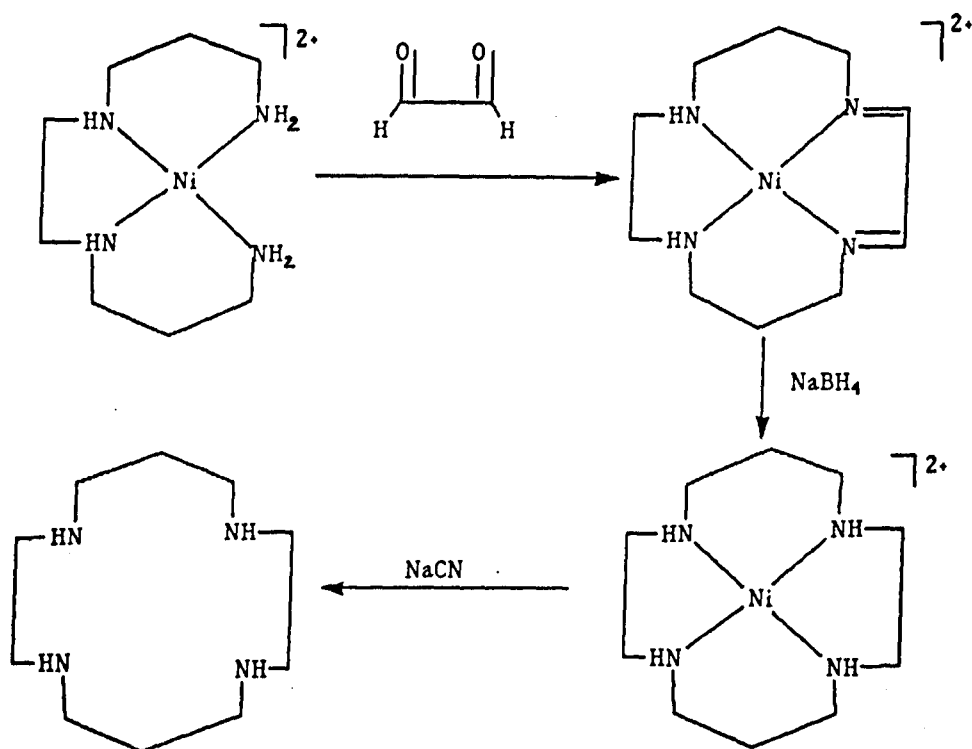


Scheme 4.1

Recently Kellogg^{6 3} showed that improved yields could be achieved by replacing the sodium of the sulphonamide (1) (Scheme 4.1) with cesium, by addition of Cs₂CO₃. The Cs₂CO₃ acts as a strong enough base for deprotonation, and ring closure. The Cs₂CO₃ method is now widely used in the synthesis of more elaborate macrocycles,⁵ but it is a costly material for simpler azamacrocycle syntheses

The main advantage of the Richman-Atkins method is that high dilution is not required; saturated solutions usually give best yields because of increased rates of cyclisation. Also, the ligand can be fully characterised before metal complexation. The main drawback of this method is the removal of the protecting groups, which is carried out under severe hydrolysis conditions (*e.g.* conc H_2SO_4). However, milder detosylation methods have been examined, for example sodium amalgam in buffered methanol.⁶³

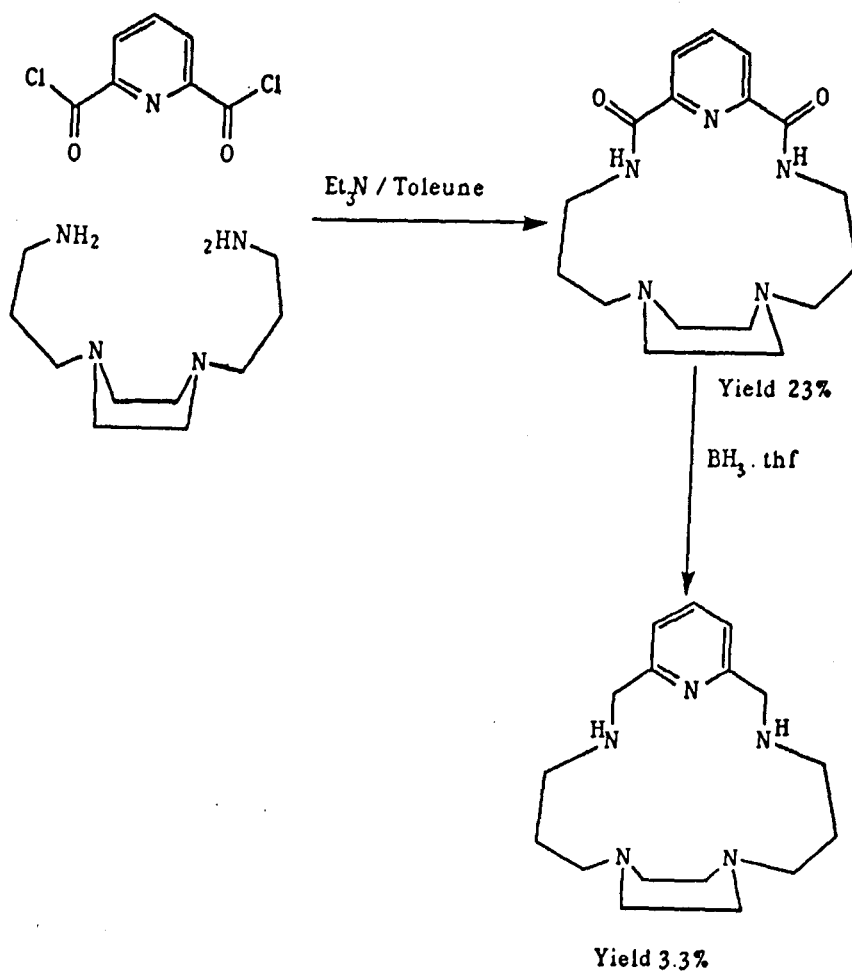
The template method has been used in a number of macrocyclic ligand synthesis.⁶⁴⁻⁶⁷ The first template reaction was carried out by Curtis³ (Scheme 1.1), where the nickel held the reacting species in close proximity for reaction. One of the most widely used template reactions is in the synthesis of [14]ane N_4 (cyclam), by Barefield⁶⁸ (Scheme 5.1).



Scheme 5.1

The ligand cyclam has found a number of uses, and as good precursor for other macrocycles.^{69,71}

The final method of high dilution typically involves cyclisation usually using a diacid chloride and a corresponding amine to produce an amide bond. The amide linkage can usually be reduced out by $\text{BH}_3 \cdot \text{thf}$ or LiAlH_4 . An example of this was carried out by Moore⁷⁰ in the synthesis of a structurally rigid penta-azamacrocyclic (Scheme 6.1).



Scheme 6.1

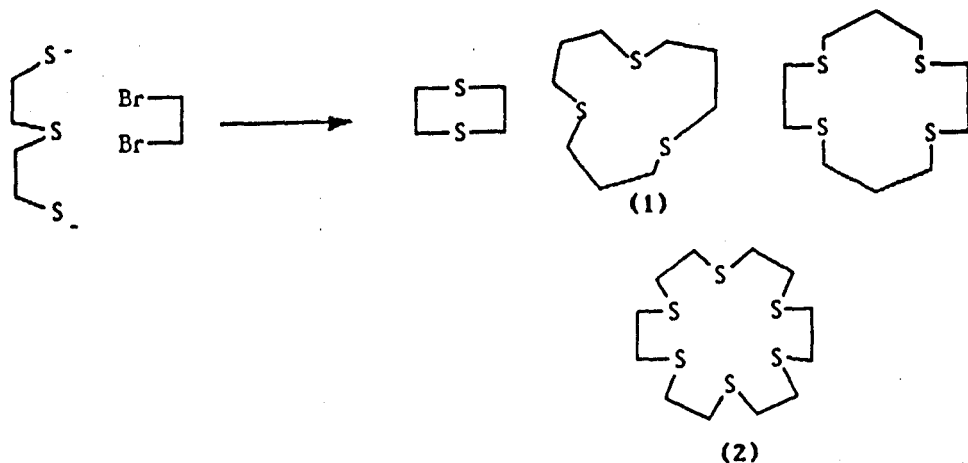
The low yield of the final product was attributed to the presence of the rigid piperazine backbone.

The main disadvantage of the high dilution method is the very dilute conditions which have to be used to avoid polymerization.

Thia-Macrocycles

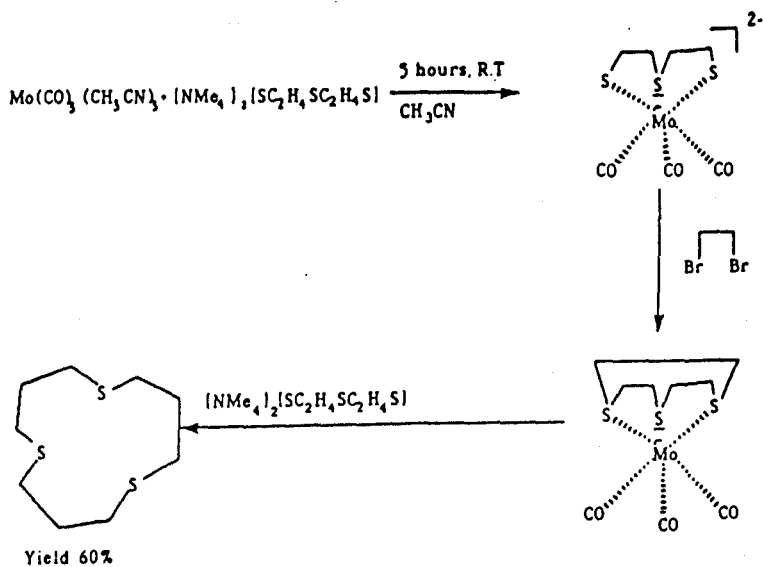
These macrocycles are of interest because the larger covalent radius of sulphur means that M-S bond lengths are increased, and also a "softer" atom is introduced.

The early synthesis used the reaction of 3-thiapentane-1,5-dithiol and ethylene bromide to give a mixture of products. (Scheme 7.1)^{7 2}



Scheme 7.1

An improved synthetic route to the tri-thiamacrocycle (1) has been achieved by Sellmann, using molybdenum as a metal template. (Scheme 8.1).^{7 3}



Scheme 8.1

Cooper^{7 4} used the hexathiamacrocycle (2) to stabilise an octahedral low spin complex of cobalt(II), utilising the fact that the M-S bond lengths are ideal for low spin cobalt(II).

Other donor Macrocycles (Arsenic, Phosphorous, Selenium)

The incorporation of other "softer" atoms into the backbone of macrocycles has been attempted. However, these macrocycles are synthetically more demanding because of problems with handling procedures and lack of suitable precursors. Phosphorous, selenium and arsenic are often incorporated into macrocycles containing other sets (*e.g* N,O,S). For example, the first macrocycle produced by Meek^{7 5} contained a N₃P set of donors (Figure 10.1). Conversely the first arsenic macrocycle by Kyba^{7 6} was based on a tri-dentate ligand (Figure 10.1).

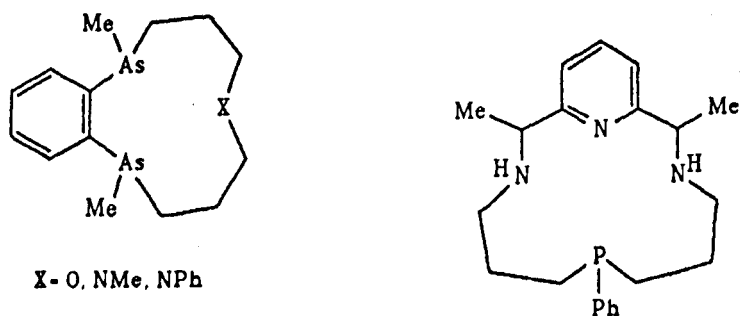
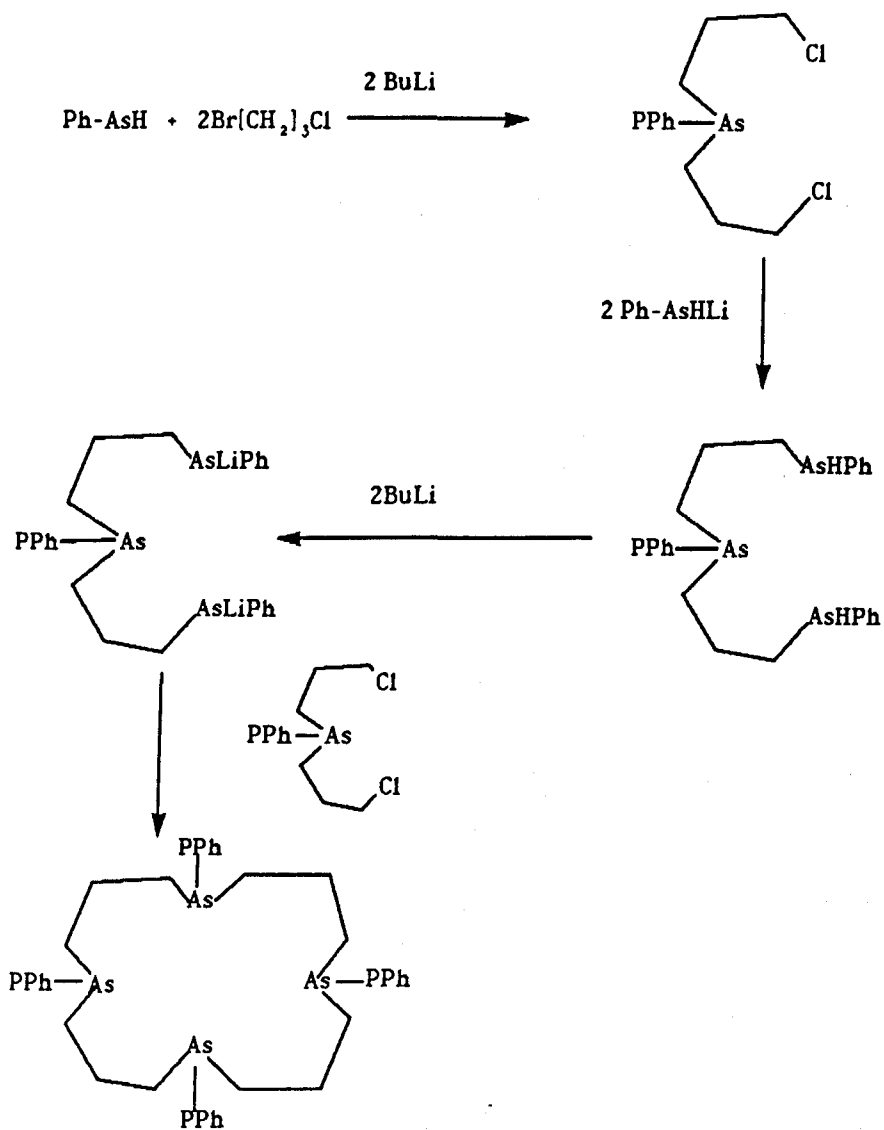


Figure 10.1

A fully arsenic macrocycle was synthesised by Kauffman^{7 7} in a moderately good yield (18%)(Scheme 9.1).



Scheme 9.1

A synthetic route to a fully arsenic macrocycle, taken from reference 77.

Recently Tomoda^{7 8} has synthesised a macrocycle containing selenium centres (Figure 11.1). Whether this macrocycle will bind to metals through the selenium atoms is debatable.

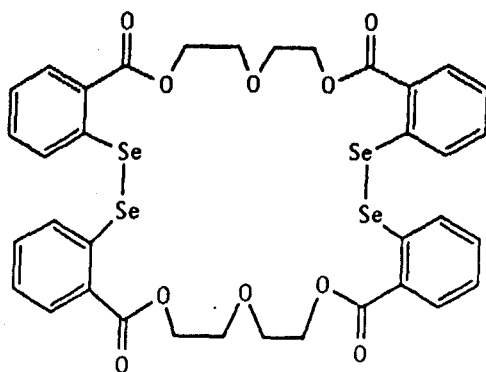


Figure 11.1

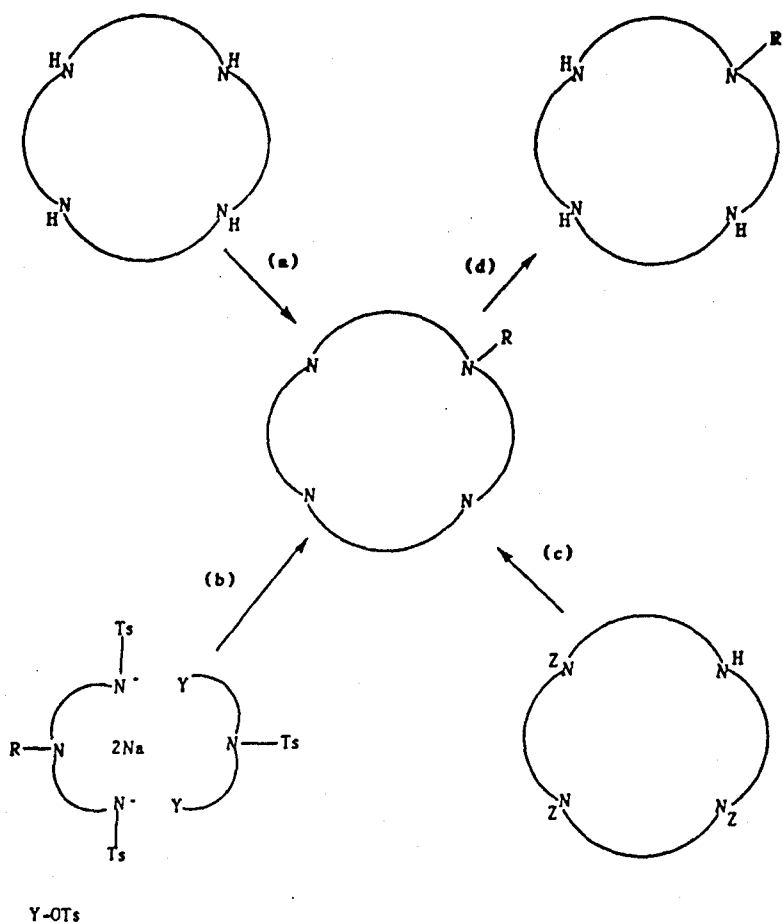
Section 6.1

Functionalised Macrocycles

This is an area which has grown recently, because of the interesting effects of having extra donor groups attached to a macrocycle. Functionalised tetra-azamacrocycles^{7 9} have received the most attention, but more recently triazamacrocycles^{5 3} have gained in popularity.

The syntheses of tetra-N-substituted azamacrocycles^{8 0}, and tri-substituted triazamacrocycles^{8 1, 8 2} are the most straightforward.

The preparation of mono functionalised macrocycles requires the use of more skilful synthesis. Four synthetic pathways are shown in Scheme 10.1.^{7 9}

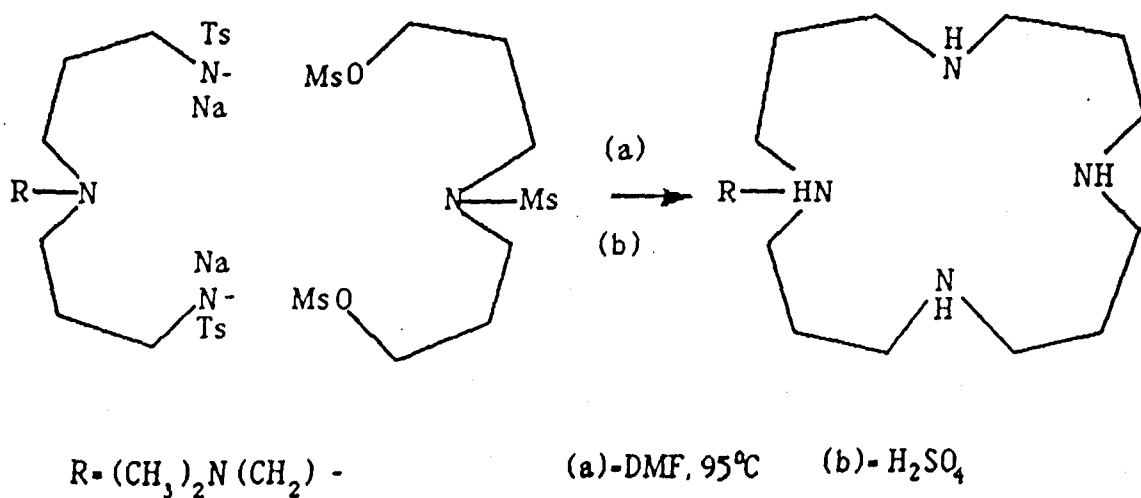


Scheme 10.1

(a) selective alkylation, (b) synthesis of pendant arm in place, (c) selective protection (d) further functionalisation.

The selective alkylation is the most simple, and involves adding alkylating agent to excess macrocycle. This method has not been used to a great extent, because of the difficulty of separation of products from starting materials.

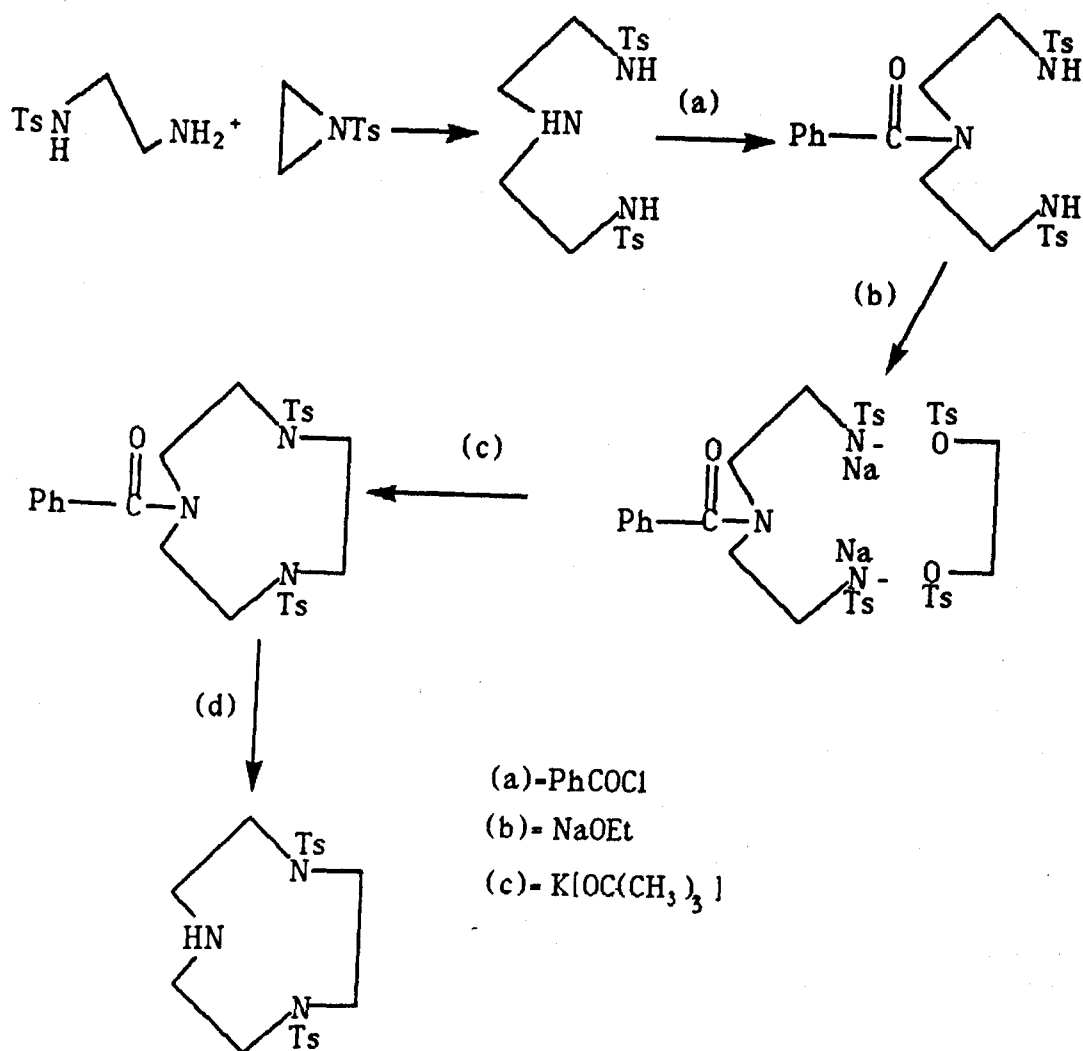
The cyclisation with the side arm already present is a popular method, and involves cyclisation using either template condensation, high dilution, or Richman-Atkins. Moore *et al.*,^{8 3} have used this method in the synthesis of a tetra-azamacrocycle containing a dimethylamino-ethyl pendant arm (Scheme 11.1).



Scheme 11.1

When the appropriate side chain has been introduced then further modification can be carried out. This has been demonstrated by Kaden^{8 4} by the hydrogenation of a pendant nitrile to an amino group.

The final approach has the greatest advantage, because once the "free" nitrogen is produced many different functionalisations can be undertaken. This has been used to a great advantage by Kaden^{84,85} in the synthesis of mono-functionalised tetra-azamacrocycles. Bukowski⁸⁶ has applied the same technique to produce a diprotected triazamacrocycle (Scheme 12.1).



Scheme 12.1

However, no further functionalisation of the "free" amine was attempted, but a great deal of potential is held by this compound in the synthesis of single pendant arm triazamacrocycles.

Redox active Macrocycles

There is a current interest in the synthesis of macrocycles containing redox active centres, especially those containing metallocene^{87,88}, quinone⁸⁹ and nitrobenzene⁹⁰ moieties. The interest in such systems is that an interaction between a redox active centre and a closely bound metal cation may occur. Redox active centres such as ferrocene are chosen because of the relatively simple reversible electrochemistry, which can be studied using cyclic voltammetry. (Section 8.1)

One of the first ferrocene containing macrocycles was synthesised by Vogtle⁹¹ in 1979 (Figure 12.1).

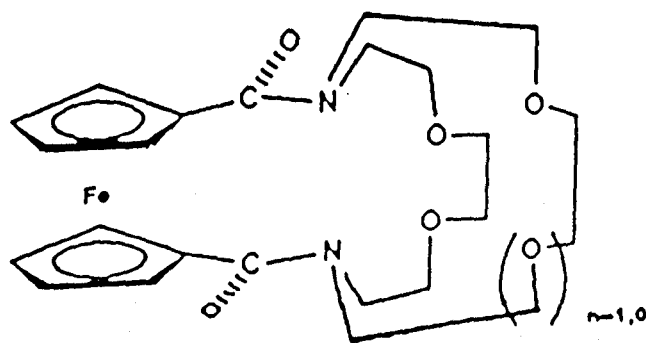
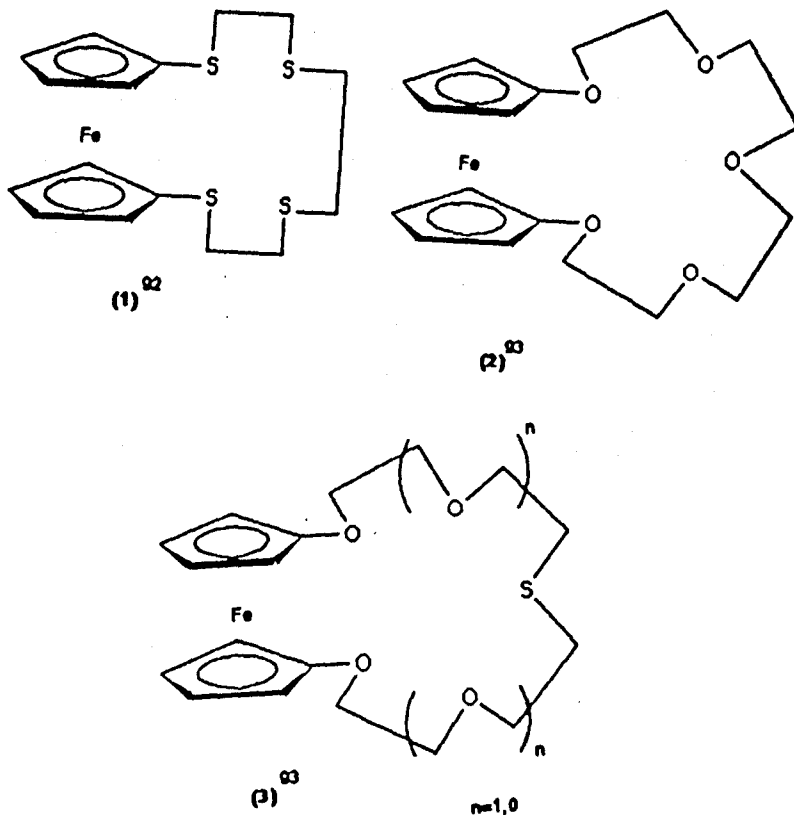


Figure 12.1

There have also been a number of oxygen, sulphur and mixed ferrocene macrocycles synthesised since then.



Saji⁹⁴ using macrocycle (2) found that a positive shift in the $E_{1/2}$ occurred on the addition of alkali metals. This shift occurred because of the decrease in cation binding of the oxidised form, compared to the neutral species. Binding enhancement by electrochemical switching has been observed with other redox active systems. For example, the lariat crown ether⁹⁰ (Figure 13.1) has been found to have an increased cation binding when the nitro group is electrochemically reduced.

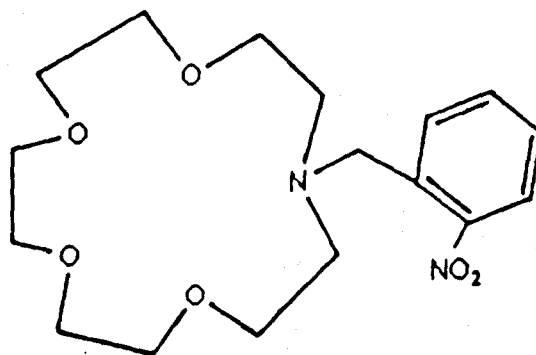
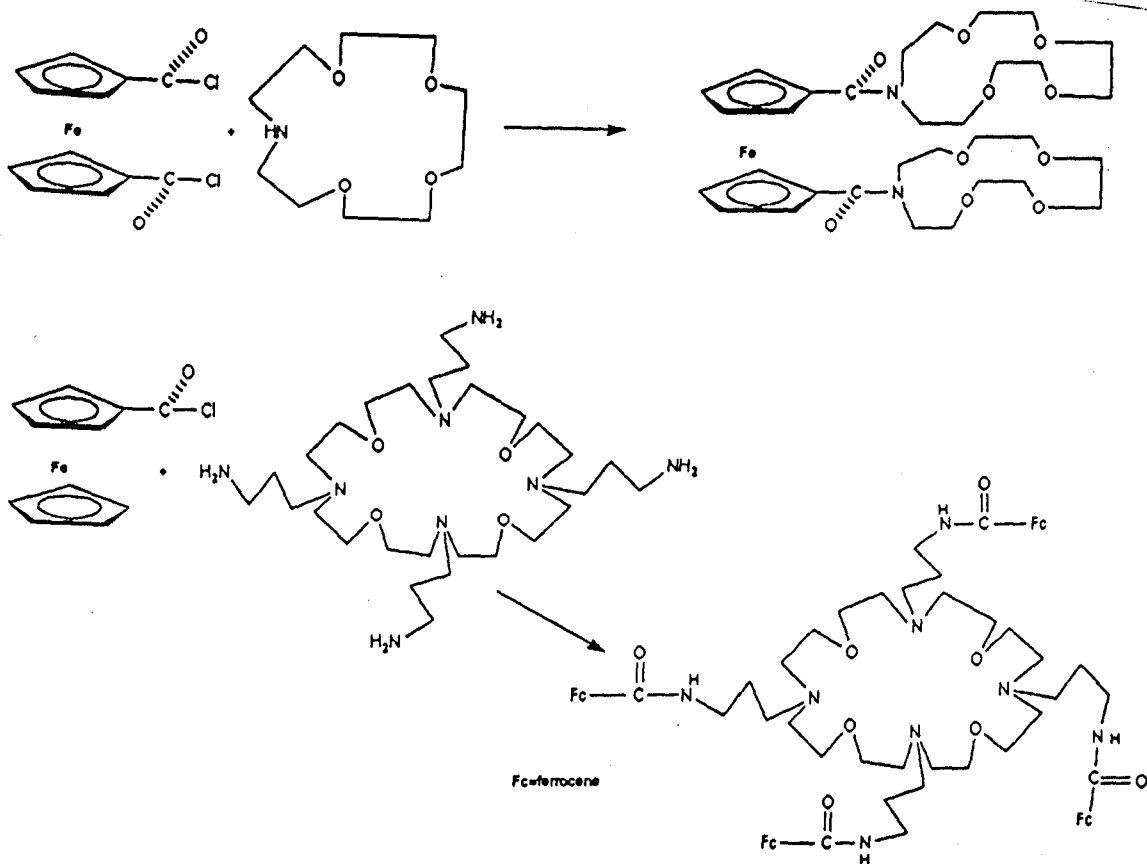


Figure 13.1

Synthesis of ferrocene containing Macrocycles

Synthesis usually involves the reaction of ferrocenoyl chloride, or 1,1'-bis(chlorocarbonyl)ferrocene with a corresponding amine (Scheme 13.1).^{95,96}



Scheme 13.1

Recently the reaction of a phosphorous ylid and a corresponding aldehyde has been used (Figure 14.1).⁸⁷

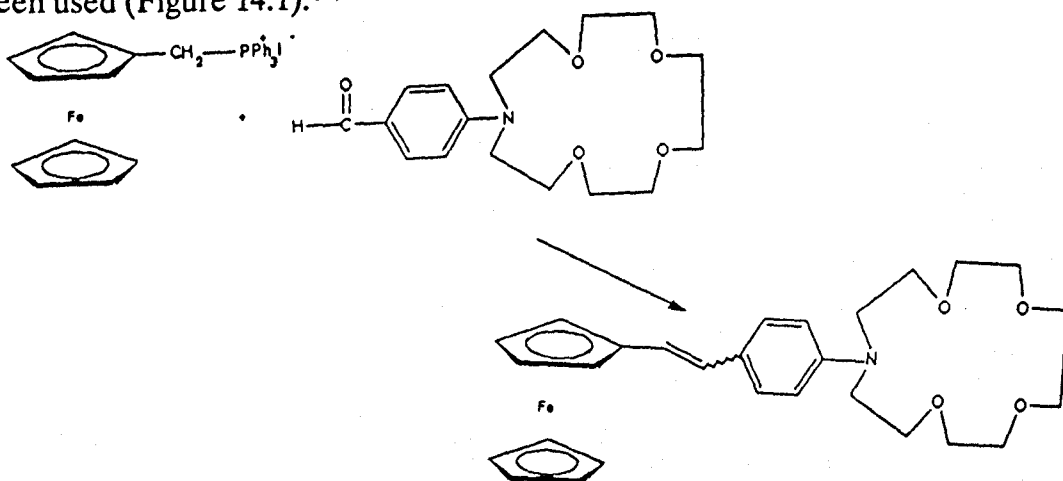


Figure 14.1

Cyclic Voltammetry

Cyclic voltammetry is a widely used tool in electroanalytical chemistry, mainly because it is straightforward to use, and can give a great deal of information on electrochemical processes. The usual experimental set up (Diagram 1.1), consists of a working electrode (W.E), counter electrode (C), and a reference electrode (R.E).

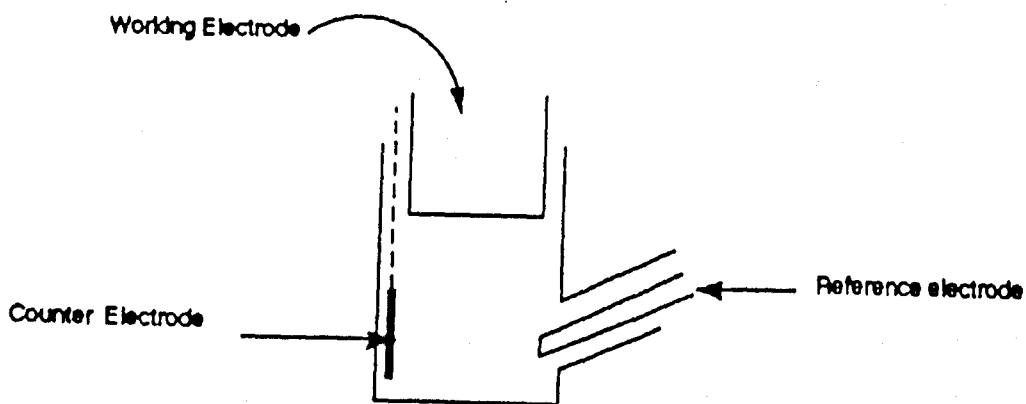
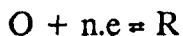


Diagram 1.1

The working electrode potential is varied between the limits(E_1) and (E_2), at a constant scan rate(ν), followed by a reversal ($E_2 \rightarrow E_1$). The corresponding currents (i) are recorded as a function of the potential (E). Usually a qualitative study is carried out by varying the limits(E_1) and (E_2) and the scan rate (ν). Repeat scanning is often carried out, as this gives information on how processes represented by peaks in the cyclic voltammogram are related.

Reversible Reactions



O = oxidised form, R = reduced form

Initially only "O" is present in solution, and concentrations above a certain distance from the electrode are maintained by convection. The current measured depends solely on the mass transport of "O" to the electrode surface. A typical cyclic voltammogram of a reversible system is shown in Figure 15.1.⁹⁷ The shape is the result of potential dependant surface changes in the surface concentrations of the redox systems and simultaneous diffusion processes. The peak current (i_p) can be determined by the Randles-Sevcik equation :-

$$i_p = -(2.69 \times 10^5) \cdot n^{3/2} \cdot C_O \cdot D^{1/2} \cdot \nu^{1/2} \cdot A.$$

n = number of electrons, C_O = bulk concentration (mol cm^{-3}) D = diffusion coefficient ($\text{cm}^2 \text{ s}^{-1}$), A = area of electrode (cm^2), ν = sweep rate (V s^{-1}).

To determine whether a system is reversible a number of diagnostic tests can be performed (Table 4.1).⁹⁷

Table 4.1.

- 1: $\Delta E_p = E_p^A - E_p^C = 59/n \text{ mV}$
- 2: $(E_p - E_{p/2}) = 59/n \text{ mV}$.
- 3: $i_p^A / i_p^C = 1$.
- 4: $i_p \propto \nu^{1/2}$.
- 5: E_p independent of ν .

A more realistic situation is the quasi-reversible system where both charge transfer and mass transport determine the current observed. Again certain diagnostic tests can be used to determine such systems (Table 5.1).^{9 7}

Table 5.1

- 1: i_p increases with $\nu^{1/2}$ but not proportional.
- 2: $i_p^A/i_p^C = 1$
- 3: $\Delta E_p > 59/n$ mV and increases with increasing ν
- 4: E_p^C shifts negatively with increasing ν .

Irreversible

In such cases the charge transfer at the electrode is slow, and so becomes the rate determining step. Usually the most marked feature of such cyclic voltammograms is the absence of a reverse peak. However, reverse peaks can be missing if a further chemical reaction occurs after oxidation. Diagnostic tests for irreversible systems are shown in Table 6.1.^{9 7}

Table 6.1

- 1: No reverse peak.
- 2: $i_p^C \propto \nu^{1/2}$
- 3: E_p^C shift = $-30/\alpha_c n_\alpha$ mV for each decade increase in ν .
- 4: $|E_p - E_{p/2}| = 48/\alpha_c n_\alpha$ mV

where n_α = number of electrons transferred up to, and including, the rate determining step. α_c = transfer coefficient.

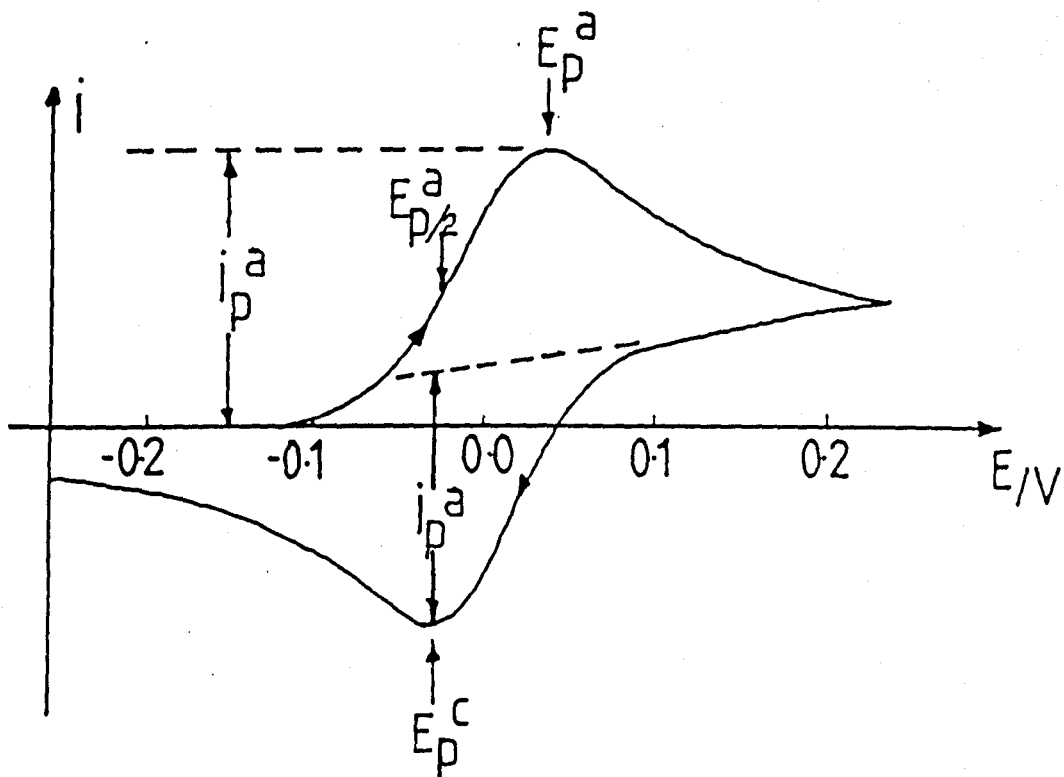


Figure 15.1

A typical reversible cyclic voltammogram. Symbols defined in text.

CHAPTER 2

The synthesis and study of redox active macrocycles based on 1,4,8,11-tetraazacyclotetradecane (cyclam)

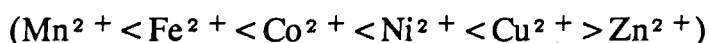
Section 1.2

Introduction

As described previously (page 29) redox active macrocycles have received considerable attention, especially in the sensing of alkali and alkaline earth metal ions.⁹⁹ To date there has been very little interest in the sensing of transition metal ions, even though these metals are important in a large number of biological processes. Beer¹⁰⁰ recently synthesised two Schiff base crown ether ligands, with a potential for transition metal ion recognition. In this study, we have undertaken the synthesis of a series of cyclam based ligands of related importance ($L^1 - L^5$). Some of these ligands combine the properties of azamacrocycles in forming highly stable complexes with transition metal ions, and have a ferrocenyl redox centre which can be used to sense metal ion complexation.

The main problem area is:-

1: Metal ion selectivity- Most macrocycles will form complexes with a number of transition metals; for the first row transition metal ions ($Mn \rightarrow Zn$), the stability constants generally follow the Irving-Williams sequence:



Therefore, to produce a specific transition metal ion sensor is more difficult than for the alkali metals, where size selectivity is more pronounced for a given ligand.^{24,101}

Because of its relatively easy synthesis, the ligand 1,4,8,11-tetraazacyclotetradecane (cyclam) was chosen as the base macrocycle.¹²⁵

In this chapter the syntheses of a series of ferrocene containing azamacrocycles based on cyclam, and their electrochemistry, are described.

Results and Discussion

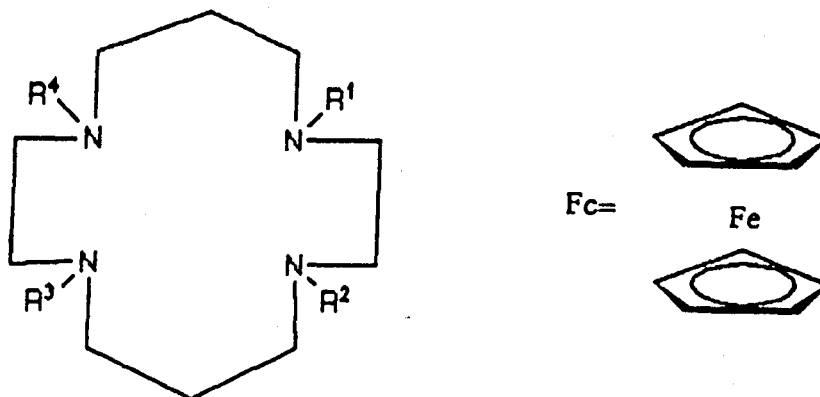
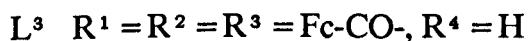
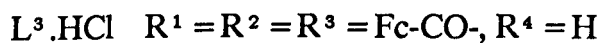
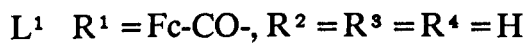


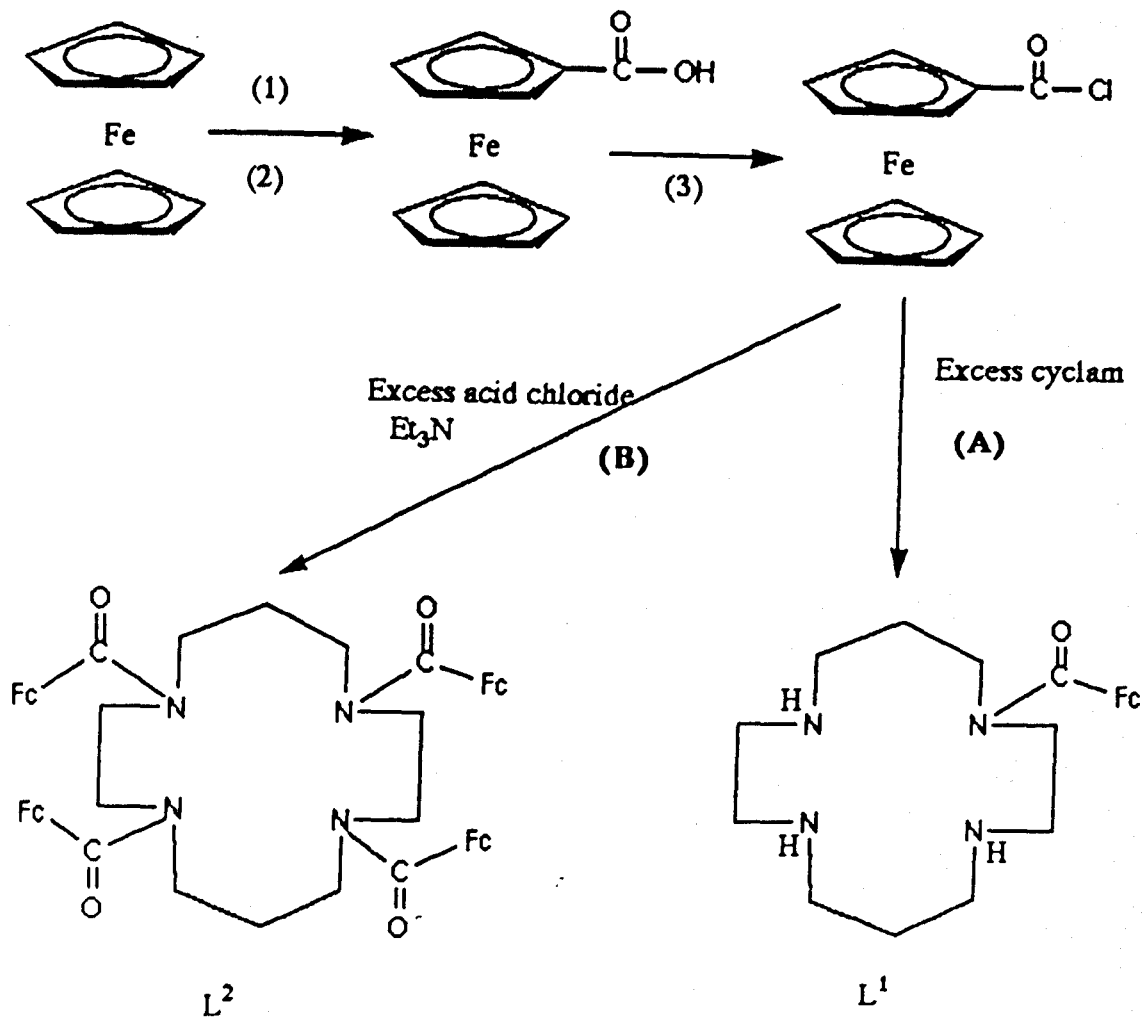
Figure 1.2



Section 2.2

The synthesis and electrochemistry of L¹ (Figure 1.2)

The general synthesis of this macrocycle is outlined in Scheme 1.2. The mono-carboxylic acid was synthesised by the procedure of Reeves¹⁰² in preference to other reported procedures,^{103,104} because of the good yields (62%), and experimental ease. A number of reported procedures for the synthesis of the mono-acid chloride were attempted,^{105,106} but oxalyl chloride¹⁰⁷ was found to give the best yields (77%).



Scheme 1.2

(1): AlCl_3 , 2-chlorobenzoyl chloride, CH_2Cl_2 , 0°C .

(2): Potassium *t*-butoxide, H_2O .

(3): Oxalyl chloride.

To obtain the ligand L¹ an excess of cyclam was used (~10 fold), to ensure that only the mono functionalised macrocycle was produced. The excess cyclam could be easily removed by dissolving the product in acetonitrile, and filtering off the insoluble cyclam. Column chromatography on silica gave the desired product as a yellow solid on good yield (76%). The structure was verified by elemental analysis (Table 3.2), F.A.B mass spectrometry (Table 5.2) (Figure 8.2), ¹H and ¹³C n.m.r spectroscopy (Tables 1.2, 2.2). The asymmetry of the cyclam is shown in both the ¹H and ¹³C n.m.r, by the number of resonances. Interestingly besides the main resonances in the ¹³C n.m.r for the cyclam backbone, a series of smaller resonances are observed, indicating a further species is present. This could be attributed to a hindered rotation (Figure 2.2) around the N-CO bond, or a "locked in" conformer of the macrocyclic ring (Figure 2.1, page 7).

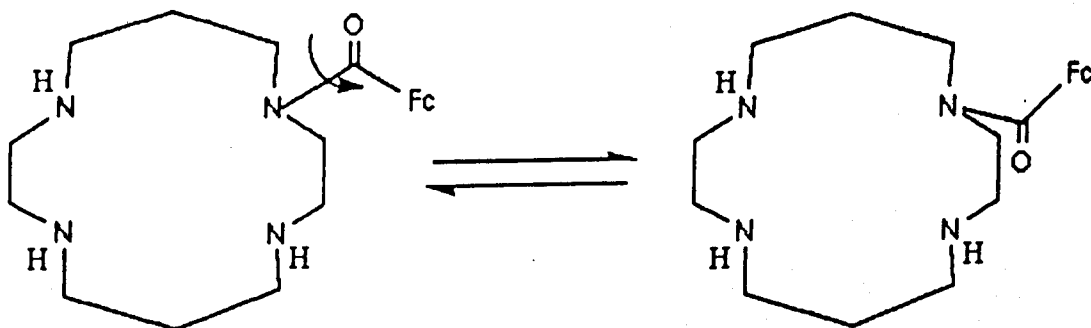


Figure 2.2

However, Beer^{9 5} has shown for a ferrocene bis-crown ether, N-CO bond rotation is fast on the n.m.r timescale, and only at low temperatures ($\sim -20^\circ\text{C}$) does resolution occur. Even at elevated temperatures ($\sim 50^\circ\text{C}$), the ^{13}C n.m.r of L¹ shows very little change (Figure 3.2); thus hindered rotation is unlikely. Therefore, conformational "locking in" is the most likely explanation, especially if the amide nitrogen is sp^2 hybridised. Crystals were obtained to try and solve this problem, but were found to be unsuitable for X-ray structure determination.

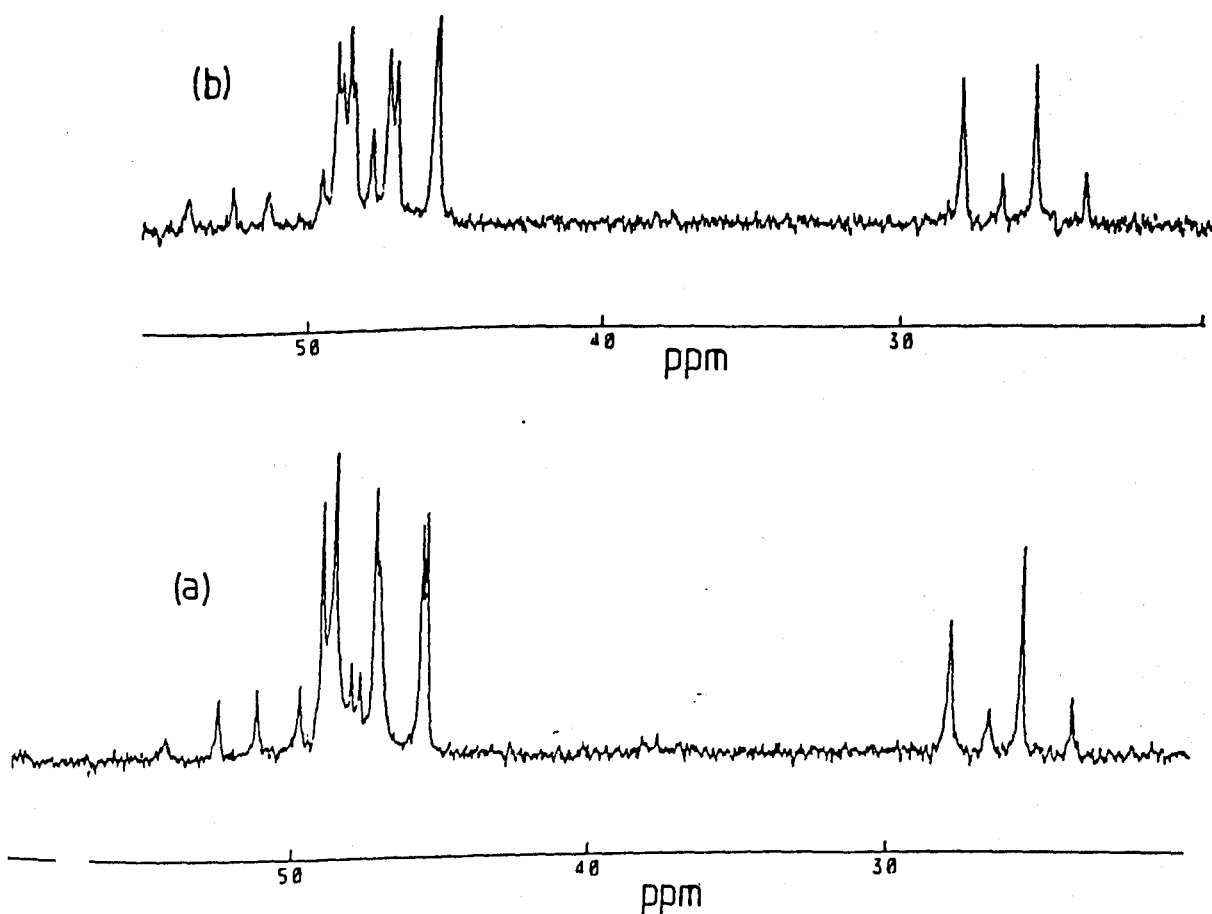


Figure 3.2

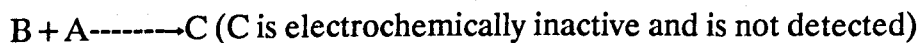
^1H decoupled ^{13}C n.m.r of ligand L¹ in D_2O (reference dioxan $\delta = 67.4$), at 300K (a), and 323K (b).

Section 3.2

Electrochemistry of L¹

The electrochemistry of L¹ is very interesting and depends on the solvent of study. The cyclic voltammetry in CH₃CN (Tetraethylammonium tetrafluoroborate TEATFB background) contains only a partial reverse peak even at high scan rates (Figure 4.2), and no reverse peak at low scan rates. Therefore, the oxidised form is removed from the electrode surface, as detection is only possible with fast experimental technique. Titration with Zn²⁺ causes the reverse peak current (*i*_{pc}) to increase to a point where a reversible system is produced. The titration curve (Figure 5.2) shows that at an equivalence of 1:1 the current (*i*_{pc}) ceases to increase, and so saturation occurs. No shift in the half wave potential (*E*_{1/2}) occurs, thus indicating no interaction occurs between the bound metal and the ferrocene unit. This poor communication between the bound metal and ferrocene unit is not surprising, as other work has shown that electronic effects are not transmitted by carboxylato¹¹¹, amino¹¹², and dithiocarbamates¹¹³. Addition of other transition metal ions (e.g. Cu²⁺, Ni²⁺) caused similar increases in the reverse current. However, electrode fouling occurs probably due to precipitation of the metal complexes, and so was not studied further.

The instability of the oxidised form must be related to the secondary nitrogen atoms of the macrocyclic ring, because once "blocked" (e.g. by complexation) reversibility occurs. Possibly the lone pair of a nitrogen atom attacks the iron centre of the oxidised form of the ferrocene:-



where A = reduced form of L¹, B = oxidised form of L², C = breakdown product. When cyclic voltammetry is conducted in H₂O (NaNO₃ background) a reversible system is observed, as indicated by the linear dependance of peak current on the square root of the scan rate (Figure 6.2). The breakdown of the oxidised form is again removed, probably due to solvation of the nitrogens by H₂O. Again the

addition of Zn^{2+} has no effect on the $E_{1/2}$ value in the cyclic voltammogram.

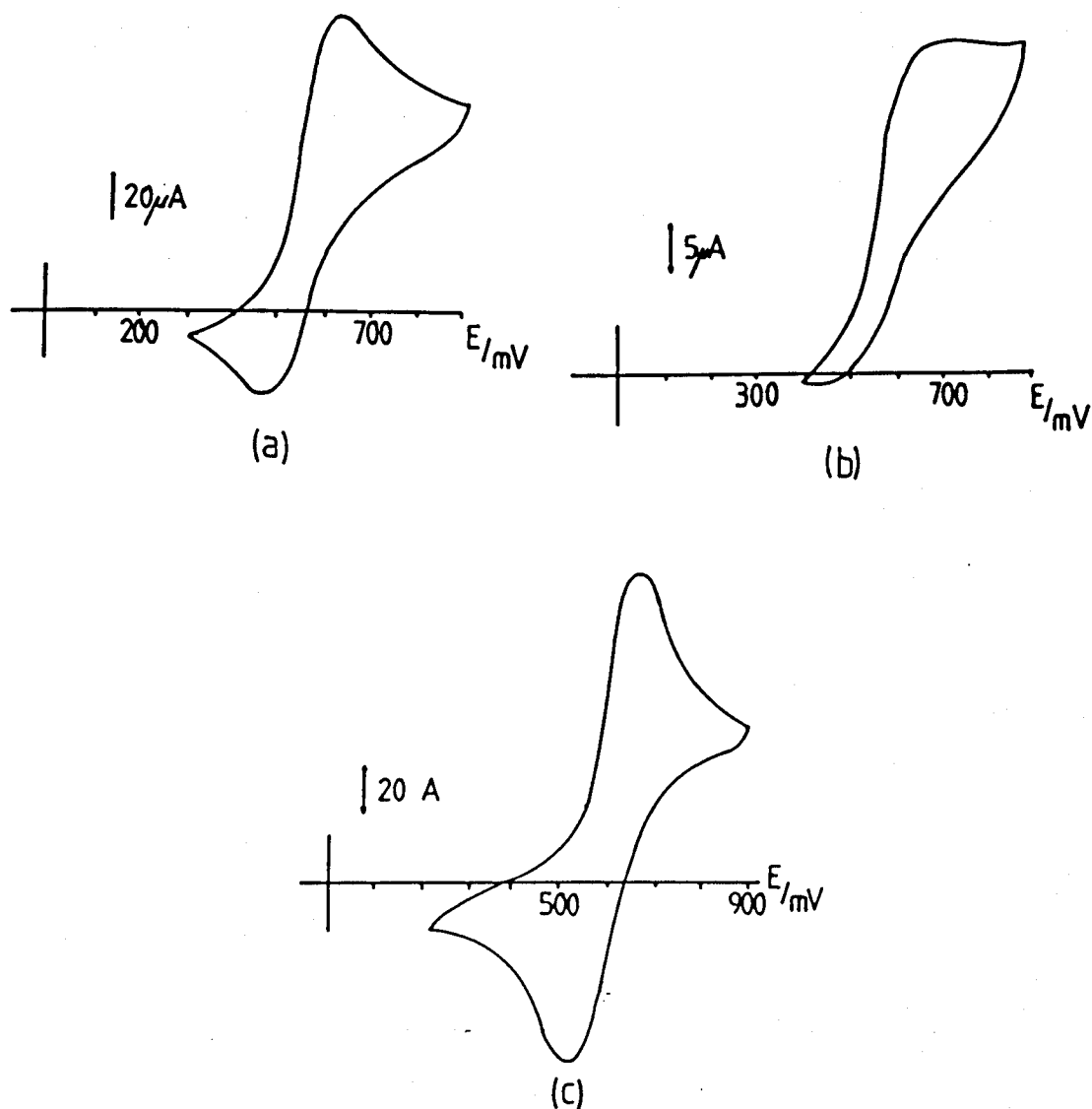
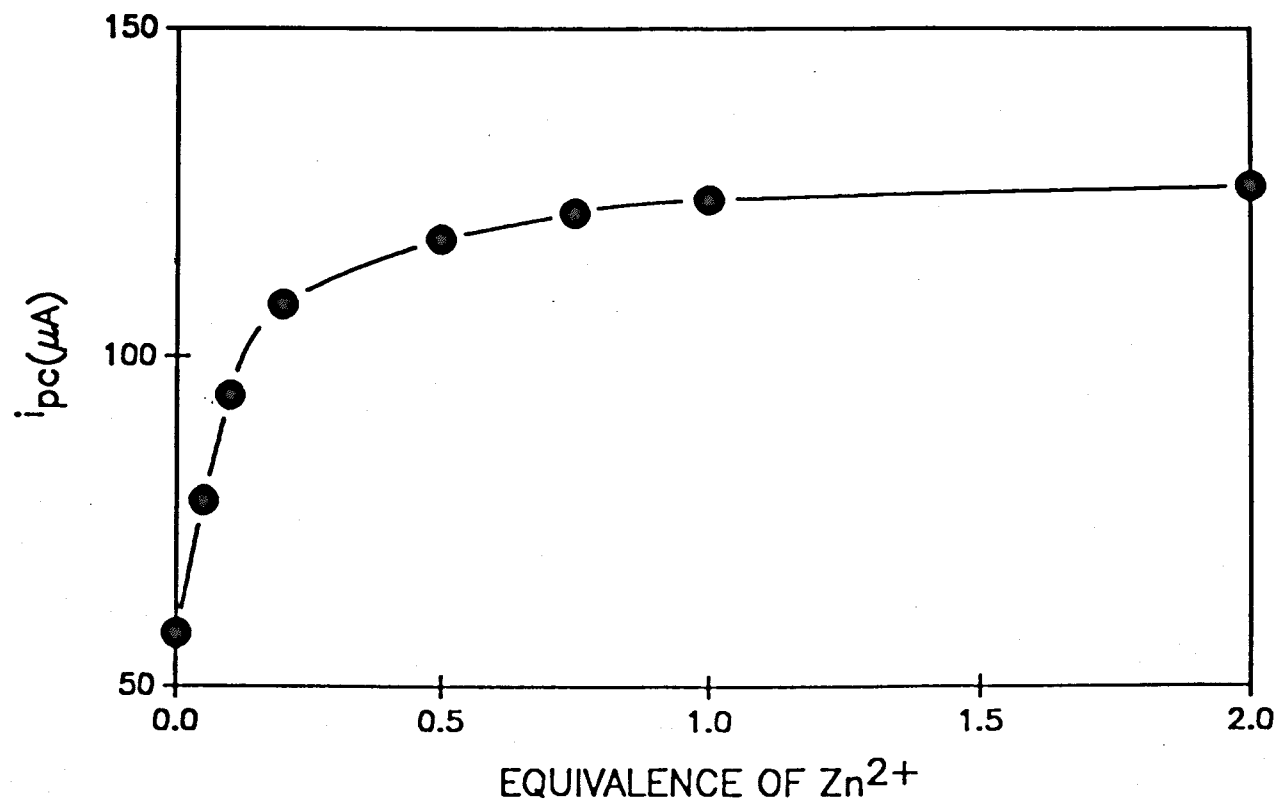


Figure 4.2

The electrochemistry of the ligand L^1 (3.2 mM) in CH_3CN , 0.2 M Tetraethylammonium tetrafluoroborate (TEATFB) background, Pt electrode, vs S.C.E. $E_{1/2} = 590 mV$, $i_{pa}/i_{pc} = 1.24$. (a) = 100 mV/s, (b) = 5 mV/s, (c) = 100 mV/s, excess Zn^{2+} added.

Figure 5.2

A titration curve for the addition of Zn^{2+} to the ligand L^1 . Experimental conditions are given in Figure 4.2



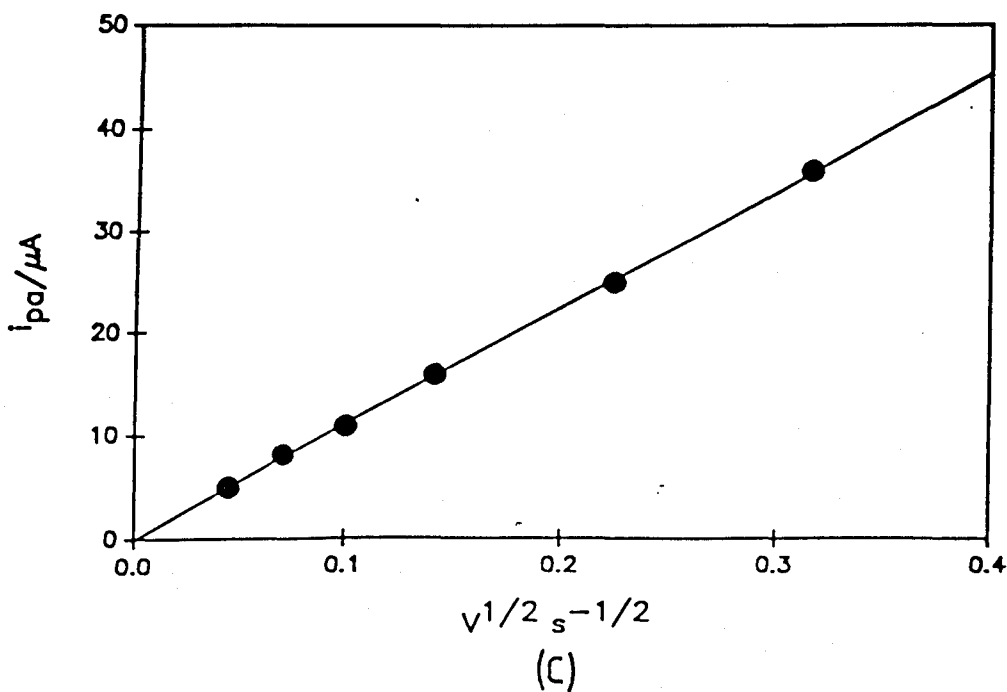
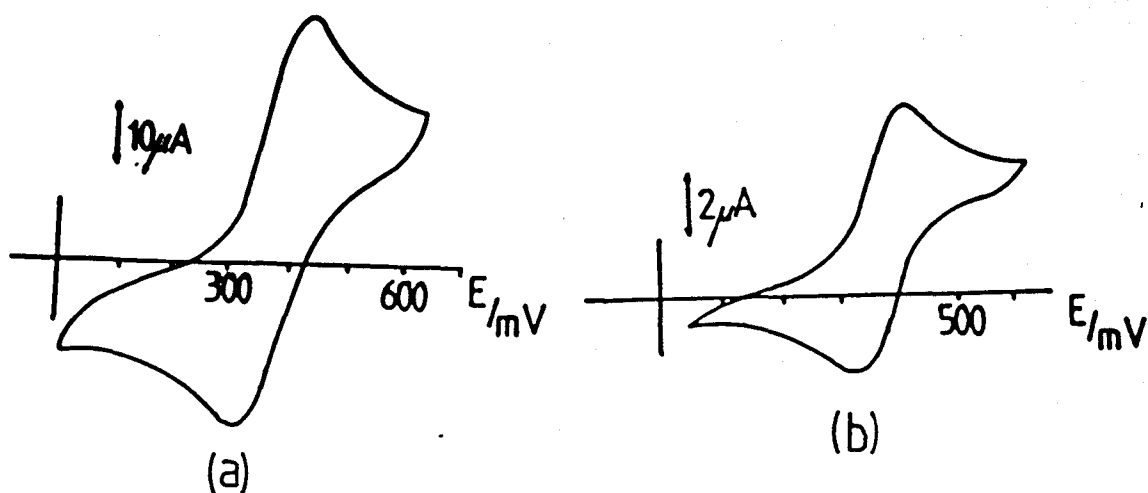


Figure 6.2

The electrochemistry of L^1 (3.98mM) in H_2O , 0.2M $NaNO_3$ background electrolyte, Pt electrode, vs S.C.E. $E_{1/2} = 367\text{mV}$, $i_{pa}/i_{pc} = 1.2$. (a) = 100mV/s, (b) = 2mV/s, (c) = Plot of peak current (i_{pa}) against the square root of scan rate.

Section 4.2

The synthesis and electrochemistry of L^2

To obtain the macrocycle L^2 , the ferrocenoyl chloride was used in a large excess (~ 10 fold) to ensure tetrasubstitution. Column chromatography on silica yielded the desired product as a yellow solid in good yield (73%). The structure is verified by elemental analysis, ^1H and ^{13}C n.m.r spectrometry (Table 1.2-3.2), F.A.B mass spectrometry (Figure 8.2, Table 5.2), and X-ray crystallography (Section 5.2).

The ^1H n.m.r shows no differentiation of the four ferrocene units at 298K, but on cooling to 253K the three resonances each split into two, indicating a set of two ferrocenes are becoming inequivalent (Figure 7.2 (a)). However, no resolution of the cyclam protons occurs. A better indication of the conformation of the cyclam framework is obtained using ^{13}C n.m.r. At 298K the carbon resonances of the cyclam are broad, but on cooling to 233K the resonances resolve (Figure 7.2 (b)). A fast process must be occurring at room temperature which makes the ferrocenes equivalent, and broadens the carbon resonances. On cooling a single conformer is frozen out. To obtain a better picture, a single crystal X-ray structure was undertaken.

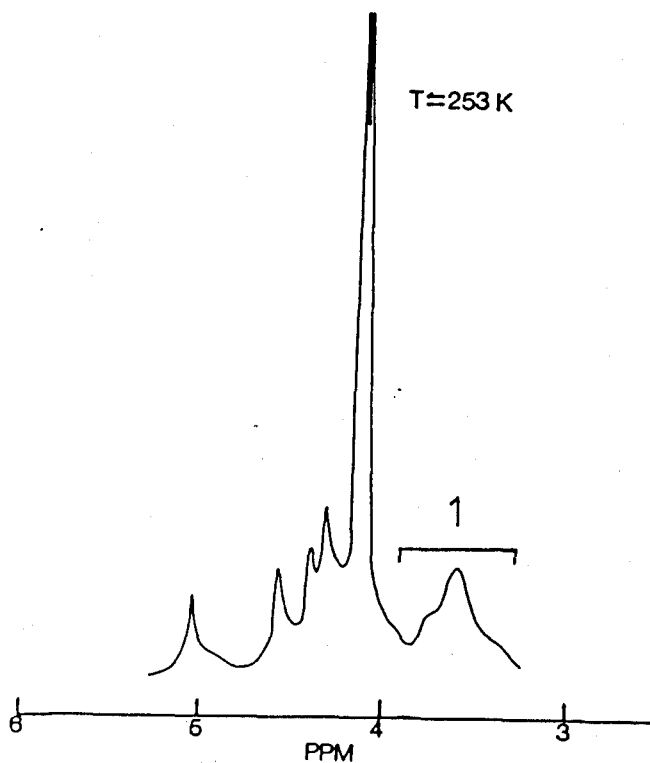
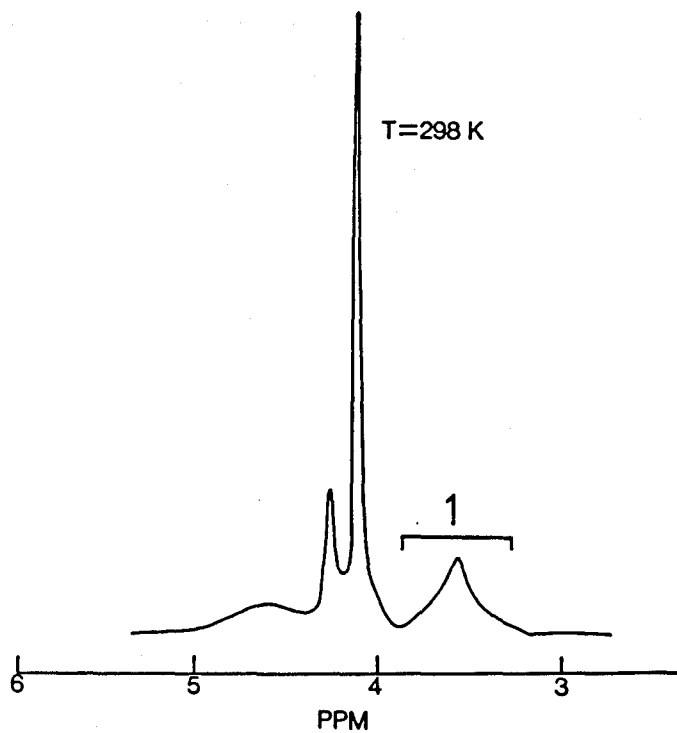
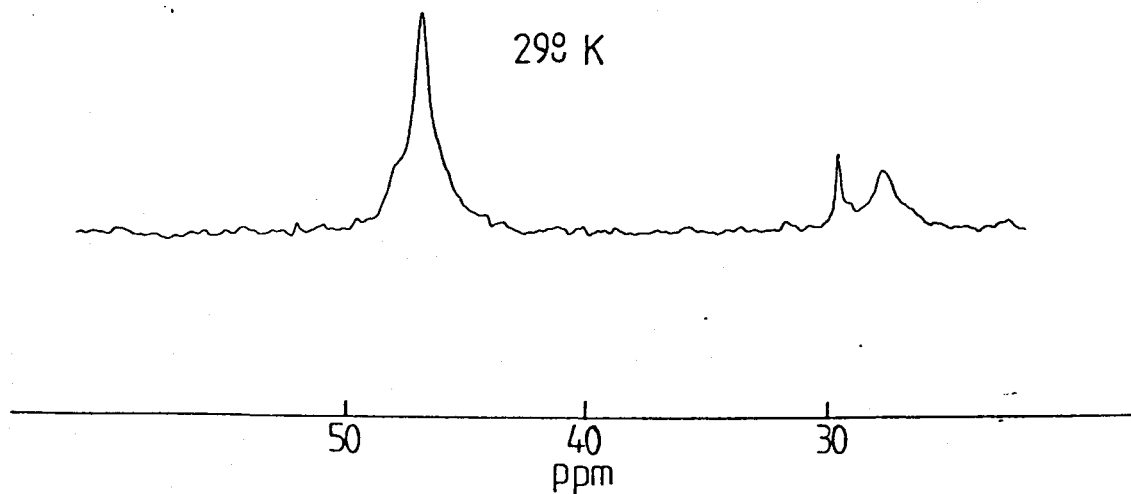
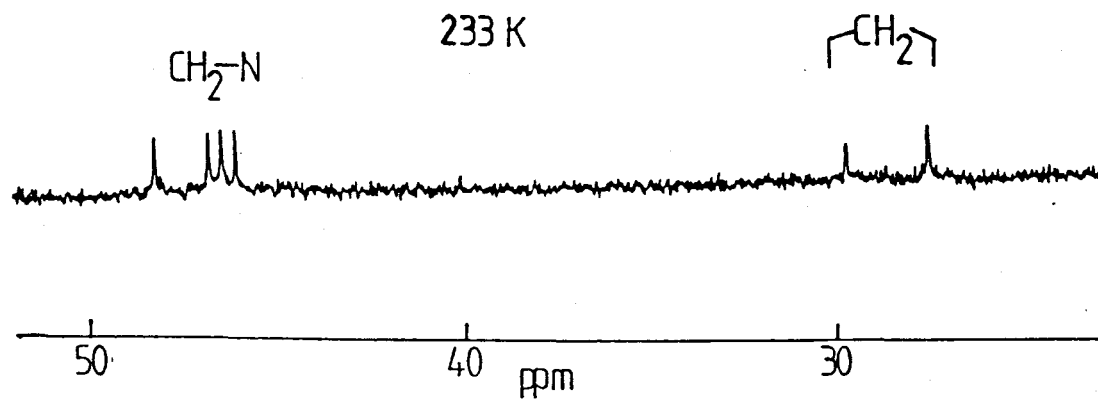


Figure 7.2(a)

A variable temperature ^1H n.m.r of L^2 in CDCl_3 (reference Me_4Si $\delta = 0.0$). Resonances (1) correspond to cyclam protons $-\text{N}[\text{CH}_2]-\text{C}$

Figure 7.2(b)

^1H decoupled ^{13}C n.m.r. of L^2 in CDCl_3 (ref. Me_4Si at $\delta = 0$)



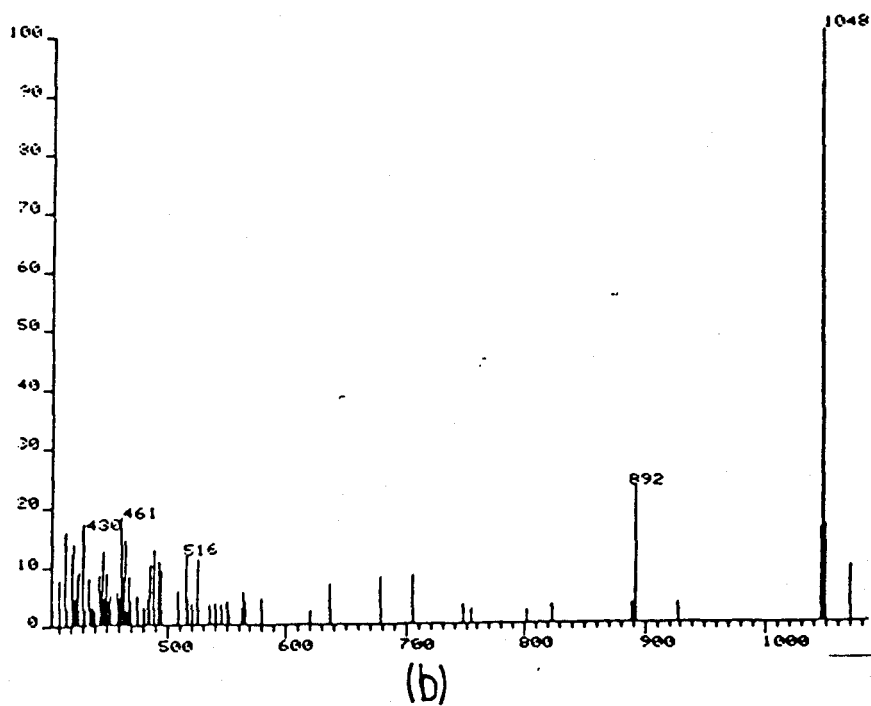
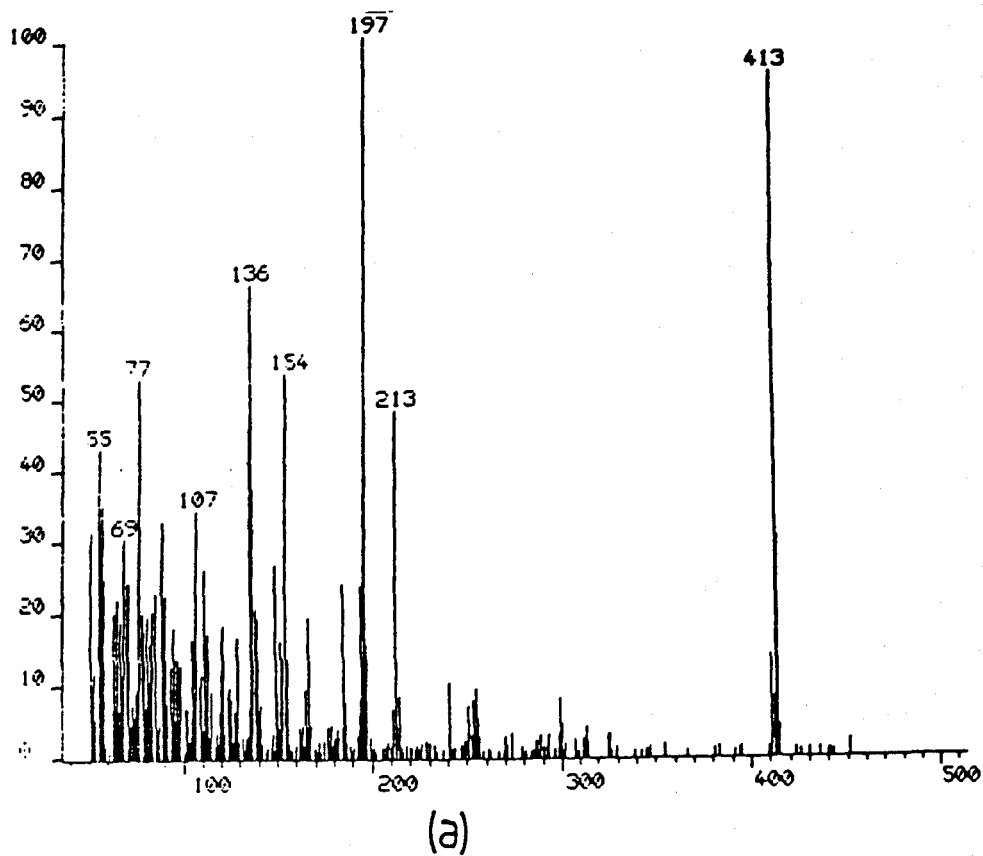


Figure 8.2

F.A.B mass spectral data for the ligands L^1 (a), L^2 (b), in a *m*-nitrobenzylalcohol matrix. L^1 (m/z calc-413 for $[M+H]^+$), L^2 (m/z calc-1048 for M^+).

The crystal structure of L^2

The geometry of the macrocycle is shown in Figure 9.2 (a), and is centrosymmetric; thus a set of two ferrocenes are equivalent. The structure fits in well with the ^{13}C and ^1H n.m.r data, which indicates a set of two equivalent ferrocenes at low temperatures. The nitrogen atoms are sp^2 hybridised with bond angles attached to C atoms of $120 \pm 3^\circ$. The sp^2 nature of the nitrogens means that the macrocycle is unsuitable for chelation. This is better seen in Figure 9.2 (b), which shows that the macrocyclic ring adopts a pseudo chair conformation. The iron centres are at a distance apart of 8.580\AA [Fe(1)-Fe(2)] and 9.593\AA [Fe(2)-Fe(1a)], indicating no interaction should be observed between the ferrocene units. L^2 shows relatively simple cyclic voltammetry in line with this conclusion. Interestingly the molecule crystallised with four moles of chloroform, which are shown in the packing diagram. The chloroform molecules sit in the spaces left by the packing of the individual units (Figure 9.2(c)).

Figure 9.2(a)

The geometry of L^2 showing atomic labelling.

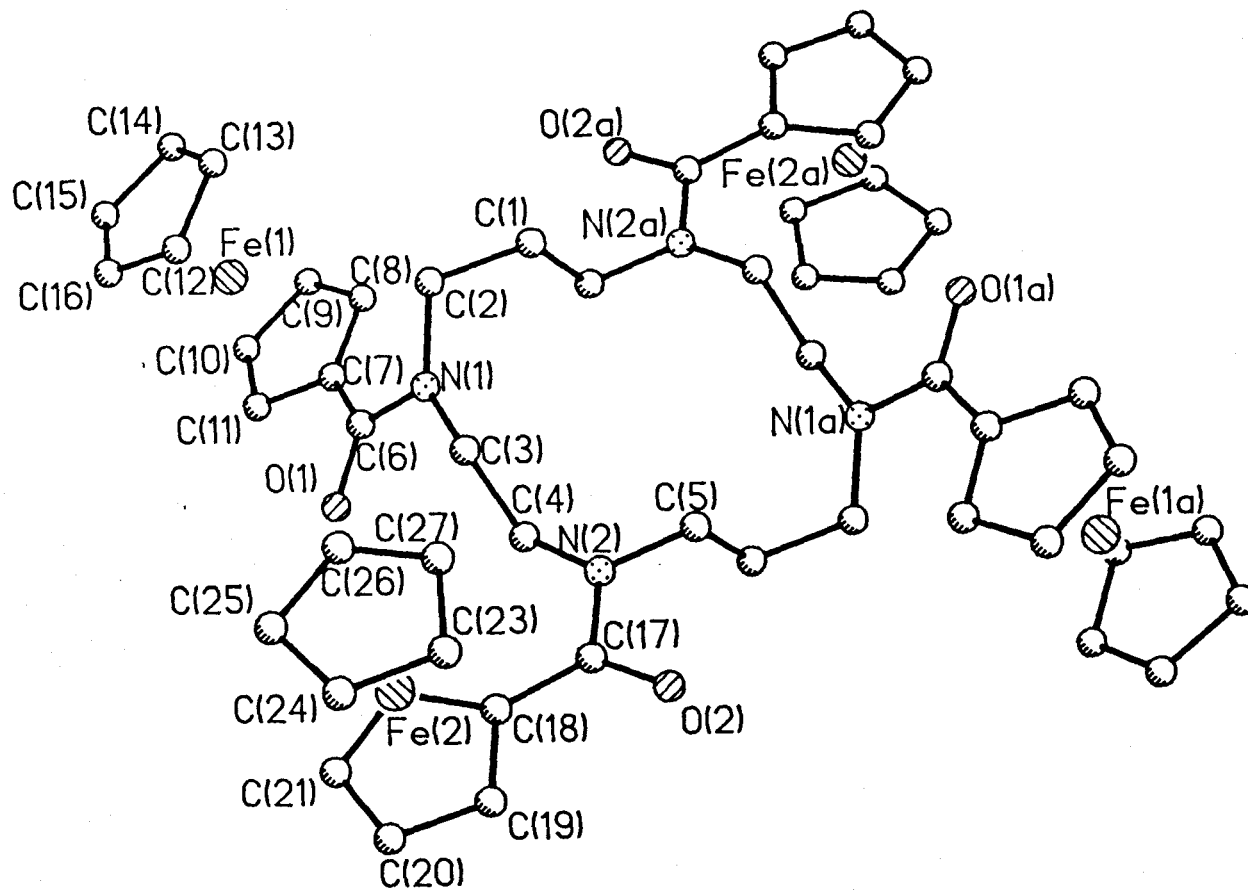


Figure 9.2(b)

Structure of the macrocyclic ring, showing the pseudo chair conformation. Ferrocene groups removed for clarity.

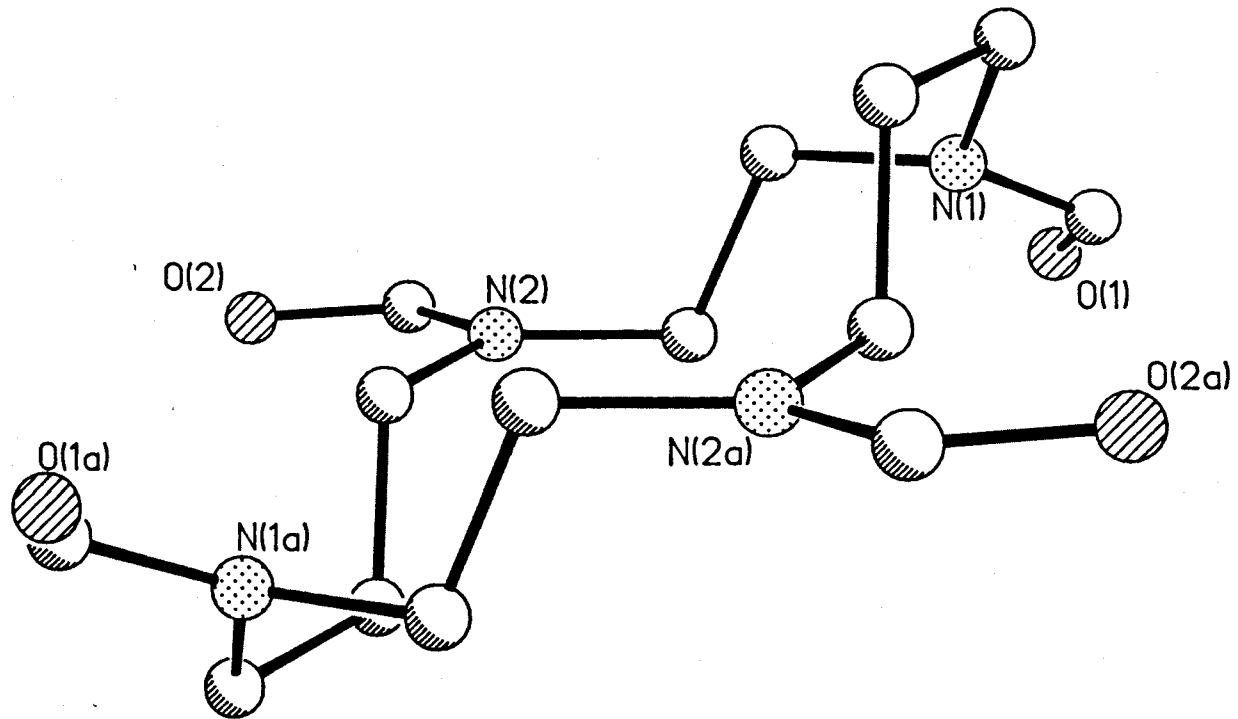


Figure 9.2(c)

Packing diagram of L^2 showing chloroform molecules marked X

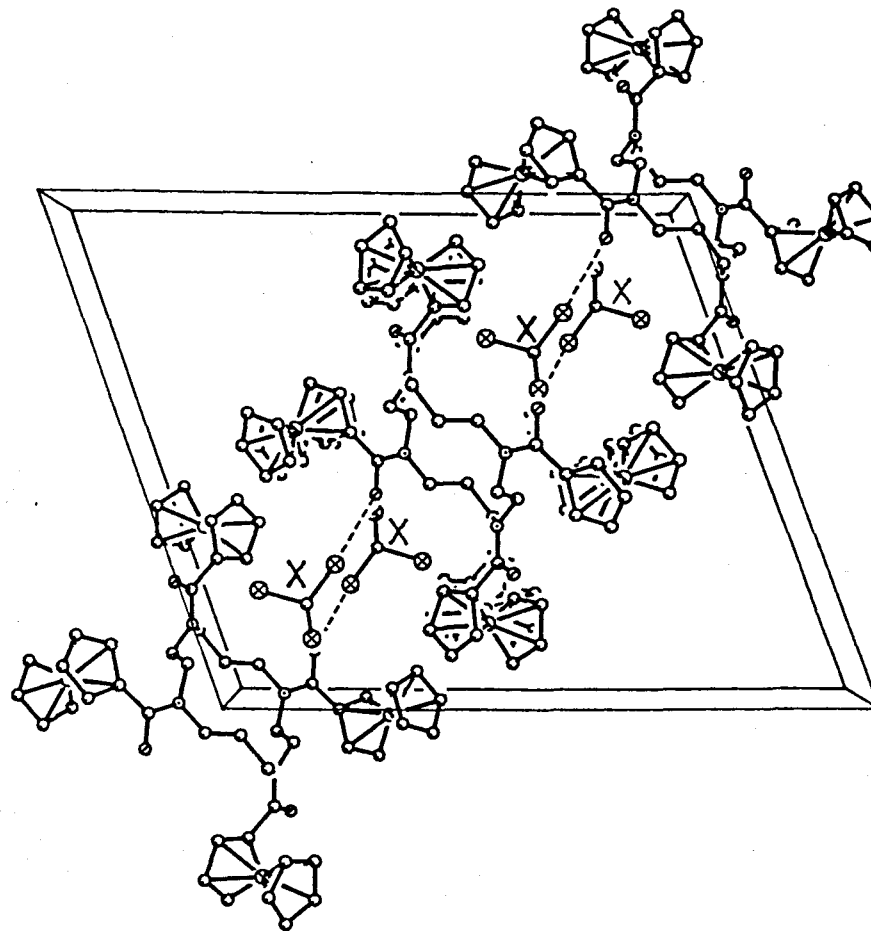


Table 6.2

Selected bond lengths for L²

Bond lengths (Å)

Fe(1)-C(7)	2.090 (29)	Fe(1)-C(8)	2.053 (31)
Fe(1)-C(9)	2.060 (30)	Fe(1)-C(10)	2.012 (29)
Fe(1)-C(11)	2.016 (29)	Fe(1)-C(12)	2.051 (30)
Fe(1)-C(13)	2.058 (28)	Fe(1)-C(14)	2.063 (31)
Fe(1)-C(15)	2.066 (40)	Fe(1)-C(16)	2.003 (46)
Fe(2)-C(18)	2.044 (26)	Fe(2)-C(19)	2.043 (26)
Fe(2)-C(20)	2.084 (28)	Fe(2)-C(21)	2.046 (29)
Fe(2)-C(22)	2.030 (25)	Fe(2)-C(23)	2.040 (31)
Fe(2)-C(24)	1.985 (30)	Fe(2)-C(25)	2.045 (39)
Fe(2)-C(26)	2.015 (32)	Fe(2)-C(27)	2.026 (37)
Cl(1)-C(201)	1.720 (23)	Cl(2)-C(201)	1.716 (26)
Cl(3)-C(201)	1.724 (33)	Cl(4)-C(101)	1.713 (29)
Cl(5)-C(101)	1.703 (34)	Cl(6)-C(101)	1.728 (31)
O(1)-C(6)	1.225 (35)	O(2)-C(17)	1.249 (31)
N(1)-C(2)	1.458 (30)	N(1)-C(3)	1.455 (27)
N(1)-C(6)	1.346 (35)	N(2)-C(4)	1.431 (25)
N(2)-C(5)	1.431 (35)	N(2)-C(17)	1.407 (31)

Selected bond angles for L²

Bond angles (°)

C(2)-N(1)-C(3)	118.0(16)	C(2)-N(1)-C(6)	120.3(20)
C(3)-N(1)-C(6)	116.8(21)	C(4)-N(2)-C(5)	118.6(18)
C(4)-N(2)-C(17)	123.4(21)	C(5)-N(2)-C(17)	117.2(19)
C(2)-C(1)-C(5A)	114.4(19)	N(1)-C(2)-C(1)	113.7(21)
N(1)-C(3)-C(4)	114.8(17)	N(2)-C(4)-C(3)	112.4(16)
N(2)-C(5)-C(1A)	114.9(18)	O(1)-C(6)-N(1)	121.1(23)
O(1)-C(6)-C(7)	115.5(23)	N(1)-C(6)-C(7)	122.1(26)

Electrochemistry of L²

The tetraamide derivative L² shows a single reversible cyclic voltammogram (Figure 10.2), which by coulometric titration is shown to be a four electron process (Appendix II); this is as expected for four independent ferrocenyl units (Section 5.2). Similar behaviour has been observed in meso-tetrakis(4-ferrocenylphenyl)porphyrin, where the ferrocenyl groups are also independent of each other.¹⁰⁸ The linear dependence of peak current with the square root of sweep rate again is consistent with a reversible system (Figure 10.2). On addition of Zn²⁺ to a solution of the tetraamide there is no change in the cyclic voltammetry. This can be attributed to the poor donor ability of tertiary amides, and the sp² hybridisation of the nitrogens which makes chelation to a metal impossible.

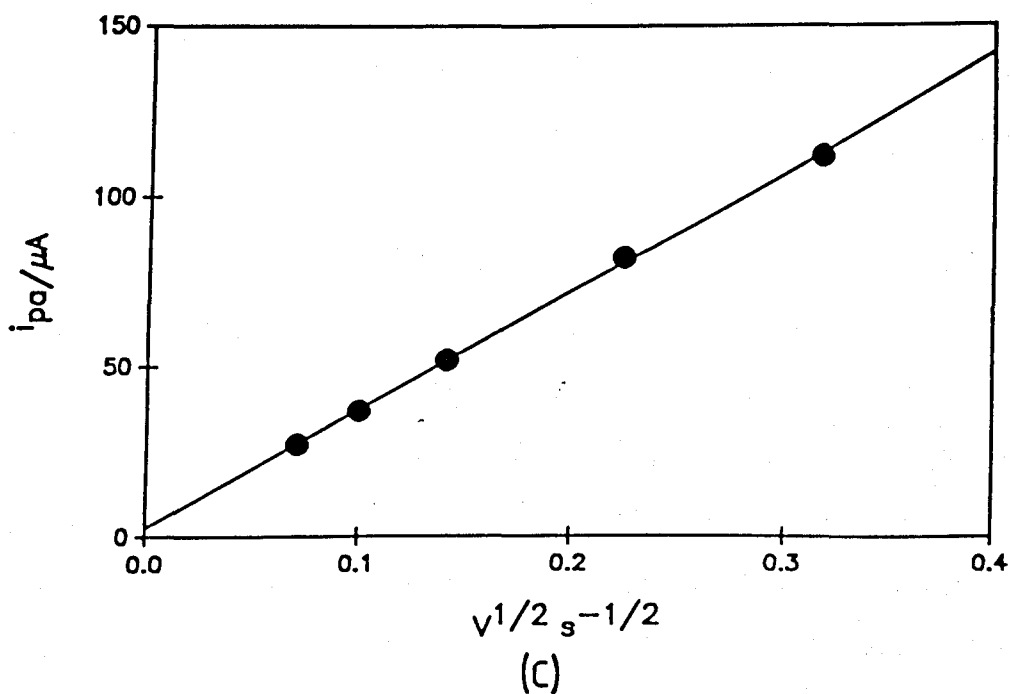
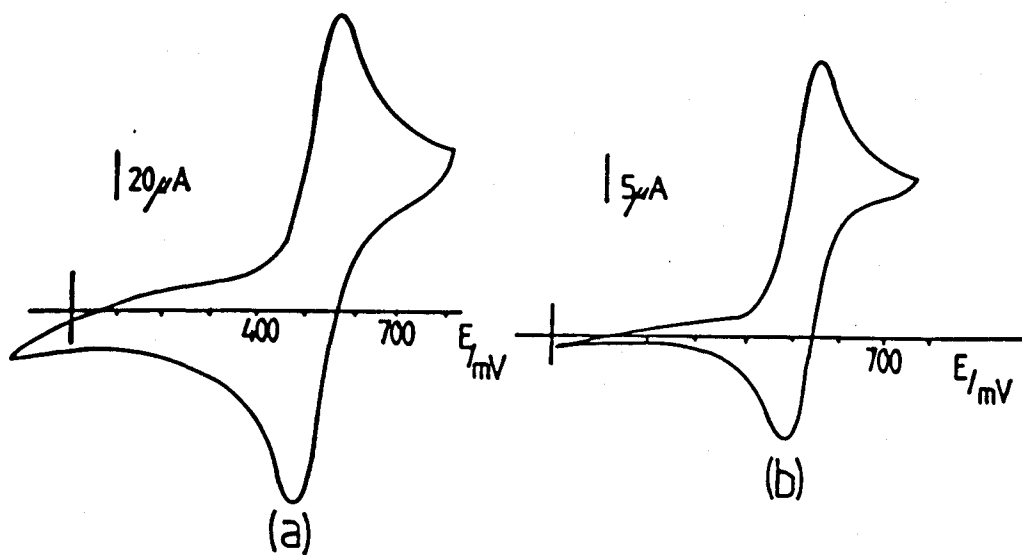


Figure 10.2

The electrochemistry of L^2 (0.32mM) in CH_3CN , 0.2M Tetrabutylammonium perchlorate background, Pt electrode, vs S.C.E, $E_{1/2} = 533\text{mV}$, $i_{pa}/i_{pc} = 1.08$.
 (a) = 100mv/s, (b) = 5mV/s, (c) = plot of peak current(i_{pa}) against the square root of scan rate.

Section 7.2

The synthesis and electrochemistry of $L^3.HCl$ and L^3

In order to obtain a better ligand, attempts were made to reduce all four amide linkages of L^2 . A number of reagents were used; $LiAlH_4$, $BH_3.thf$, and triethyloxonium fluoroborate (the latter caused alkylation of the ferrocene ring), but after a number of attempts, including repetitive reduction, a pure product could not be obtained. Therefore, a new synthetic procedure was adopted, which entailed the reaction of a halomethylferrocene with cyclam, hopefully in order to produce a tetra-alkylated macrocycle. Interestingly, this method failed to yield the desired product, but gave instead a trisubstituted derivative (Section 8.2).

Section 8.2

Synthesis of $L^3.HCl$ and L^3

The synthetic procedure for $L^3.HCl$ and L^3 is outlined in Scheme 2.2. The hydroxymethylferrocene can be easily obtained in good yield (89%) using standard organic procedures.¹⁰⁹ The chloromethylferrocene is more difficult to obtain, because of its instability and reactivity. However, by adaptation of the method of Schlögl,¹¹⁰ and immediate use of material without purification, problems can be overcome. To ensure that the reaction goes to completion, the reaction mixture is stirred for a least 72 hours. After work up and purification, two products are obtained, the desired product $L^3.HCl$ in moderately good yield (55%), and the side product $2L^b.Fe_2OCl_6$. The structures were established by 1H and ^{13}C n.m.r spectrometry (Table 5.2) and single crystal X-ray crystallography (Section 9.2/11.2). Good evidence that only tri-substitution occurs is shown by the ^{13}C n.m.r (Figure 11.2 (a)). The number of resonances in both the ferrocene and cyclam regions indicate the unsymmetric nature of the molecule. The F.A.B mass spectrum contains a cluster of peaks around $m/z = 795$, with an isotopic pattern which fits well with the data expected for $[L^3 + H]^+$. To obtain a better insight into the structure of $L^3.HCl$, a single crystal structure X-ray structure determination was undertaken.

Figure 11.2(a)
 ^1H decoupled ^{13}C n.m.r of $\text{L}^3\cdot\text{HCl}$ in CDCl_3 (ref Me_4Si $\delta = 0$). Y-Y = expansion of ferrocene region. X-X = expansion of cyclam
N-(CH_2)-C carbons.

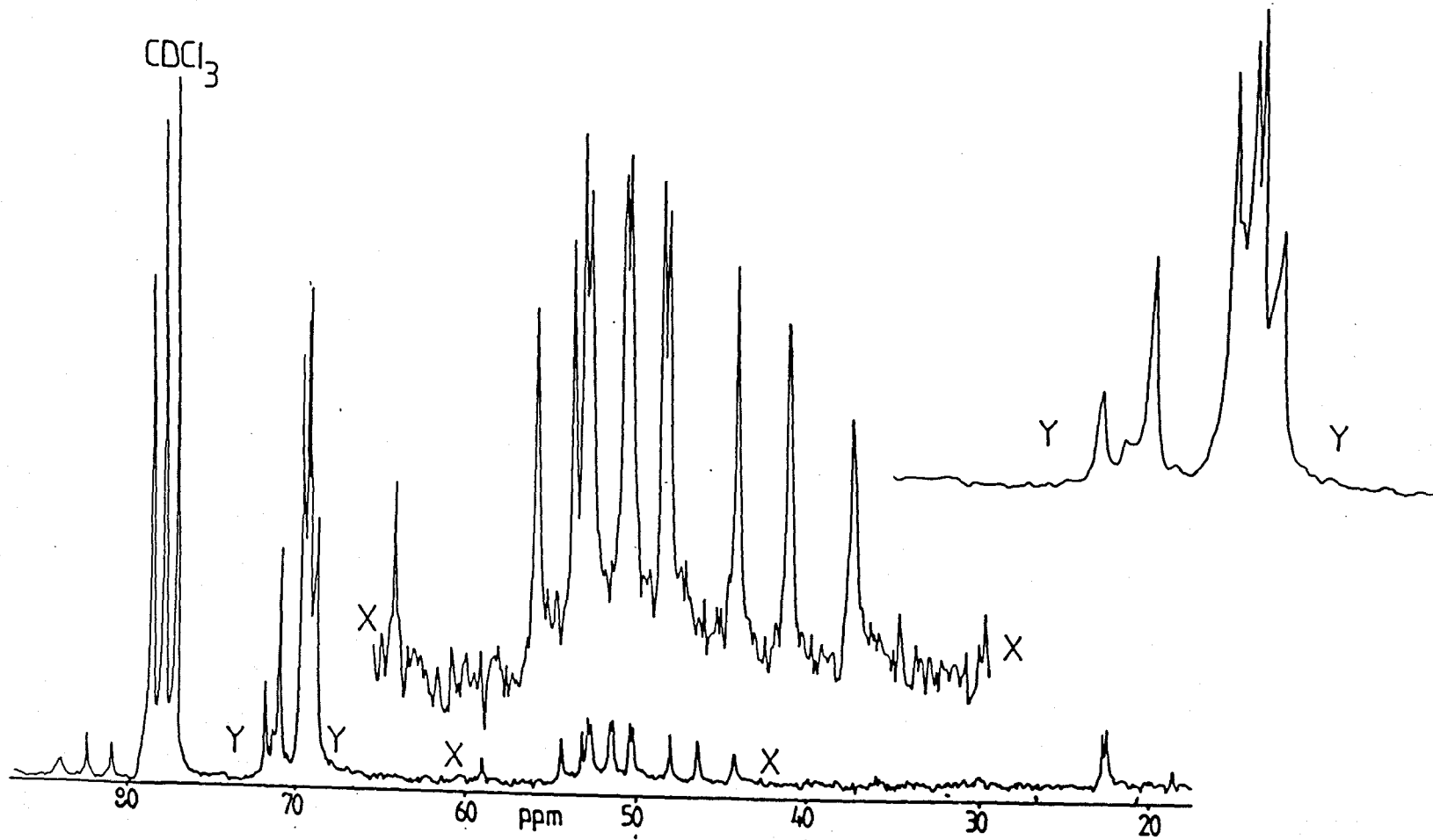
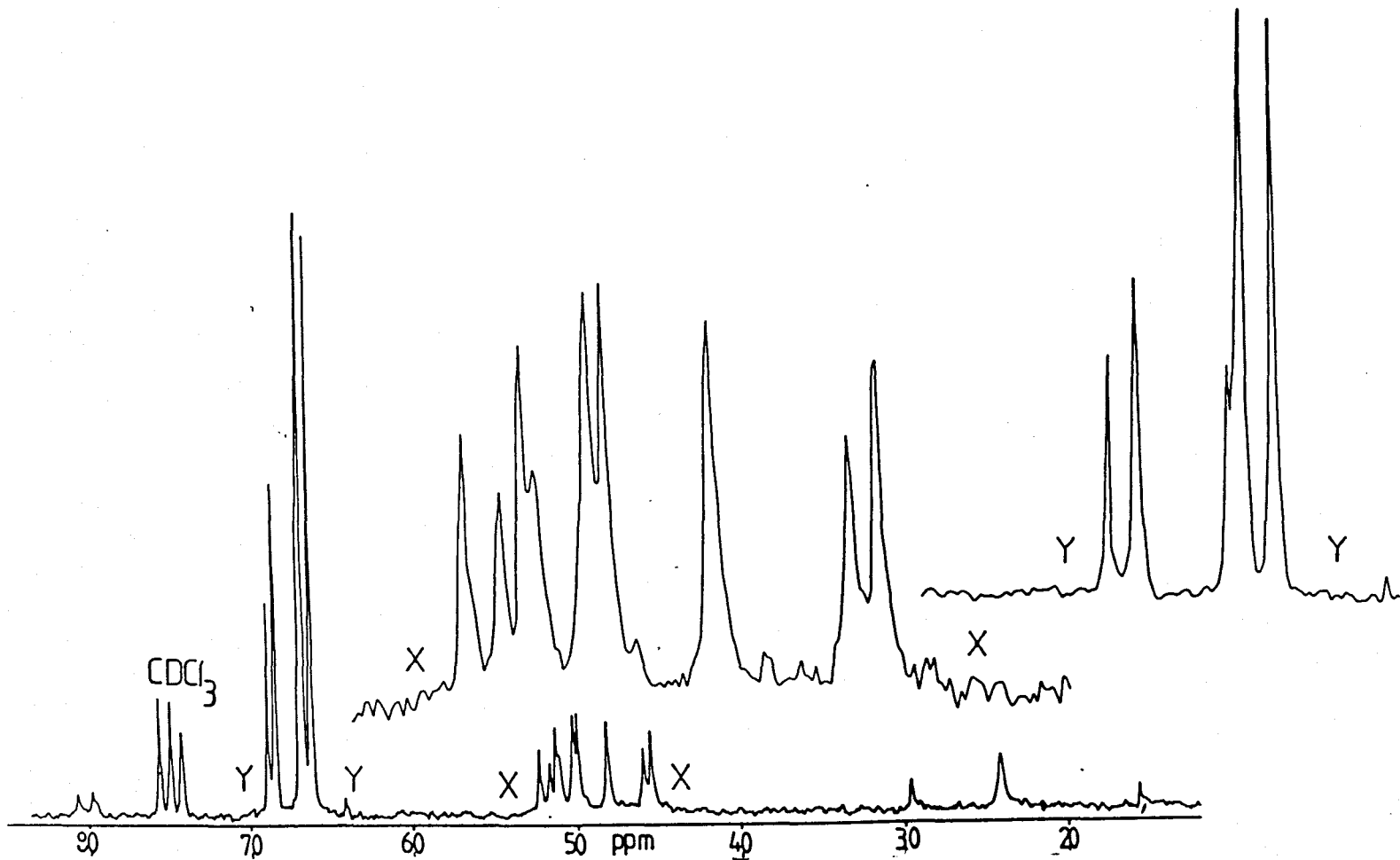
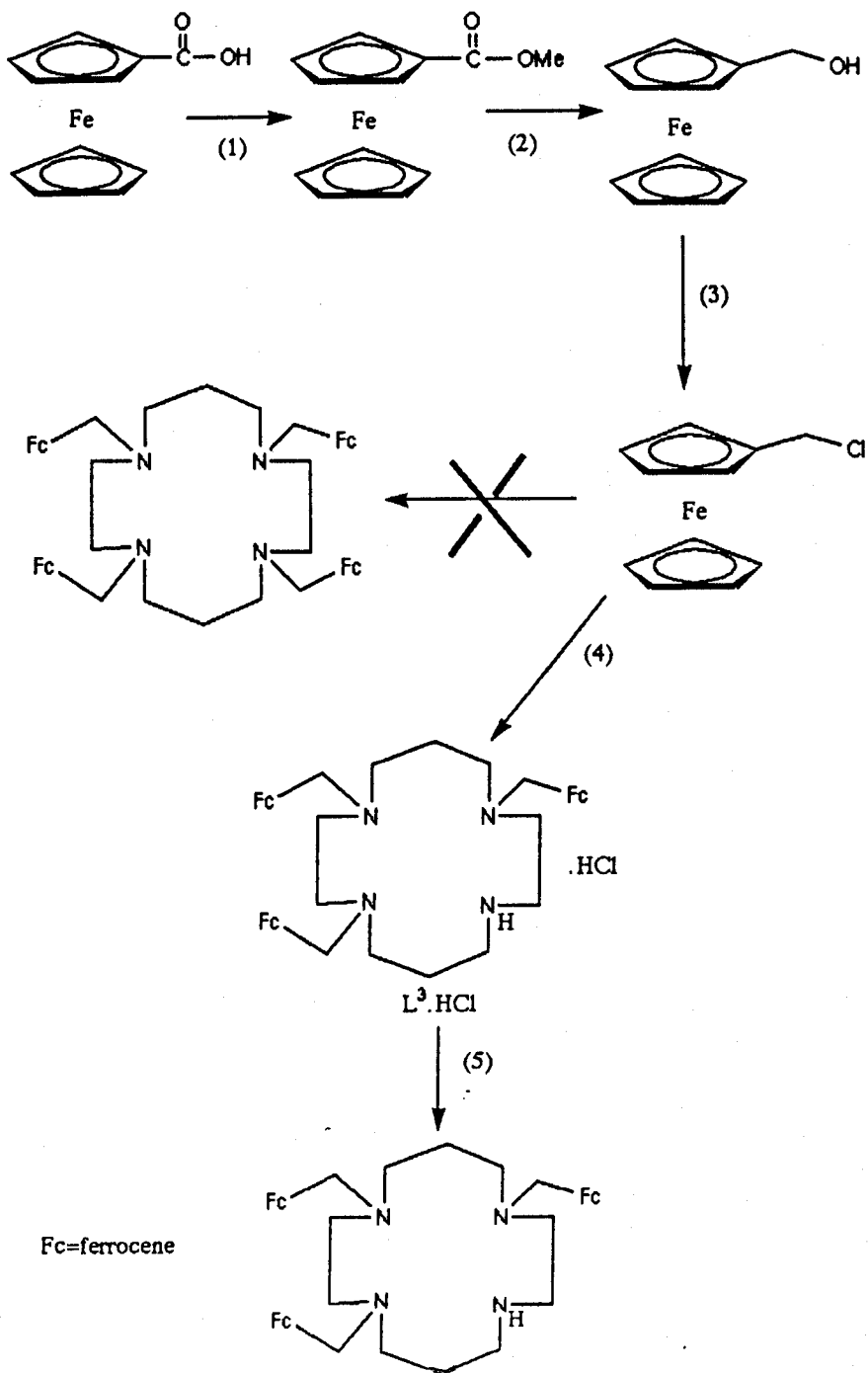


Figure 11.2(b)
 ^1H decoupled ^{13}C n.m.r spectrum of L^3 in CDCl_3 (ref Me_4Si $\delta = 0$). Y-Y = expansion of ferrocene carbons, X-X = expansion of cyclam N-(CH_2)-C carbons.





Scheme 2.2

(1) MeOH/H⁺ (2) LiAlH₄ (3) PCl₃ (4) Cyclam, Et₃N, CH₂Cl₂ (5) NaOH

Crystal structure of $L^3 \cdot HCl$

The crystal structure of $L^3 \cdot HCl$ is shown in Figures 12.2 (a)/(b). The structure clearly shows that the monohydrochloride of the functionalised macrocycle is produced. The unalkylated secondary nitrogen is protonated, with the proton forming a hydrogen bridge to a chloride ion [N(4)-H(4)-Cl(4)-166° ;H(4)-Cl(4)-1.975Å]. As indicated in the space fill diagram (Figure 12.2 (b)) two of the ferrocenes are on the same side of the macrocyclic ring, but at a distance apart of 7.473Å [Fe(1)-Fe(3)]. It appears from the space fill diagram that there is no reason why alkylation of the remaining secondary amino group should not have taken place. It also seems that steric hindrance is not the explanation for the failure of tetrasubstitution (Section 10.2).

Figure 12.2(a)

The geometry of $L^3.HCl$ showing atomic numbering

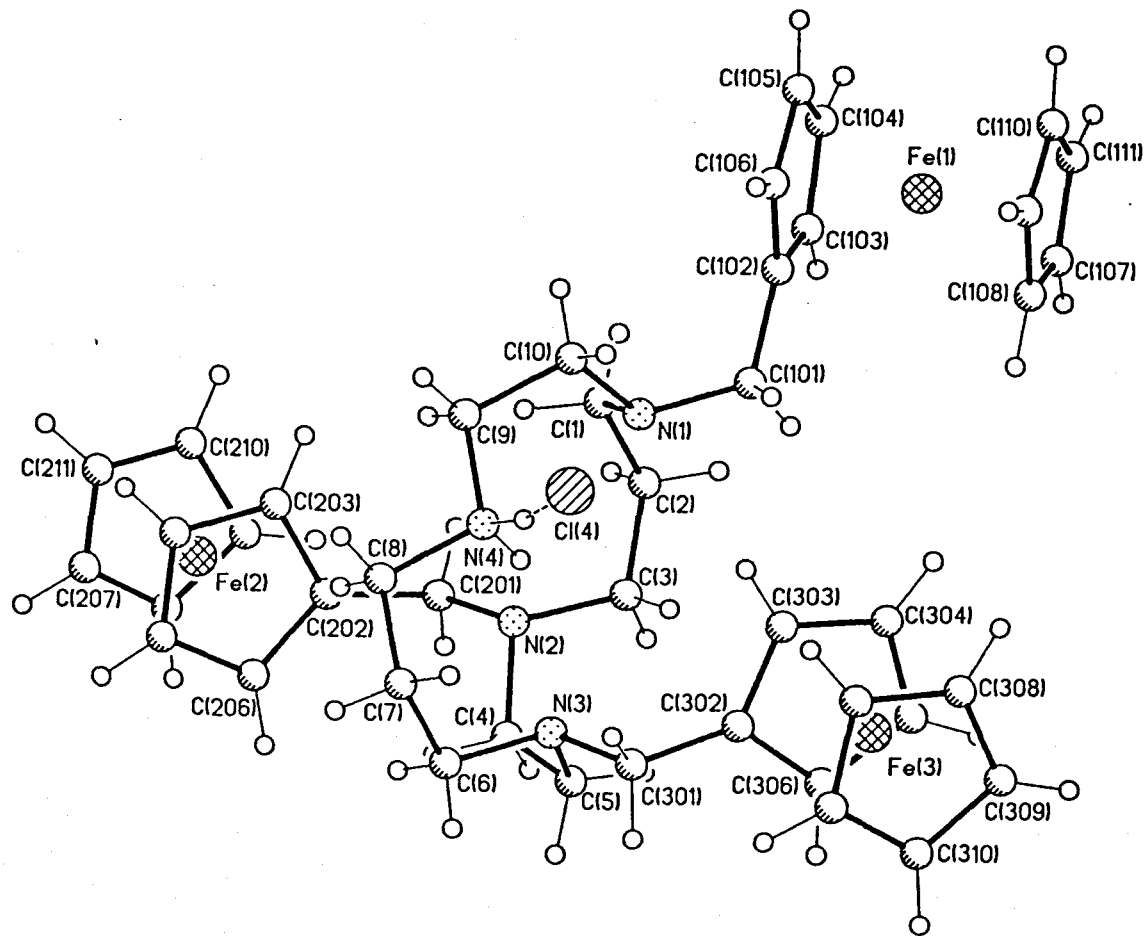


Figure 12.2(b)
Space fill diagram of $L^3.HCl$.

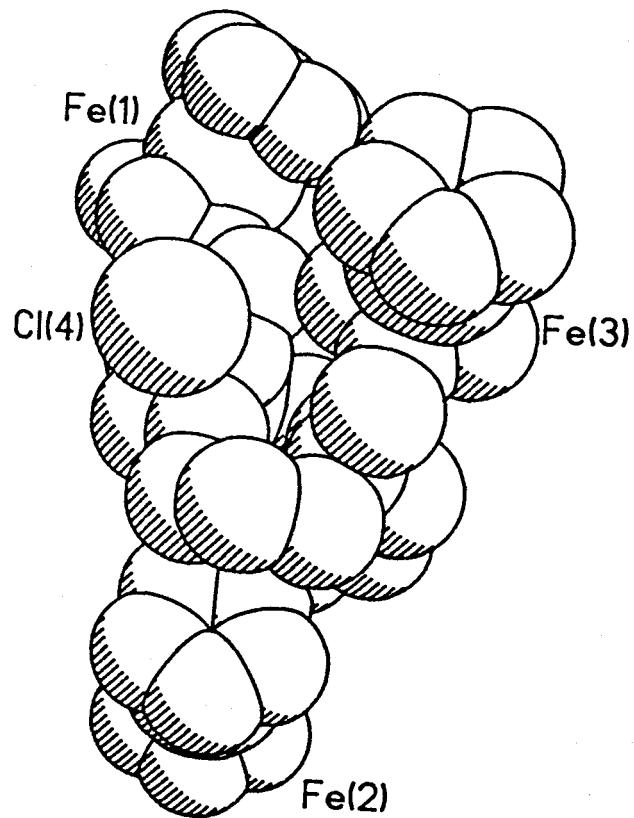


Table 7.2

Selected bond lengths of L³.HCl

Bond lengths (Å)

Fe(1)-C(102)	2.047 (12)	Fe(1)-C(103)	2.031 (12)
Fe(1)-C(104)	2.024 (14)	Fe(1)-C(105)	2.052 (15)
Fe(1)-C(106)	2.042 (11)	Fe(1)-C(107)	2.002 (16)
Fe(1)-C(108)	2.010 (26)	Fe(1)-C(109)	2.015 (15)
Fe(1)-C(110)	2.039 (16)	Fe(1)-C(111)	2.046 (14)
Fe(2)-C(202)	2.048 (12)	Fe(2)-C(203)	2.031 (13)
Fe(2)-C(204)	2.024 (14)	Fe(2)-C(205)	2.043 (18)
Fe(2)-C(206)	2.028 (16)	Fe(2)-C(207)	2.002 (24)
Fe(2)-C(208)	1.988 (21)	Fe(2)-C(209)	2.007 (22)
Fe(2)-C(210)	1.999 (25)	Fe(2)-C(211)	2.033 (20)
Fe(3)-C(302)	2.033 (11)	Fe(3)-C(303)	2.007 (14)
Fe(3)-C(304)	2.023 (17)	Fe(3)-C(305)	2.010 (13)
Fe(3)-C(306)	2.009 (12)	Fe(3)-C(307)	2.040 (16)
Fe(3)-C(308)	1.998 (24)	Fe(3)-C(309)	2.034 (20)
Fe(3)-C(310)	2.010 (22)	Fe(3)-C(311)	2.000 (17)
		N(1)-C(1)	1.469 (13)
N(1)-C(10)	1.452 (14)	N(1)-C(101)	1.456 (15)
N(2)-C(3)	1.503 (14)	N(2)-C(4)	1.491 (19)
N(2)-C(201)	1.496 (13)	N(3)-C(5)	1.466 (13)
N(3)-C(6)	1.488 (15)	N(3)-C(301)	1.468 (13)
N(4)-H(4C)	0.960	N(4)-H(4)	1.082 (105)
N(4)-C(8)	1.503 (16)	N(4)-C(9)	1.492 (20)

Selected bond angles of L³.HCl

C(1)-N(1)-C(101)	112.6(9)	C(1)-N(1)-C(10)	110.3(9)
C(3)-N(2)-C(4)	108.3(9)	C(10)-N(1)-C(101)	112.3(9)
C(4)-N(2)-C(201)	106.5(9)	C(3)-N(2)-C(201)	111.6(9)
C(5)-N(3)-C(301)	110.3(8)	C(5)-N(3)-C(6)	111.1(9)
C(6)-C(7)-C(8)	114.6(11)	C(6)-N(3)-C(301)	108.5(9)
C(8)-N(4)-C(9)	111.5(9)	C(1)-C(2)-C(3)	114.4(10)
N(4)-C(9)-C(10)	109.5(9)	N(4)-C(8)-C(7)	110.8(10)
N(3)-C(6)-C(7)	112.8(12)	N(3)-C(5)-C(4)	114.1(10)
N(2)-C(3)-C(2)	115.0(10)	N(2)-C(4)-C(5)	115.8(10)
		N(1)-C(10)-C(9)	111.5(11)

Section 10.2

Conclusions to synthesis

The reason for only the formation of the trisubstituted product $L^3.HCl$ becomes apparent when the side product of the reaction is examined. As discussed earlier, the bulkiness of the ferrocene does not appear to hinder the alkylation of the fourth nitrogen. Excess triethylamine is used in the preparation of $L^3.HCl$ to remove the HCl produced. This excess triethylamine can react with the chloromethylferrocene to form the quaternary ammonium ferrocene salt L^b . Similar salts are known, but are usually synthesised by the reaction of the corresponding aminoferrocene and an alkylhalide¹⁰⁴. Both 1H and ^{13}C n.m.r (Tables 1.2, 2.2) confirm the existence of the Et_3N group. Interestingly the ^{13}C n.m.r spectrum indicates that some of the methyl and methylene groups are inequivalent; the reason for this is unclear considering the symmetric nature of the Et_3N unit. The F.A.B mass spectrum (Table 5.2) contains a cluster of peaks corresponding to the $Fc-[CH_2]-NEt_3^+$ unit. Initially the counter ion was thought to be chloride, as this would be the side product of the reaction. However, a single crystal X-ray structure determination confirmed that $[Fe_2OCl_8]^{2-}$ as the counter anion (Section 11.2). The $[Fe_2OCl_8]^{2-}$ has been reported previously; it is usually produced during the reaction of ferrocene and iron(III) chloride¹¹⁵, but has also been characterised as a side product in the preparation of *mer* $[Fe(phen)Cl_3.DMF]^{116}$.

Section 11.2

Crystal structure of $2L^b Fe_2 OCl_8$

The structure of L^b is shown in Figure 13.2. The Fe(III)-Cl bond lengths (2.195-2.216Å) agree well with other published values¹¹⁵⁻¹¹⁷. The Fe-O-Fe bond angle of 169.8° is slightly larger than that in previous $[Fe_2OCl_8]$ complexes (161.6° ¹¹⁶ 155.6° ¹¹⁷ 162.4° ¹¹⁵). All other bond lengths and angles agree with expected values.

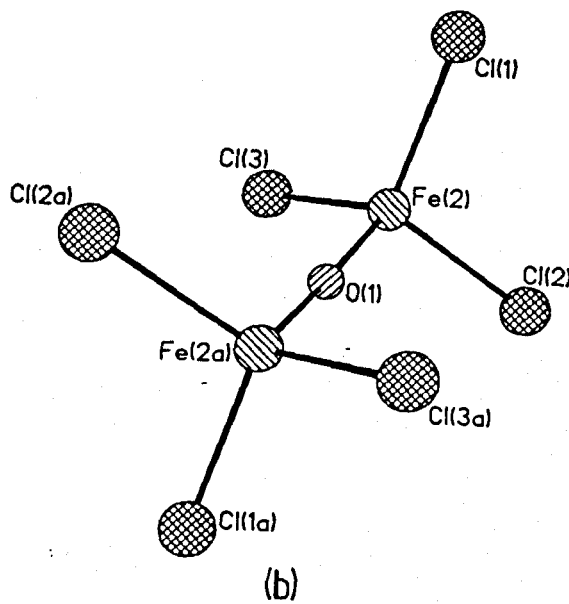
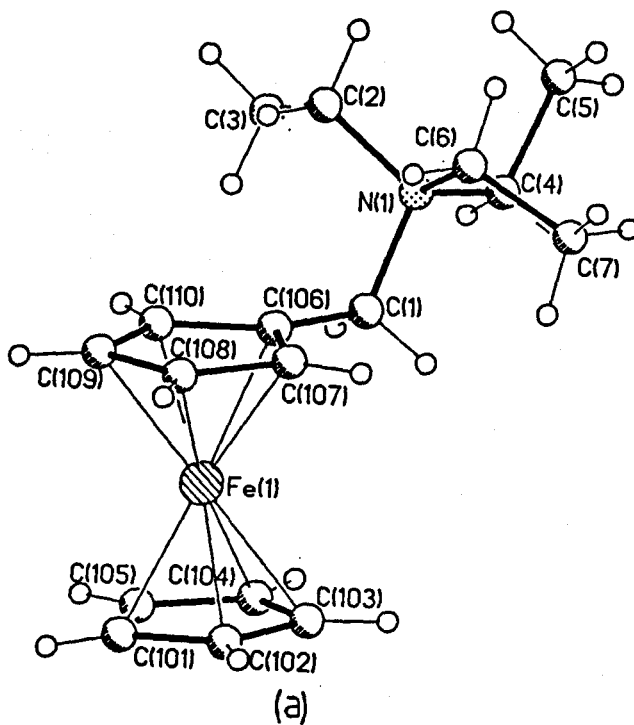


Figure 13.2

The crystal, structures of (a) $\text{Fc-}[\text{CH}_2]\text{-NEt}_3^+$ (b) $[\text{Fe}_2\text{OCl}_6]^{2-}$.

Table 8.2
Bond Lengths

Bond lengths (Å)			
Fe(1)-C(101)	2.014(14)	Fe(1)-C(102)	2.011(9)
Fe(1)-C(103)	2.023(11)	Fe(1)-C(104)	2.021(14)
Fe(1)-C(105)	2.034(9)	Fe(1)-C(106)	2.024(6)
Fe(1)-C(107)	2.010(7)	Fe(1)-C(108)	2.025(13)
Fe(1)-C(109)	2.029(10)	Fe(1)-C(110)	2.027(8)
Fe(2)-Cl(1)	2.216(3)	Fe(2)-Cl(2)	2.212(3)
Fe(2)-Cl(3)	2.195(3)	Fe(2)-O(1)	1.658(2)
Fe(2)-O(1a)	1.808(2)	O(1)-Fe(2a)	1.808(2)
O(1)-O(1a)	0.342	N(1)-C(1)	1.532(7)
N(1)-C(2)	1.514(8)	N(1)-C(4)	1.503(11)
N(1)-C(6)	1.522(7)	C(101)-C(102)	1.368(18)
C(101)-C(105)	1.420(19)	C(102)-C(103)	1.362(20)
C(103)-C(104)	1.338(17)	C(104)-C(105)	1.375(20)
C(106)-C(107)	1.414(9)	C(106)-C(110)	1.401(12)
C(106)-C(1)	1.480(11)	C(107)-C(108)	1.400(18)
C(108)-C(109)	1.399(16)	C(109)-C(110)	1.383(15)
C(2)-C(3)	1.495(9)	C(4)-C(5)	1.523(10)
C(6)-C(7)	1.508(10)		

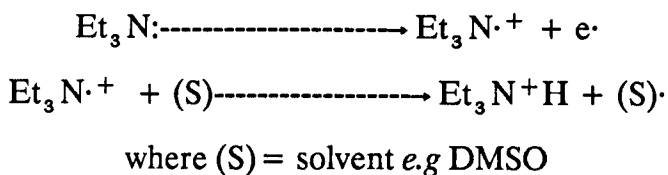
Bond Angles

Bond angles (deg.)			
C(101)-Fe(1)-C(102)	39.7(5)	C(101)-Fe(1)-C(103)	66.1(5)
C(102)-Fe(1)-C(103)	39.5(6)	C(101)-Fe(1)-C(104)	66.7(5)
C(102)-Fe(1)-C(104)	66.3(5)	C(103)-Fe(1)-C(104)	38.6(5)
C(101)-Fe(1)-C(105)	41.1(5)	C(102)-Fe(1)-C(105)	67.8(5)
C(103)-Fe(1)-C(105)	66.4(5)	C(104)-Fe(1)-C(105)	39.6(6)
C(101)-Fe(1)-C(106)	172.9(4)	C(102)-Fe(1)-C(106)	146.2(5)
C(103)-Fe(1)-C(106)	116.3(4)	C(104)-Fe(1)-C(106)	110.6(4)
C(105)-Fe(1)-C(106)	132.8(4)	C(101)-Fe(1)-C(107)	145.7(5)
C(102)-Fe(1)-C(107)	113.5(4)	C(103)-Fe(1)-C(107)	107.9(4)
C(104)-Fe(1)-C(107)	130.9(5)	C(105)-Fe(1)-C(107)	170.0(5)
C(106)-Fe(1)-C(107)	41.0(3)	C(101)-Fe(1)-C(108)	115.8(5)
C(102)-Fe(1)-C(108)	107.8(5)	C(103)-Fe(1)-C(108)	130.5(5)
C(104)-Fe(1)-C(108)	168.3(5)	C(105)-Fe(1)-C(108)	149.3(6)
C(106)-Fe(1)-C(108)	68.2(4)	C(107)-Fe(1)-C(108)	40.6(5)
C(101)-Fe(1)-C(109)	111.2(5)	C(102)-Fe(1)-C(109)	132.0(6)
C(103)-Fe(1)-C(109)	169.5(5)	C(104)-Fe(1)-C(109)	151.0(5)
C(105)-Fe(1)-C(109)	118.9(5)	C(106)-Fe(1)-C(109)	67.7(4)
C(107)-Fe(1)-C(109)	68.2(4)	C(108)-Fe(1)-C(109)	40.4(5)
C(101)-Fe(1)-C(110)	134.3(4)	C(102)-Fe(1)-C(110)	171.3(6)
C(103)-Fe(1)-C(110)	149.1(5)	C(104)-Fe(1)-C(110)	119.5(4)
C(105)-Fe(1)-C(110)	111.8(4)	C(106)-Fe(1)-C(110)	40.5(3)
C(107)-Fe(1)-C(110)	68.5(3)	C(108)-Fe(1)-C(110)	67.8(4)
C(109)-Fe(1)-C(110)	39.9(4)	Cl(1)-Fe(2)-Cl(2)	109.8(1)
Cl(1)-Fe(2)-Cl(3)	107.3(1)	Cl(2)-Fe(2)-Cl(3)	109.1(1)
Cl(1)-Fe(2)-O(1)	116.1(1)	Cl(2)-Fe(2)-O(1)	107.0(1)
Cl(3)-Fe(2)-O(1)	107.4(1)	Cl(1)-Fe(2)-O(1a)	106.0(1)
Cl(2)-Fe(2)-O(1a)	110.8(1)	Cl(3)-Fe(2)-O(1a)	113.7(1)
O(1)-Fe(2)-O(1a)	10.2(1)	Fe(2)-O(1)-Fe(2a)	169.8(1)
Fe(2)-O(1)-O(1a)	110.7(1)	Fe(2a)-O(1)-O(1a)	59.1(1)
C(1)-N(1)-C(2)	110.5(5)	C(1)-N(1)-C(4)	106.5(5)
C(2)-N(1)-C(4)	112.6(5)	C(1)-N(1)-C(6)	110.0(4)
C(2)-N(1)-C(6)	106.4(5)	C(4)-N(1)-C(6)	111.0(5)

Tables showing bond lengths and angles for $2L^b\text{Fe}_2\text{OCl}_6$

Electrochemistry of $L^3.HCl$ and L^3

Selected cyclic voltammograms of the macrocycle $L^3.HCl$ are shown in Figure 14.2. At fast scan rates (100mV/s) only one anodic peak is observed, whilst at slower scan rates (50mV/s-10mV/s) two are evident. This is attributed to protonation of tertiary amines, by protons produced during oxidation. Tertiary amines such as triethylamine form ammonium salts when oxidised in DMSO (Scheme 2.2).¹¹⁸



Scheme 2.2

This behaviour was also observed with the unprotonated ligand L^3 (Figure 15.2(a),(b)), where on the second scan a second anodic peak is observed. The protonation problem is removed by stirring the solution well after each scan, which removes any protonated product from the electrode surface. Interestingly, after the first scan, another couple is observed at a lower potential (Figure 15.2 (i)). This is attributed to a breakdown product of the species forming the main peak, because cycling in the region 0–400mV (*i.e.* not cycling through the main peaks), causes no wave at $E_{1/2} = 94\text{mV}$ vs S.C.E to be produced. By holding the potential at +800mV, enough of this side product could be generated to study its electrochemistry (Figure 16.2). The side product has fairly good reversible electrochemistry ($i_p \propto \text{scan rate}^{1/2}$, $i_{pa}/i_{pc} = 0.95$, $\Delta E_p = 98\text{mV}$). No other detailed study of this product was attempted.

In the sensing of metal ions L^3 has interesting prospects, for on titration of zinc(II), a shift to a more positive potential of 42mV in the $E_{1/2}$ value is observed (Figure 15.2(c)). Thus binding of the zinc(II) to the macrocycle perturbs the ferrocene moiety, and makes oxidation/reduction more difficult. To ensure this was not a spurious effect, the unligated ferrocene/ferrocenium couple

in the presence and absence of zinc(II) was studied using cyclic voltammetry. No real effect on the $E_{1/2}$ value ($< 5\text{mV}$) was observed on adding zinc(II).

With L^3 even though the observed shift of 42mV is not large when compared to that reported for the oxygen macrocyclic systems used for sensing alkali and alkaline earth metals [e.g. $\Delta E_{1/2}$ 90mV (Na^+)⁹⁹, 110mV (Mg^{2+})⁹⁹, 170mV (Na^+)⁹⁴], it does show potential for transition metal ion sensing. Addition of other transition metals such as Cu^{2+} , Ni^{2+} , also caused comparable shifts in the $E_{1/2}$ values, and results are summarised below:-

Electrochemistry Results^(a)

Metal ion	$\Delta E_{1/2}$ (mV)
Zn^{2+} (b)	42
Cu^{2+} (c)	60
Ni^{2+} (d)	55

(a) = 100mV/s , Pt electrode, vs S.C.E in DMSO, 0.2M TBAP. (b) conc = 2.1mM . (c) conc = 2.0mM . (d) conc = 2.2mM .

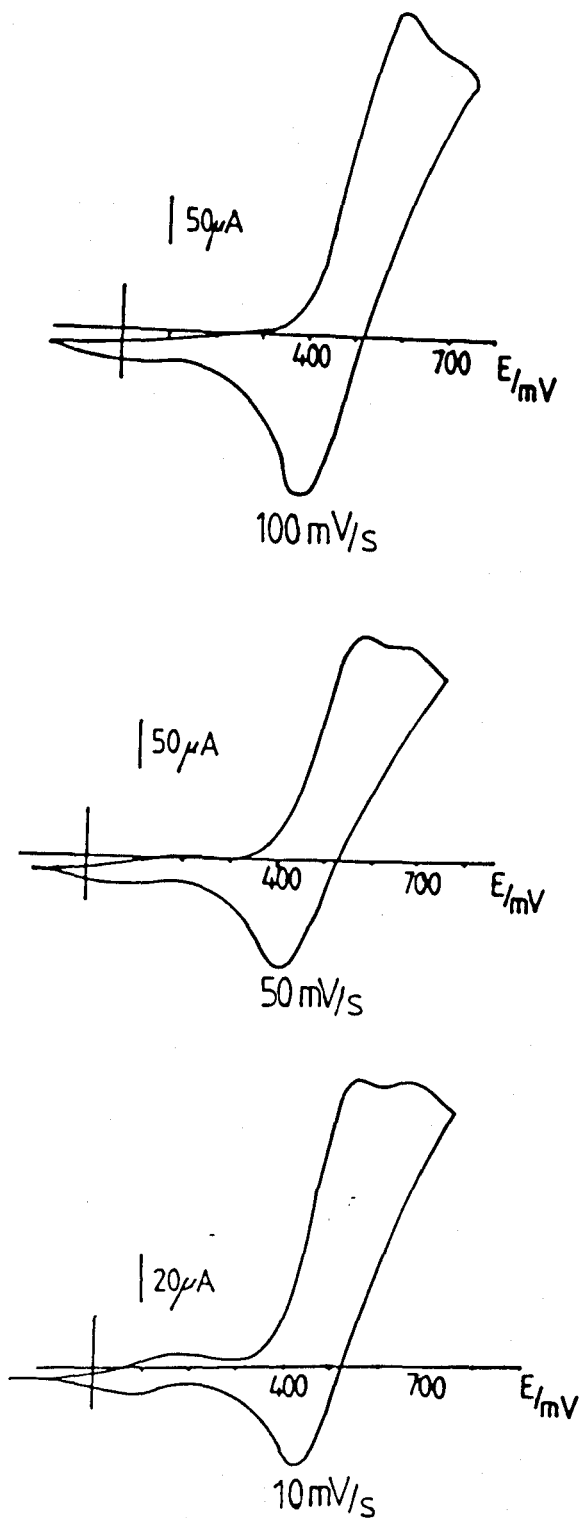


Figure 14.2

The electrochemistry of $L^3 \cdot HCl$ (4.8mM) in DMSO, 0.2M Tetrabutylammonium perchlorate background, Pt electrode, vs S.C.E. $E_{1/2}(\dagger) = 494mV$.
 (\dagger) = first peak only

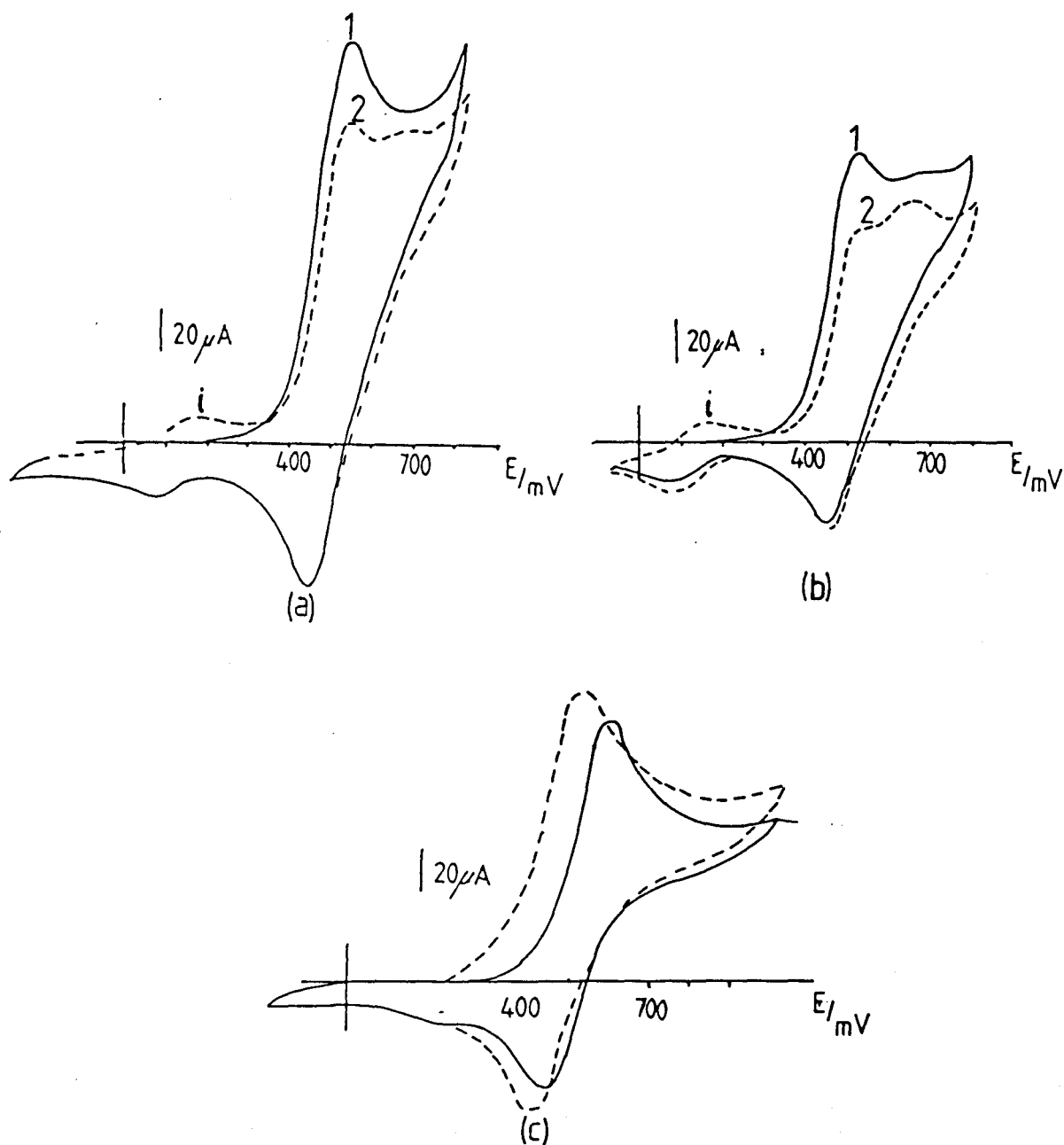


Figure 15.2

The electrochemistry of L^3 (2.1mM), in DMSO, 0.2M Tetrabutylammonium perchlorate background, Pt electrode, vs S.C.E. (a) 100mV/s (b) 50mV/s; (1) = scan 1, (2) = scan2, (i) = breakdown product (c) 100mV/s, cleaned electrode, solid line zinc(II) complex, dashed line free ligand.

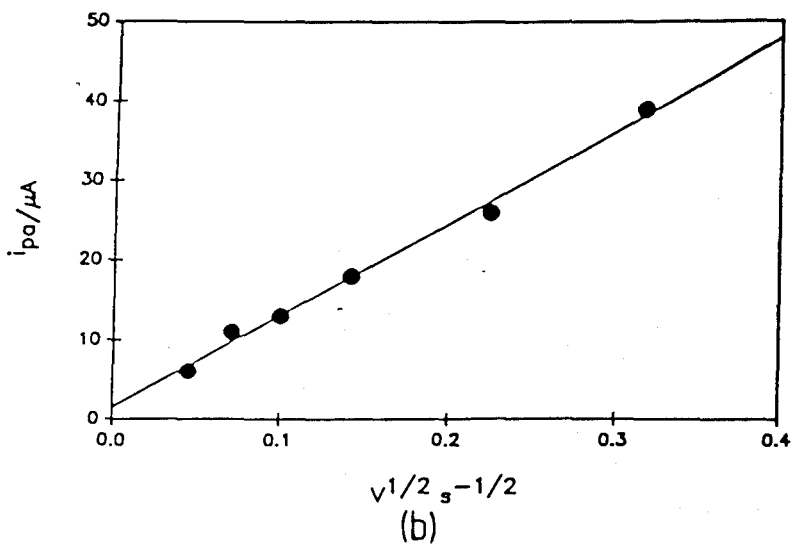
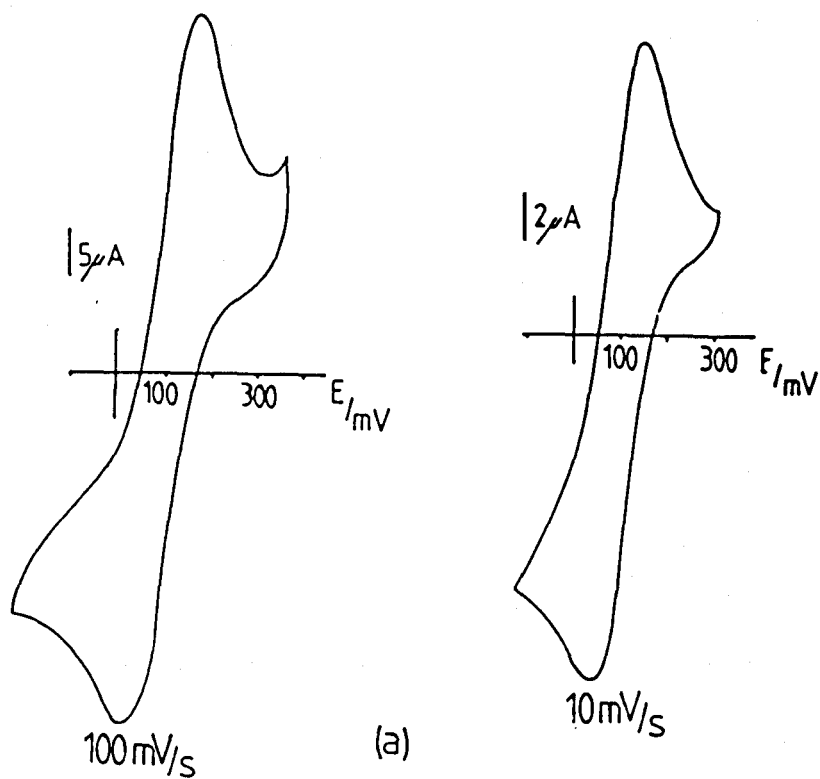


Figure 16.2

(a) The electrochemistry of the breakdown product from L^3 . $E_{1/2} = 94\text{mV}$. (b) A plot of peak current (i_{pc}) against the square root of scan rate.
Section 13.2

Conclusions

The macrocycles L^1 and L^3 show a certain potential for the sensing of transition metal ions; the former by the increase in the cathodic current, whilst the latter by the shift in the half wave potential. However, the main problems are:-

1: **No selectivity-** Both L^1 and L^3 give similar results with a range of transition metal ions (*e.g* Zn^{2+} , Cu^{2+} , Ni^{2+}). Thus a size/match selectivity needs to be introduced.

2: **Effect not large enough-** The shift of 42mV in the half wave potential for L^3 needs to be increased, so that sensitivity is increased. Therefore, macrocycles with the ferrocene moiety forming part of the macrocyclic ring need to be synthesised. Hopefully, the bound metal ion and ferrocene centre will be in close proximity, and so interact (Chapter 3).

CYCLAM PROTONS

	C-CH ₂ -C	NH	C-CH ₂ -N
	1.15(m,2H)	1.80(br,1H)	{2.70(m),2.85(m),2.95(m)}-10H
L ¹	1.25(m,2H)	1.90(br,2H)	3.70(m,6H)
	1.30(br,2H)		3.70(br,16H)
L ²	2.15(br,2H)		

CYCLAM PROTONS

	1.24(br,2H), 1.67(br,4H), 2.24(br,6H)
L ³ .HCl	2.82(br,4H), 3.44(br,4H)

TRIETHYLAMINE PROTONS

	CH ₃ -C-N	C-(CH ₂)-N
2.L ^b	1.40(t,9H)	3.35(q,6H)
Fe ₂ OCl ₆		

FERROCENE PROTONS

Cp	Cp-C=O
4.2(s,5H)	4.3(d,2H)
4.30(s,20H)	4.40(s,8H)
	4.80(br,8H)

FERROCENE + Fc-CH₂-N-PROTONS

{4.04,4.06,4.08,4.10,4.12,4.14,4.19}-42H

FERROCENE PROTONS

Cp	Cp-C=O
4.35(s,7H)(*)	4.40(s,2H)
	4.60(s,2H)

Table 1.2

¹H n.m.r data for ligands shown, in CDCl₃ (ref Me₄Si delta = 0). All recorded at 298K. (*) = accidental equivalence of Fc-(CH₂)-N protons. Cp = cyclopentadiene

	CYCLAM REGION		FERROCENE REGION			
	C-(CH ₂)-C	C-(CH ₂)-N	Cp	Cp-C=O	ipso	C=O
L ^{1a}	23.92(*) 25.57(1C) 26.61(*) 27.94(1C)	45.52(1C),45.62(2C),47.25(2C) 47.76(*),48.63(2C),49.05(2C) 49.82(*),51.24(*),52.53(*)	70.86(5C)	71.72(2C) 71.83(2C) 76.66(*)	76.33(3C) 77.21(*)	175.04(1C) 176.42(*)
L ^{1b}	23.88(*) 25.56(1C) 26.66(*) 28.01(1C)	45.63(2C),47.04(1C),47.32(1C),47.84(*) 48.66(1C),48.91(1C),49.08(1C) 49.55(1C),51.34(*),52.55(*),54.01(*)	70.82 71.66 73.69		76.72(1C)	174.80(1C)
L ^{2c}	29.60(2C)	47.05(8C)	69.90(20C)	70.09(8C) 70.35(8C)	ipso buried	171.62(4C)
L ^{2d}	27.40(1C) 29.62(1C)	46.19(2C),46.57(2C) 46.92(2C),48.42(2C)	69.64(10C) 69.55(10C)	70.10(4C) 70.17(4C) 70.67(4C) 70.98(4C)		171.41(2C) 172.03(2C)

Table 2.2

¹H decoupled ¹³C n.m.r data in CDCl₃ (ref Me₄Si delta = 0) unless otherwise stated. Number of carbons in parentheses. a = D₂O ref dioxan = 67.4, 300K. b = D₂O ref dioxan delta = 67.4, 323K. c = 298K, d = 233k, * = minor species

CYCLAM REGION				FERROCENE REGION		
	C-(CH ₂)-C	C-(CH ₂)-N + N-(CH ₂)-Fc		Cp	ipso	Cp-C=O
L ³ .HCl	18.44(3C)* 22.26(1C) 22.49(1)	43.63(1C),45.73(1C),47.34(1C) 49.54(1C),48.74(1C),50.76(1C) 50.93(1C),52.01(1C),52.21(1C) 52.57(1C),53.75(1C),58.32(2C)*		68.45(5C) 68.61(5C) 68.91(5C)	80.06(1C) 81.53(1C) 83.11(1C)	68.09,68.22,68.78 69.80,70.19,71.05 71.05
L ³	15.29(3C) 24.20(1C) 29.72(1C)	46.22(2C),46.72(1C),49.12(2C) 50.93(2C),51.22(1C),52.34(1C) 52.70(1C),53.39(1C)		67.89(5C) 68.42(5C) 68.52(5C)	82.03(1C) 82.98(2C)	68.65,70.22,70.72
TRIETHYLAMINE CARBONS				FERROCENE CARBONS		
	CH ₃ -C-N	C-(CH ₂)-N	-(CH ₂)-Fc	Cp		Cp-C=O
2.L ^b Fe ₂ OCL ₆	{8.88,9.11}-3C	{46.13,52.47}-3C	60.16(1C)	70.26(5C)		70.6 2(2C),71.74(2C)

Table 2.2(cont'd)

¹H decoupled ¹³C n.m.r data for compounds shown, in CDCl₃ (ref Me₄Si delta = 0).* = trace of diethylether present.

	Formula	%C	%H	%N
L ²	(C ₂₁ H ₅₆ N ₄ Fe ₄ O ₄) ^a	61.36(61.58)	5.38(5.49)	5.34(5.64)
L ¹	(C ₂₁ H ₃₂ N ₄ O ₁ Fe ₁) _x .CHCl ₃ ^b _{x = 7/8}	50.84(50.57)	6.41(6.72)	10.84(10.73)
	(C ₂₁ H ₃₂ N ₄ O ₁ Fe ₁) _x .CHCl ₃ _{x = 1}	49.69(50.57)	6.26(6.72)	10.54(10.73)
	(C ₂₁ H ₃₂ N ₄ O ₁ Fe ₁) _x .CHCl ₃ _{x = 3/4}	52.04(50.57)	6.58(6.72)	11.16(10.73)
	(C ₂₁ H ₃₂ N ₄ O ₁ Fe ₁) _x .CHCl ₃ _{x = 8/9}	50.70(50.57)	6.39(6.72)	10.81(10.73)
	(C ₂₁ H ₃₂ N ₄ O ₁ Fe ₁) _x .CHCl ₃ _{x = 6/7}	51.00(50.57)	6.43(6.72)	10.89(10.73)
	(C ₂₁ H ₃₂ N ₄ O ₁ Fe ₁) _x .CHCl ₃ _{x = 9/10}	50.60(50.57)	6.38(6.72)	10.78(10.73)

Table 3.2

Combustion analysis results. (a) = bulk sample, before being used to grow crystals for x-ray study. (b) = sample unsuitable for X-ray analysis, but crystallised with chloroform; either $x = 7/8, 9/10$. Found values in parentheses

Table 4.2

	Crystal data for compounds of Chapter 2 L^2	$L^3 \cdot HCl$	$2 L^b Fe_2 OCl_6$
Formula	$C_{54}H_{56}N_4Fe_4O_{4.4}CHCl_3$	$C_{43}H_{55}ClFe_3N_{4.3}CHCl_3$	$C_{34}H_{52}N_2Fe_4OCl_6$
RMM	1526.0	1189.1	940.876
System	Monoclinic	Triclinic	Monoclinic
Space group	$P2_1/n$	$P\bar{1}$	$P2_1/n$
Systematic	$h,k,0;k=2n+1$	none	$h,k,0;k=2n+1$
Absences	$0,0,l;l=2n+1$		$0,0,l;l=2n+1$
$a/(\text{\AA})$	18.649(12)	10.559(5)	13.554(8)
$b/(\text{\AA})$	8.058(5)	11.846(5)	9.273(8)
$c/(\text{\AA})$	22.217(13)	23.215(12)	17.10(1)
$\alpha/^\circ$	\	83.9(84)	\
$\beta/^\circ$	110.06(4)	78.17(4)	99.72(5)
$\gamma/^\circ$	\	70.55(4)	\
$U/\text{\AA}^3$	3136(3)	2678(2)	2119(2)
D_c/gcm^{-3}	1.62	1.475	1.47
Z	2	2	2
$\mu(\text{Mo-K}\alpha)/\text{cm}^{-1}$	14.7	13.4	28.0
F(0000)	1552	1220	1292
Total Reflections			
$I/\sigma(I) \geq 3.0$	1287	4113	1547
2θ (max)	40	45	45
Range(2θ) about			
$K\alpha_1-K\alpha_2$	+0.50,-0.60	+0.55,-0.50	+0.50,-0.50
Speed(2θ) $^\circ \text{min}^{-1}$	3-29	4-29	2-29
Crystal Dimensions	0.1x0.1x0.1	0.1x0.1x0.1	0.71x0.16x0.29
Max/Min Transmission			
Factors	0.93, -0.89	0.84, -0.74	0.721/-0.67
Final R(R^1)	0.0870/0.0798	0.0877/0.0922	0.0413/0.0462
Weighting (g)	0.001302	0.001460	0.00066
Largest peak on ΔF map/ $e \text{\AA}^3$	+0.63/-0.57	+0.8/-0.6	+0.5/-0.4

[L¹ + H]⁺

m/z (calc)	m/z(found)
411-(6%)	411-(15%)
412-(2%)	412-(9%)
413-(100%)	413-(100%)
414-(28%)	414-(32%)
415-(4%)	415-(50%)
416-(< 1%)	416-(< 1%)

[L²]⁺

m/z (calc)	m/z (found)
1045-(1%)	1045-(16%)
1046-(24%)	1046-(26%)
1047-(17%)	1047-(91%)
1048-(100%)	1048-(100%)
1049-(69%)	1049-(46%)
1050-(27%)	1050-(17%)
1051-(7%)	1051-(/)

[L³ + H]⁺

m/z (calc)	m/z (found)
792-(< 1%)	792-(/)
793-(19%)	793-(/)
794-(10%)	794-(6%)
795-(100%)	795-(100%)
796-(57%)	796-(49%)
797-(17%)	797-(8%)
798-(4%)	798-(/)
799-(< 1%)	799-(7%)

[L^b]

m/z (calc)	m/z (found)
298-(6%)	298-(7%)
299-(1%)	299-(3%)
300-(100%)	300-(100%)
301-(22%)	301-(22%)
302-(3%)	302-(3%)
303-(< 1%)	303-(< 1%)

Table 5.2

Mass spectral data. Relative heights expressed as % of main peak in parentheses.

Spectra run in *m*-nitrobenzylalcohol matrix

Experimental

The experimental techniques and instrumentation are discussed in Chapter 7. 1,4,8,11-Tetraazacyclotetradecane (cyclam) was produced by a standard organic preparation.^{1 2 5} All spectra referenced to Me₄Si $\delta = 0$, unless stated otherwise. ¹³C n.m.r (CDCl₃): 29.52(2C), 49.45(4C), 50.76(4C). ¹H n.m.r (CDCl₃): 1.7(m, 4H), 2.2(br, NH, 4H), 2.7(t, 16H)

Solvents and Chemicals

All chemicals were obtained from Aldrich and used without further purification unless stated. The background electrolytes for electrochemistry were kindly supplied by Dr.P.N.Bartlett's group; these were already recrystallised and dried. Standard calomel electrodes were also supplied by them. Deuterated solvents 99.9% [²H] were used as supplied or dried over 4A molecular sieves before use. Dried A.R solvents were used to obtain U.V-visible spectra, as well as in electrochemical experiments. Milli"Q" quality water was used for electrochemical experiments, and all glassware was thoroughly soaked in Decon for 24 hours, washed with millipore water, and dried in an oven at 100° C. All standard solvents for reactions were dried by a literature method^{1 2 1} before use. Elemental analyses were carried out either by Medac or Butterworths. [Zn(DMSO)₄](ClO₄)₂ was produced by a standard literature method.^{1 2 2}

Preparation of Ferrocenecarboxylic acid (1) (Scheme 1.2)

A three necked flask (1dm³) was dried and charged with ferrocene (18.6g, 100mmol) and 2-chlorobenzoylchloride (17.5g, 100mmol) in CHCl₃ (200cm³). The solution was cooled to 0-5° C and AlCl₃ (14.0g, 100mmol) added in small portions to the stirring solution under nitrogen. The reaction was stirred for a further 30 minutes at 0-5° C, and 2 hours at room temperature. The mixture was cooled to ice temperature and H₂O (100cm³) was added slowly, and the two phase mixture stirred for 30 minutes. The two layers were separated, and the aqueous layer extracted with CH₂Cl₂ (2x50cm³). The combined CH₂Cl₂

portions were washed with H_2O (50cm^3) and 10%NaOH ($2 \times 50\text{cm}^3$), dried over MgSO_4 , and the solvent removed on a rotary evaporator to give a red oily liquid, which solidified (29g, crude 2-chlorobenzoylferrocene).

A three necked flask was dried, and 1,2-dimethoxyethane (250cm^3), KBu^tO (46.0g, 410mmol) added. The stirring mixture was put under nitrogen and H_2O (2.2cm^3) added. The crude 2-chlorobenzoylferrocene was added in portions. The mixture was refluxed for 1 hour, cooled, and added to H_2O (1dm^3). The aqueous solution was washed with Et_2O ($3 \times 150\text{cm}^3$), and the Et_2O layers combined and back extracted with 10%NaOH(aq) ($2 \times 50\text{cm}^3$). The aqueous layers were combined and acidified with HCl(conc), to precipitate ferrocenemonocarboxylic acid. The yellow solid was collected, air dried and recrystallised from toluene (14.36g, 62%yield). I.r (Nujol Mull) 1655cm^{-1} , (C=O stretch), mp $> 200^\circ\text{C}$, lit $\sim 220^\circ\text{C}^{119}$.

Preparation of Ferrocenoyl chloride (2) (Scheme 1.2)

Ferrocenemonocarboxylic acid (0.62g, 2.7mmol) was dissolved in dry CH_2Cl_2 (100cm^3). Oxalyl chloride (1.03g, 8.1mmol) in dry CH_2Cl_2 (10cm^3) was added over a period of 15 minutes, under nitrogen, with ice cooling. The mixture was stirred at room temperature for 1 hour, and refluxed for 25 minutes (50°C , oil bath temperature). The solvent was removed on a rotary evaporator to give an oily residue, which was extracted with boiling pentane ($3 \times 25\text{cm}^3$). The pentane was removed *in vacuo* to give a red solid (0.52g, 77% yield). I.r (Nujol Mull) 1755cm^{-1} , (C=O stretch), mp 55°C , lit 49.1°C^{120} .

Preparation of L^1

Ferrocenoyl chloride (0.25g, 1mmol) was dissolved in dry CHCl_3 (200cm^3), and added dropwise to a stirred solution of cyclam (2.5g, 12.5mmol) in dry CHCl_3 (50cm^3), under nitrogen. The mixture was stirred overnight, and the solvent then removed on a rotary evaporator. The residue was dissolved in CH_3CN (50cm^3) and the insoluble cyclam filtered off. The solvent was removed to give an oily red solid. Gravity chromatography on silica using $\text{MeOH}(3\%):\text{CHCl}_3(97\%)$ as

eluant gave a red solid, which was recrystallised from $\text{CH}_2\text{Cl}_2/\text{Et}_2\text{O}$ (1:1) to give a yellow solid (0.31g, 76% yield). Analytical data is shown in Tables 1.2-3.2/ 5.2.

Preparation of L^2

Ferrocenoyl chloride (1.06g, 4.23mmol) and cyclam (0.14g, 0.7mmol) were dissolved in dry CHCl_3 (50cm^3), under nitrogen, with Et_3N (0.3g, 2.9mmol) present. The mixture was stirred overnight, and washed with H_2O (10cm^3), dried over anhydrous MgSO_4 and the CHCl_3 removed on a rotary evaporator. Gravitational chromatography of the red oily residue, on silica, using $\text{MeOH}(2\%)/\text{CHCl}_3(98\%)$ as eluant gave an orange/yellow solid after solvent removal. The product was recrystallised from $\text{CHCl}_3/\text{Et}_2\text{O}$ (1:1) to give an orange solid (0.54g, 73% yield). Analytical data is in Tables 1.2-3.2/ 5.2. I.r (Nujol Mull) 1620cm^{-1} , (C=O stretch), U.V/visible (CH_2Cl_2) / $\epsilon_{\text{max}}(\text{mol}^{-1}\text{dm}^3\text{cm}^{-1})$, 446 (34), 340(sh, 54), 302 (164).

Preparation of Ferrocenemonomethyl ester

Ferrocenemonocarboxylic acid (2.0g, 8.7mmol) was dissolved in MeOH (50cm^3) with a few drops of H_2SO_4 (98%w/v). The mixture was refluxed for 4 hours, cooled, and CHCl_3 (50cm^3) added. The mixture was washed with H_2O (20cm^3), and the organic layer separated, dried over anhydrous MgSO_4 , and the solvent removed on a rotary evaporator, to give ferrocenemonomethyl ester (1.98g, 94% yield). ^1H n.m.r (CDCl_3): 3.9(s, 3H), 4.3(s, 5H), 4.5(s, 2H), 4.9(s, 2H). I.r(Nujol Mull): 1690cm^{-1} , (C=O stretch).

Preparation of Hydroxymethylferrocene

Ferrocenemonomethyl ester (1.98g, 8.1mmol) was dissolved in dry THF (50cm^3), and added dropwise to a stirred solution of LiAlH_4 (0.6g, 16mmol), in dry THF (30cm^3), under nitrogen. After addition the mixture was refluxed overnight, then cooled to ice temperature, and H_2O (20cm^3) added to destroy any remaining LiAlH_4 . The solution was filtered and the residue washed with CHCl_3 ($3 \times 50\text{cm}^3$). The combined CHCl_3 extracts were dried with anhydrous MgSO_4 , and the solvent then removed on a rotary evaporator to give an orange

solid, which was recrystallised from hexane to give hydroxymethylferrocene. (1.56g, 89% yield). I.r (Nujol Mull), loss of absorbance at 1690cm^{-1} . ^1H n.m.r (CDCl_3): 4.20(s, 7H), 4.29(br, 2H), 4.37(br, 2H). ^{13}C n.m.r (CDCl_3): 60.76(1C), 67.89(2C), 68.29(7C), 88.40(1C, ipso). E.I mass spectrum: m/z found 199, calc 199 $[\text{M-OH}]^+$.

Preparation of Chloromethylferrocene

Hydroxymethylferrocene (2.78g, 13mmol) was dissolved in dry benzene (40cm^3), containing pyridine (0.3cm^3) and cooled to $0-5^\circ\text{C}$. Freshly distilled PCl_3 (0.7g, 5mmol) in dry benzene (10cm^3) was added slowly, and the mixture stirred for 4 hours at room temperature. The solution was washed with NaHCO_3 (0.1M, 10cm^3), dried over CaCl_2 , and the solvent removed *in vacuo* at $0-5^\circ\text{C}$ to give chloromethylferrocene (2.35g, 77% yield). Due to the instability of the chloromethylferrocene it was used without immediately and without further purification. I.r (Nujol Mull): 1270, 1130, 1100, 1020cm^{-1} - changes in the fingerprint region.

Preparation of $\text{L}^3\cdot\text{HCl}$

Cyclam (0.16g, 0.83mmol) was dissolved in dry CH_2Cl_2 (100cm^3) with Et_3N (0.83g, 8.3mmol), and add dropwise to a stirring solution of chloromethylferrocene (1.94g, 8.3mmol), in dry CH_2Cl_2 (50cm^3). The mixture was stirred for 72 hours under nitrogen, and the solvent removed *in vacuo*. Gravitational chromatography on silica using $\text{MeOH}(2\%)/\text{CHCl}_3(98\%)$ as eluant removed any hydroxymethylferrocene produced. The desired product $\text{L}^3\cdot\text{HCl}$ was eluted using $\text{MeOH}(10\%)/\text{CHCl}_3(90\%)$, and after solvent removal and recrystallisation from $\text{CHCl}_3/\text{Et}_2\text{O}$ (1:1) gave an orange/red solid (0.38g, 55% yield). Analytical data is in Tables 1.2/ 2.2/ 5.2. Further eluting with MeOH gave the side product $2\text{L}^b\cdot\text{Fe}_2\text{OCl}_6$ (0.45g, 0.48mmol). Analytical data is in Tables 1.2/ 2.2/ 5.2.

Preparation of L³

L³.HCl (0.112g, 0.14mmol) was dissolved in MeOH (30cm³), with NaOH (0.060g, 0.14mmol), and stirred for 10 minutes. The solvent was removed, and the product taken up in CHCl₃ (50cm³), washed with H₂O (10cm³), dried over anhydrous MgSO₄, and the solvent removed on a rotary evaporator give an orange solid (0.09g, 84% yield). Analytical data is in Tables 1.2/ 2.2/ 5.2. U.V/visible (DMSO) / ϵ_{\max} (mol⁻¹ dm³ cm⁻¹): 432 (316).

Crystallography

For all three compounds data were collected with a Nicolet R3 four circle diffractometer using graphite monochromated Mo-K α radiation in the ω -2 θ mode. Reflections were scanned around K α_1 -K α_2 angles, with variable scan speeds depending on the intensity of the 2s pre scan; backgrounds were measured at each end of the scan of 0.25 of the scan time. All data were taken at 293K. Standard reflections were monitored every 200 reflections; in all cases a slight decrease occurred during data collection (4%-L², 5%-L³.HCl, 2.L^b.Fe₂OCl₆-0%), the data were rescaled to correct for this. Unit cell dimensions and standard deviations were obtained by least-squares fit to 15 reflections. Reflections with $I/\sigma(I) \geq 2.0$ were considered observed, and used in refinement, and corrected for Lorentz polarisation and absorption effects; the last by a Gaussian method. Heavy atoms were located by Patterson interpretation, and light atoms found on successive Fourier syntheses. Anisotropic temperature factors were used for all non-H atoms (except in the case of L² where carbons and nitrogens of macrocyclic ring were isotropic). Hydrogen atoms were placed in calculated positions (except for H atom bridging N(4)-Cl(4) in L³.HCl which was located), and given fixed isotropic temperature factors $U = 0.07 \text{ \AA}^2$. Methyl groups (only 2.L^b.Fe₂OCl₆) were treated as rigid CH₃ units with their initial orientations taken from the strongest H-atom peak on a difference Fourier synthesis. Final refinement was on F by least squares methods refining {306-L², 572-L³.HCl, 214-2.L^b.Fe₂OCl₆} parameters, including an isotropic extinction parameter. A weighting scheme of the form $W = 1/[\sigma^2(F) + g(F^2)]$ (for g values see Table 4.2) were used and found to be satisfactory by a weight analysis. Computing was with SHELXTL PLUS^{1 2 3} on a DEC Microvax II with scattering factors in the analytical form and anomalous dispersion factors taken from International Tables^{1 2 4}. All crystals were mounted on a fine quartz fibre using epoxy resin, then held in a grub screw. Specific data for each crystal is shown in Table 4.2.

Compound L²

Crystals potentially suitable for X-ray diffraction were obtained from a slow evaporation of a saturated chloroform solution, which gave thin red needles. All of the crystals obtained were twinned, but by careful cutting, a single crystal was obtained. The smallness of the crystal and weak diffracting ability, meant that data collection was slow, and maximum 2θ was only 40° . Selected bond lengths and angles are in Table 6.2. All bond lengths and angles plus atomic co-ordinates are in Appendix I.

Compound L³.HCl

Crystals suitable for X-ray diffraction were obtained from a slow evaporation of a saturated chloroform solution, which gave red needles. Selected bond lengths and angles are in Table 7.2. All bond lengths and angles, plus atomic co-ordinates are in Appendix I.

Compound 2.L^b.Fe₂OCl₆

Crystals suitable for X-Ray study were obtained by slow evaporation of a saturated chloroform solution into diethylether (~ 1:4), and gave clumps of red crystals. By careful cutting red diamond shaped crystals were obtained. Bond lengths and angles are in Table 8.2. Atomic co-ordinates are in Appendix I.

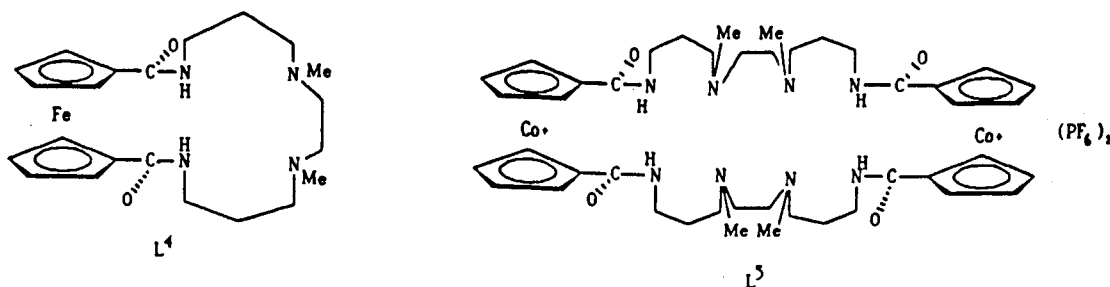
CHAPTER 3

The synthesis and electrochemistry of further redox active macrocycles

Section 1.3

Introduction

Towards the end of Chapter 2 (Section 13.2), the synthesis of ligands with redox active centres in the macrocyclic ring was discussed. This chapter discusses the synthesis of two such ligands L^4 and L^5 , and their electrochemical properties. The two ligands were prepared by a high dilution technique.



Dioxo-tetraazamacrocycles such as 5,7-dioxo-1,4,8,11-tetraazacyclotetradecane have interesting properties. Firstly, co-ordination to Ni^{2+} and Cu^{2+} causes deprotonation of the two amido protons to form neutral complexes. Also dissociation is relatively fast, when compared to tetra-amine complexes. Finally, Ni^{2+} and Cu^{2+} complexes can be oxidised to form stable trivalent complexes.^{1 2 9} With this in mind, complexes of L^4 with Cu^{2+} , Ni^{2+} , Zn^{2+} have been synthesised and characterised by ^{13}C n.m.r, F.A.B mass spectrometry, and U.V/visible spectrometry (Section 4.3).

Results and Discussion

Section 2.3

Synthesis of L⁴

The synthetic route to L⁴ is outlined in Scheme 1.3. 1,1'-Ferrocenedicarboxylic acid is readily obtained by the oxidation of 1,1'-Diacetylferrocene with sodium hypobromide in dioxan/water, keeping the temperature below 5°C.^{1 2 6} Conversion of the dicarboxylic acid to the corresponding diacid chloride is carried out by the reaction with oxalyl chloride, in the absence of light.^{1 2 7} The amine N,N'-dimethyl-N,N'-bis(3-aminopropyl)ethane (2) is produced by two standard organic reactions; a Michael addition of acrylonitrile to N,N'-dimethyl-ethylenediamine is followed by reduction of the di-nitrile with sodium metal. The high dilution reaction to produce L⁴ is based on that used by Hall,^{1 2 8} and gives the desired product in reasonable yield (36%). The work up yielded no product which can be assigned to a 2 + 2 addition. The structure of L⁴ was determined by ¹H and ¹³C n.m.r spectroscopy and F.A.B mass spectrometry (Tables 1.3, 2.3, 4.3). The ¹³C n.m.r of L⁴ (Figure 1.3) shows the symmetric nature of the ligand, as indicated in Figure 2.3.

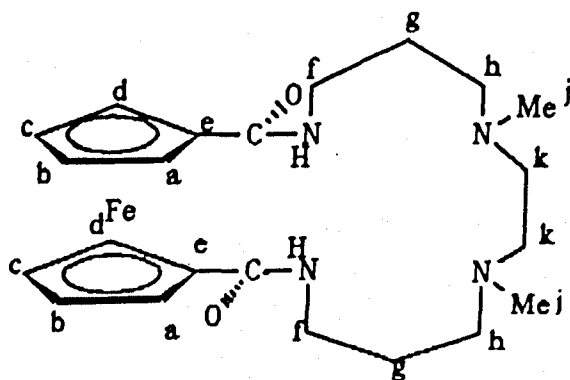
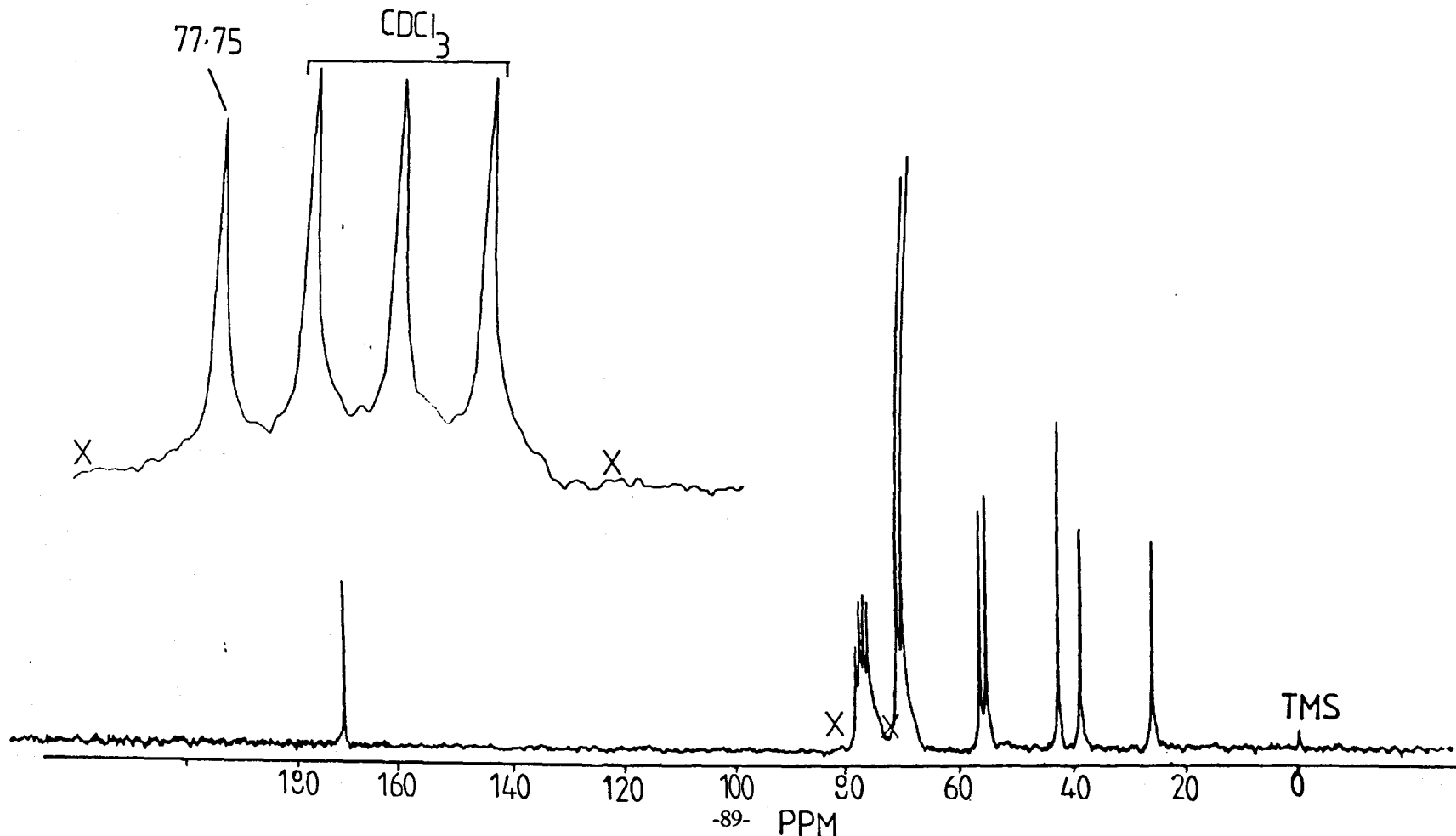


Figure 2.3

The carbonyls are probably planar in the trans configuration, as for similar crown ether ferrocene macrocycles.^{1 2 8} The cis configuration cannot be ruled out, but symmetry is only allowed if the two carbonyls are eclipsed; which is energetically unfavourable due to parallel dipoles of the carbonyl groups.^{1 2 8} Rather interestingly the carbonyl resonance in the ¹³C n.m.r is strong, indicating faster than usual relaxation (short T₁). The F.A.B mass spectrum contains a cluster of peaks around m/z = 441, which are assigned to [L⁴ + H]⁺, and constitute the main peaks in the spectrum. No peaks at higher m/z are observed, thus ruling out the possibility that the product is the 2 + 2 adduct. The electrochemistry of L⁴ is discussed in Section 4.3.

Figure 1.3

^1H decoupled ^{13}C n.m.r spectra of L^4 in CDCl_3 (ref Me_4Si $\delta = 0$), at 45.28MHz



Section 3.3

Metal complexes of L⁴

Metal complexes are prepared by refluxing the ligand in the presence of M(acetate)₂ (M = Cu²⁺, Ni²⁺, Zn²⁺), for 12 hours. The general formula of the complexes formed is [M(L⁴)](CH₃COO)₂.xH₂O (M = Cu²⁺, x = 3; Ni²⁺, x = 4; Zn²⁺, x = 2.5). All analytical data is in Tables 1.3, 2.3, 3.3, 4.3.

The metal acetates were used to try to promote deprotonation of the amide nitrogens, a process which occurs with other dioxo-tetraazamacrocycles.^{130,131} However, conductivity measurements (Table 4.3), indicate the complexes are 1:2 electrolytes, as expected for non-deprotonated complexes. Fabbrizzi¹²⁹ has found similar behaviour for non-rigid dioxo-macrocycles where MLH³⁺, ML²⁺, MLH₋₁⁺ and MLH₋₂ species are formed. More recently, the same behaviour has been observed by Reader.¹³² The lack of deprotonation in L⁴ is probably due to the geometrical constraints imposed by the ferrocene moiety. F.A.B mass spectra of the complexes show a cluster of peaks corresponding to [M(L⁴-H)]⁺ (Table 3.3). However, no peaks are observed corresponding to [M(L⁴)(CH₃COO)]⁺ as might be expected. This is attributed to the instability of such an ion. The I.r spectrum of the ligand L⁴ contains an amide I band at 1625cm⁻¹ {ν(CO)} and a further band at 1544cm⁻¹ (amide II band), which can be assigned to δ(NH) mixed with ν(CN).¹³³ In the I.r spectra of the metal complexes a new band appears at ~1580cm⁻¹ due to the acetate ion, with no sign of deprotonation in the amideI/amideII band. The U.V/visible of the free ligand contains a single absorbance at 444nm, which is characteristic of the ferrocene unit. The copper(II) complex again shows an absorbance corresponding to the ferrocene unit, but at a shorter wavelength (436nm). Although this could be interpreted as some interaction between the copper(II) and ferrocene centre, with complexes of the other metal ions there is no sign of a change in the wavelength maximum (Ni²⁺, 444nm, Zn²⁺, 444nm).

A further absorbance at 652nm, characteristic of a copper(II) d^9 spectrum, is observed at a longer wavelength than other corresponding dioxo-tetraazamacrocycles.¹³⁰ This can be attributed to the smaller ligand field, caused by the lack of deprotonation of the amide groups. The magnetic moment of the copper(II) complex (1.7 B.M) is as expected for a single unpaired electron, therefore confirming that no interaction is occurring between the copper(II) and iron(II) centres. Since numerous planar complexes of copper(II) are known it is most likely that the complex formed with L^4 is four co-ordinate. The nickel(II) complex formed is diamagnetic and therefore square planar. Further insight into the nickel(II) and zinc(II) complexes were obtained by ^{13}C n.m.r spectroscopy.

The integration of the ferrocene group into the macrocycle L^4 makes it interesting for two reasons:-

- (1) The carbonyls will be co-planar, with the cis/trans arrangements. For complexation the amide nitrogens will be sp^3 hybridised.
- (2) The ferrocene rings can be skew or tilted to allow release of ring strain.

Therefore, L^4 is a fairly flexible macrocycle. The number of possible conformations for the macrocycle are numerous (~ 15), but using molecular models it is possible to construct the least sterically strained systems. The conformations shown in Figure 3.3 have the carbonyls co-planar with the ferrocene rings, but with the N-Me, N-H groups in different orientations.

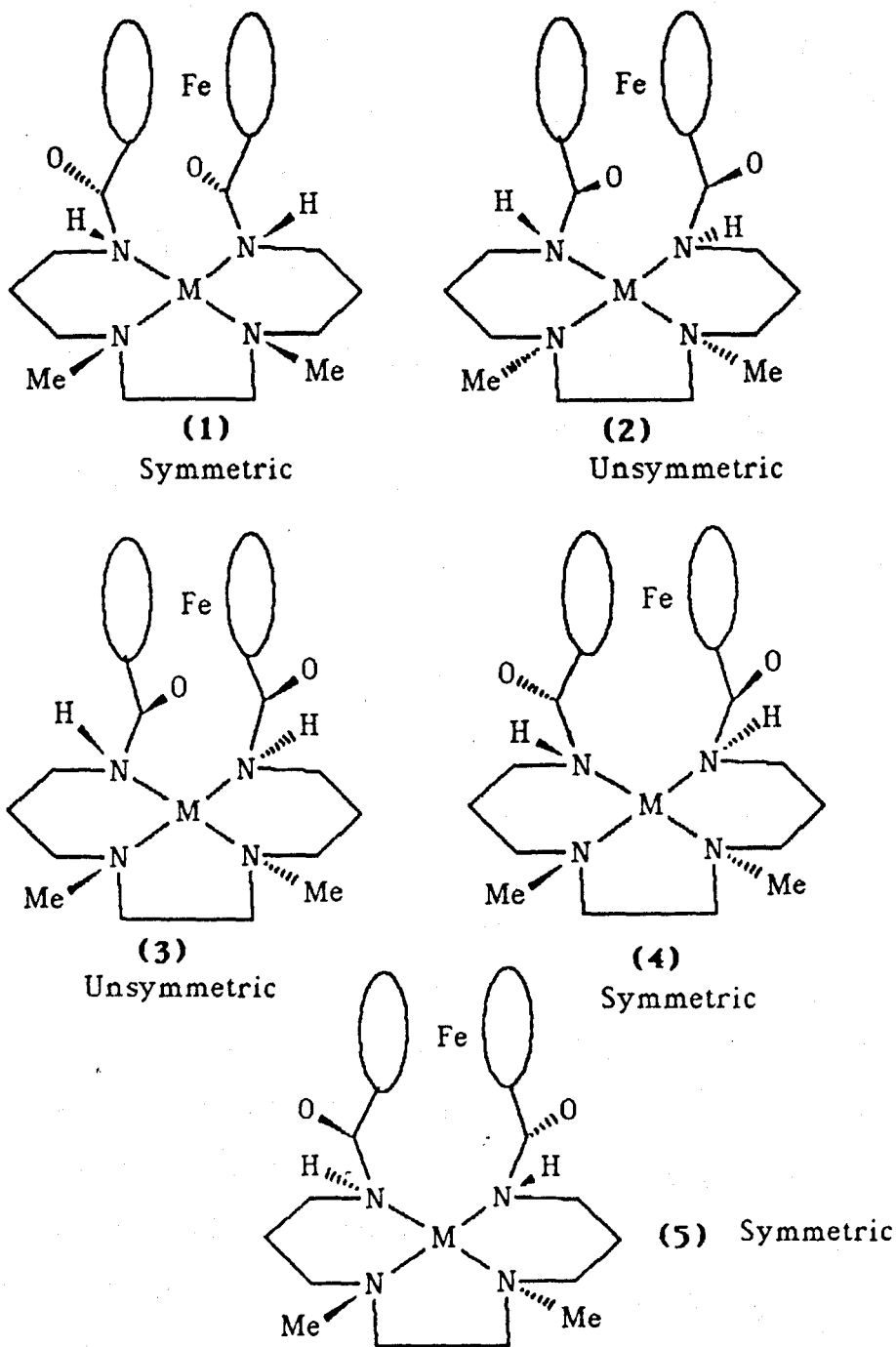
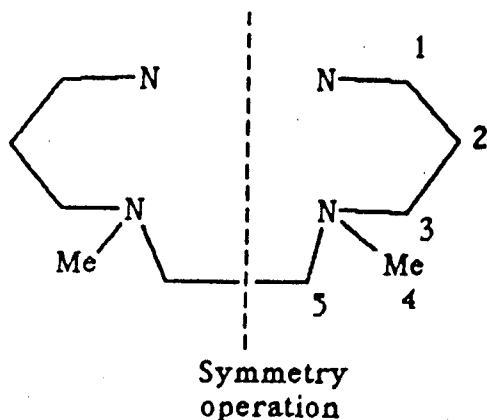


Figure 3.3

Some of the possible conformations of $[ML_4]^{2+}$ with the carbonyls cis/cis and cis/trans.

As discussed previously the carbonyls are thought to be disposed trans to one another. Therefore, this only leaves two of the five possible conformations shown in Figure 3.3 [(4) and (5)]. The possibility of having all the nitrogens with the same configuration is not possible for trans carbonyls (*i.e* analogous to conformation (1)). In conformer (4) the ferrocene rings are slightly askew, but there is a pseudo C_2 axis through the Fe atom, and bisects the N-C-C-N group. The conformer (5) has the ferrocene rings eclipsed with a proper C_2 axis.

The ^{13}C n.m.r spectra of $[\text{Ni}(\text{L}^4)]^{2+}$ and $[\text{Zn}(\text{L}^4)]^{2+}$ are shown in Figure 4.3 (a)/ (b). Both spectra show that the two complexes have a pseudo symmetry, because only five resonances are observed for the macrocyclic ring (see below).



The spectrum of $[\text{Ni}(\text{L}^4)]^{2+}$ shows that the ferrocene carbons are inequivalent, indicating that the cyclopentadiene rings are slightly askew. The $[\text{Zn}(\text{L}^4)]^{2+}$ spectrum is interesting since the macrocyclic ^{13}C resonances are broad, and accidental equivalence of the ferrocene carbons occurs. On cooling the sample to 233K no resolution of the ferrocene carbons in the spectrum is observed, but some splitting of the macrocyclic resonances occurs, suggesting the formation of other isomers. A very tentative interpretation to this data is that the two complexes adopt the conformation (4), with a pseudo C_2 axis, and the ferrocene rings slightly askew. No other structural determination was obtained on these complexes. However, in view of the tendency for zinc(II) to form five co-ordinate complexes a likely formulation for the complex is $[\text{Zn}(\text{L}^4)(\text{OH}_2)](\text{CH}_3\text{COO})_2 \cdot 1.5\text{H}_2\text{O}$.

Figure 4.3(a)

^1H decoupled ^{13}C n.m.r spectrum of $[\text{Zn}(\text{L}^4)](\text{CH}_3\text{COO})_2$ in CD_3NO_2 (ref Me_4Si $\delta = 0$) at 100.62MHz

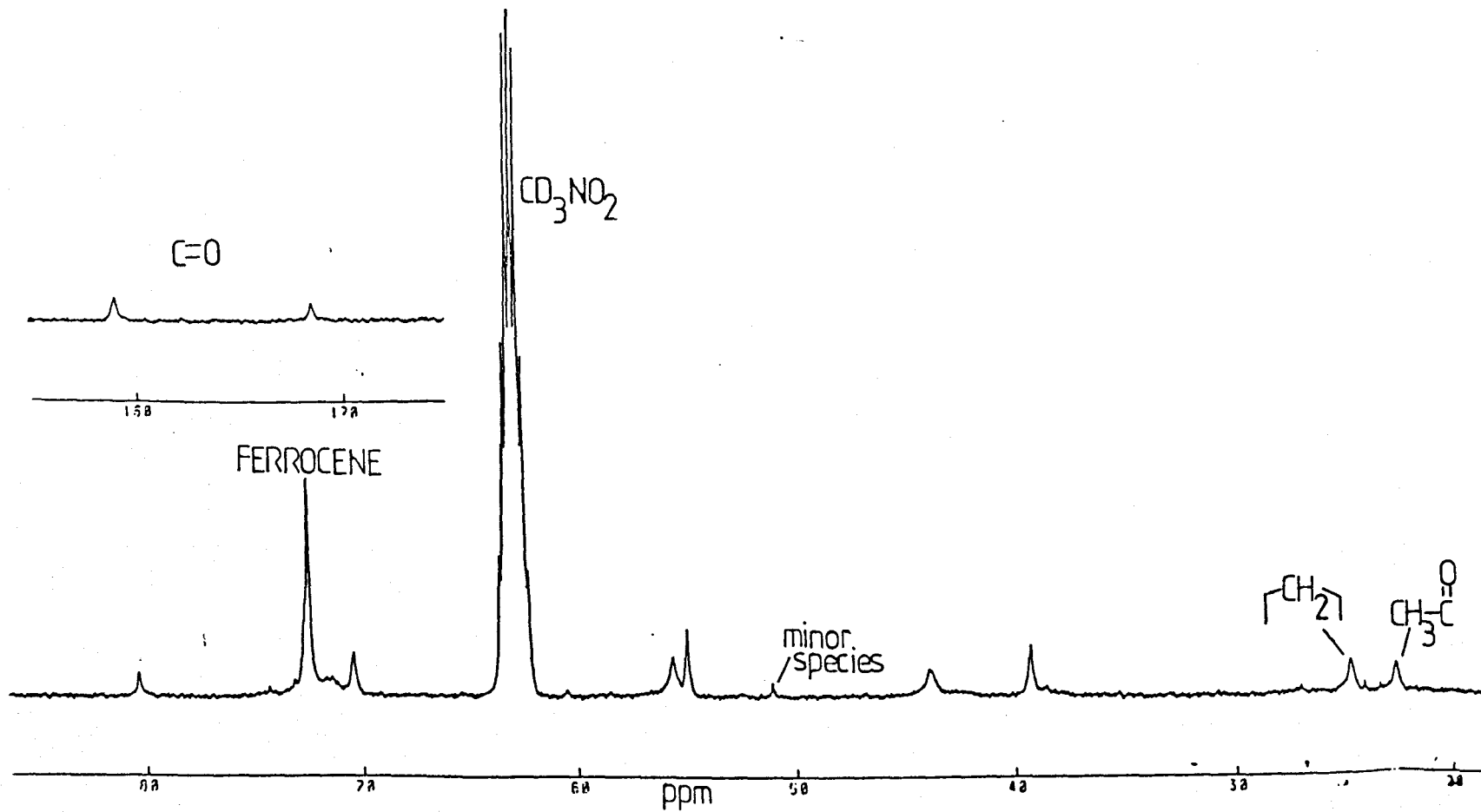
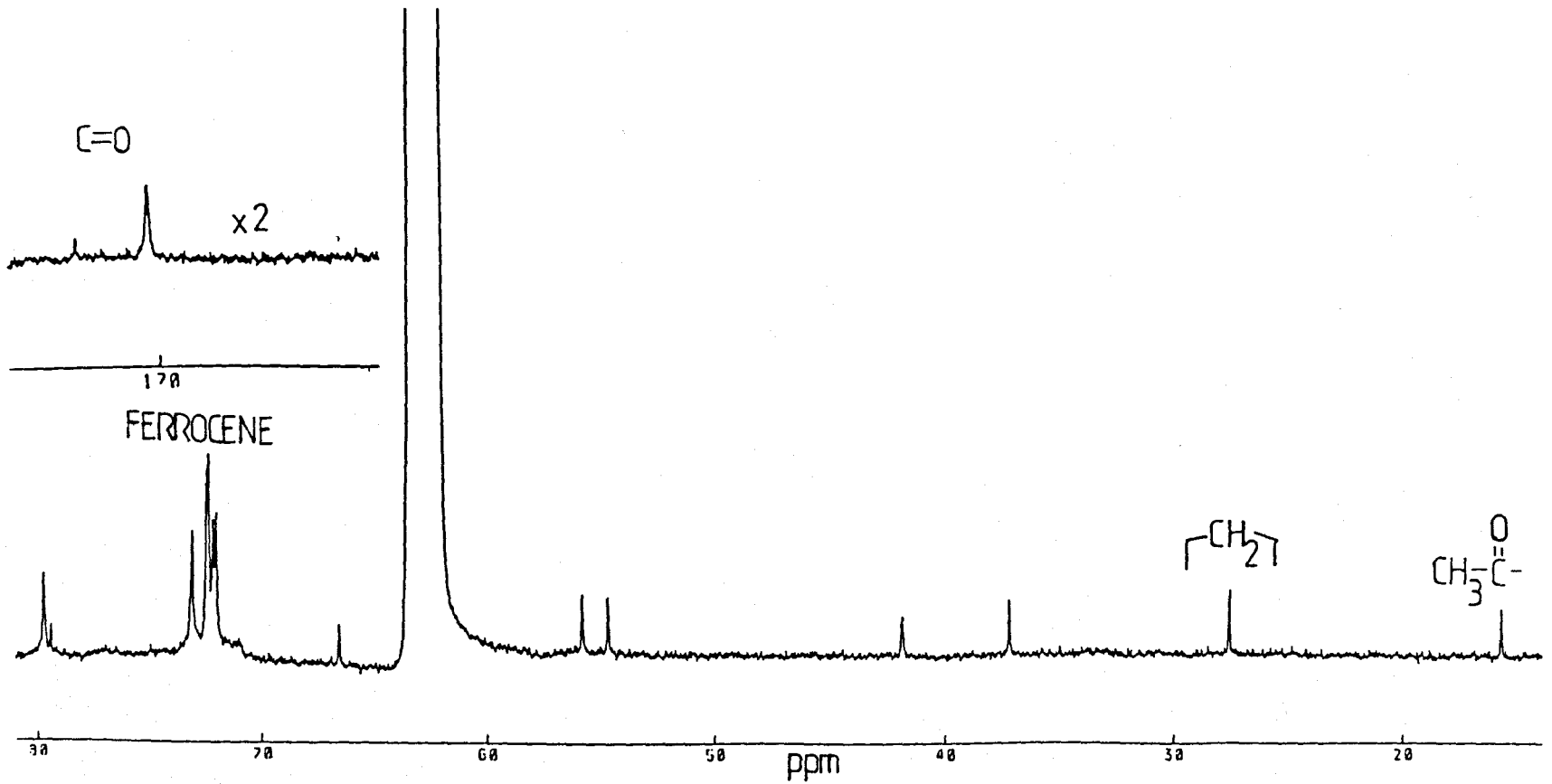


Figure 4.3(b)

^1H decoupled ^{13}C n.m.r spectrum of $[\text{Ni}(\text{L}^4)](\text{CH}_3\text{COO})_2$ in $\text{CD}_3\text{NO}_2/\text{CD}_3\text{CN}$ at 100.62 MHz.



Electrochemistry of L⁴

The cyclic voltammetry of L⁴ in DMSO is shown in Figure 5.3 (a). Again as discussed in Chapter 2 (Section 12.2) the problem of oxidation of the tertiary amines is evident. In this case the electrochemistry of the ferrocene unit is masked by the added current. At low scan rates the system becomes totally irreversible, indicating that electron transfer at the electrode surface is slow. Also after the first scan there is evidence of the same breakdown product, as observed for the macrocycles L³.HCl and L³. To overcome these problems the electrochemistry of L⁴ was studied in a strong acid (Trifluoroacetic acid), so that the tertiary amine groups were protonated. The cyclic voltammetry in strongly acidic solution is shown in Figure 5.3 (b). In this case the electrochemistry is almost reversible, with a linear dependence of peak current to square root of scan rate (Figure 5.3 (c)). The peak separation (ΔE) is larger than expected at high scan rates (170mV), but decreases to 110mV at lower scan rates, suggesting sluggish electron transfer.

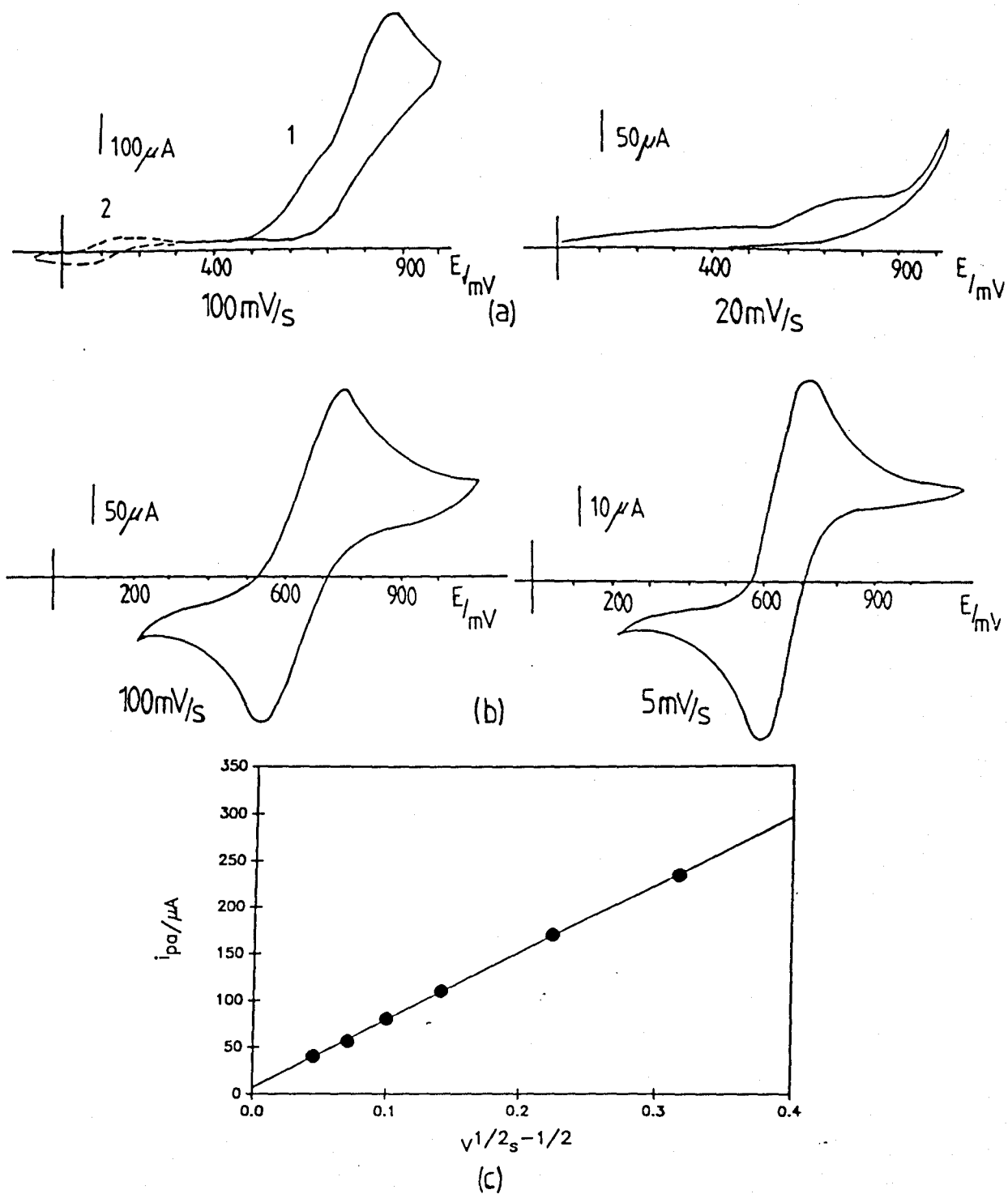


Figure 5.3

The electrochemistry of L^4 in (a) DMSO, 0.2M Tetrabutylammonium perchlorate, Pt electrode, vs S.C.E, conc = 6.5mM: (1) = scan 1, (2) = scan 2. (b) Trifluoroacetic acid 0.2M Tetrabutylammonium perchlorate, Pt electrode, vs S.C.E, conc = 6.9mM, ΔE (average) = 150mV, $i_{pa}/i_{pc} = 1.02$, $E_{1/2} = 658mV$. (c) plot of peak current (i_{pa}) against the square root of scan rate.

However, overcoming the problem of tertiary amine oxidation renders the macrocycle L^4 unsuitable for co-ordination. To overcome this problem, it was decided to move the electrochemistry of the redox centre to a region where oxidation of tertiary amines is not possible. One way to achieve this is to replace the ferrocenes with cobalticenium centres and use the cobalticenium/cobaltocene (Co^{3+}/Co^{2+}) couple, as discussed in Section 7.3.

Section 5.3

The electrochemistry of metal complexes of L^4

The cyclic voltammetry of $[Ni(L^4)]^{2+}$ and $[Cu(L^4)]^{2+}$ are shown in Figure 6.3. In both complexes no reverse peak is observed, but at all scan rates the anodic peak (E_{pa}) is observed. A possible explanation is that the oxidised form is unstable and breakdown occurs before detection is possible. For both systems no detection of higher oxidation states (*e.g.* Ni(III), Cu(III)) are observed. This is similar to the related work by Fabbrizzi,^{1 3 4} who concluded that the attainment of trivalent copper is only possible in the presence of deprotonated amido groups.

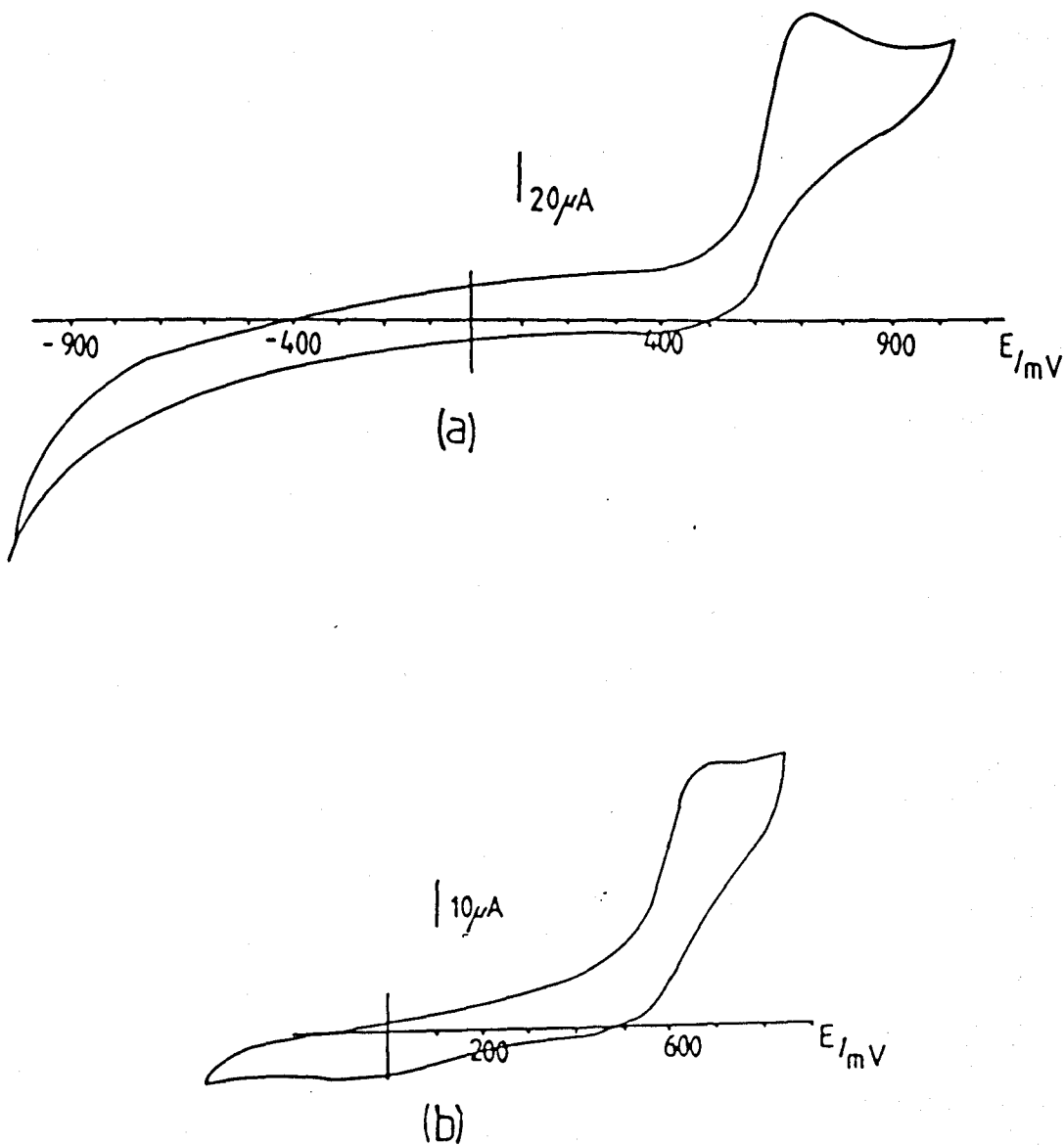


Figure 6.3

The electrochemistry of (a): $\text{Ni}(\text{L}^4)^{2+}$, 50mV/s, H_2O , 0.2M NaNO_3 vs S.C.E, glassy carbon electrode. conc = 1.5mM, pH = 7.2. (b): $\text{Cu}(\text{L}^4)^{2+}$, 50mV/s, H_2O , 0.2M NaNO_3 , vs S.C.E, Pt electrode, conc = 1.4mM, pH = 7.2

Section 6.3

Synthesis of L⁵

Beer⁹ has recently synthesised a series of cobalticenium macrocycles, in an attempt to detect anions. However, no attempt has been made to produce a cobalticenium macrocycle which could bind cations, using nitrogen donors.

In this study the main object was to produce a ligand, similar to L⁴, but with a cobalticenium centre instead of ferrocene. Although a synthetic route analogous to that used for L⁴ was adopted it became apparent from the ¹³C, ¹H n.m.r and mass spectra (Tables 1.3, 3.3) of the product, that a 2+2 addition occurred, instead of a 1+1. As described later the ¹³C n.m.r of L⁴ and L⁵ are quite different, supporting the proposal that the similar synthetic procedures give different products. The difference in the outcome of the two preparations is not so dramatic if the synthetic conditions are examined closely. Firstly different solvents are used in the two preparations, and the yields of the two products vary dramatically. The most important point, is that the starting material diacid chloride in the cobalticenium macrocycle preparation, is mixture of chloride and hexafluorophosphate salts (see experimental), which probably causes an imbalance in the stoichiometry of the reaction.

The synthesis of L⁵ is outlined in Scheme 1.3. The diacidchloride is easily synthesised by the method of Sheats and Rausch.¹³⁵ The diacid chloride is obtained by refluxing the dicarboxylic acid in thionyl chloride for 24 hours¹³⁶ instead of only 6 hours.¹³⁷ The diacid chloride was handled in a dry box, as it was found to be extremely moisture sensitive. A similar high dilution method to that used in the synthesis of L⁴ was carried out, using acetonitrile as solvent. After purification on silica, the brown solid obtained was dissolved in water and slurried with excess KPF₆, to ensure that the complex was entirely the hexafluorophosphate salt. However, even after recrystallisation from water/Et₂O, some KPF₆ remained (Table 2.3). The presence of co-crystallised KPF₆ was established by atomic absorption spectrophotometry.

The ^{13}C n.m.r spectrum of L^5 is shown in Figure 7.3. The resonances corresponding to the five aliphatic carbons of the macrocyclic ring are all split into two, indicating some loss of symmetry. A total loss of symmetry is ruled out, as this would lead to a far more complicated spectrum. In the dimeric structure the complication of the carbonyls being trans/trans; cis/cis; cis/trans, with the possibility of skew rings makes interpretation difficult. However, the dimeric nature of L^5 is evident in the ^1H n.m.r (Figure 8.3), where four equal intensity methyl resonances are observed. The ^1H n.m.r also indicates the presence of two moles of diethylether, which are probably sitting in the cavity of the macrocycle. The use of F.A.B mass spectrometry is not at first totally convincing of the dimeric nature of the macrocycle; m/z is the same for both monomer and dimer (for a monomer $z=1$, for a dimer of mass $2m$ $z=2$). To try and produce $[\text{L}^5]^+$ instead of $[\text{L}^5]^2+$, sodium chloride was slurried with the sample prior to F.A.B mass spectral analysis. A cluster of peaks around $m/z=923$ are observed, corresponding to $[\text{L}^5\text{Cl}]^+$ (m/z calc = 921).

Section 7.3

Electrochemistry of L^5

The electrochemistry of L^5 in the presence and absence of Zn^{2+} is shown in Figure 9.3. Titration of Zn^{2+} into a solution of the ligand, in acetonitrile, causes the cyclic voltammogram to change shape and a new peak to appear at a lower potential (less reducing) (Figure 9.3(b)), as expected. As a positive metal ion enters the cavity reduction of $\text{Co}^{3+} \rightarrow \text{Co}^{2+}$ should become easier, as positive repelling charges are being removed. After addition of excess zinc(II) a new cyclic voltammogram appears at $E_{1/2} = -520\text{mV}$ versus S.C.E, and corresponds to a shift of 280mV in the half wave potential. A titration curve (Figure 10.3) seems to confirm that saturation occurs at a metal/ligand ratio of 2:1, but questions remain of how genuine the slight plateau region of the curve is. A very tentative interpretation of this data is that two zinc(II) ions are binding to all eight nitrogens of the macrocyclic ring. Titration of Ni^{2+} to a solution of L^5 , in acetonitrile, again

causes the cyclic voltammogram to change shape and a new cyclic voltammogram to appear at a less reducing potential. The shift in the half wave potential ($E_{1/2}$) is less than for the zinc(II) ($\Delta E_{1/2} = 180\text{mV}$), and saturation seems to occur at a metal/ligand ratio of only 1:1 (Figure 11.3). Therefore, only one nickel(II) ion appears to be co-ordinating to the macrocycle, which accounts for the smaller shift in the half wave potential. The results seem to contradict each other with nickel(II) appearing to form a 1:1 complex, and the zinc(II) a 2:1 complex; which seems unlikely as this would bring positive centres closer together. This apparent dilemma will only be solved when the nickel(II) and zinc(II) complexes are analysed and the metal ion content found.

Varying the background electrolytes (e.g ClO_4^- , BF_4^-) had no effect on the phenomena observed. Therefore, the ligand L^5 shows no response to anions. To ensure no spurious effect occurred the electrochemistry of 1,1'-dimethylcobalticenium hexafluorophosphate was studied in the presence and absence of Zn^{2+} . No real shift ($< 5\text{mV}$) is observed in the half wave potential, except on the addition of a large excess of Zn^{2+} the cobalticenium/cobaltocene couple becomes more irreversible.

Rather disappointingly studies using Cu^{2+} gives very irreversible electrochemistry, possibly due to slow copper(II)→copper(I) reduction.

Figure 7.3

^1H decoupled ^{13}C n.m.r spectrum of L^5 in CDCl_3 (ref Me_4Si $\delta = 0$) at 45.28MHz

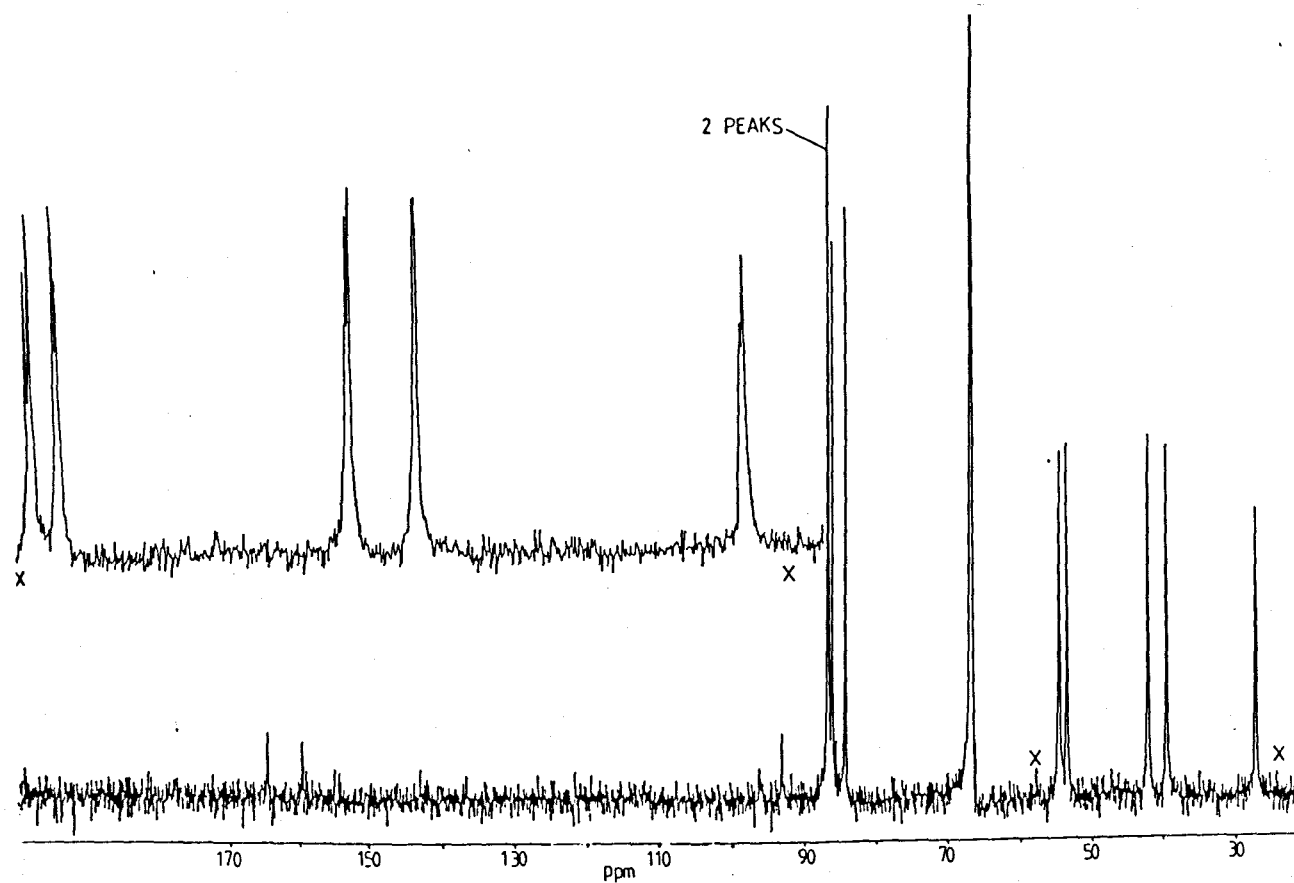
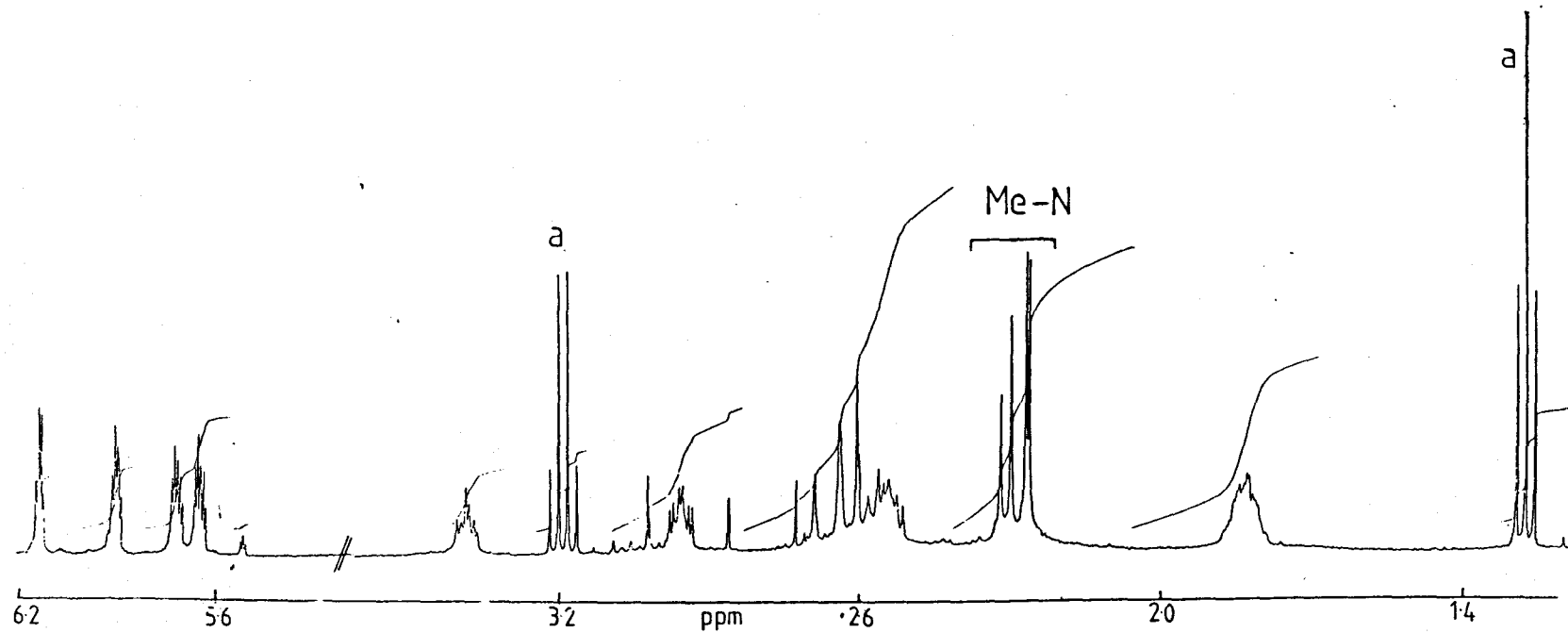


Figure 8.3

A 400MHz ^1H n.m.r spectrum of L^5 in CDCl_3 (ref Me_4Si $\delta = 0$), showing the four different methyl resonances.



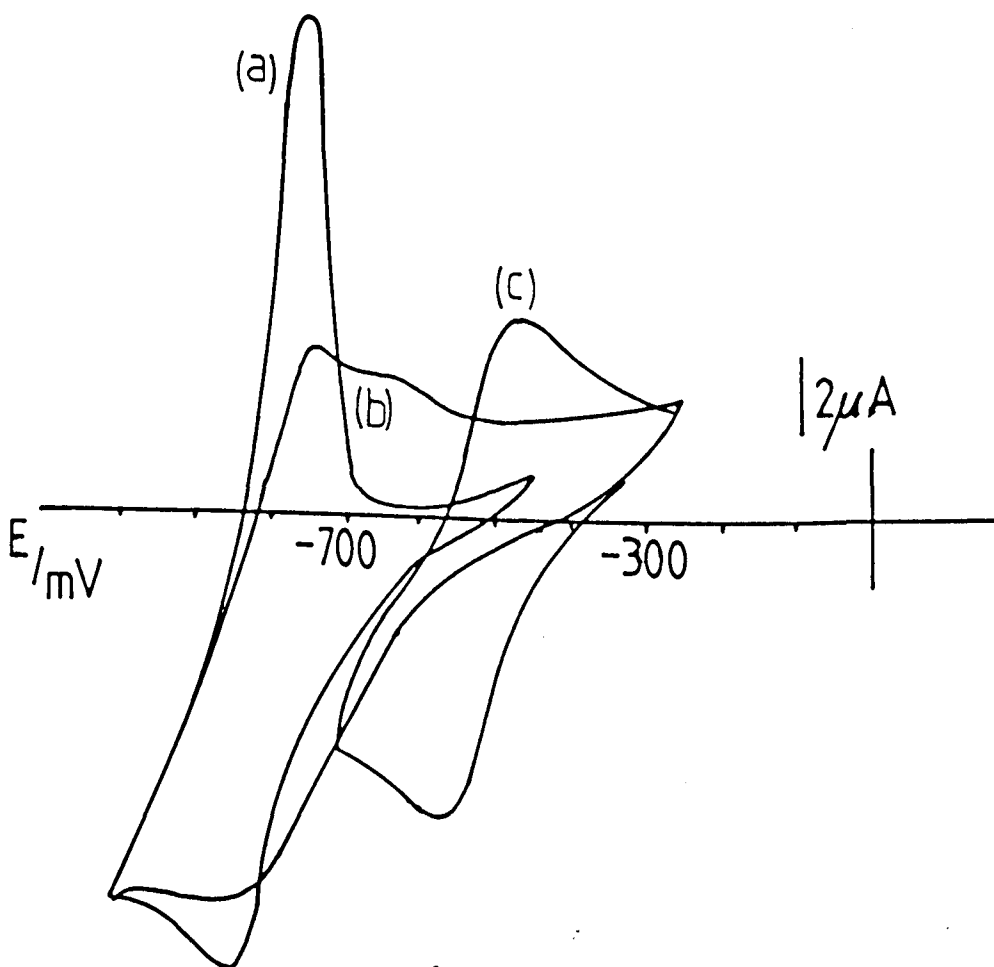


Figure 9.3

The electrochemistry of L^5 in CH_3CN , 0.2M tetrabutylammonium hexafluorophosphate, Pt electrode, vs S.C.E, conc = 0.34mM . (a) free ligand. (b) 0.32 equivalents of Zn^{2+} . (c) excess Zn^{2+} . $\Delta E_{1/2} = 280\text{mV}$.

Figure 10.3

A titration curve for the addition of Zn^{2+} to L^5 , showing the shift in the half wave potential ($E_{1/2}$) against equivalence of Zn^{2+} added. Experimental conditions as in Figure 9.3

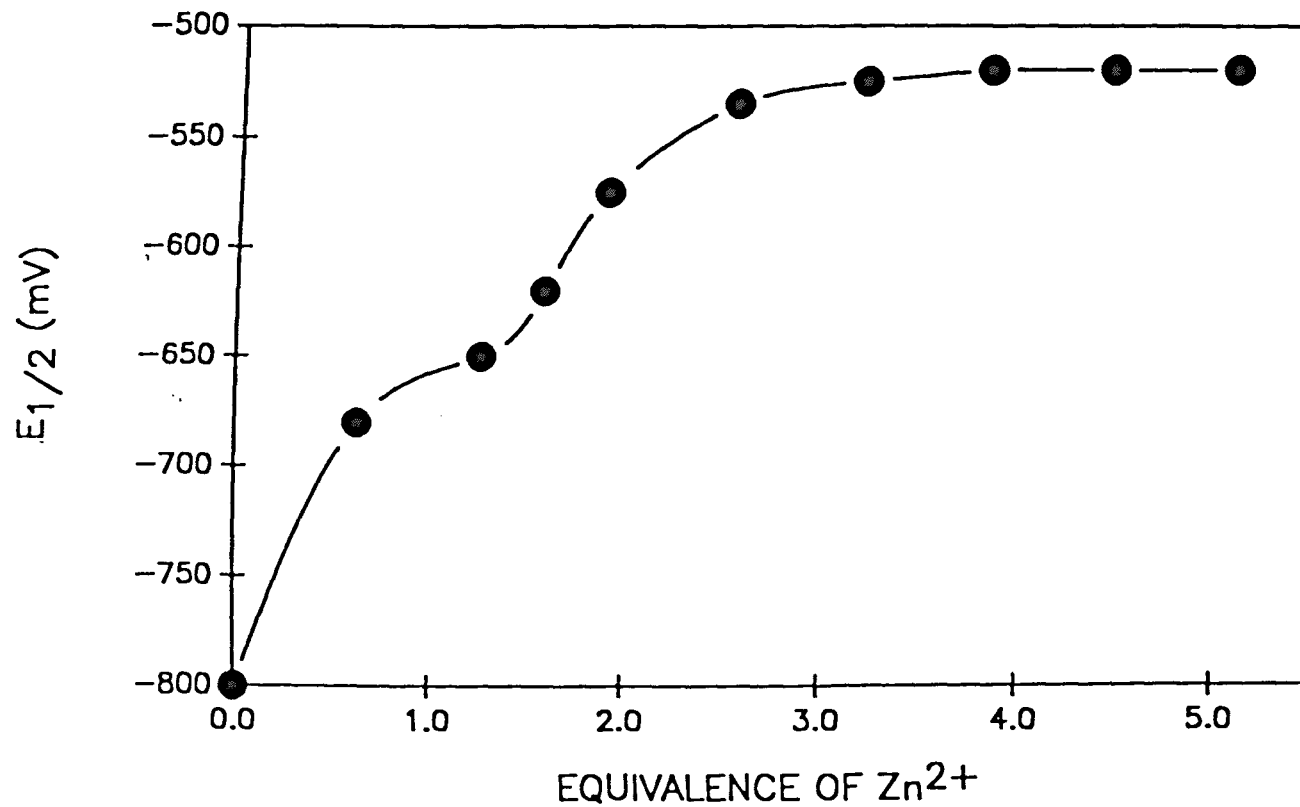
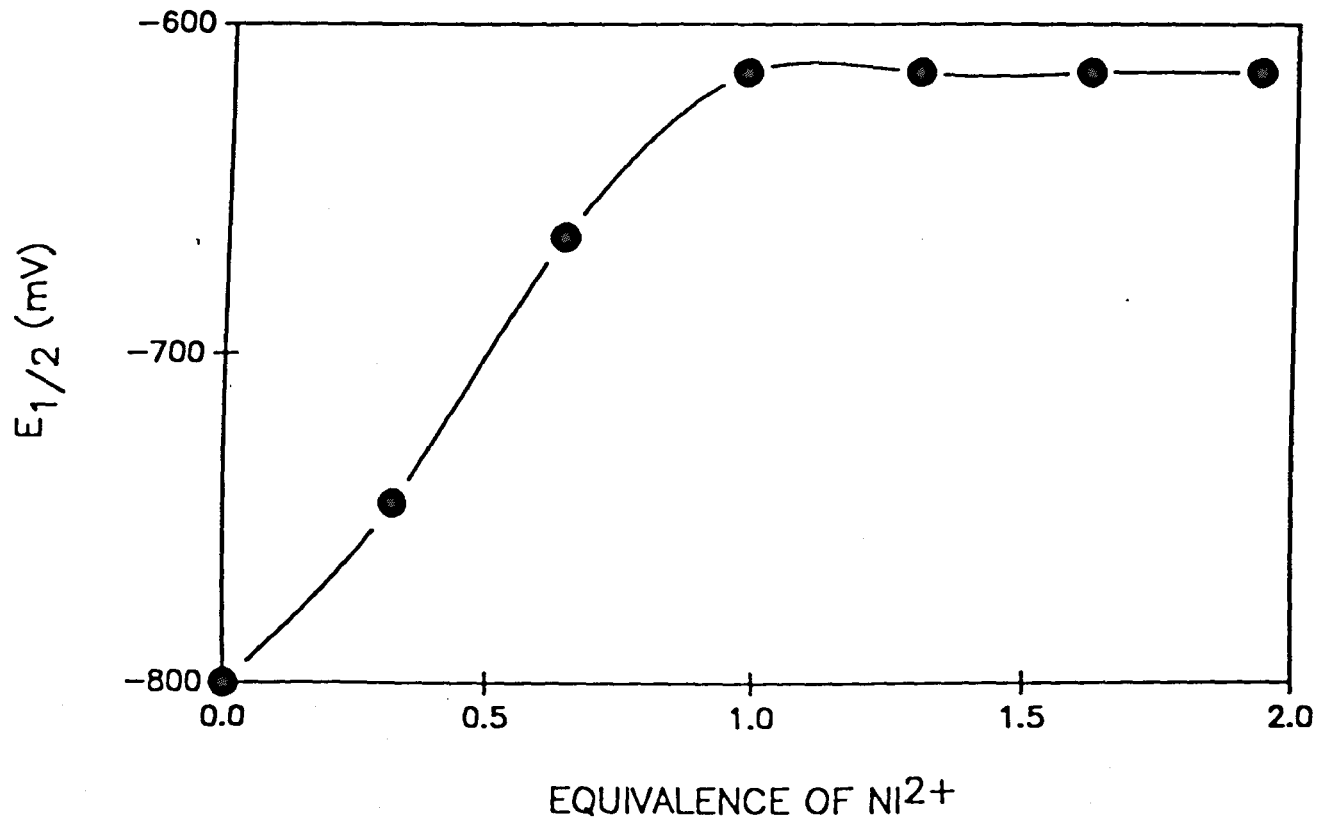


Figure 11.3

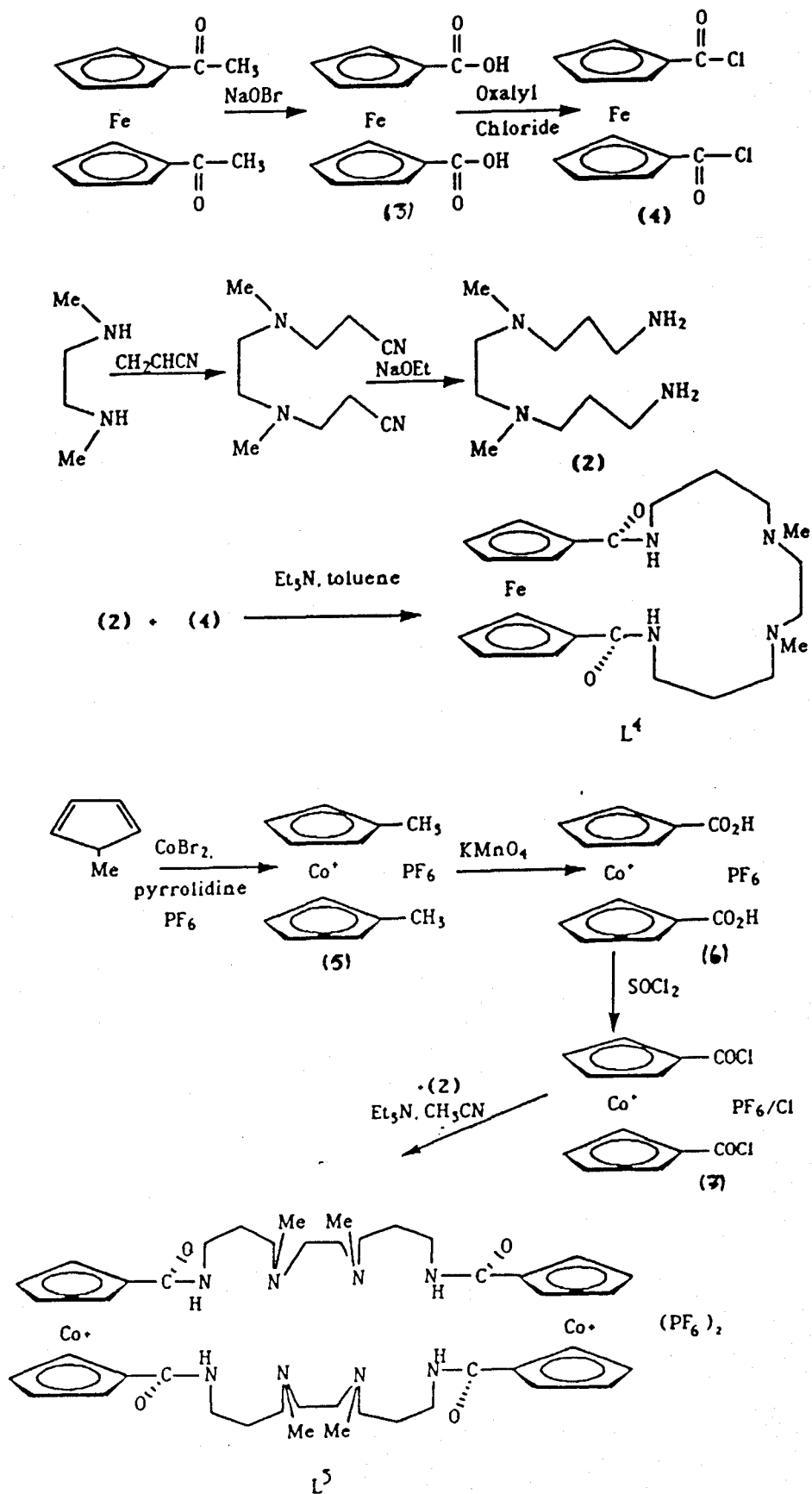
A titration curve for the addition of Ni^{2+} to L^5 , showing the shift in half wave potential ($E_{1/2}$) against the equivalence of Ni^{2+} added. Conc of $\text{L}^5 = 0.3\text{mM}$, in acetonitrile (0.2M Tetrabutylammonium perchlorate), vs S.C.E, Pt electrode.



Conclusions

The ligand L⁴ readily forms complexes with the transition metals copper(II), nickel(II) and zinc(II), without deprotonation of the amido nitrogens. The ligand is unable to stabilise higher oxidation states of copper(II) and nickel(II), presumably due to this lack of deprotonation. The use of the free ligand L⁴ as a transition metal sensor is hampered by the oxidation of the tertiary amines which "masks" the electrochemistry of the ferrocene/ferrocenium couple. However, the ligand L⁵ shows more potential as a chemical sensor as large shifts are observed in the E_{1/2} value on addition of zinc(II) and nickel(II). The main problem areas are:-

- (1) **Crystallised potassium hexafluorophosphate-** This needs to be removed possibly by using ammonium hexafluorophosphate in the synthesis. At the moment the electrochemistry may not be reflecting the true interaction of the transition metal ions and the ligand, but exchange of a transition metal for potassium.
- (2) **Yield of ligand-** The synthesis gives a poor yield, which needs to be improved to enable workable amounts of ligand to be obtained. Better yields would then allow characterisable metal complexes to be obtained, and perhaps the electrochemistry to be understood fully.



Scheme 1.3

The scheme for the synthesis of L^4 and L^5

Ligand	C-(CH ₂)-C	C-(CH ₂)-N, Me-N	FERROCENE CARBONS COBALTICENIUM CARBONS	C=O
L ⁴ (a)	26.14(2C)	38.76(2C), 42.67(2C), 55.30(2C), 56.42(2C)	70.22(4C), 71.24(4C) 77.75(2C, ipso)	170.24(2C)
L ⁵ (b)	26.24(2C) 26.80(2C)	39.26(4C), 41.92(2C) 42.02(2C), 53.95(4C) 53.95(4C), 54.97(2C) 54.97(2C), 55.12(2C)	85.32(4C), 87.16(4C) 87.72(4C), 87.82(4C) 94.41(2C, ipso), 97.75(2C, ipso)	164.22(2C) 169.15(2C)
[Zn(L ⁴) (acetate) ₂ (c)]	22.65(2C)(*) 24.75(2C)	39.33(2C), 43.97(2C) 54.95(2C), 55.62(2C)	{70.40, 71.65, 72.53}8C 80.36(2C, ipso)	171.50(2C) 180.92(1C*)
[Ni(L ⁴) (acetate) ₂ (d)]	15.64(2C) 27.57(2C)	37.19(2C), 41.82(2C) 54.72(2C), 55.86(2C)	{72.05, 72.19, 72.41 72.48, 73.11}8C {79.40, 79.73}(2C, ipso)	170.39(2C) 172.94(2C)

Table 1.3

¹H decoupled ¹³C n.m.r spectra. (a) CDCl₃ (ref Me₄Si delta = 0). (b) D₂O (ref dioxan delta 67.4). (c) CD₃NO₂ (ref Me₄Si delta = 0). (d) CD₃NO₂/CD₃CN (ref Me₄Si delta = 0). (*) = CH₃COO group.

Compound	Colour	Recrystallised from	Yield	Formula	(C) found in parentheses	(H) found in parentheses	(N) found in parentheses
$[\text{Zn}(\text{L}^4)]$ $(\text{CH}_3\text{COO})_2$ $2.5\text{H}_2\text{O}$	yellow	acetonitrile/ diethylether(1:1)	60%	$\text{C}_{26}\text{H}_{38}\text{N}_4\text{Fe}_1\text{O}_6\text{Zn}_1$ $2.5\text{H}_2\text{O}$	46.68 (46.58)	6.48 (6.16)	8.38 (8.78)
$[\text{Ni}(\text{L}^4)]$ $\text{CH}_3\text{COO})_2$ $4\text{H}_2\text{O}$	yellow	acetonitrile/ diethylether(1:1)	62%	$\text{C}_{26}\text{H}_{46}\text{Fe}_1\text{N}_4\text{Ni}_1\text{O}_{10}$	45.31 (45.52)	6.73 (6.40)	8.13 (8.07)
$[\text{Cu}(\text{L}^4)]$ $(\text{CH}_3\text{COO})_2$ $3\text{H}_2\text{O}$	green	acetonitrile/ diethylether(1:1)	76%	$\text{C}_{26}\text{H}_{44}\text{Cu}_1\text{Fe}_1\text{N}_4\text{O}_9$	46.19 (46.60)	6.56 (6.30)	8.23 (7.88)
$(\text{L}^5)(\text{Et}_2\text{O})_2$ $(\text{PF}_6)_2 \cdot 8\text{KPF}_6$	brown	water/ diethylether(1:2)	10%	$\text{C}_{52}\text{H}_{84}\text{Co}_2\text{F}_{60}$ $\text{K}_8\text{N}_8\text{O}_6\text{P}_{10}(\text{a})$	22.32 (22.24)	3.02 (2.79)	4.00 (3.88)

Table 2.3

Combustion analysis results for complexes synthesised in Chapter 3. (a) Potassium content calculated using atomic absorption spectrophotometry %cal(11.18):%found (11.11)

$[L^4 + H]^+$	
m/z(calc)	m/z(found)
438-(6%)	439-(13%)
440-(2%)	440-(11%)
441-(100%)	441-(100%)
442-(29%)	442-(25%)
443-(5%)	443-(5%)
444-(< 1%)	444-(< 1%)

$[Zn(L^4)-H]^+$	
m/z(calc)	m/z(found)
501-(6%)	501-(14%)
502-(< 1%)	502-(10%)
503-(100%)	503-(100%)
504-(29%)	504-(23%)
505-(62%)	505-(63%)
506-(29%)	506-(29%)
507-(42%)	507-(39%)
508-(11%)	508-(18%)

$[Cu(L^4)-H]^+ + 1$	
m/z(calc)	m/z(found)
501-(6%)	501-(18%)
502-(1%)	502-(60%)
503-(100%)	503-(100%)
504-(29%)	504-(53%)
505-(48%)	505-(46%)
506-(13%)	506-(10%)
507-(2%)	507-(/)

$[Ni(L^4)-H]^+$	
m/z(calc)	m/z(found)
495-(6%)	495-(13%)
496-(1%)	496-(16%)
497-(100%)	497-(100%)
498-(29%)	498-(61%)
499-(43%)	499-(57%)
500-(13%)	500-(28%)
501-(8%)	501-(20%)

Table 3.3

F.A.B mass spectral data. Relative isotopic abundances in parentheses expressed as % of main isotopic peak. All samples run in *m*-nitrobenzylalcohol matrix.

Complex	Colour	Magnetic Moment(B.M) ^e	$\lambda_{\max}(\text{nm})$ $\epsilon_{\max}(\text{mol}^{-1}\text{dm}^3\text{cm}^{-1})$ DMSO ^c	$\epsilon_{\max}(\text{mol}^{-1}\text{dm}^3\text{cm}^{-1})$ H ₂ O ^c	Molar Conductivity $\Omega^{-1}\text{mol}^{-1}\text{cm}^2$	I.r.(cm ⁻¹) ^b (C=O stretch)	ref
L ⁴	red/ brown	diamagnetic	444(115)			1625 1544	this work
[ZnL ⁴](CH ₃ COO) ₂ ·2.5H ₂ O	yellow	diamagnetic		448(340) 344(sh,658)	207 ^a	1618 1588 1548	this work
[CuL ⁴](CH ₃ COO) ₂ ·3H ₂ O	green	1.7	652(162)	436(380)	192 ^a	1631 1578 1542	this work
[NiL ⁴](CH ₃ COO) ₂ ·4H ₂ O	yellow	diamagnetic		444(399) 352(sh,670) 256(10,054)	169 ^a	1629 1546 1536	this work
[NiL]1.5H ₂ O	purple			464(77)	12	1640 ^d 1595 1535	130
[CuL]1.5H ₂ O	orange			506(86)	18	1580 ^d 1550	130

Table 4.3

Analytical data for compounds of Chapter 3. (a) H₂O solvent, 1x10⁻³M solutions at 25 C. (b) Nujol Mull (c) Solvent (d) KBr disc.

(e) Evans method ~ 1x10⁻²M solutions at 25 C. L = 5,7-Dioxo-1,4,8,11-tetraazacyclotetradecane

Experimental

For chemicals and solvents see Chapter 2 (Section 14.2), and experimental techniques Chapters 2 (Section 14.2) and Chapter 7.

Pyrrrolidine was dried by refluxing over anhydrous CaSO_4 for 24 hours, followed by distillation under dry nitrogen. Methylcyclopentadiene was obtained by the procedure of Reynolds and Wilkinson.^{1 3 8}

Preparation of $[\text{CH}_2\text{-N(Me)-(CH}_2\text{)-CN}]_2\text{-}(1)$

N,N'-dimethylethane-1,2-diamine (10.63g, 120mmol) was dissolved in acrylonitrile (170cm^3) with glacial acetic acid (13.56g, 226mmol), and refluxed for 12 hours. The excess acrylonitrile was removed *in vacuo*, and the residue taken up in CH_2Cl_2 (300cm^3), washed with 0.88 NH_3 (aq) ($\sim 60\text{cm}^3$). The organic layer was washed with H_2O (125cm^3), dried over anhydrous MgSO_4 , and solvent removed with a rotary evaporator. The oily residue was vacuum distilled to give a colourless oil (bp 150°C , 0.03mmHg, 16.9g, 73% yield). ^{13}C n.m.r (CDCl_3): 16.21(2C), 42.02(2C), 53.19(2C), 55.17(2C), 118.8(CN).

Preparation of $[\text{CH}_2\text{-N(Me)-(CH}_2\text{)}_3\text{-NH}_2]_2\text{-}(2)$

Compound (1) (8.55g, 4.4mmol) was dissolved in dry EtOH (200cm^3). Freshly cut sodium (16g, 700mmol) was added slowly over a period of 4 hours. The solution was refluxed under nitrogen for 12 hours, cooled and added to H_2O (200cm^3). The solution was extracted with CH_2Cl_2 ($6 \times 50\text{cm}^3$), dried over anhydrous MgSO_4 , and the solvent removed by rotary evaporation to give a yellow oil. The oil was distilled under vacuum to give a colourless oil (bp 120° , 0.02mmHg, 4.01g, 45% yield). ^1H n.m.r (CDCl_3): 1.20(br, NH, 4H), 1.65(q, 4H), 2.30(s, 6H), 2.45(t, 4H), 2.50(s, 4H), 2.78(t, 4H). ^{13}C n.m.r (CDCl_3): 31.48(2C), 41.02(2C), 43.02(2C), 56.07(2C), 56.27(2C).

Preparation of 1,1'-Ferrocenedicarboxylic acid → (3)

Dioxane (243cm³) was added in portions to a stirring solution of H₂O (500cm³), NaOH (80.63g, 2moles), and bromine (92.75g, 580mmol) at 0-10° C. At a temperature of 0-5° C, 1,1'-diacetylferrocene (25g, 92.6mmol) was added in small portions. After addition, stirring was continued at 0-5° C for 1 hour, the solution filtered, and washed with CH₂Cl₂ (3x100cm³). The aqueous layer was heated to 80° C and acidified with conc HCl to precipitate a brown solid, which was collected and dried in a oven at 100° C (18.91g, 75% yield). I.r (Nujol Mull): 1680cm⁻¹ (C=O). ¹H n.m.r (d⁴ MeOH): 4.90 (s, 8H).

Preparation of 1,1'-Ferrocenediacid chloride→(4)

1,1'-Ferrocenedicarboxylic acid (2g, 7.3mmol) in dry CH₂Cl₂ (30cm³), with oxalyl chloride (4cm³, 40mmol) and pyridine (~ 1 drop) was stirred in the dark at room temperature for 12 hours. The mixture was refluxed for 6 hours, and the solvent removed with a rotary evaporator. The residue was continuously extracted at 80° C with petrol (100-140) to yield, on removal of solvent, a dark red solid (1.56g, 66% yield). I.r (Nujol mull): 1770cm⁻¹ (C=O).

Preparation of L⁴

A 1dm³ dry three necked flask was charged with dry toluene (100cm³), and flushed with nitrogen. Two oven dried 100cm³ all glass syringes were charged separately with solutions of (2) (0.64g, 3.2mmol) and (4) (0.99g, 3.2mmol), each dissolved in dry toluene (100cm³). The two syringes were connected to the flask via two long stainless steel needles passing through a suba seal, and positioned above a vigorously stirred solvent in the flask. The syringes were mounted on a Sage Instrument model 355 syringe pump, to allow slow addition of the two reagents over a period of 12 hours. Triethylamine (1.62g, 16mmol) was added to the toluene flask, and the solution cooled in a ice bath to below 5° C before, and during addition of the two reagents from the syringes. After addition was complete, the solution was stirred for 24 hours. The precipitated triethylammonium chloride was filtered off, and the solvent removed on a rotary evaporator to give a

red oil. Gravitational column chromatography on silica with $\text{CHCl}_3(96\%)/\text{MeOH}(4\%)$ removed unreacted starting material. The desired product was obtained by eluting with $\text{MeOH}(98\%)/0.88\text{NH}_3(2\%)$ to give, after recrystallisation from $\text{CHCl}_3/\text{Et}_2\text{O}(1:1)$, a red/brown solid (0.5g, 36% yield). I.r (Nujol Mull): 1625cm^{-1} (C=O), U.V/visible (DMSO)/ ϵ_{max} ($\text{mol}^{-1} \text{dm}^3 \text{cm}^{-1}$): 444nm (115). Analytical data in Tables 1.3, 3.3, 4.3. ^1H n.m.r (CDCl_3): 1.80(m, 4H), 2.30(s, 6H), 2.60(t, 4H), 2.70(s, 4H), 3.50(m, 4H), 4.40(d, 4H), 4.60(d, 4H).]

Preparation of 1,1'-Dimethylcobalticenium hexafluorophosphate →(5)

Anhydrous cobalt(II) bromide (34.4g, 150mmol) was added in small portions with continuous stirring to a solution of methylcyclopentadiene (33.16g, 410mmol) in pyrrolidine (150cm^3) at 0°C , under nitrogen. The solution was allowed to warm up to room temperature and stirred for a further 12 hours. The solvent was removed on a rotary evaporator, and the purple residue dissolved in hot water (500cm^3). The aqueous layer was extracted with $\text{Et}_2\text{O}(2 \times 100\text{cm}^3)$ to remove unreacted methylcyclopentadiene. Addition of $\text{KPF}_6(16-20\text{g})$ in hot water (100cm^3) precipitated a yellow solid which was collected and air dried (9.71g, 18% yield). I.r (KBr disc): $\{3100\text{cm}^{-1}, 1470\text{cm}^{-1}, 1450\text{cm}^{-1}\}$ (C-H), $1390\text{cm}^{-1}, 1370\text{cm}^{-1}, 1030\text{cm}^{-1}, 840\text{cm}^{-1}$ (PF_6). ^1H n.m.r (CD_3CN): 1.90(s, 6H), 5.50(s, 8H).

Preparation of 1,1-Dicarboxycobalticenium hexafluorophosphate → (6)

A solution of $\text{KMnO}_4(5.37\text{g}, 34\text{mmol})$, $\text{NaOH}(0.72\text{g}, 18\text{mmol})$ and 1,1'-dimethylcobalticenium hexafluorophosphate (5g, 13mmol) in $\text{H}_2\text{O}(100\text{cm}^3)$ were heated at 95°C for 3 hours. The hot mixture was filtered through a sinter to remove manganese dioxide. Addition of 6M HCl precipitated a yellow solid which was collected and air dried. The yellow solid was recrystallised from acetone (Yield 4.1g, 70%). I.r (Nujol Mull): 1710cm^{-1} (C=O), 840cm^{-1} (PF_6).

Preparation of 1,1'-Dichlorocarbonylcobalticenium hexafluorophosphate → (7)

1,1'-dicarboxycobalticenium hexafluorophosphate (2g, 4.8mmol) was dissolved in thionyl chloride (100cm³), and refluxed for 24 hours, under dry nitrogen. The solution was cooled to 0° C, and the precipitate collected under dry nitrogen, washed with dry benzene, and dried for 24 hours at 60° C/0.1mmHg, to give a yellow solid* (1.8g, ~ 3.9 mmol). I.r (Nujol mull): {1770cm⁻¹, 1740cm⁻¹} (C=O), 830cm⁻¹ (PF₆). *- literature¹³⁹ reveals this to be a mixture of PF₆/Cl salt in a ratio of 80% PF₆/20% Cl, and was taken as so in preparations.

Preparation of L⁵

A experimental method similar to that used for the preparation of L⁴ was used, except that acetonitrile was used as solvent.

Mass of (2) = 0.22g, 1.1mmol. Mass of (7) = 0.4g, ~ 1.1 mmol. Mass of triethylamine = 0.22g, 2.2mmol). Purification using gravitational chromatography on silica using MeOH(95%)/0.88 NH₃ (5%) removed unreacted starting material. Further eluting with MeOH(50%)/0.88 NH₃ (50%) gave after solvent removal a brown solid. The solid was dissolved in H₂O (10cm³), excess KPF₆ added, and stirred for 12 hours under nitrogen. The excess KPF₆ was filtered off and dry Et₂O added to precipitate a brown solid which was collected and dried *in vacuo* (0.32g, 10% yield). All analytical data in Tables 1.3, 2.3, 3.3. I.r (KBr disc): ~ 3000cm⁻¹ (C-H), 1664cm⁻¹ (C=O), 834cm⁻¹ (PF₆). U.V/visible (H₂O)/ ε_{max} (mol⁻¹ dm³ cm⁻¹): 408sh (1237).

Preparation of [Zn(L⁴)](CH₃COO)₂.2.5H₂O

The macrocycle L⁴ (0.20g, 0.45mmol) was dissolved in ethanol (10cm³), and added to stirring solution of zinc acetate (0.098g, 0.45mmol) in ethanol (10cm³). The mixture was refluxed for 12 hours under nitrogen, cooled, and filtered. The solvent was removed *in vacuo*, and the yellow solid recrystallised from CH₃CN/Et₂O (1:1), collected under nitrogen, and dried in a desiccator (0.18g, 60% yield). Analytical data is in Tables 1.3, 2.3, 3.3, 4.3.

Preparation of $[\text{Ni}(\text{L}^4)](\text{CH}_3\text{COO})_2 \cdot 4\text{H}_2\text{O}$

The macrocycle L^4 (0.24g, 0.55mmol) was dissolved in ethanol (10cm^3), and added to a stirring solution of nickel(II) acetate (0.13g, 0.55mmol). The resulting solution was refluxed for 12 hours under nitrogen. The solution was cooled and filtered, and the solvent removed *in vacuo*. The resulting solid was recrystallised from $\text{CH}_3\text{CN}/\text{Et}_2\text{O}$ (1:1), to give a very hygroscopic yellow solid, which was collected under nitrogen, and dried in a desiccator (0.23g, 62% yield). Analytical data is in Tables 1.3, 2.3, 3.3, 4.3.

Preparation of $[\text{Cu}(\text{L}^4)](\text{CH}_3\text{COO})_2 \cdot 3\text{H}_2\text{O}$

The macrocycle L^4 (0.19g, 0.43mmol) was dissolved in EtOH (10cm^3) and added to copper(II) acetate (0.08g, 0.43mmol), and refluxed for 12 hours under nitrogen. The solvent was cooled, filtered, and the solvent removed *in vacuo*. The resulting dark green solid was recrystallised from $\text{CH}_3\text{CN}/\text{Et}_2\text{O}$ (1:1). The green product was collected, and dried in a desiccator (0.22g, 76% yield). Analytical data is in Tables 2.3, 3.3, 4.3.

CHAPTER 4

The synthesis and study of two pyrrolidinyl pendant arm Triazamacrocycles

Section 1.4

Introduction

Triazamacrocycles such as 1,4,7-triazacyclononane have been shown by crystallography^{1 4 0, 1 4 1} and models, to be too small to accommodate metal ions in the ligand cavity. Therefore, facial co-ordination occurs with the metal to ligand ratio of 1:2 (*e.g.* $[\text{Ni}([\text{9}] \text{aneN}_3)_2]^{2+}$).^{1 4 2} Extensive studies of triazamacrocycles have been carried out by the group of Weighardt, especially complexes of the early transition metals.^{5 3} Only recently has the work on functionalised triazamacrocycles flourished, especially the readily prepared tri-N-substituted macrocycles. As usual mono-functionalised triazamacrocycles have been slow to develop, undoubtedly because of the more difficult synthetic routes. However, Studer and Kaden^{1 4 3} have prepared a mono-substituted triazamacrocycle containing a carboxylic pendant group. Recently, a triazamacrocycle containing a single pendant bipyridyl group has been prepared by Moore^{1 4 4}, along with the Ni^{2+} , and Zn^{2+} complexes, which adopt six and seven co-ordinate geometries respectively. Therefore, to extend this work two related pendant arm triazamacrocycles L^6 and L^7 have been synthesised, and their co-ordination chemistry studied (Figure 1.4), especially to see if tetrahedrally co-ordinating ligands could be produced.

Further functionalisation of L^6 was attempted to try and introduce two bulky substituents on the secondary nitrogens. It was hoped that metals could be "forced" into different geometries, by relief of steric crowding. However, as discussed in Section 9.4 this failed to give the desired product.

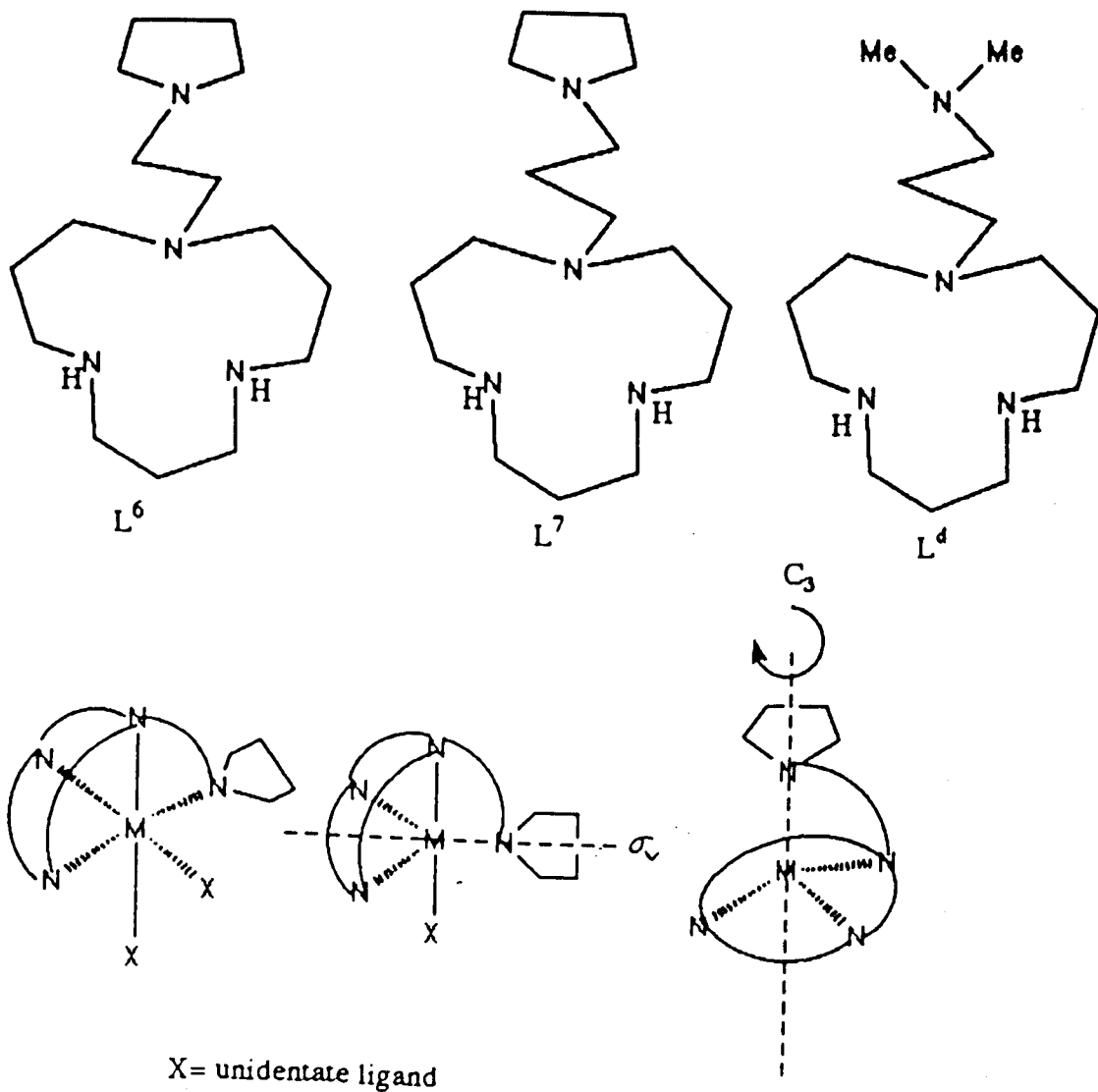


Figure 1.4

Diagrams of the ligands discussed in this chapter and some of the possible geometries of the metal complexes.

Results and Discussion

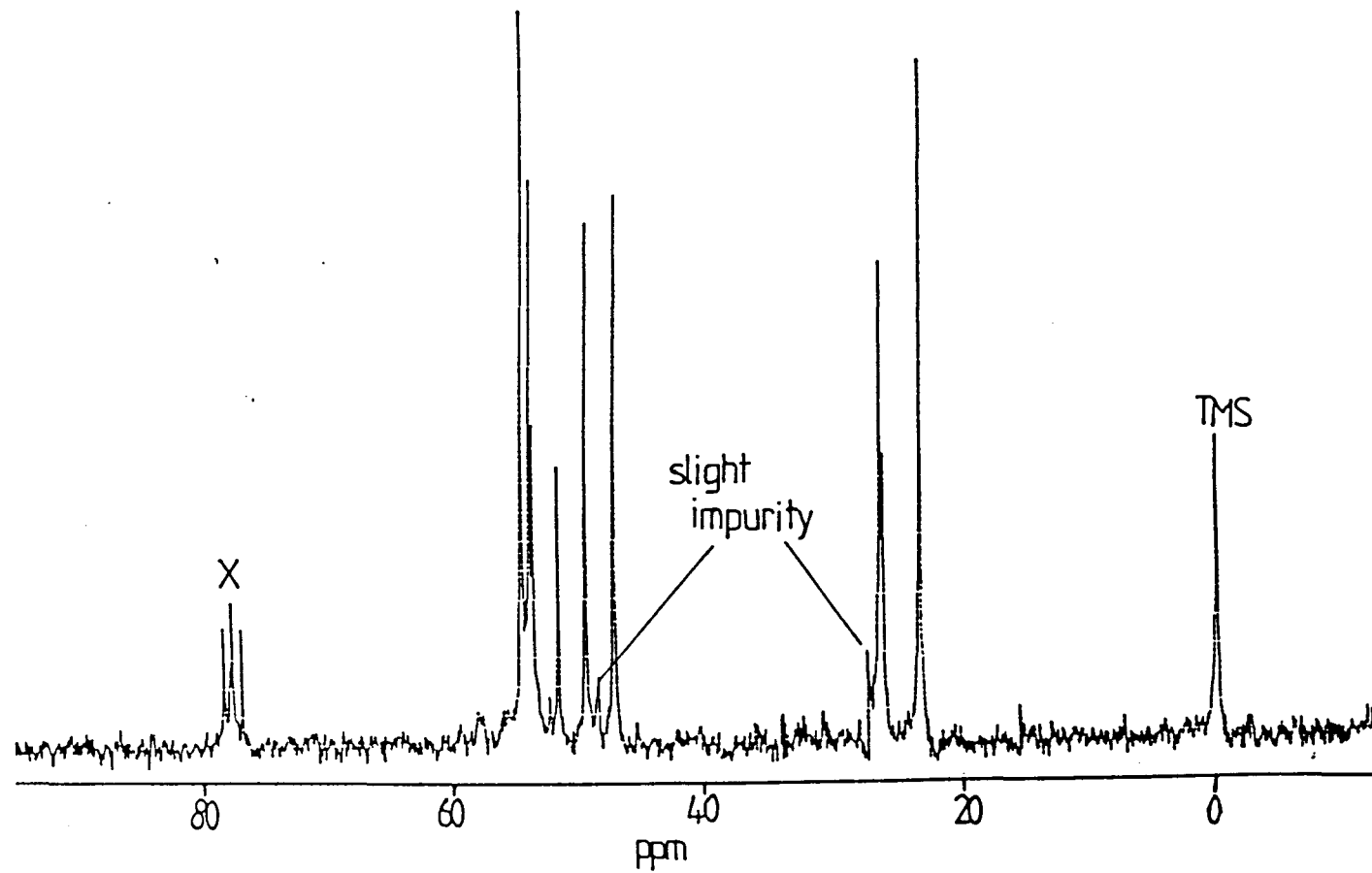
Section 2.4

The synthesis of L⁶ and L⁷

The synthesis of L⁶ and L⁷ is outlined in Scheme 1.4, and follows the general method of Richman and Atkins. The pendant arms are synthesised already in place; a method used in the production of pendant arm tetraazamacrocycles.^{1 4 5} The starting material amines (2) and (10) are prepared by the method described by Moore.^{1 4 5} Both amines are ditosylated in good yields, and converted to the corresponding sodium salts by reaction with sodium ethoxide (2mol). The sodium salts are coupled to form the ditosylated macrocycles, by reaction with the ditosyl derivative of 1,3-propandiol. The tosyl protecting groups are removed by acid hydrolysis, using concentrated H₂SO₄. The macrocycles are obtained as viscous oils in average yield (L⁶-12%, L⁷-24%). The structures are confirmed by C.I mass spectrometry, and ¹H and ¹³C n.m.r spectrometry (Table 1.4). A typical ¹³C n.m.r spectrum of a pendant pyrrolidinyl triazamacrocycle L⁶ is shown in Figure 2.4, revealing the symmetric nature of the molecule.

Figure 2.4

^1H decoupled ^{13}C n.m.r spectrum of L^6 in CDCl_3 (ref Me_4Si $\delta = 0$), run at 45.28 MHz. X = CDCl_3



Section 3.4

Metal complexes of L⁶ and L⁷ (General)

The metal complexes, except those of nickel(II), are prepared by mixing equimolar amounts of ethanolic solutions of ligand and $[M(\text{DMSO})_x](\text{ClO}_4)_2$ $\{M = \text{Cu, Co } x = 6; M = \text{Zn, } x = 4\}$. In the attempts to prepare cobalt(II) complexes the solutions are thoroughly degassed with nitrogen to remove traces of oxygen. Cobalt(III) complexes are prepared by bubbling oxygen through ethanolic solutions of the ligands and $[\text{Co(II)(DMSO)}_6](\text{ClO}_4)_2$. The nickel(II) complexes are prepared by adding equimolar amounts of ligands to $[\text{Ni(II)(DMSO)}_6](\text{ClO}_4)_2$ in acetonitrile, followed by addition of one equivalent of potassium thiocyanate. After removal of potassium perchlorate the metal complexes are obtained by addition of diethylether. F.A.B mass spectra of the complexes (Table 4.4) shows clusters of peaks corresponding to $[M(\text{L-H})]^+$, where $M = \text{Zn}^{2+}, \text{Cu}^{2+}, \text{Ni}^{2+}$ and $L = \text{L}^6$, and also $M = \text{Cu}^{2+}, L = \text{L}^7$. Also observed are clusters of peaks corresponding to $[M(\text{L})\text{OClO}_3]^+$, where $M = \text{Zn}^{2+}, L = \text{L}^6, \text{L}^7, M = \text{Ni}^{2+}, L = \text{L}^6$. Further analytical data are in Tables 2.4, 3.4 and 4.4.

Section 4.4

Synthesis of Zinc(II) and Copper(II) complexes of L⁶

The general formula of the complexes are $[M(\text{L}^6)\text{X}]^{n+}(\text{ClO}_4)_n$, where $M = \text{Zn}^{2+}, X = \text{ClO}_4, n = 1; M = \text{Cu}^{2+}, X = \text{OH}_2, n = 2$. The two complexes are obtained in good yields as white and dark green solids respectively. The copper(II) complex is very moisture sensitive, but the zinc(II) complex less so, and can be handled easily in the open air.

Insight into the structure of the zinc(II) complex was obtained by ¹³C n.m.r and X-ray crystallography (Section 13.4). The later confirms a five coordinate distorted trigonal bipyramidal configuration, with a bound perchlorate occupying the fifth co-ordination site. The ¹³C n.m.r (Figure 3.4) confirms the symmetric nature of the complex. Interestingly, a series of minor resonances are

also observed, suggesting another symmetric species present. These resonances are attributed to small amounts of DMSO solvate present which forms $[\text{Zn}(\text{L}^6)(\text{DMSO})]^{2+}$. Surprisingly conductivity experiments, in nitromethane, indicate a 1:2 electrolyte present, suggesting a weakly bound perchlorate group. Supporting evidence is gained by infrared spectroscopy, which shows no splitting of the absorbance around 620cm^{-1} , usually seen for bound perchlorate.¹⁴⁶

The conductivity of the copper(II) complex indicates a 1:2 electrolyte, as expected, but does not distinguish between the four and five co-ordination possibilities. This dilemma is further evident in the U.V/visible spectrum, where only a single broad absorbance at 600nm is observed. Infrared spectroscopy indicates the presence of lattice bound water by absorbances at 3400cm^{-1} and 523cm^{-1} ; the later being tentatively assigned to bound water.¹⁴⁷ The magnetic moment at room temperature is 1.7 B.M, in good agreement with a d^9 system. Owing to the five co-ordinate nature of the zinc(II) complex, and the similar radii of copper(II) and zinc(II) ($\text{Cu}^{2+} - 0.72\text{\AA}$, $\text{Zn}^{2+} - 0.69\text{\AA}$)¹⁴⁸, the copper(II) complex is postulated as being five co-ordinate with a bound water molecule.

Section 5.4

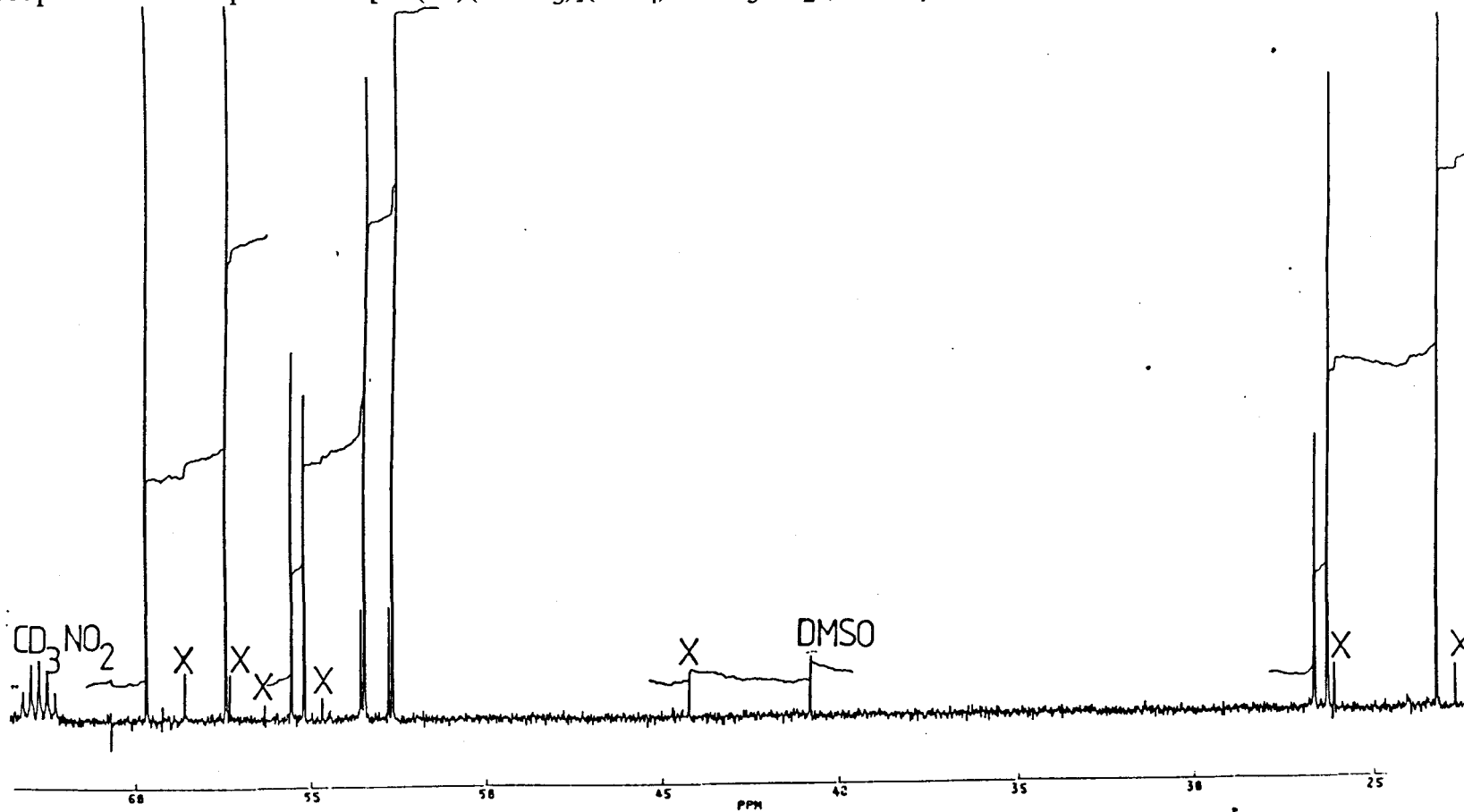
Synthesis of Nickel(II) and Cobalt(III) complexes of L^6

The nickel(II) complex produced is formulated as $[\text{Ni}(\text{L}^6\text{H})(\text{NCS})(\text{OCIO}_3)](\text{ClO}_4) \cdot 0.25 \text{Et}_2\text{O}$, and is a dark green solid. The pendant arm is protonated and non co-ordinating. Conductivity and U.V/visible spectroscopy are in full agreement with a five co-ordinate complex. The Infrared spectrum contains a single absorbance at 2070cm^{-1} , indicative of nitrogen bound thiocyanate, and further bands due to perchlorate ($\nu \sim 1100\text{cm}^{-1}$). Also two bands at 620cm^{-1} and 630cm^{-1} indicate a bound perchlorate. The magnetic moment at room temperature is 2.8 B.M which indicates a high spin complex, as seen in the analogous $[\text{Ni}(\text{trenMe})]^{2+}$ complex.¹⁴⁹

Attempts to prepare cobalt(II) complexes of L⁶ failed, even when solutions are thoroughly degassed with nitrogen. This suggests that the shorter pendant arm macrocycle is not able to stabilise the cobalt(II) centre sufficiently to stop oxidation. If oxygen is passed through the cobalt(II) solutions, a brown precipitate forms, which is formulated as [Co(III)₂(L⁶)₂O₂(OClO₃)(OH₂)](ClO₄)₃.2H₂O; and contains two cobalt(III) centres joined by a peroxo bridge. Conductivity experiments confirm a 1:3 electrolyte as expected, and a F.A.B spectrum contains a cluster of peaks, which can be assigned to [Co(III)L⁶-2H]⁺. Infrared spectroscopy also confirms the existence of lattice bound water, with absorbances at 3440cm⁻¹ and 1635cm⁻¹. No other detailed study of this complex was undertaken.

Figure 3.4

^1H decoupled ^{13}C n.m.r spectrum of $[\text{Zn}(\text{L}^6)(\text{OCIO}_3)](\text{ClO}_4)$ in CD_3NO_2 (ref Me_4Si $\delta = 0$) run at 100.62 MHz. X = minor species.



Section 6.4

Synthesis of Zinc(II), Copper(II), Cobalt(II) and Cobalt(III) complexes of L⁷

The formulae of the complexes are $[\text{Zn}(\text{L}^7)](\text{ClO}_4)_2$, and $[\text{M}(\text{L}^7\text{H})(\text{OCIO}_3)_x(\text{DMSO})_y](\text{ClO}_4)_z$, where $\text{M} = \text{Cu}(\text{II})$, $x=2$, $y=0$, $z=1$; $\text{M} = \text{Co}(\text{II})$, $x=0$, $y=2$, $z=3$, with the pendant arm protonated and uncoordinating.

The zinc(II) complex is obtained in good yield as white solid, and its structure verified by ^{13}C n.m.r spectroscopy and X-ray crystallography (Section 13.4). In contrast to the shorter pendant arm macrocycle L⁶, the zinc(II) complex adopts a tetrahedral geometry, as seen for a closely related pendant dimethylaminopropyl-triazamacrocycle L^d (Figure 1.4).¹⁵⁰ Again the ^{13}C n.m.r (Figure 4.4) confirms the symmetric nature of the complex.

The copper(II) complex is a dark green solid, and is extremely moisture sensitive and becomes "sticky" on exposure to air for long periods. The infrared spectrum indicates the existence of bound perchlorate by two resonances observed at 620cm^{-1} and 630cm^{-1} . Interestingly the U.V/visible spectrum contains only a single absorbance similar to $[\text{Cu}(\text{L}^6)]^{2+}$, but at longer wavelength (644nm), which is due to the smaller ligand field splitting caused by two oxygen bound perchlorates. The magnetic moment at room temperature is slightly lower than expected (1.44 B.M), which is possibly due to some interaction between two copper(II) ions, through a bridging perchlorate. This matter was not pursued further, but similar behaviour has been seen in other pendant arm macrocyclic systems.¹⁴⁵

The cobalt(II) macrocycle can be easily prepared as purple/red solid, which can be handled in air for short periods with no sign of oxidation. However, in solution oxidation occurs more rapidly, making measurement of the magnetic moment difficult. A U.V/visible spectrum can be obtained in a thoroughly nitrogen degassed nitromethane solution, in a well stoppered cell, and contains a single absorbance at 560nm, which is removed by the passage of oxygen through

the solution (Figure 5.4). The cobalt(III) complex obtained from passage of oxygen through a solution of the cobalt(II) complex is formulated as $[\text{Co(III)}_2(\text{L}^7\text{H})(\text{DMSO})_2\text{O}_2(\text{OCIO}_3)(\text{OH}_2)_2](\text{ClO}_4)_3 \cdot 4\text{H}_2\text{O}$ by elemental analysis. Surprisingly the formula suggests two peroxo bridged cobalt(III) centres, but only one macrocycle. Conductivity experiments confirm the 1:3 electrolyte, and infrared spectroscopy the existence of water by absorbances at 3440cm^{-1} , 1600cm^{-1} . The cobalt(III) complex fits in well with the starting material cobalt(II) complex, but why only macrocycle should be present is not clear. A possible explanation is that the cobalt(II) complex is stable enough for only a partial oxidation product to be observed. The nature of the cobalt(III) complex was not pursued further.

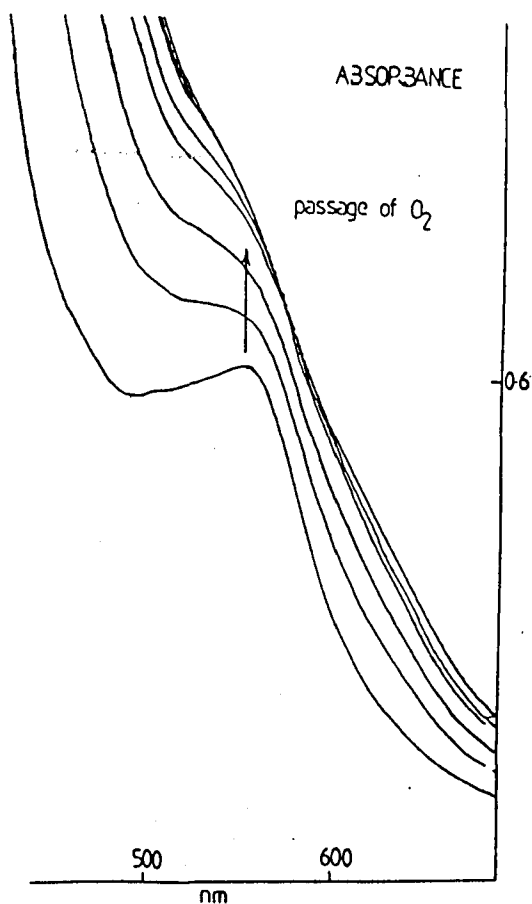
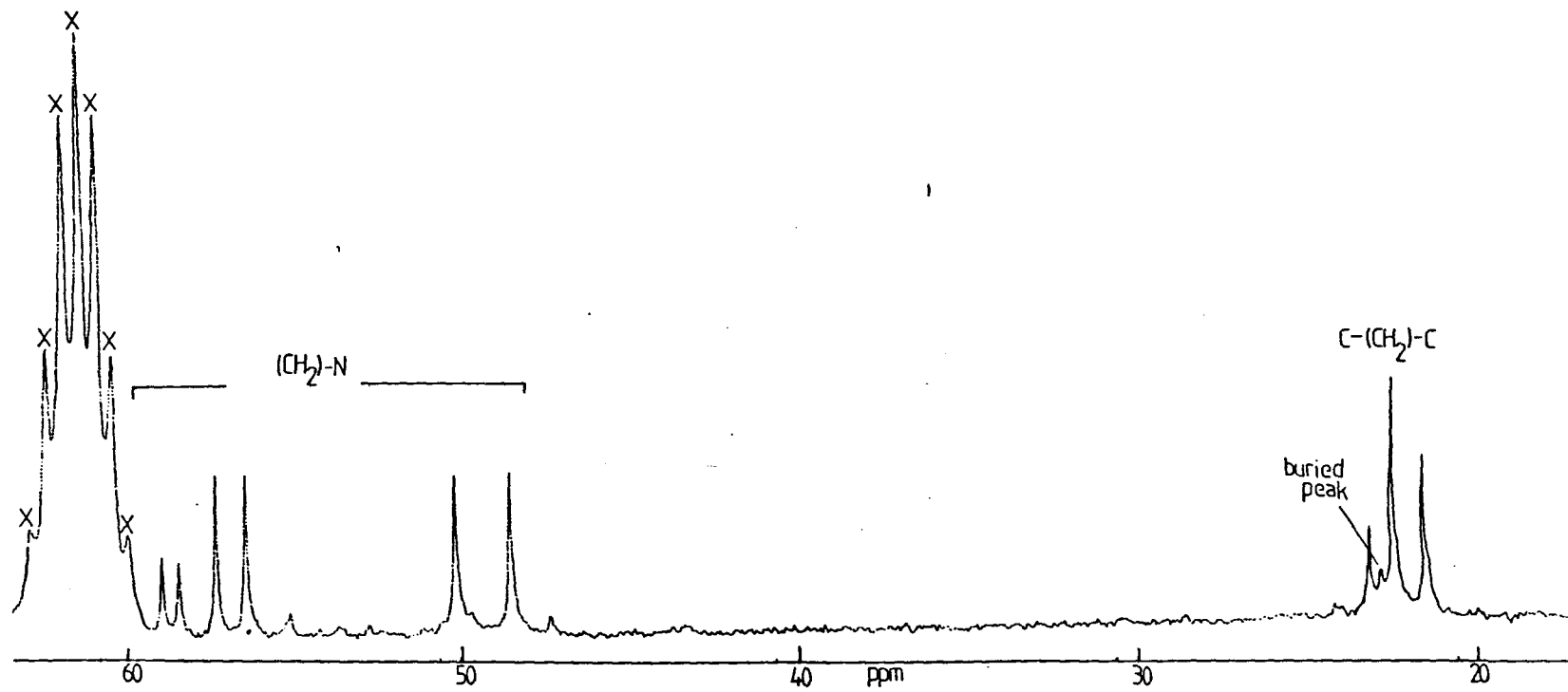


Figure 5.4

A U.V/visible spectrum of $[\text{Co(II)}(\text{L}^7\text{H})(\text{DMSO})_2](\text{ClO}_4)_3$ in CH_3NO_2
(conc = 4.7 mM)

Figure 4.4

^1H decoupled ^{13}C n.m.r spectrum of $[\text{Zn}(\text{L}^7)](\text{ClO}_4)_2$ in CD_3NO_2 (Me_4Si $\delta = 0$) run at 45.28MHz. X = solvent resonances.



Section 7.4

Attempted synthesis of a nickel(II) complex of L⁷

The nickel(II) complex obtained is formulated as $[\text{Ni}_2(\text{L}^7\text{H})_2(\text{OCIO}_3)_2(\text{NCS})](\text{ClO}_4)_3 \cdot 5\text{H}_2\text{O}$, but also containing one mole of potassium perchlorate impurity. Again the pendant arm is protonated and unco-ordinating as with the copper(II) and cobalt(II) complexes. The dimeric nature of the complex is evident from the F.A.B mass spectrum, where a cluster of peaks are observed corresponding to $[\text{Ni}_2(\text{L}^7)_2(\text{OCIO}_3)_2-\text{H}]^+$ (Figure 7.4). The infrared spectrum contains an absorbance at 2090cm^{-1} which is assigned to N bound non bridging thiocyanate.¹⁴⁷ Other absorbances at 1100cm^{-1} are assigned to perchlorate, with two absorbances at 630cm^{-1} and 620cm^{-1} to bound perchlorate.

The similarity of the U.V/visible spectrum to that of $[\text{Ni}(\text{L}^6\text{H})(\text{NCS})(\text{OCIO}_3)]^+$ indicates five co-ordinate nickel(II) centres. Therefore the proposed structure is two five co-ordinate nickel(II) centres bridged by a perchlorate group (Figure 6.4).

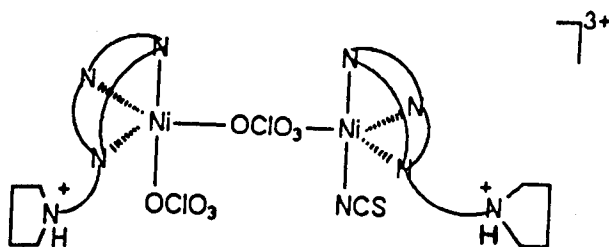


Figure 6.4

The proposed structure of the nickel(II) complex of L⁷

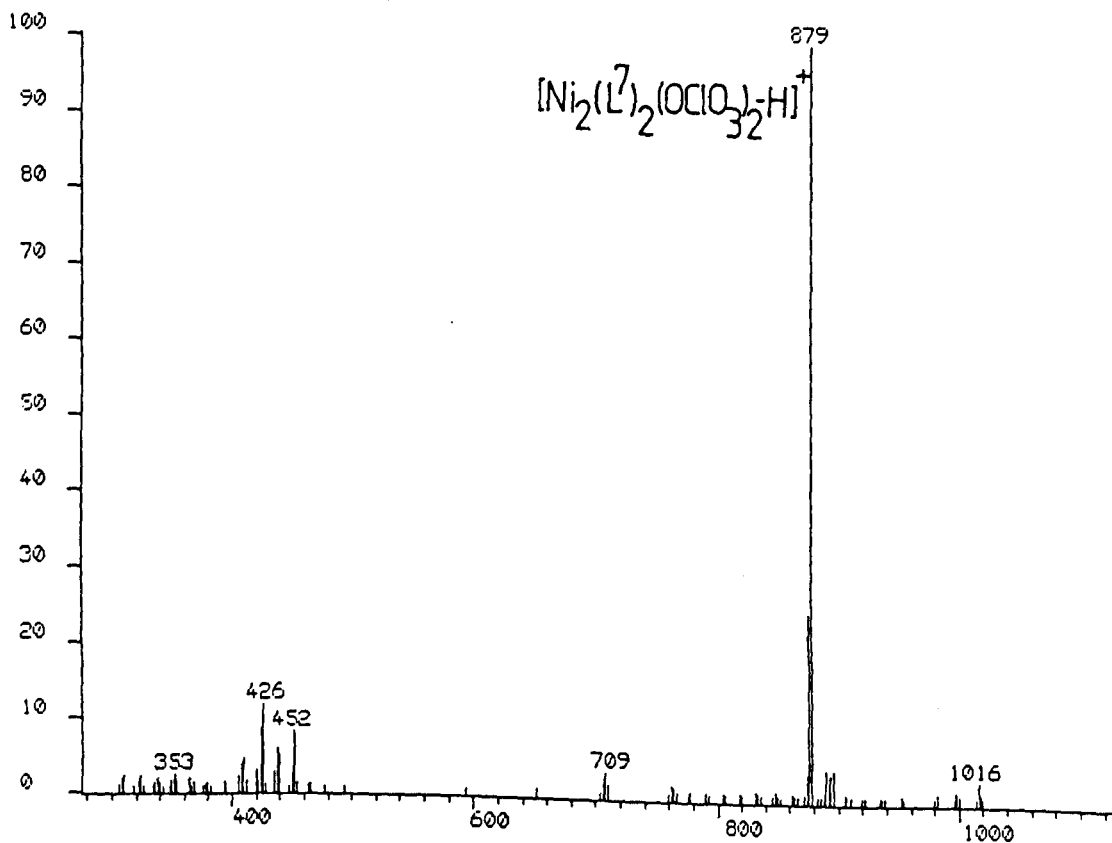


Figure 7.4

F.A.B mass spectrum of $Ni_2(L')_2(OCIO_3)_2-H]^+$ in *m*-nitrobenzylalcohol matrix.

The slightly low magnetic moment ($\mu_{eff} = 4.4$ B.M) is probably due to some interaction between the two nickel(II) centres via the bridging perchlorate. The failure to remove all the potassium perchlorate is unclear, considering its insolubility in acetonitrile.

Section 8.4

Crystal structures of $[\text{Zn}(\text{L}^6)\text{OClO}_3]^+$ and $[\text{Zn}(\text{L}^7)]^{2+}$

The structures of $[\text{Zn}(\text{L}^6)\text{OClO}_3]^+$ and $[\text{Zn}(\text{L}^7)]^{2+}$ are shown in Figure 8.4 and Figure 9.4 respectively. These two structures are compared with that of $[\text{ZnL}^d]^{2+}$, in Figure 10.4. Clearly the shorter arm ligand L^6 gives a distorted trigonal bipyramidal geometry, whilst the "longer" arm ligand a pseudo tetrahedral geometry. The high R factor of $[\text{Zn}(\text{L}^7)]^{2+}$, discussed in Section 13.4, means that only a semi qualitative comparison to the structure of $[\text{ZnL}^d]^{2+}$ will be given. All experimental details about the two structures are given in Section 13.4. Bond lengths and angles are in Table 6.4 and Table 7.4.

The average Zn-N bond lengths for the macrocyclic ring of $[\text{Zn}(\text{L}^6)\text{OClO}_3]^+$ are $2.041(10)\text{\AA}$, in good agreement to that found by Kimura (average Zn-N: $2.073(5)\text{\AA}$), in a similar five co-ordinate single phenolic pendant arm triazamacrocycle.^{1 5 1} The Zn-OClO₃ bond length of $2.680(10)\text{\AA}$, is slightly longer than that for Zn-OH₂ ($2.219(4)\text{\AA}$) of Kimura's structure, but can be attributed to the bulkiness of the perchlorate group. The distortion from a regular trigonal bipyramid is evident from the O(21)-Zn-N(1) bond angle of $162.1(2)^\circ$, and N(2)-Zn-N(4) and N(4)-Zn-N(3) bond angles of $122.9(7)^\circ$ and $99.8(6)^\circ$ respectively. Angles within the macrocyclic differ greatly from the expected tetrahedral angle 109.47° , and fall within the range of C(1)-N(1)-C(9): $105.6(12)^\circ$ ---- C(7)-C(8)-C(9): $129.00(25)^\circ$, showing how distortion of the macrocyclic ring occurs upon co-ordination.

The average Zn-N bond lengths for the macrocyclic ring of $[\text{Zn}(\text{L}^7)]^{2+}$ are $2.05(4)\text{\AA}$, which is comparable with the Zn-N bond lengths found in $[\text{ZnL}^d]^{2+}$ {average = $1.997(10)\text{\AA}$ }, especially in view of the errors involved. Both values are in good agreement with the bond lengths found by Shaber^{1 5 2} in $[\text{Zn}([\text{12}] \text{aneN}_3)\text{Br}]^+$ {average = $2.039(10)\text{\AA}$ }. The distorted tetrahedral geometry is evident in the N(11)-Zn-N(13), N(11)-Zn-N(12), N(12)-Zn-N(13), N(11)-Zn-N(14), N(12)-Zn-N(14), N(13)-Zn-N(14), bond angles of $99.50(15)^\circ$,

103.00(12)°, 111.10(16)°, 115.10(10)°, 116.80(14)° respectively. Again as seen in $[\text{Zn}(\text{L}^6)\text{OClO}_3]^+$, angles within the macrocyclic ring differ from the expected tetrahedral angle, C(101)-N(11)-C(109):102.20(31)°, C(103)-N(12)-C(104):113.60(27)°. But ignoring atoms with high thermal parameters (C104, C106, N13), the ring of L^7 is less distorted by co-ordination than for the shorter arm complex of L^6 .

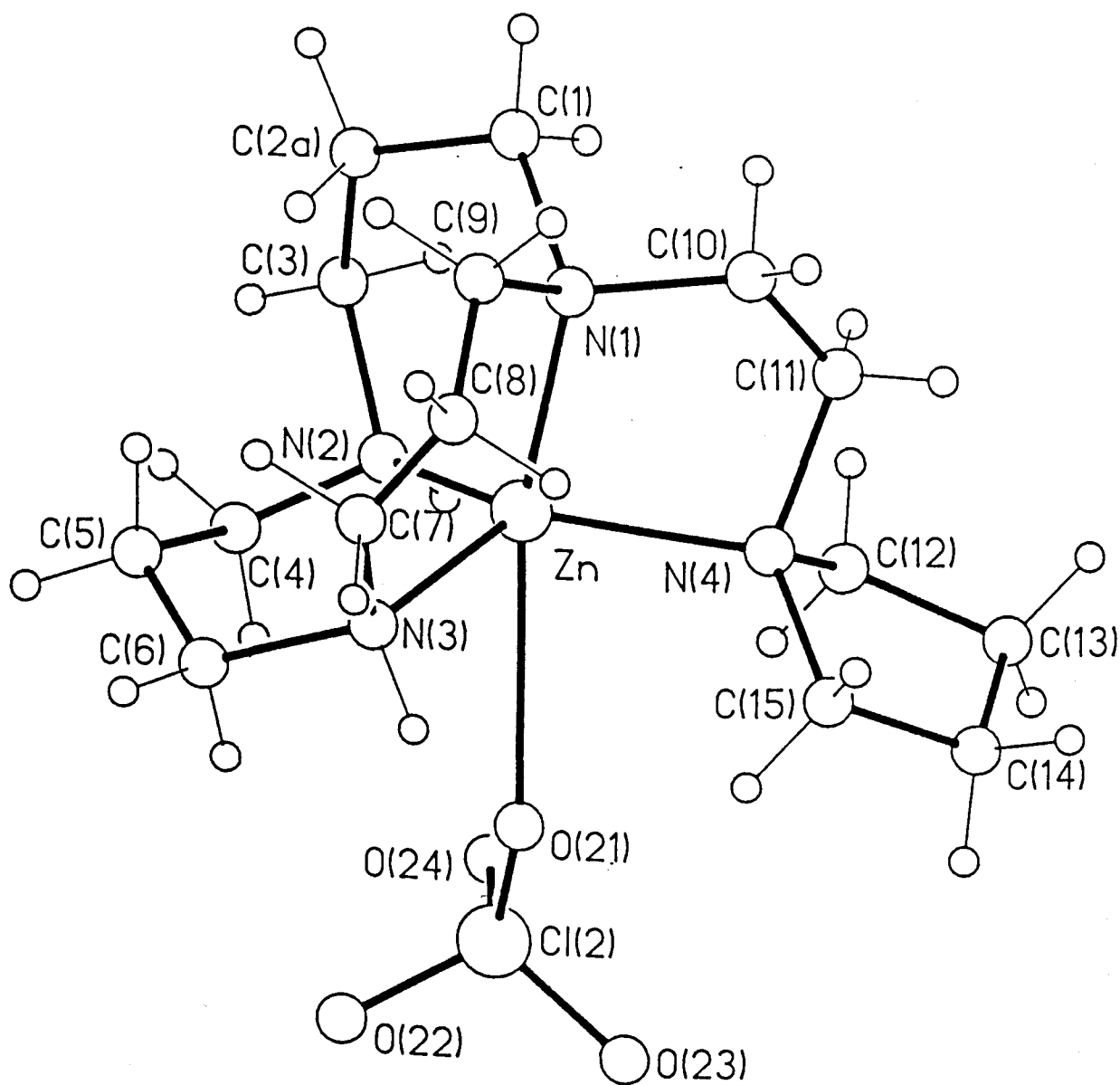


Figure 8.4

Crystal structure of $[\text{Zn}(\text{L}^6)\text{OClO}_3]^+$ showing the atomic numbering scheme and a perchlorate group occupying the fifth co-ordination site. The non coordinated perchlorate is omitted for clarity.

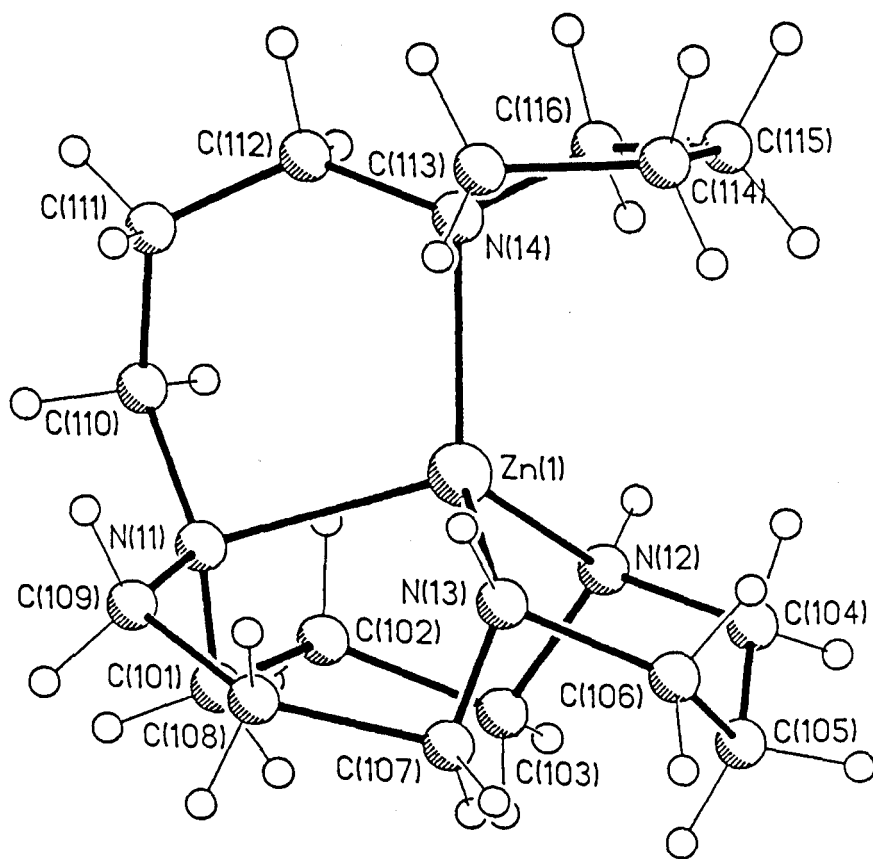


Figure 9.4

Crystal structure of $[\text{Zn}(\text{L}^7)]^{2+}$ showing the atomic numbering scheme. Two unco-ordinated perchlorates are omitted for clarity.

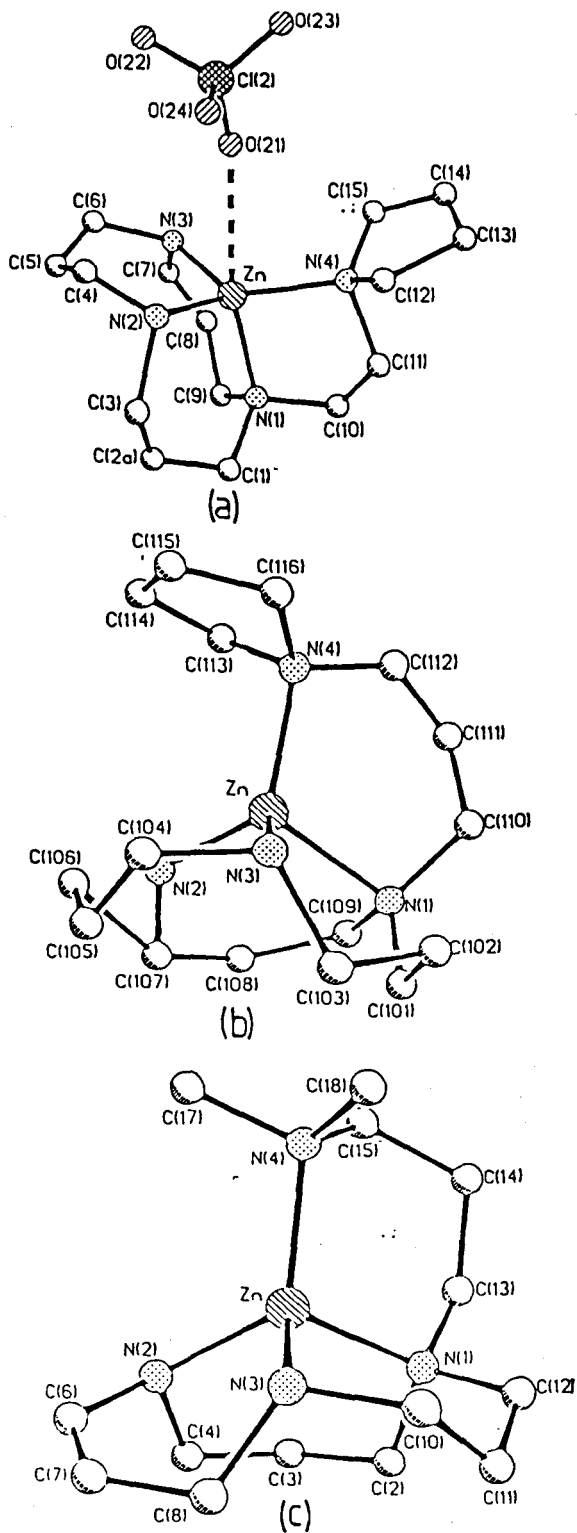


Figure 10.4

Crystal structures of (a) $[\text{Zn}(\text{L}^6)\text{OCIO}_3]^+$, (b) $[\text{Zn}(\text{L}^7)]^{2+}$, (c) $[\text{Zn}(\text{L}^d)]^{2+}$.
Hydrogens omitted for clarity.

Table 6.4

Bond lengths and angles for $[\text{Zn}(\text{L}^e)\text{OClO}_3]^+$

Bond lengths (Å)

Zn-N(1)	2.088(9)	Zn-N(2)	1.971(12)
Zn-N(3)	2.063(12)	Zn-N(4)	2.035(7)
Cl(1)-O(11)	1.437(21)	Cl(1)-O(12)	1.420(9)
Cl(1)-O(13)	1.356(11)	Cl(1)-O(14)	1.341(18)
Cl(2)-O(21)	1.430	Cl(2)-O(22)	1.430
Cl(2)-O(23)	1.430	Cl(2)-O(24)	1.430
N(1)-C(1)	1.548(28)	N(1)-C(9)	1.486(27)
N(1)-C(10)	1.506(17)	N(2)-C(3)	1.450(33)
N(2)-C(4)	1.338(18)	N(3)-C(6)	1.605(19)
N(3)-C(7)	1.508(24)	N(4)-C(11)	1.535(16)
N(4)-C(12)	1.369(32)	N(4)-C(15)	1.499(32)
C(1)-C(2a)	1.544(28)	C(1)-C(2b)	1.684(50)
C(2a)-C(2b)	1.504(51)	C(2a)-C(3)	1.617(38)
C(2b)-C(3)	1.754(56)	C(4)-C(5)	1.675(40)
C(5)-C(6)	1.273(44)	C(7)-C(8)	1.166(37)
C(8)-C(9)	1.280(32)	C(10)-C(11)	1.249(19)
C(12)-C(13)	1.464(34)	C(13)-C(14)	1.429(44)
C(14)-C(15)	1.507(43)		

Bond angles (deg.)

N(1)-Zn-N(2)	110.4(6)	N(1)-Zn-N(3)	99.8(6)
N(2)-Zn-N(3)	106.8(5)	N(1)-Zn-N(4)	87.8(3)
N(2)-Zn-N(4)	122.9(7)	N(3)-Zn-N(4)	123.3(7)
O(11)-Cl(1)-O(12)	112.7(15)	O(11)-Cl(1)-O(13)	107.2(15)
O(12)-Cl(1)-O(13)	108.3(6)	O(11)-Cl(1)-O(14)	106.4(11)
O(12)-Cl(1)-O(14)	105.3(15)	O(13)-Cl(1)-O(14)	117.0(15)
O(21)-Cl(2)-O(22)	109.5	O(21)-Cl(2)-O(23)	109.5
O(22)-Cl(2)-O(23)	109.5	O(21)-Cl(2)-O(24)	109.5
O(22)-Cl(2)-O(24)	109.5	O(23)-Cl(2)-O(24)	109.5
Zn-N(1)-C(1)	110.9(12)	Zn-N(1)-C(9)	112.9(12)
C(1)-N(1)-C(9)	105.6(12)	Zn-N(1)-C(10)	99.6(7)
C(1)-N(1)-C(10)	95.4(17)	C(9)-N(1)-C(10)	130.7(19)
Zn-N(2)-C(3)	116.2(14)	Zn-N(2)-C(4)	116.6(11)
C(3)-N(2)-C(4)	103.3(16)	Zn-N(3)-C(6)	105.6(11)
Zn-N(3)-C(7)	109.1(10)	C(6)-N(3)-C(7)	118.4(14)
Zn-N(4)-C(11)	102.3(7)	Zn-N(4)-C(12)	119.6(17)
C(11)-N(4)-C(12)	92.4(18)	Zn-N(4)-C(15)	114.1(13)
C(11)-N(4)-C(15)	126.0(14)	C(12)-N(4)-C(15)	101.9(15)
N(1)-C(1)-C(2a)	114.6(15)	N(1)-C(1)-C(2b)	117.8(21)
C(2a)-C(1)-C(2b)	55.3(19)	C(1)-C(2a)-C(2b)	67.1(21)
C(1)-C(2a)-C(3)	122.2(19)	C(2b)-C(2a)-C(3)	68.3(23)
C(1)-C(2b)-C(2a)	57.6(19)	C(1)-C(2b)-C(3)	107.2(27)
C(2a)-C(2b)-C(3)	58.9(21)	N(2)-C(3)-C(2a)	118.7(21)
N(2)-C(3)-C(2b)	112.8(25)	C(2a)-C(3)-C(2b)	52.8(19)
N(2)-C(4)-C(5)	116.3(13)	C(4)-C(5)-C(6)	113.4(16)
N(3)-C(6)-C(5)	119.7(15)	N(3)-C(7)-C(8)	124.7(21)
C(7)-C(8)-C(9)	129.0(25)	N(1)-C(9)-C(8)	114.8(17)
N(1)-C(10)-C(11)	126.4(11)	N(4)-C(11)-C(10)	115.9(14)
N(4)-C(12)-C(13)	114.2(21)	C(12)-C(13)-C(14)	97.1(21)
C(13)-C(14)-C(15)	112.1(27)	N(4)-C(15)-C(14)	102.8(23)

Table 7.4

Bond lengths and angles for $[\text{Zn}(\text{L}^7)]^{2+}$

Bond lengths (Å)

Zn(1)-N(11)	2.150 (36)	Zn(1)-N(12)	2.134 (36)
Zn(1)-N(13)	1.872 (30)	Zn(1)-N(14)	2.015 (23)
Zn(2)-N(21)	1.884 (35)	Zn(2)-N(22)	2.006 (35)
Zn(2)-N(23)	2.004 (26)	Zn(2)-N(24)	2.022 (38)
Cl(1)-O(11)	1.312 (19)	Cl(1)-O(12)	1.312 (23)
Cl(1)-O(13)	1.312 (18)	Cl(1)-O(14)	1.312 (23)
Cl(2)-O(21)	1.312 (30)	Cl(2)-O(22)	1.312 (25)
Cl(2)-O(23)	1.312 (20)	Cl(2)-O(24)	1.312 (32)
Cl(3)-O(31)	1.312 (18)	Cl(3)-O(32)	1.312 (24)
Cl(3)-O(33)	1.312 (19)	Cl(3)-O(34)	1.312 (26)
Cl(4)-O(41)	1.312 (23)	Cl(4)-O(42)	1.312 (17)
Cl(4)-O(43)	1.312 (27)	Cl(4)-O(44)	1.312 (25)
N(11)-C(101)	1.333 (56)	N(11)-C(109)	1.470 (47)
N(11)-C(110)	1.489 (55)	N(12)-C(103)	1.561 (42)
N(12)-C(104)	1.470 (51)	N(13)-C(106)	1.470 (73)
N(13)-C(107)	1.235 (48)	N(14)-C(112)	1.383 (47)
N(14)-C(113)	1.556 (42)	N(14)-C(116)	1.420 (44)
C(101)-C(102)	1.596 (60)	C(102)-C(103)	1.486 (56)
C(104)-C(105)	1.288 (53)	C(105)-C(106)	1.540 (70)
C(106)-C(107)	1.891 (71)	C(107)-C(108)	1.540 (46)
C(108)-C(109)	1.540 (49)	C(110)-C(111)	1.424 (63)
C(111)-C(112)	1.360 (63)	C(113)-C(114)	1.446 (54)
C(114)-C(115)	1.383 (59)	C(115)-C(116)	1.382 (54)
N(21)-C(201)	1.525 (56)	N(21)-C(209)	1.555 (54)
N(21)-C(210)	1.394 (55)	N(22)-C(203)	1.512 (52)
N(22)-C(204)	1.470 (68)	N(23)-C(206)	1.470 (38)
N(23)-C(207)	1.425 (43)	N(24)-C(212)	1.496 (59)
N(24)-C(213)	1.394 (54)	N(24)-C(216)	1.583 (58)
C(201)-C(202)	1.528 (57)	C(202)-C(203)	1.315 (53)
C(204)-C(205)	1.540 (70)	C(205)-C(206)	1.540 (41)
C(207)-C(208)	1.400 (49)	C(208)-C(209)	1.538 (55)
C(210)-C(211)	1.344 (59)	C(211)-C(212)	1.411 (63)
C(213)-C(214)	1.418 (70)	C(214)-C(215)	1.340 (74)
C(215)-C(216)	1.533 (63)		

Table 7.4 (contd)

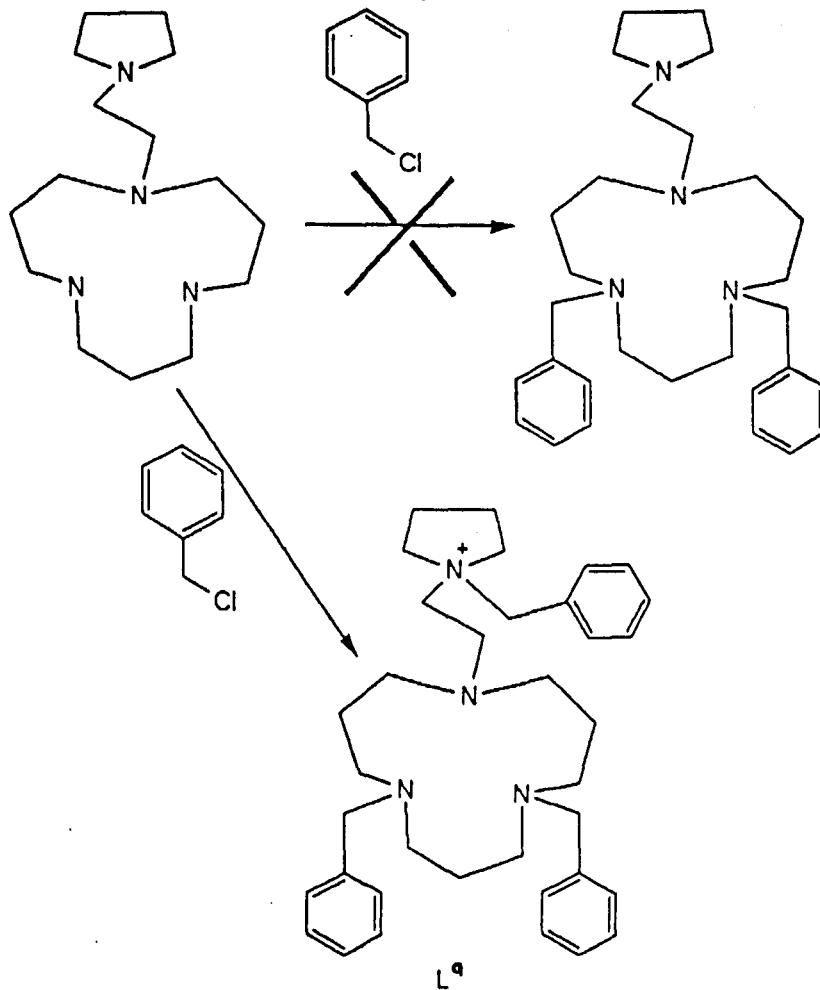
Bond angles (°)

N(11)-Zn(1)-N(12)	103.0(12)	N(11)-Zn(1)-N(13)	99.5(15)
N(12)-Zn(1)-N(13)	111.1(16)	N(11)-Zn(1)-N(14)	109.1(12)
N(12)-Zn(1)-N(14)	115.1(10)	N(13)-Zn(1)-N(14)	116.8(14)
N(21)-Zn(2)-N(22)	108.7(14)	N(21)-Zn(2)-N(23)	109.7(13)
N(22)-Zn(2)-N(23)	97.7(15)	N(21)-Zn(2)-N(24)	102.6(15)
N(22)-Zn(2)-N(24)	120.8(15)	N(23)-Zn(2)-N(24)	117.1(13)
O(11)-Cl(1)-O(12)	109.5(16)	O(11)-Cl(1)-O(13)	109.5(13)
O(12)-Cl(1)-O(13)	109.5(19)	O(11)-Cl(1)-O(14)	109.5(15)
O(12)-Cl(1)-O(14)	109.5(15)	O(13)-Cl(1)-O(14)	109.5(17)
O(21)-Cl(2)-O(22)	109.5(23)	O(21)-Cl(2)-O(23)	109.5(22)
O(22)-Cl(2)-O(23)	109.5(20)	O(21)-Cl(2)-O(24)	109.5(21)
O(22)-Cl(2)-O(24)	109.5(23)	O(23)-Cl(2)-O(24)	109.5(23)
O(31)-Cl(3)-O(32)	109.5(18)	O(31)-Cl(3)-O(33)	109.5(18)
O(32)-Cl(3)-O(33)	109.5(18)	O(31)-Cl(3)-O(34)	109.5(18)
O(32)-Cl(3)-O(34)	109.5(17)	O(33)-Cl(3)-O(34)	109.5(18)
O(41)-Cl(4)-O(42)	109.5(16)	O(41)-Cl(4)-O(43)	109.5(17)
O(42)-Cl(4)-O(43)	109.5(16)	O(41)-Cl(4)-O(44)	109.5(18)
O(42)-Cl(4)-O(44)	109.5(17)	O(43)-Cl(4)-O(44)	109.5(19)
Zn(1)-N(11)-C(101)	106.5(27)	Zn(1)-N(11)-C(109)	105.4(24)
C(101)-N(11)-C(109)	102.2(31)	Zn(1)-N(11)-C(110)	97.2(24)
C(101)-N(11)-C(110)	119.4(35)	C(109)-N(11)-C(110)	124.0(32)
Zn(1)-N(12)-C(103)	108.6(21)	Zn(1)-N(12)-C(104)	96.0(23)
C(103)-N(12)-C(104)	113.6(27)	Zn(1)-N(13)-C(106)	105.1(36)
Zn(1)-N(13)-C(107)	122.2(30)	C(106)-N(13)-C(107)	88.3(39)
Zn(1)-N(14)-C(112)	105.1(22)	Zn(1)-N(14)-C(113)	110.4(18)
C(112)-N(14)-C(113)	116.2(27)	Zn(1)-N(14)-C(116)	110.2(19)
C(112)-N(14)-C(116)	107.7(27)	C(113)-N(14)-C(116)	107.2(24)
N(11)-C(101)-C(102)	104.7(34)	C(101)-C(102)-C(103)	109.2(33)
N(12)-C(103)-C(102)	103.6(30)	N(12)-C(104)-C(105)	121.5(38)
C(104)-C(105)-C(106)	111.4(43)	N(13)-C(106)-C(105)	123.8(49)
N(13)-C(106)-C(107)	40.8(23)	C(105)-C(106)-C(107)	110.7(40)
N(13)-C(107)-C(106)	51.0(31)	N(13)-C(107)-C(108)	99.0(33)
C(106)-C(107)-C(108)	149.8(34)	C(107)-C(108)-C(109)	129.9(29)
N(11)-C(109)-C(108)	118.0(28)	N(11)-C(110)-C(111)	119.3(37)
C(110)-C(111)-C(112)	117.2(42)	N(14)-C(112)-C(111)	129.1(37)
N(14)-C(113)-C(114)	98.1(28)	C(113)-C(114)-C(115)	110.0(35)
C(114)-C(115)-C(116)	112.0(37)	N(14)-C(116)-C(115)	103.2(30)
Zn(2)-N(21)-C(201)	110.2(26)	Zn(2)-N(21)-C(209)	109.1(25)
C(201)-N(21)-C(209)	107.8(32)	Zn(2)-N(21)-C(210)	121.5(29)
C(201)-N(21)-C(210)	103.7(32)	C(209)-N(21)-C(210)	103.7(33)
Zn(2)-N(22)-C(203)	106.9(23)	Zn(2)-N(22)-C(204)	96.8(32)
C(203)-N(22)-C(204)	118.0(37)	Zn(2)-N(23)-C(206)	110.5(22)
Zn(2)-N(23)-C(207)	114.9(21)	C(206)-N(23)-C(207)	129.9(28)
Zn(2)-N(24)-C(212)	109.0(26)	Zn(2)-N(24)-C(213)	116.2(27)
C(212)-N(24)-C(213)	126.3(37)	Zn(2)-N(24)-C(216)	109.0(26)
C(212)-N(24)-C(216)	99.0(31)	C(213)-N(24)-C(216)	92.4(30)
N(21)-C(201)-C(202)	117.5(35)	C(201)-C(202)-C(203)	117.4(37)
N(22)-C(203)-C(202)	116.9(35)	N(22)-C(204)-C(205)	126.1(48)
C(204)-C(205)-C(206)	116.7(36)	N(23)-C(206)-C(205)	93.2(25)
N(23)-C(207)-C(208)	117.3(29)	C(207)-C(208)-C(209)	118.1(31)
N(21)-C(209)-C(208)	117.6(33)	N(21)-C(210)-C(211)	117.1(38)
C(210)-C(211)-C(212)	123.3(40)	N(24)-C(212)-C(211)	123.2(37)
N(24)-C(213)-C(214)	102.2(37)	C(213)-C(214)-C(215)	117.7(47)
C(214)-C(215)-C(216)	94.8(41)	N(24)-C(216)-C(215)	107.0(35)

Section 9.4

Attempted functionalisation of L⁶

As discussed earlier (page 119) further functionalisation of the ligand L⁶ was attempted, by the addition of excess benzyl chloride (Scheme 2.4).



Scheme 2.4

However, ¹³C n.m.r (Table 1.4) contains more resonances than expected, and so it is evident that quaternarisation occurs, which is slightly surprising considering the bulkiness of the benzyl group. Inspection of the breakdown products in the mass spectrum confirms that quaternisation occurs at the pyrrolidinyl nitrogen. Synthesis of metal complexes of L⁹ were not attempted.

Conclusions

The two single pendant arm triazamacrocycles L^6 and L^7 can be synthesised in reasonable yields by using Richman-Atkins preparations. Interestingly, the two macrocycles can impose different geometries on zinc(II); the ligand L^6 a distorted trigonal bipyramid, and L^7 a distorted tetrahedron. The change in geometry is due to the increase in pendant arm length and not the pyrrolidinyl group, as demonstrated by the similarity of the $[Zn(L^7)]^{2+}$ and $[Zn(L^d)]^{2+}$ structures. The effect of the increase in the pendant arm length is further evident in the stabilisation of cobalt(II), where the shorter arm macrocycle is unable to stop oxidation to cobalt(III). The impurity of the nickel(II) complex of L^7 makes comparison to that of L^6 difficult, but further work (crystallographic) may prove the dimeric / monomeric nature of the two complexes. Whether further functionalisations of the two macrocycles can produce changes in geometry will only be evident after successful modifications.

Compound	C-(CH ₂)-C	-(CH ₂)-N, + Ph-(CH ₂)
L ⁷	23.52(2C), 25.43(1C) 26.35(2C)	47.39(2C), 49.53(2C), 50.52(1C), 53.02(2C) 54.36(3C), 54.86(1C)
L ⁶	23.41(2C), 26.30(1C) 26.53(2C)	47.28(2C), 49.41(2C), 51.58(1C), 53.56(1C) 53.85(2C), 54.51(2C)
L ^a	20.84(2C), 21.27(2C) 23.11(1C)	48.49(2C), 48.85(2C), 49.22(1C), 50.56(2C), 55.89(1C) 58.92(2C), 60.89(2C), 63.12(1C), 126.84(2C), 128.19(4C)
[ZnL] ^{2+a}	22.85(2C), 23.74(2C) 24.098(1C)	49.87(2C), 51.49(2C), 56.38(2C), 57.76(2C), 58.65(1C) 59.80(1C)
[ZnL ⁶ OCO ₃] ^{+a}	22.76(*), 23.26(2C) 26.11(*), 26.29(2C) 26.66(1C)	40.87(*), 44.28(*), 52.82(*), 53.51(2C), 53.58(*), 53.63(2C), 54.72(*) 55.23(1C), 55.60(1C), 56.36(*), 57.48(2C), 58.64(*), 59.74(2C)

Table 1.4

¹H decoupled ¹³C n.m.r spectra in CDCl₃ unless stated (ref Me₄Si delta = 0) (a) CD₃NO₂ (ref Me₄Si delta = 0). (*) minor species.

Compound	Magnetic Moment (B.M) ^b	λ max(nm) (ϵ_{max} mol ⁻¹ dm ³ cm ⁻¹)		Molar Conductivity $\sigma_{\text{mol}^{-1}\text{cm}^2}^{-1}$
		CH ₃ CN	CH ₃ NO ₂	
[Co(II)L ⁷ (DMSO) ₂](ClO ₄) ₃ ·4H ₂ O	*		560(112)	*
[Co(III) ₂ (L ⁷ H)(DMSO) ₂ O ₂ (OCIO ₃) ₃ (OH ₂) ₂](ClO ₄) ₃ ·4H ₂ O	diamagnetic	468(sh,340)		217(1:3 electrolyte) ^a
[Cu(II)(L ⁷ H)(OCIO ₃) ₂](ClO ₄)	1.4		647(104)	117(1:1 electrolyte) ^a
[Ni(II) ₂ (L ⁷ H) ₂ (OCIO ₃) ₂ (NCS)](ClO ₄) ₃ ·5H ₂ O(!)	4.4	600(45) 328(sh,318)	637(57)	315(3:1 electrolyte) ^a
[Ni(II)(L ⁶ H)(NCS)(OCIO ₃)](ClO ₄)·0.25Et ₂ O	2.8	590(150) 328(274)		98(1:1 electrolyte) ^a
[Cu(II)(L ⁶)(OH ₂)](ClO ₄)·0.5H ₂ O	1.7		600(144)	149(1:2 electrolyte) ^a
[Co(III)(L ⁶) ₂ O ₂ (OCIO ₃)(OH ₂)](ClO ₄)·2H ₂ O	diamagnetic		528(sh, 241)	266(1:3 electrolyte) ^a

Table 2.4

Analytical data for complexes of Chapter 5. (a) CH₃NO₂ ~ 1x10⁻³ solutions at 25°C. (*) unable to obtain. (b) Evans method ~ conc = 1x10⁻²M solutions at 25 C. (!) plus 1 mole of KClO₄

Compound	Colour	Yield	Formula	(C)	(H)	(N)
				(found in parentheses)		
$[\text{ZnL}^6(\text{OCIO}_3)](\text{ClO}_4)$	white	50%	$\text{C}_{15}\text{H}_{32}\text{Cl}_2\text{N}_4\text{Zn}_1\text{O}_8$	33.82 (33.57)	6.05 (5.86)	10.52 (10.67)
$[\text{Ni}(\text{II})(\text{L}^6\text{H})(\text{NCS})(\text{OCIO}_3)](\text{ClO}_4) \cdot 0.25\text{Et}_2\text{O}^{\text{a}}$	dark green	71%	$\text{C}_{16}\text{H}_{33}\text{Cl}_2\text{N}_5\text{Ni}_1\text{O}_8\text{S}_1 \cdot 0.25\text{Et}_2\text{O}$	34.74 (34.74)	6.16 (6.49)	11.26 (10.76)
$[\text{Cu}(\text{II})(\text{L}^6)(\text{OH}_2)](\text{ClO}_4) \cdot 0.5\text{H}_2\text{O}^{\text{b}}$	dark green	66%	$\text{C}_{15}\text{H}_{34}\text{Cl}_2\text{Cu}_1\text{N}_4\text{O}_9 \cdot 0.5\text{H}_2\text{O}$	32.29 (32.02)	6.27 (5.68)	10.04 (9.74)
$[\text{Co}(\text{III})(\text{L}^6)_2\text{O}_2(\text{OCIO}_3)(\text{OH}_2)](\text{ClO}_4) \cdot 2\text{H}_2\text{O}$	brown	41%	$\text{C}_{30}\text{H}_{70}\text{Cl}_4\text{Co}_2\text{N}_8\text{O}_{21}$	31.60 (31.28)	6.19 (5.71)	9.84 (10.10)
$[\text{ZnL}^7](\text{ClO}_4)_2$	white	60%	$\text{C}_{16}\text{H}_{34}\text{Cl}_2\text{N}_4\text{O}_8\text{Zn}_1$	35.13 (33.82)	6.26 (5.82)	10.24 (9.98)
$[\text{Co}(\text{II})\text{L}^7(\text{DMSO})_2](\text{ClO}_4)_3 \cdot 4\text{H}_2\text{O}$	purple/ red	74%	$\text{C}_{20}\text{H}_{55}\text{Cl}_3\text{Co}_1\text{N}_4\text{O}_{18}\text{S}_2$	27.63 (27.72)	6.33 (5.77)	6.45 (6.02)
$[\text{Co}(\text{III})_2(\text{L}^7\text{H})(\text{DMSO})_2\text{O}_2(\text{OCIO}_3)_3(\text{OH}_2)_2](\text{ClO}_4)_3 \cdot 4\text{H}_2\text{O}$	brown	47%	$\text{C}_{20}\text{H}_{59}\text{Cl}_6\text{Co}_2\text{N}_4\text{O}_{34}\text{S}_2$	18.54 (18.15)	4.67 (4.35)	4.33 (4.35)
$[\text{Cu}(\text{II})(\text{L}^7\text{H})(\text{OCIO}_3)_2](\text{ClO}_4)^{\text{c}}$	green	60%	$\text{C}_{16}\text{H}_{35}\text{Cl}_3\text{Cu}_1\text{N}_4\text{O}_{12}$	29.78 (29.72)	5.43 (5.41)	8.69 (9.26)
$[\text{Ni}(\text{II})_2(\text{L}^7\text{H})_2(\text{OCIO}_3)_2(\text{NCS})](\text{ClO}_4)_3 \cdot 5\text{H}_2\text{O}(!)^{\text{d}}$	light green	39%	$\text{C}_{33}\text{H}_{80}\text{Cl}_6\text{K}_1\text{N}_9\text{Ni}_1\text{O}_{29}\text{S}_1$	26.99 (26.75)	5.49 (5.26)	8.58 (8.19)

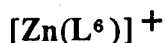
Table 3.4

Analytical results. (a) %Ni(calc)-9.43,(found)-9.80, (b)%Cu(calc)-11.39, (found)-11.02, (c)%Cu(calc)-9.85, (found)-9.40, (d) %Ni(calc)-7.99, (found)-8.13

(!) plus 1 mole of KClO_4



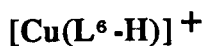
m/z(calc)	m/z(found)
431-(100%)	431-(8%)
432-(19%)	432-(26%)
433-(91%)	433-(100%)
434-(25%)	434-(50%)
435-(60%)	435-(92%)
436-(29%)	436-(29%)
437-(16%)	437-(48%)



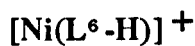
m/z(calc)	m/z(found)
331-(100%)	331-(100%)
332-(19%)	332-(13%)
333-(71%)	333-(71%)
334-(19%)	334-(32%)
335-(41%)	335-(59%)
336-(7%)	336-(13%)
337-(2%)	337-(/)



m/z(calc)	m/z(found)
325-(100%)	325-(100%)
326-(18%)	326-(100%)
327-(2%)	327-(26%)



m/z(calc)	m/z(found)
330-(100%)	330-(100%)
331-(19%)	331-(76%)
332-(46%)	332-(56%)
333-(8%)	333-(28%)



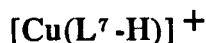
m/z(calc)	m/z(found)
325-(100%)	325-(100%)
326-(19%)	326-(54%)
327-(40%)	327-(54%)
328-(9%)	328-(6%)
329-(6%)	329-(15%)
330-(1%)	330-(7%)



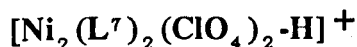
m/z(calc)	m/z(found)
425-(100%)	425-(100%)
426-(19%)	426-(98%)
427-(73%)	427-(99%)
428-(15%)	428-(39%)
429-(20%)	429-(50%)



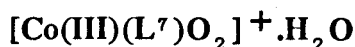
m/z(calc)	m/z(found)
445-(100%)	445-(100%)
446-(20%)	446-(15%)
447-(91%)	447-(63%)
448-(26%)	448-(12%)
449-(60%)	449-(55%)
451-(16%)	451-(17%)



m/z(calc)	m/z(found)
344-(20%)	344-(60%)
345-(100%)	345-(100%)
346-(47%)	346-(/)



m/z(calc)	m/z(found)
877-(66%)	877-(25%)
878-(27%)	878-(/)
879-(100%)	879-(100%)
880-(41%)	880-(35%)
881-(67%)	881-(50%)
882-(27%)	882-(8%)



m/z(calc)	m/z(found)
390-(/)	390-(3%)
391-(100%)	391-(100%)
392-(20%)	392-(18%)
393-(/)	393-(7%)

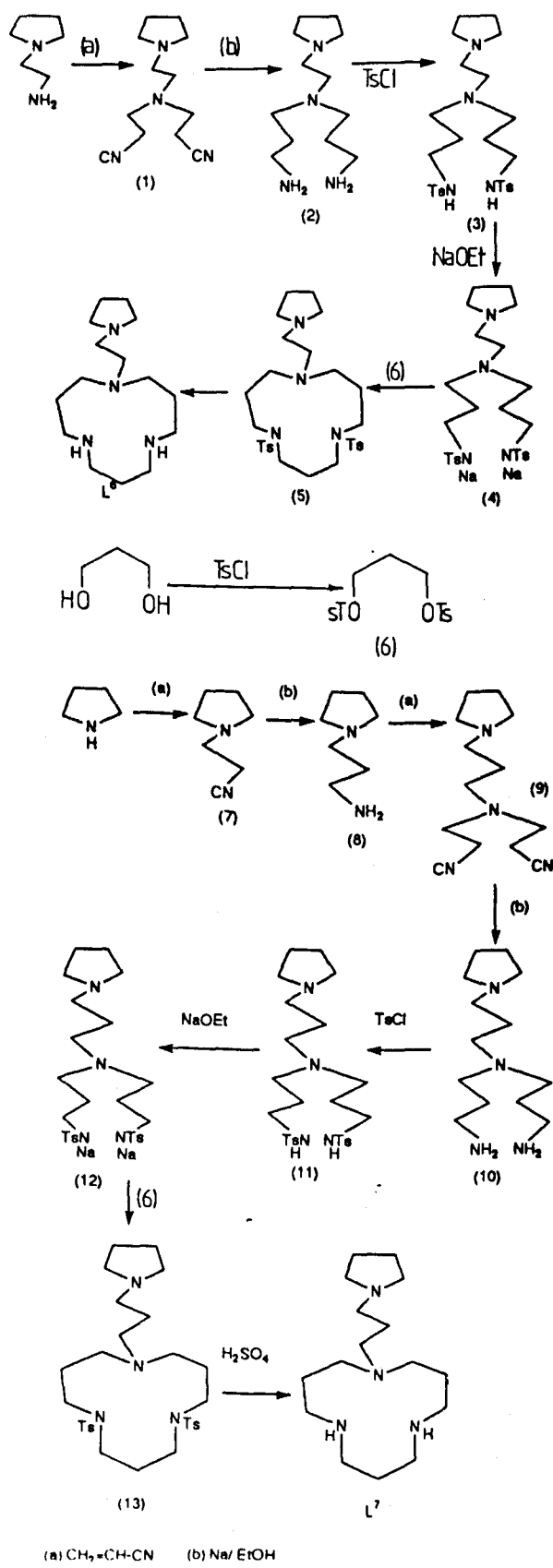
Table 4.4

Mass spectral data for metal complexes of Chapter 4. Relative isotopic abundances in parentheses expressed as % of main isotopic peak. All spectra run in *m*-nitrobenzyl alcohol matrix.

	$[\text{Zn}(\text{L}^7)](\text{ClO}_4)_2$	$[\text{Zn}(\text{L}^6)\text{OClO}_3](\text{ClO}_4)$
R.M.M	546.76	532.82
System	Orthorhombic	Orthorhombic
Space Group	Pbca	$\text{Pn}2_1\text{a}$
a/Å	36.344(12)	13.875(13)
b/Å	16.373(6)	9.811(6)
c/Å	15.766(10)	16.186(9)
$\alpha/^\circ$	/	/
$\beta/^\circ$	/	/
$\gamma/^\circ$	/	/
U/Å ³	9382	2203
D _c /gcm ³	1.48	1.61
$\mu(\text{M}_\text{O}-\text{K}_\alpha)/\text{cm}^{-1}$	14.3	14.3
Unique		
Reflections	6431	2034
Total		
Reflections		
I/σ(I) ≥ 2.0	2155	1224
2θ max	45	50
Range 2θ about	+0.55	+0.55
K _{α1} - K _{α2}	-0.50	-0.50
Speed 2θ /° min ⁻¹	4-29	2-29
Dimensions	0.5x0.1x0.1	0.5x0.1x0.1
Max/Min		
Transmission		
Factors	No absorption correction	0.899/0.849
Final R(R ¹)	0.125(0.113)	0.0593(0.0576)
Weighting(g)	0.0005	0.00073
Largest peak		
on ΔF map		
e Å ³	+/- 1.0	+0.6/-0.3

Table 5.4

Crystallographic data for $[\text{Zn}(\text{L}^6)\text{OClO}_3]^+$ and $[\text{Zn}(\text{L}^7)]^{2+}$



Scheme 1.4

Schematic diagram of the synthesis of L^6 and L^7

Experimental

Experimental procedures and instrumentation are discussed in Chapter 7.

For chemicals and solvents see Chapter 2 (Section 14.2).

The salts $[M(\text{DMSO})_x](\text{ClO}_4)_2$ where $M = \text{Cu}^{2+}$, Ni^{2+} , Co^{2+} , $x=6$ and $m = \text{Zn}^{2+}$, $x=4$ were prepared by a standard literatures method.^{1 2 2} *p*-Toluenesulphonyl chloride was recrystallised from diethylether, and dried *in vacuo*.

Preparation of 1,3-propandiol bis-(4-methylbenzenesulphonate)---(6)

1,3-propandiol (20g, 26.3mmol) was dissolved in CHCl_3 (200 cm^3) with Et_3N (53.16g, 526mmol). *p*-Toluenesulphonyl chloride (100.3g, 526mmol) was dissolved in CHCl_3 (300 cm^3) and added dropwise to the mixture over a period of 2 hours. After addition was complete the solution was stirred for a further 3 hours, and H_2O (200 cm^3) added, and the organic layer separated. The organic layer was dried over anhydrous MgSO_4 , and solvent removed on a rotary evaporator to give a white solid, which was recrystallised from EtOH (Yield 71%, 72g). ^1H n.m.r (CDCl_3): 2.00 (pentet, 2H), 2.46(s, 6H), 4.08(t, 2H), 7.33(d, 4H), 7.73(d, 4H).

Preparation of 1-(2-cyanoethyl)pyrrolidine ---(7)

Pyrrolidine (50g, 700mmol) was dissolved in acrylonitrile (100 cm^3 , 1.52mol) and the mixture heated under reflux at 90° C for 3 days, under nitrogen, with the reaction mixture protected from light. The excess acrylonitrile was removed by vacuum distillation, and the crude product distilled at 0.5mmHg (bp 60° C) to give a colourless oil (82g, 96% yield). ^1H n.m.r (CDCl_3): 1.80(m, 4H), 2.59(m,6H), 2.80(t, 2H).

Preparation of 1-(3-aminopropyl)pyrrolidine ---(8)

1-(2-cyanoethyl)pyrrolidine (25g, 0.20mol) was dissolved in dry EtOH (300 cm^3). Freshly cut sodium (39g, 1.26mol) was added slowly, and after addition the mixture was refluxed for 24 hours under nitrogen. The solvent was removed and the residue taken up in CH_2Cl_2 (300 cm^3), washed with H_2O (100 cm^3) and the

organic layer separated. The solvent was removed on a rotary evaporator to give a yellow oil which was vacuum distilled at 35° C (0.5mmHg) to give a colourless oil (13.33g, 52% yield). ¹H n.m.r (CDCl₃): 1.40(br, 2H), 1.70(t, 2H), 1.80(m, 4H), 2.50(m, 6H), 2.80(t, 2H).

Preparation of 1,5-dicyano-3-(3'-(pyrrolidinyl)-propyl)-3-azapentane---(9)

1-(3-aminopropyl)pyrrolidine (13.3g, 0.14mol) was dissolved in acrylonitrile (148cm³, 2.2mol) with glacial acetic acid (12.5g, 0.2mol), and refluxed for 24 hours. The excess acrylonitrile was removed *in vacuo*, and the residue dissolved in CH₂Cl₂ (300cm³), washed with 0.88 NH₃ (aq) (100cm³) and H₂O (100cm³). The organic layer was separated, dried over anhydrous MgSO₄, and solvent removed on a rotary evaporator to give a yellow oil, which was distilled at 180° C (0.1mmHg) to give a colourless oil (21.7g, 66% yield). ¹H n.m.r (CDCl₃): 1.65(t, 2H), 1.80(m, 6H), 2.50(m, 12H), 2.90(t, 4H). I.r (thin film): 2240cm⁻¹ (C=N).

Preparation of 1,7-diamino-4-(3'-(1"-pyrrolidinyl)-propyl)-4-azaheptane ---(10)

Compound (9) (21.7g, 92.7mmol) was dissolved in dry EtOH (300cm³). Freshly cut sodium (35.5g, 1.5mol) was added slowly, and after addition the mixture was refluxed for 24 hours, under nitrogen. The solvent was removed, and the residue taken up in CH₂Cl₂ (300cm³), washed with H₂O (100cm³), and the organic layer separated. The solvent was removed on rotary evaporator to give a yellow oil, which was distilled at 117° C (0.05mmHg) to give a colourless oil (10.49g, 47% yield). ¹H n.m.r (CDCl₃): 1.30(NH, 4H), 1.60(m, 6H), 1.80(m, 4H), 2.50(m, 12H), 2.75(t, 4H).

Preparation of compound (11)

Compound (10) (4.2g, 17mmol) and Et₃N (3.4g, 34mmol) were dissolved in CH₂Cl₂ (100cm³) and p-toluenesulphonyl chloride (6.48g, 34mmol) in CH₂Cl₂ (50cm³) was added dropwise over a period of 2 hours. After addition, the mixture was stirred for a further 6 hours, and H₂O (100cm³) added. The organic layer was separated, dried over anhydrous MgSO₄, and removed on a rotary evaporator to give a yellow glass (8.05g, 86% yield). ¹H n.m.r (CDCl₃): 1.35(t,

4H), 1.65(m, 2H), 2.10(m, 6H), 2.40(m, 10H), {2.95, 3.09, 3.30}(10H), 7.35(d, 4H), 7.85(d, 4H).

Preparation of compound (12)

Compound (11) (8.05g, 14.6mmol) was dissolved in dry EtOH (400cm³). Freshly prepared NaOEt{0.67g of Na in EtOH (20cm³)} was added, and the mixture stirred for 12 hours under nitrogen. The solvent was removed *in vacuo*, and the white solid dried in a desiccator over silica gel for several hours (Yield 98%, 8.7g). I.r (Nujol Mull): loss of N-H stretch.

Preparation of Tosylated macrocycle (13)

Compound (12) (30.15g, 50mmol) was dissolved in dry DMF (400cm³), and heated to 95° C under nitrogen. 1,3-propanediol-bis(4-methylbenzene sulpho-nate) (19.2g, 50mmol) in dry DMF (100cm³) was added slowly over a period of 5 hours to the stirring solution, and after addition stirring was continued for a further 12 hours. The DMF was removed by vacuum distilled off, and the residue taken up in CH₂Cl₂ (200cm³), washed with H₂O (50cm³), and the organic layer separated, dried over anhydrous MgSO₄, and removed on a rotary evaporator. The oily residue was heated to 90° C (0.1mmHg) to remove any remaining DMF, and used without purification.

Preparation of L⁷

The crude macrocycle from the reaction above (22g, 37mmol) was dissolved in 98%H₂SO₄ (150cm³), and heated to 100° C for 2 days. After cooling the acid was neutralised using 10%NaOH, keeping the temperature below 10° C, and the Na₂SO₄ filtered off. The water layer was extracted several times with CH₂Cl₂ (6x100cm³), the combined extracts dried over anhydrous MgSO₄, and removed on a rotary evaporator to give a brown oil. The oil was distilled on a Kugelröhr apparatus at 140° C (0.05mmHg) to give a colourless oil (3.56g, 24% yield). ¹H n.m.r (CDCl₃): 1.65(m, 8H), 1.80(m, 4H), 2.50(m, 12H), 2.75(m, 8H). C.I mass spectrum m/z calculated-283, m/z found-283 [M + 1]⁺. ¹³C n.m.r data is in Table 1.4

Preparation of 1,5-dicyano-3-(2'-(1"-pyrrolidinyl)-3-azapentane---(1)

1-(2-aminoethyl)pyrrolidine (20g, 0.17mol) was dissolved in acrylonitrile (250cm³, 3.8mol) with glacial acetic acid (21g, 0.35mol), and refluxed for 24 hours. The excess acrylonitrile was removed on a rotary evaporator, and the residue taken up in CH₂Cl₂ (300cm³), washed with 0.88NH₃ (aq) (100cm³) and H₂O (100cm³). The organic layer was separated, dried over anhydrous MgSO₄, and the solvent removed a rotary evaporator to give a yellow oil. Fractional distillation of the crude oil at 160° C (0.07mmHg) gave a colourless oil (26g, 70% yield). ¹H n.m.r (CDCl₃): 1.75(m, 4H), 2.55(m, 10H), 2.70(m, 2H), 2.90(t, 4H).

Preparation of 1,7-diamino-4-(2'-(1"-pyrrolidinyl)-ethyl)-4-azaheptane---(2)

Compound (1) (20g, 90mmol) was dissolved in dry EtOH (300cm³) under nitrogen. Freshly cut sodium (35g, 1.5mol) was added slowly, and the mixture refluxed for 24 hours. The solvent was removed on a rotary evaporator and the residue taken up in CHCl₂ (300cm³), washed with H₂O (50cm³), and the organic layer separated and dried over anhydrous MgSO₄. Removal of the solvent gave a yellow oil which was distilled at 105° C (0.05mmHg) to give a colourless oil (11.79, 57% yield). ¹H n.m.r (CDCl₃): 1.60(m, 4H), 1.75(m, 4H), 2.0(br, 4H), 2.50(m, 12H), 2.70(t, 4H).

Preparation of compound (3)

Compound (2) (11.79g, 50mmol) was dissolved in CH₂Cl₂ (200cm³) containing Et₃N (10g, 0.1mol). *p*-Toluenesulphonyl chloride (19.06g, 0.1mol) in CH₂Cl₂ (100cm³) was added to the stirring solution over 2 hours, after which the solution was stirred for a further 6 hours. The organic layer was washed with H₂O (100cm³), separated, dried over anhydrous MgSO₄, and the solvent removed on a rotary evaporator to give a yellow glass (25.72g, 96% yield). ¹H n.m.r (CDCl₃): 1.55(m, 4H), 1.80(m, 4H), 2.50(m, 18H), 3.00(t, 4H), 7.30(d, 4H), 7.75(d, 4H).

Preparation of compound (4)

Compound (3) (25.72g, 48mmol) was dissolved in dry EtOH (250cm³), under

nitrogen. Freshly prepared NaOEt{2.2g of Na in EtOH (50cm³)} was added, and the mixture stirred for 12 hours. The solvent was removed *in vacuo* to give a white solid, which was dried in a desiccator over silica gel (27.28g, 98% yield). I.r (Nujol Mull): No N-H stretch.

Preparation of tosylated macrocycle (5)

Compound (4) (27.78g, 47mmol) was dissolved in dry DMF (400cm³), and heated to 95° C, under nitrogen. 1,3 propanediol bis-(4-methylbenzene sulphonate) (18.05g, 47mmol) in dry DMF (150cm³) was added to the stirring solution, and after addition was complete the mixture was stirred for a further 12 hours. The DMF was vacuum distilled off, and the residue taken up in CH₂Cl₂ (300cm³), and washed with H₂O (100cm³). The organic layer was dried over anhydrous MgSO₄, and removed on a rotary evaporator to give a brown oil which was heated at 90° C (0.1mmHg) to remove remaining DMF. The crude product was used in the next step without further purification.

Preparation of L⁶

The crude tosylated macrocycle from the reaction above (26.39g, 46mmol) was dissolved in 98% H₂SO₄ (200cm³), and heated to 100° C for 2 days. The acid was neutralised using 10% NaOH, keeping the temperature below 10° C, and the Na₂SO₄ filtered off. The water layer was extracted several times with CH₂Cl₂ (6x100cm³), and the organic layer separated, then dried over anhydrous MgSO₄. Removal of the organic solvent gave a brown oil, which on was distilled on a Kugelröhr apparatus at 160° C (0.05mmHg) to give a slightly yellow oil (1.58g, 12% yield). ¹H n.m.r (CDCl₃): 1.70(m, 6H), 1.80(m, 4H), 2.60(m, 14H), 2.80(m, 6H). C.I mass spectrum m/z calculated-269, m/z found-269 [M + 1]⁺. ¹³C n.m.r data in Table 1.4.

Preparation of L^a

The macrocycle L⁶ (0.22g, 0.82mmol) was dissolved in EtOH (25cm³) with excess NaOH (0.32g, 8mmol), and benzoyl chloride (1g, 8mmol). The mixture was refluxed for 48 hours, and the solvent removed to give a yellow residue, which

was dried *in vacuo* at 25° C (0.1mmHg) to remove excess benzoyl chloride. The residue was taken up in CH₂Cl₂ (50cm³), washed with H₂O (10cm³), separated and dried over anhydrous MgSO₄. Removal of the solvent yielded a yellow oil which passed down an alumina column (gravity elution), using Et₂O(80%)/MeOH(20%) as eluant, to give a white solid after solvent removal (0.20g, 42% yield). C.I mass spectrum m/z calculated 449, m/z found 449 [M-CH₂-Ph]⁺. ¹³C n.m.r data in Table 1.4

Section 12.4

Metal complexes of L⁶ and L⁷

Preparation of [Zn(L⁶)OCIO₃](ClO₄)

The ligand L⁶ (0.20g, 0.75mmol) in EtOH (10cm³) was added to a stirred solution of [Zn(DMSO)₄](ClO₄)₂ (0.43g, 0.75mmol) in EtOH (10cm³), under nitrogen. The resulting off white precipitate was collected and recrystallised from CH₃NO₂/Et₂O/EtOH (1:2:2) to give a white solid which was filtered, and dried *in vacuo* (0.20g, 50% yield). I.r (Nujol Mull): 1100cm⁻¹ (br, ClO₄), 620cm⁻¹. Analytical data is in Tables 2.4/3.4/4.4.

Preparation of [Cu(L⁶)(OH₂)](ClO₄) 0.5H₂O

The ligand L⁶ (0.20g, 0.75mmol) in EtOH (10cm³) was added to a stirred solution of [Cu(DMSO)₆](ClO₄)₂ (0.55g, 0.75mmol) in EtOH (10cm³). The solution was stirred for several hours, during which time the dark blue solution turned green, and a dark green precipitate formed. The solid was collected and recrystallised from CH₃NO₂/Et₂O (1:2), dried *in vacuo* to give a dark green solid (0.26g, 60% yield). I.r (Nujol Mull): 1100cm⁻¹ (br, ClO₄), 630cm⁻¹. Analytical data is in Tables 2.4/3.4/4.4.

Preparation of [Ni(L⁶H)(NCS)(OCIO₃)](ClO₄).0.5 Et₂O

The ligand L⁶ (0.20g, 0.75mmol) was dissolved dry CH₃CN (10cm³), and added to a stirred solution of [Ni(DMSO)₆](ClO₄)₂ (0.54g, 0.75mmol) in dry acetonitrile (10cm³). The mixture was stirred for 2 hours under nitrogen, and KNCS (0.073g, 0.75mmol) in dry acetonitrile (5cm³) added. The precipitated KClO₄

was filtered off, and the volume of solvent reduced *in vacuo* to approximately half the original volume, and filtered again. The product was precipitated by addition of dry Et₂O, and the green solid collected and dried (0.33g, 71% yield). I.r (KBr disc): {2960, 2920, 2860}cm⁻¹ (C-H), 2080cm⁻¹ (NCS), 1100cm⁻¹ (ClO₄). Analytical data is in Tables 2.4/3.4/4.4

Preparation of [Co(III)(L⁶)₂O₂(OCIO₃)(OH₂)](ClO₄)₃.3H₂O

The ligand L⁶ (0.20g, 0.75mmol) was dissolved in EtOH(10cm³), and added to a stirred solution of [Co(II)(DMSO)₆](ClO₄)₂ (0.54g, 0.75mmol) in EtOH (10cm³). The solution was stirred and oxygen bubbled through the solution for 12 hours. The brown precipitate was collected and recrystallised from CH₃NO₂/Et₂O (1:2) (Yield 41%, 0.17g). I.r (Nujol Mull): 3440cm⁻¹ (br, OH), 1635cm⁻¹ (H-OH bending), 1100cm⁻¹ (br, ClO₄). Analytical data is in Tables 2.4/3.4/4.4.

Preparation of [Zn(L⁷)](ClO₄)₂

The ligand L⁷ (0.20g, 0.71mmol) was dissolved in EtOH (10cm³), and added to a stirred solution of [Zn(DMSO)₄](ClO₄)₂ (0.41g, 0.71mmol) in EtOH (10cm³). The white precipitate formed was collected and recrystallised from CH₃NO₂/EtOH/Et₂O (1:2:2) to give a white solid (0.23g, 60% yield). I.r (Nujol Mull): 1100cm⁻¹ (br, ClO₄). Analytical data is in Tables 2.4/3.4/4.4

Preparation of [Cu(L⁷H)(OCIO₃)₂](ClO₄)

The ligand L⁷ (0.20g, 0.71mmol) was dissolved in dry EtOH (10cm³) and added to a stirred solution of [Cu(DMSO)₆](ClO₄)₂ (0.52g, 0.71mmol) in EtOH (10cm³). The dark green precipitate was collected, and recrystallised from CH₃NO₂/Et₂O (1:2) to give hygroscopic dark green solid (0.27g, 60% yield). I.r (KBr disc): 1100cm⁻¹ (br, ClO₄), {620, 630}cm⁻¹ (ClO₄). Analytical data is in Tables 2.4/3.4/4.4.

Preparation of [Co(II)(L⁷H)(DMSO)₂](ClO₄)₃.4H₂O

A thoroughly degassed solution of L⁷ (0.22g, 0.78mmol) in EtOH (10cm³) was added to a nitrogen degassed solution of [Co(DMSO)₆](ClO₄)₂ (0.56g,

0.78mmol) in EtOH (10cm³). The purple/red solid formed was collected under dry nitrogen, and dried *in vacuo* (0.50g, 74% yield). I.r (Nujol Mull): 1090cm⁻¹ (ClO₄), 958cm⁻¹ (DMSO). Analytical data is in Tables 2.4/3.4/4.4.

Preparation of [Co(III)₂(L⁷H)(DMSO)₂O₂(OCIO₃)₃(OH₂)₂](ClO₄)₃.4H₂O
The ligand L⁷ (0.20g, 0.71mmol) was dissolved in EtOH (10cm³) and added to stirred solution of [Co(II)(DMSO)₆](ClO₄)₂ (0.52g, 0.71mmol) in EtOH (10cm³). The solution remained purple for a few minutes, and started to darken on passage of oxygen through the solution. The brown solid formed was collected and recrystallised from CH₃NO₂/Et₂O (1:2) (Yield 47%, 0.21g). I.r (Nujol Mull): 3400cm⁻¹ (br, OH), 1100cm⁻¹ (v.br, ClO₄). Analytical data is in Tables 2.4/3.4/4.4.

Preparation of [Ni₂(L⁷H)₂(OCIO₃)₂(NCS)](ClO₄)₃.5H₂O.KClO₄
The ligand L⁷ (0.23g, 0.81mmol) was dissolved in dry CH₃CN (10cm³), and added to a stirred solution of [Ni(DMSO)₆](ClO₄)₂ (0.59g, 0.81mmol) in dry CH₃CN (10cm³). The mixture was stirred for two hours, under nitrogen, and KNCS (0.0786g, 0.81mmol) in dry CH₃CN (5cm³) added. The precipitated KClO₄ was filtered off, and the volume of solvent reduced, and filtered again. The product was precipitated by addition of dry Et₂O to give a light green solid which was collected and dried. Even after several recrystallisations from CH₃NO₂/Et₂O (1:2) KClO₄ remained (Yield 39% 0.23g). I.r (Nujol Mull): 2080cm⁻¹ (NCS), 1100cm⁻¹ (br, ClO₄). Analytical data is in Tables 2.4/3.4/4.4.

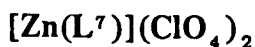
Crystallography

For both compounds data were collected on a Nicolet R3 four circle diffractometer using graphite monochromated Mo-K α angles, with variable scan speeds depending on the intensity of 2 θ pre-scan; backgrounds were measured at each end of the scan for 0.25 of the scan time. All data were taken at 293K. Three standard reflections were monitored every 200 reflections; in both cases a slight decrease (c.a 5%) occurred during data collection; the data were rescaled to correct for this. Unit cell dimensions and standard deviations were obtained by a least squares fit to 15 high angle reflections. Reflections with $I/\sigma(I) \geq 2.0$ were considered observed and used in refinement, and corrected for Lorentz polarisation and absorption effects (no absorption correction done for $[\text{Zn}(\text{L}^7)]^{2+}$). Heavy atoms were located by Patterson interpretation, and light atoms found on successive Fourier syntheses { see notes on $[\text{ZnL}^7]^{2+}$ structure}. Anisotropic temperature factors were used for all non H atoms except C(7) and C(8) of the $[\text{Zn}(\text{L}^6)\text{OCIO}_3](\text{ClO}_4)$, and only on Zn, Cl, O, N atoms for $[\text{Zn}(\text{L}^7)](\text{ClO}_4)_2$. Hydrogen atoms were given fixed isotropic temperature factors, $U = 0.07 \text{ \AA}^2$, and inserted at calculated positions and not refined (see notes on $[\text{ZnL}^7]^{2+}$). Final refinement was on F by least squares methods refining 395 $[\text{ZnL}^7]^{2+}$, 245 $[\text{ZnL}^6\text{OCIO}_3]^+$ parameters. A weighting scheme of the form $W = 1/\sigma^2(F) + gF^2$ (for g values see Table 5.4) were used and shown to be satisfactory by weight analysis. Computing was carried out with SHELXTL PLUS^{1 2 3} on a DEC Microvax-II, except the absorption correction for $[\text{Zn}(\text{L}^6)\text{OCIO}_3]^+$ which was done with SHELXTL on a Data General D.G 30. Scattering factors in the analytical form and anomalous dispersion factors were taken from International Tables(1974).^{1 2 4}



Crystals suitable for X-ray crystallography were obtained as short clear needles from slow diffusion of a saturated CH_3NO_2 solution into $\text{Et}_2\text{O}/\text{EtOH}$ (1:1)

mixture. The unbound perchlorate ion was held as a rigid group, and the remaining electron density was located around the perchlorate groups. The carbon atom C(2) of the propyl chain was disordered over two sites due to flipping of the carbon chain, and so the occupancy was refined, and approached 0.6-0.4{C(2A)-C(2B)}. Hydrogen atoms were only attached to C(2A) as it was the major component. Bond lengths and angles are in Table 6.4. Atomic co-ordinates are given in Appendix I.



Crystals suitable for X-ray crystallography were obtained as long needles from a slow diffusion of a saturated CH_3NO_2 solution into a $\text{Et}_2\text{O}/\text{EtOH}$ (1:1) mixture. Absences indicated a space group Pbcm or $\text{Pbc}2_1$ (non standard setting of $\text{Pca}2_1$). Attempted Patterson solutions in Pbcm were unsuccessful, but showed four zinc(II) atoms in $\text{Pbc}2_1$. A slow development by least squares and Fourier methods showed part of the cation structure and several perchlorate groups, and revealed that the zinc(II) atoms were centro-symmetrically related, but in Pbca and not Pbcm . The perchlorate groups were held as rigid tetrahedrons, and some of the C-N, C-C bond distances were constrained to reasonable values. The high R factor is readily understood in terms of the very weak diffraction and the high anisotropic thermal motion, not only of the perchlorate groups, but of the macrocyclic ligand itself. Bond lengths and angles are given in Table 7.4. Atomic co-ordinates are in Appendix I.

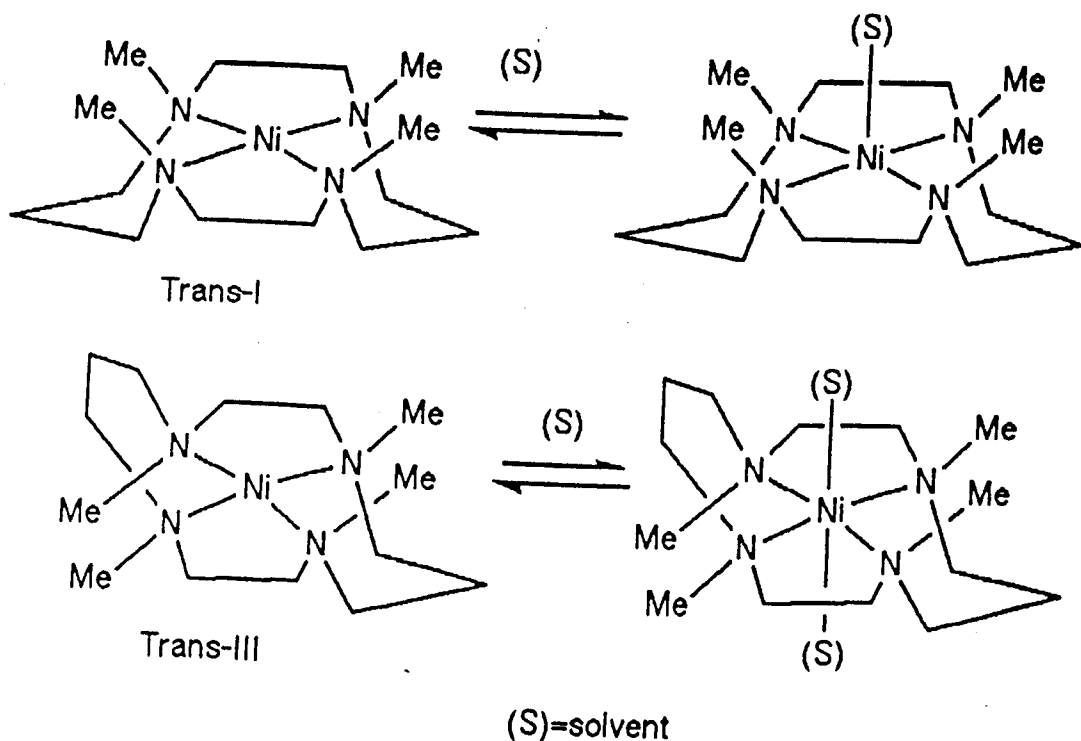
CHAPTER 5

The synthesis of two tetra-N-substituted derivatives of 1,4,8,11-Tetraazacyclotetradecane (cyclam), and their nickel(II) complexes

Section 1.5

Introduction

The ligand 1,4,8,11-tetramethyl-1,4,8,11-tetraazacyclotetradecane (TMC) has received a wide interest since its synthesis in 1973, by Barefield and Wagner.^{1 5 3} The possible conformations of metal complexes of TMC have been discussed previously in Chapter 1 (page 7). The two most common conformations for $[\text{Ni}(\text{TMC})]^{2+}$ complexes are R,S,R,S (known as Trans-I), and R,S,S,R (known as Trans-III). The Trans-I form was thought to be the kinetically favourable product, but this conclusion has been shown to be questionable. Initially it was believed that the two forms could not be interconverted, but work by Moore^{1 5 4} and Lincoln^{1 6 2} showed that in the presence of strongly co-ordinating amines (*e.g* N-propylamine) the Trans-III to Trans-I isomerisation was possible. The main interest in the two conformers is the difference in solvation properties. The Trans-I isomer has been found to mono solvate with various unidentate ligands to form five co-ordinate paramagnetic complexes, whilst the Trans-III isomer forms di-solvento complexes to produce six co-ordinate paramagnetic complexes (Scheme 1.5)



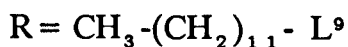
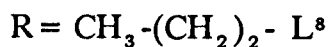
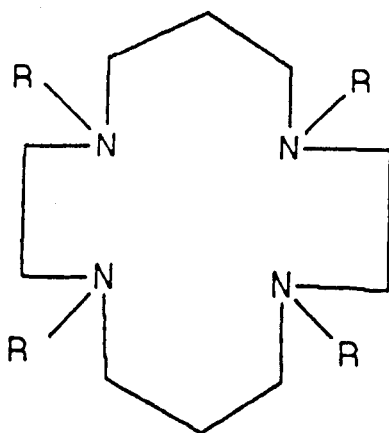
Scheme 1.5

The solvation properties of the Trans-I and Trans-III conformers of
 $[\text{Ni}(\text{TMC})]^{2+}$

The failure to form the six co-ordinate complex with the Trans-I conformer has been attributed to unfavourable steric interactions between an incoming solvent molecule, and the carbons of the macrocyclic ring. Also unfavourable steric interactions would occur between the incoming ligand and the methyl groups. A number of studies have been carried out on the calculation of equilibrium constants and rates of solvent exchange, using ^1H n.m.r shifts,¹⁵⁵ ^{17}O n.m.r line broadening,¹⁵⁶ visible spectrophotometry¹⁵⁶ and conductivity.¹⁵⁷

To date no studies of the effect of changing the methyl groups for other alkyl substituents have been attempted. Indeed routes to other tetra-N-alkylated derivatives are sparse, and so we have undertaken to produce two tetra-N-alkylated cyclam derivatives, in order to study the co-ordination properties of these ligands with nickel(II), and make comparisons to $[\text{Ni}(\text{TMC})]^{2+}$ complexes.

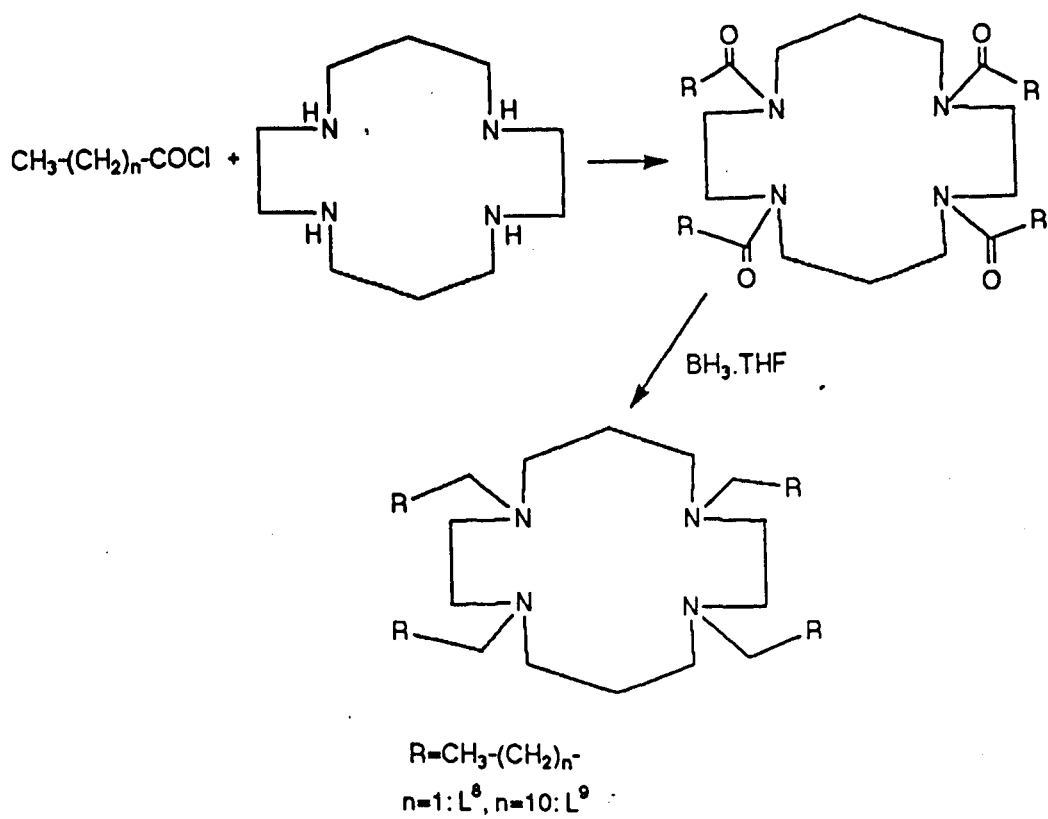
Results and Discussion



Section 2.5

Synthesis of L^8 and L^9

The synthesis of the two ligands is outlined in Scheme 2.5. Direct alkylation using an alkyl halide and cyclam gives messy products, which is attributed to quaternisation of the tertiary nitrogens produced. To overcome this problem two standard organic reactions are used. Reaction of cyclam with excess alkyl acid chloride, to produce a tertiary tetraamide, is followed by reduction with BH_3 thf to give two ligands L^8 and L^9 in good yields (85% L^8 , 72% L^9) as a yellow oil and white solid respectively. The structures were confirmed by ^1H n.m.r and ^{13}C n.m.r (Table 1.5) and F.A.B mass spectrometry. The ^{13}C n.m.r confirmed the symmetric nature of the two ligands, and are shown in Figure 1.5(a)/(b). The ligand L^8 contains a small amount of butan-1-ol, which is used during the preparation, and is not removed even after continuous pumping in *vacuo*.



Scheme 2.5

Schematic diagram for the preparation of L^8 and L^9

Figure 1.5(a)

^1H decoupled ^{13}C n.m.r spectrum of L^8 in CDCl_3 (ref Me_4Si $\delta = 0$) run at 45.28MHz. X = traces of butan-1-ol. Y = CDCl_3

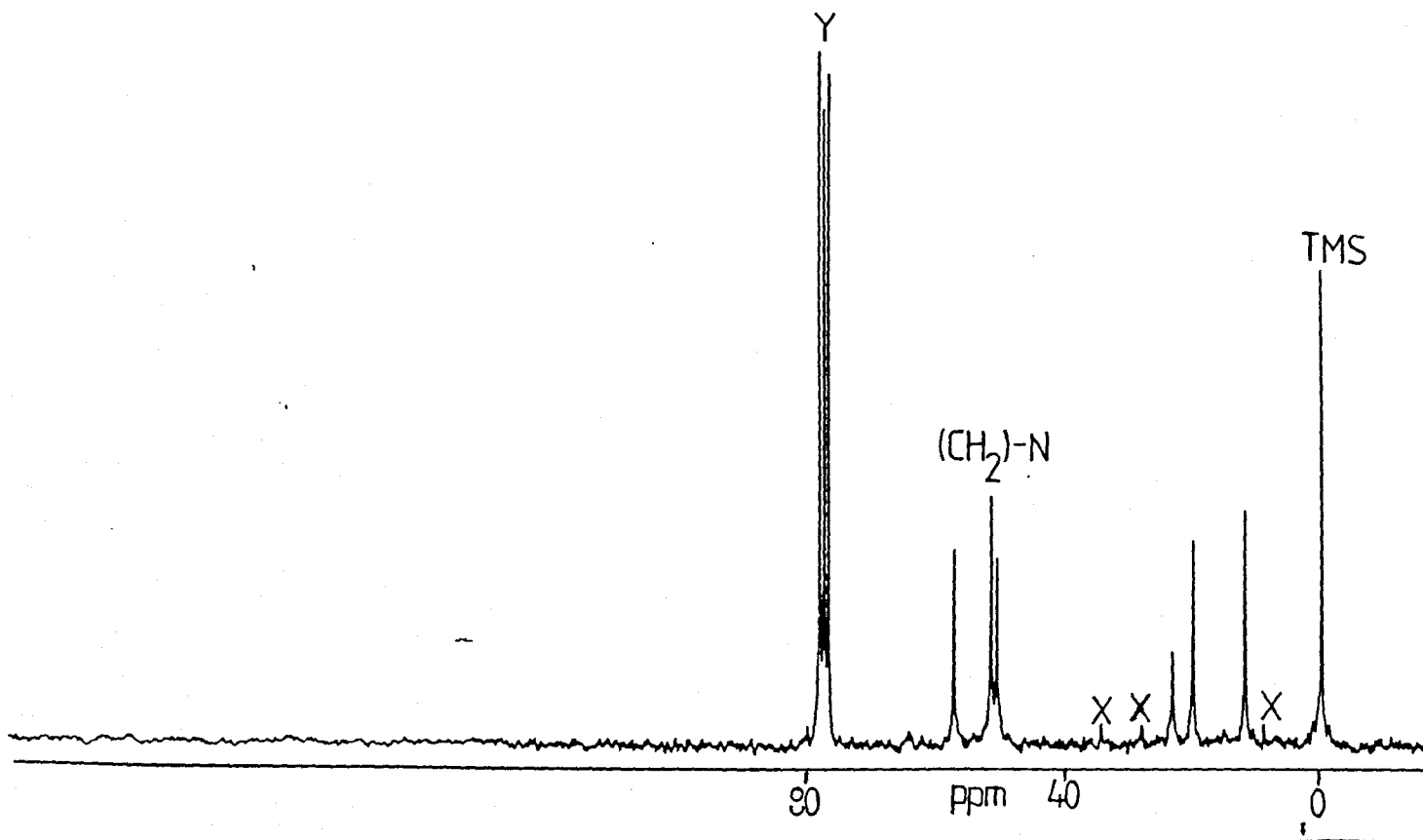
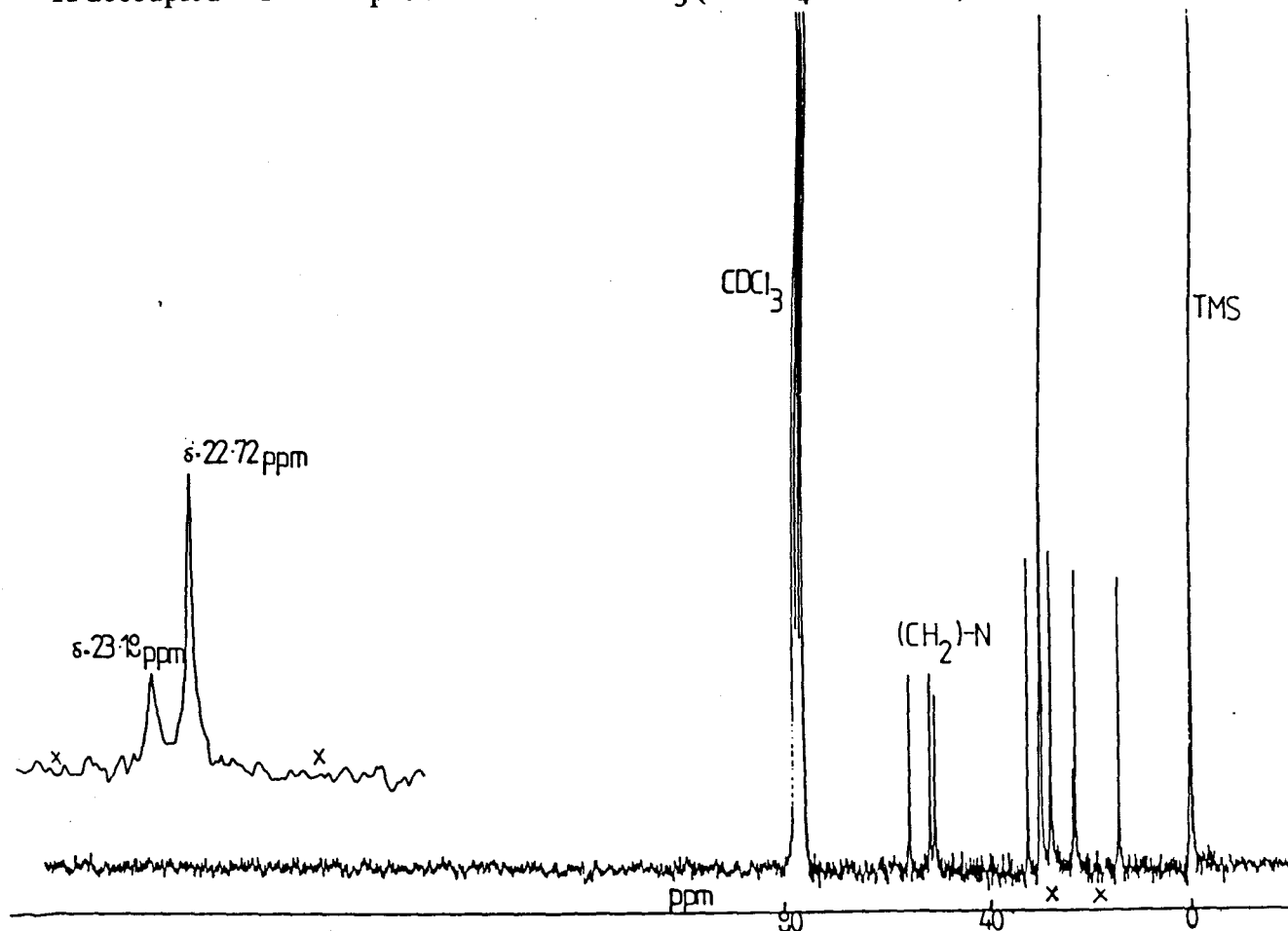


Figure 1.5(b)

^1H decoupled ^{13}C n.m.r spectrum of L^9 in CDCl_3 (ref Me_4Si $\delta = 0$) run at 45.28MHz.



Section 3.5

Nickel(II) complexes of L⁸

Addition of the ligand L⁸ to [Ni(DMSO)₆](BF₄)₂ in ethanol followed by addition of Et₂O, produces a purple product which analyses to [Ni(L⁸)](BF₄)₂.0.25Et₂O. The question of conformation of the macrocyclic ring seems to be answered by the comparison of U.V/visible spectra of Trans-I/Trans-III [Ni(TMC)]²⁺ to that of [Ni(L⁸)]²⁺. The U.V/visible spectrum in non co-ordinating nitromethane contains only a single absorbance at 544nm, with an extinction coefficient (212 mol⁻¹ dm³ cm⁻¹) consistent with square planar nickel(II). The similarity of the spectrum to that of Trans-I [Ni(TMC)]²⁺ (Table 3.5) suggests a similar structure for Trans-I [Ni(L⁸)]²⁺. U.V/visible spectra in co-ordinating solvents (*e.g.* CH₃ CN) contains additional bands, which are assigned to five co-ordinate species; this point is further supported by thermodynamic data (Section 5.5). The decrease in absorbance at 544nm corresponding to the square planar nickel(II) complex, is greater in CH₃ CN solutions than in DMSO, which is consistent with the better co-ordinating ability of the rod like CH₃ CN. A variable temperature U.V/visible spectrum of [Ni(L⁸)]²⁺ in CH₃ CN (Figure 2.5) shows how the four co-ordinate to five co-ordinate equilibrium is affected by temperature. Increasing the temperature moves the equilibrium to the four co-ordinate species as expected.

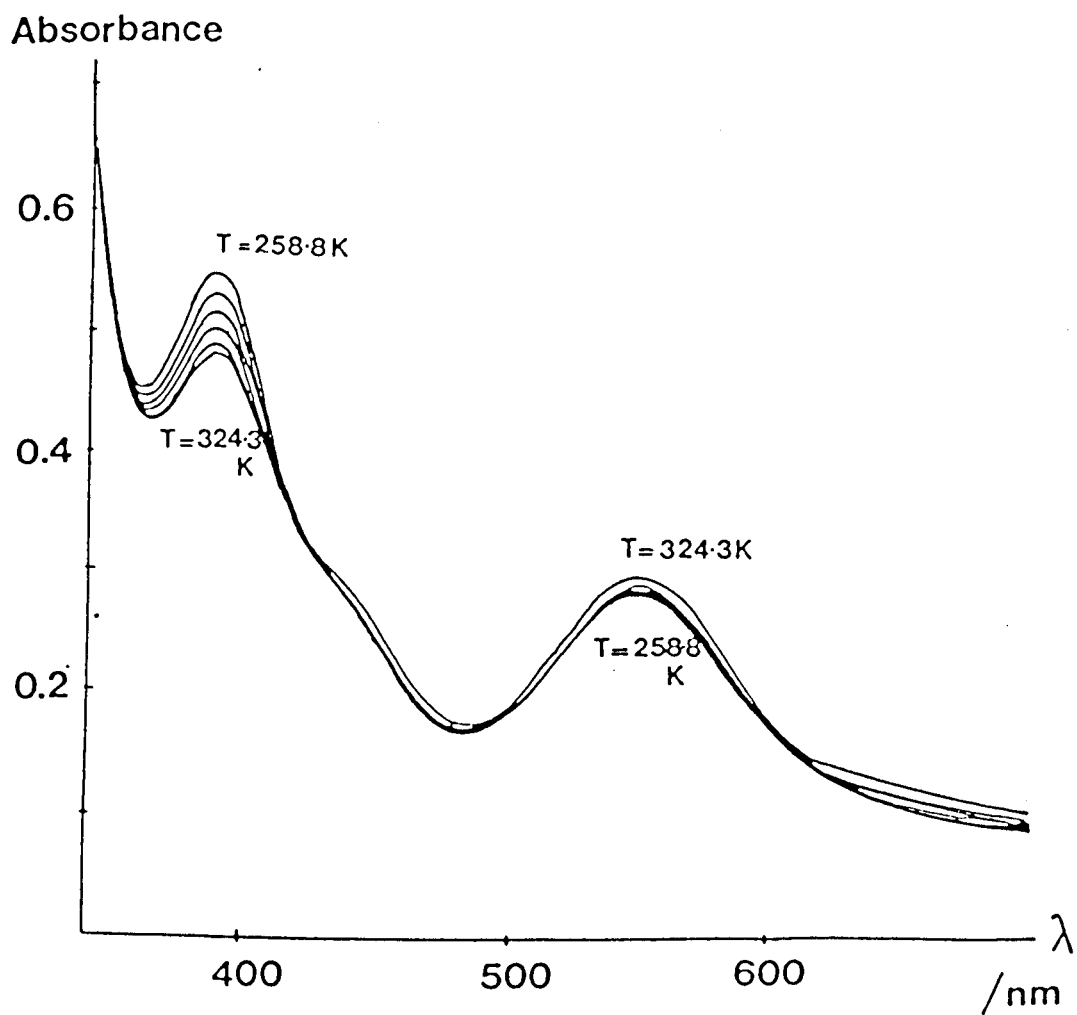


Figure 2.5

Variable temperature spectrum of $[\text{NiL}^8](\text{BF}_4)_2 \cdot 0.25\text{Et}_2\text{O}$, (0.012M) in acetonitrile, from 12.6°C to 51.1°C .

Apparent ambiguities about conformation arise when the ^1H and ^{13}C n.m.r spectra of $[\text{Ni}(\text{L}^s)]^{2+}$ are obtained in non co-ordinating CD_3NO_2 . The ^1H n.m.r (Figure 3.5) clearly shows two resonances corresponding to the methyl groups, with relative integrals of (a)/(b) = 1:1.3. The two methyls resonances correspond to two symmetric isomers in solution, and not one unsymmetric isomer, as confirmed by ^{13}C n.m.r. (see Figure 5.5 for explanation).

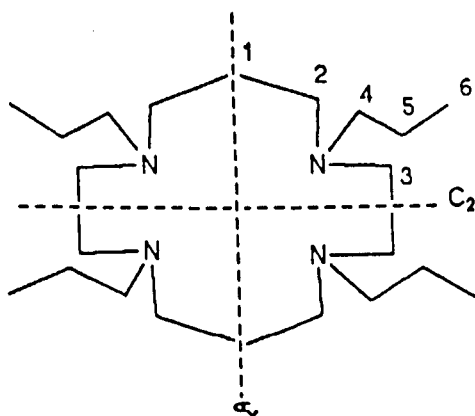


Figure 5.5

Trans-I σ_v symmetry: 6 resonances, Trans-III C_2 symmetry: 6 resonances.
 Trans-II no symmetry: 28 resonances, Trans-IV σ_v symmetry: 6 resonances.

The ^{13}C n.m.r spectrum of $[\text{Ni}(\text{L}^s)]^{2+}$ in CD_3NO_2 is shown in Figure 4.5, and contains twelve resonances as expected for two symmetric species. Interestingly the resonances for the one isomer appear sharp whilst resonances for the other species are broad. This indicates that some slow dynamic process is occurring in one isomer and not the other. The data suggests that the two isomers are not interconverting appreciably, as both sets of resonances would be broad. On cooling all the resonances become broad, and on heating ($\sim 50^\circ\text{C}$) the resonances sharpen slightly, suggesting a dynamic process of torsional "flipping" is occurring in the macrocyclic backbone (Figure 6.5).

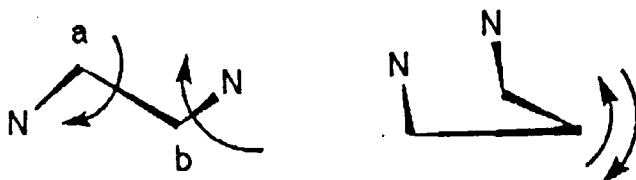


Figure 6.5
Torsional "flipping" equalates both (a) and (b)

Usually "flipping" is fast on the n.m.r timescale and so resonances appear sharp, as seen in one of the isomers, but if "flipping" is slow then broadening of resonances occurs. For both isomers at low temperature "flipping" is reduced, and all resonances appear broad, but on heating "flipping" is fast and sharpening of resonances occurs. By analysis of the gauche arrangements of the methylene groups in the macrocyclic ring it is possible to tentatively assign the sharp resonances to the Trans-I conformation. However, due to the similarity of the only other two planar symmetric conformations (Trans-III, Trans-IV), it is not possible to assign the broad resonances to one of these conformations. However, due to the Trans-IV conformer's instability, it seems likely that the other isomer present is the Trans-III arrangement.

Rather interestingly, addition of small amounts of CD_3CN to a solution of $[\text{Ni}(\text{L}^8)]^{2+}$ in CD_3NO_2 causes the downfield methyl resonance to shift, and in CD_3CN the resonance is completely removed. Therefore, one isomer is being preferentially solvated; analogous behaviour has been reported by Moore^{1 & 2} where Trans-I $[\text{Ni}(\text{TMC})]^{2+}$ was shown to be preferentially solvated over the Trans-II isomer.

Confirmation that Trans-I $[\text{Ni}(\text{L}^8)]^{2+}$ is one of the isomers present comes from the rapid destruction of this isomer by acid, as followed by U.V/visible spectrometry (Figure 7.5); Trans-I $[\text{Ni}(\text{TMC})]^{2+}$ is known to be rapidly destroyed by acid, owing to the lability of the nickel(II).^{1 6 3}

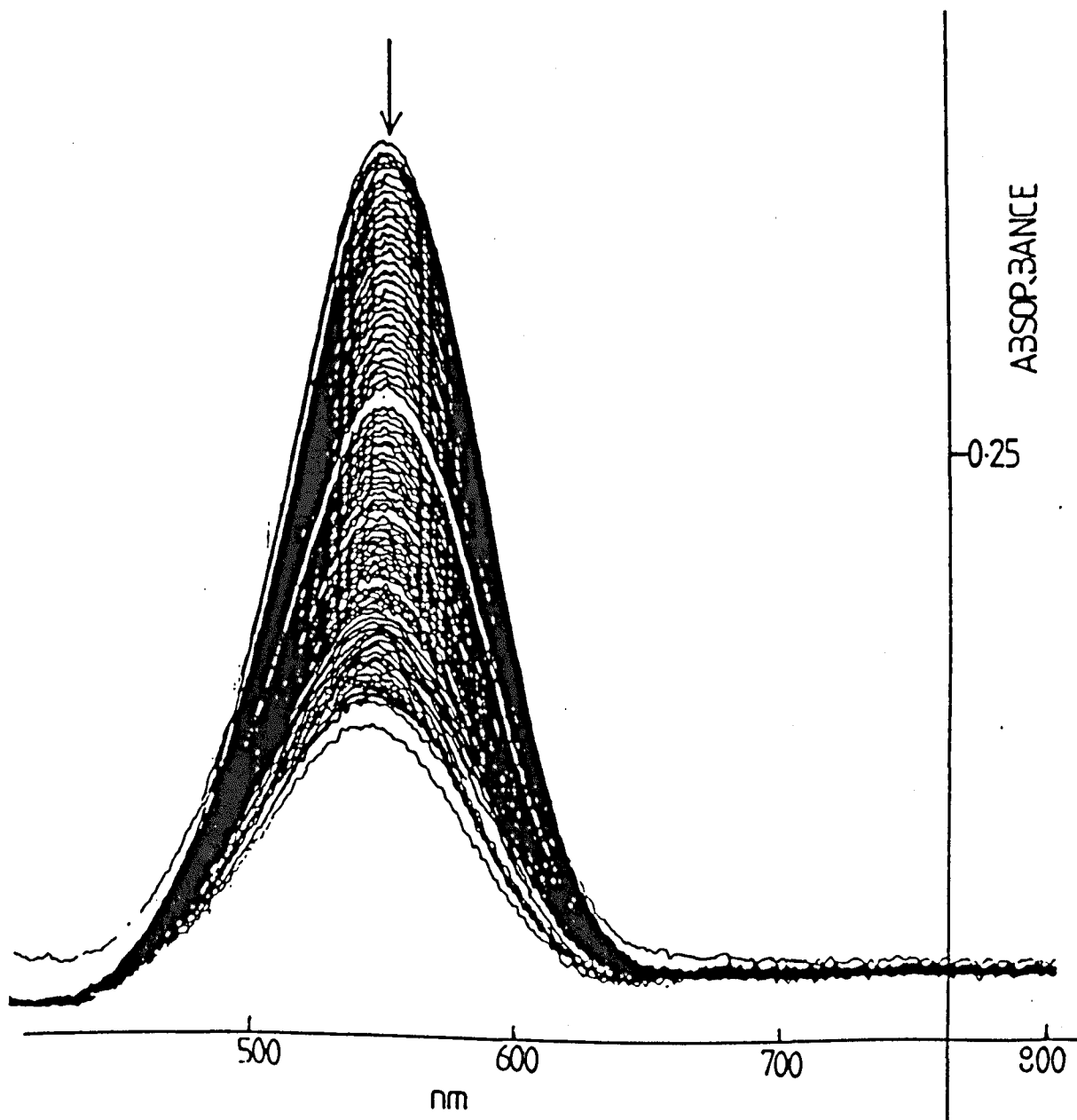


Figure 7.5

A U.V/visible spectrum of $[\text{Ni}(\text{L}^8)]^{2+}$ (conc = 1.65mM) in CH_3NO_2 , plus one drop of conc HClO_4 . Scans repeated every 10 minutes.

Figure 3.5

^1H n.m.r spectrum of $[\text{NiL}^8]^{2+}$ in CD_3NO_2 (ref Me_4Si $\delta = 0$), at 400MHz. X = Et_2O integral confirms 0.25 moles. (a)/(b) = 1.3.

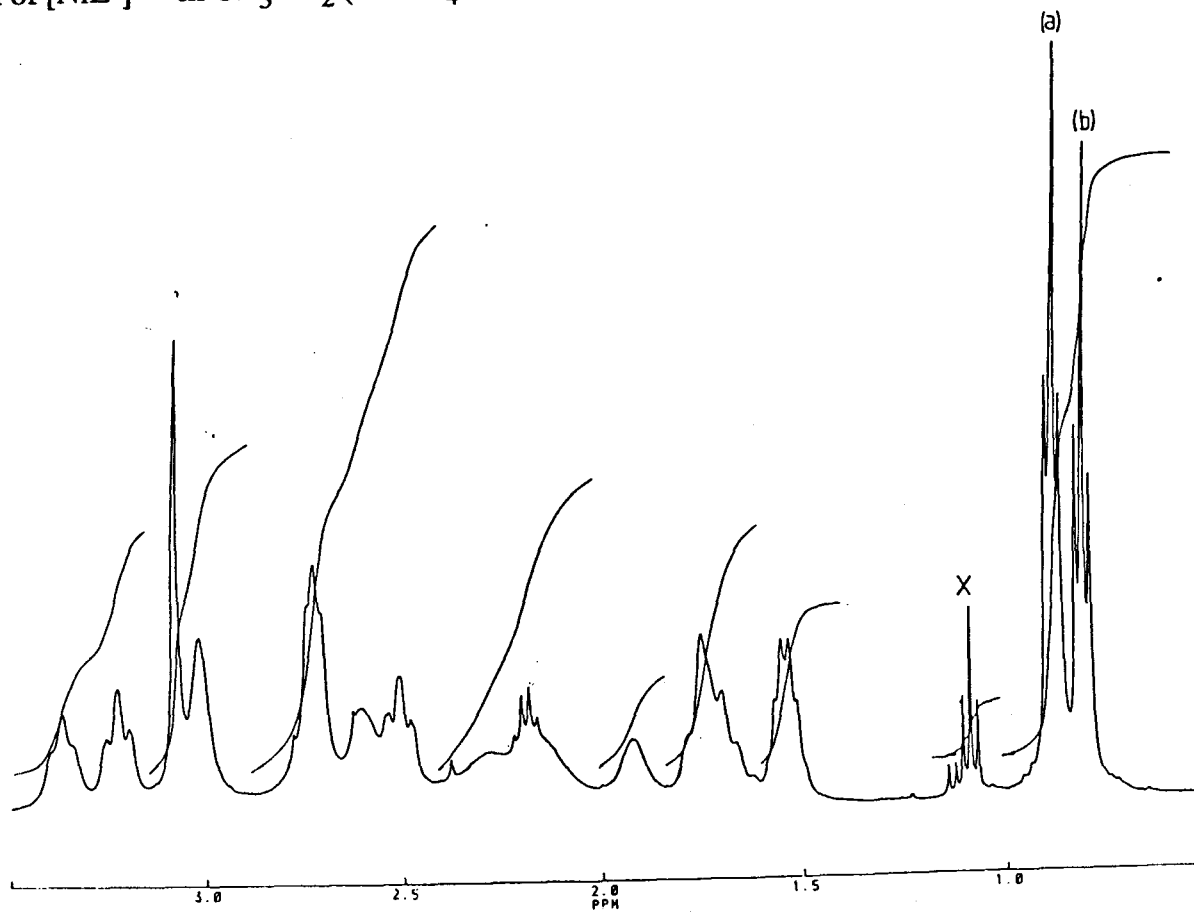
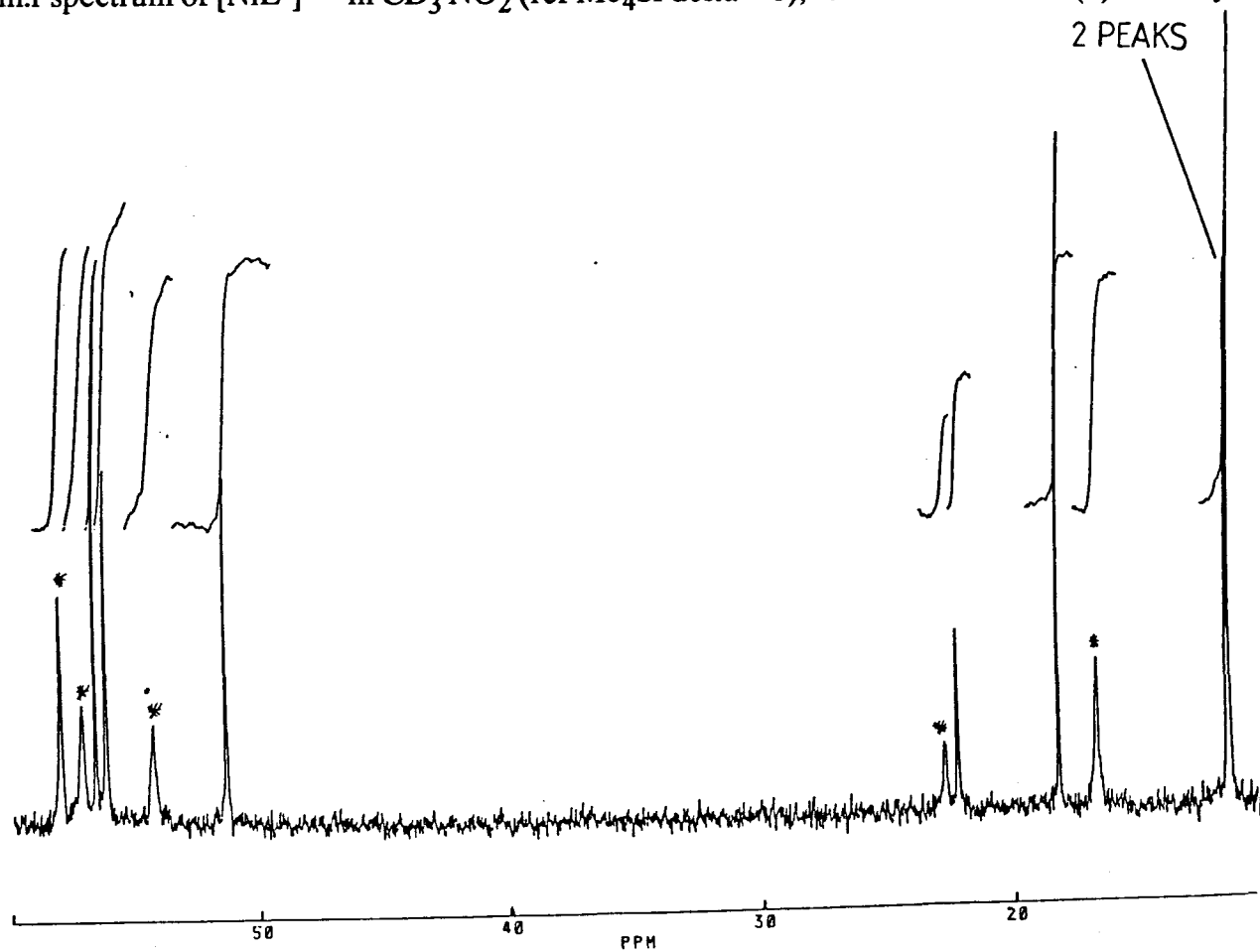


Figure 4.5

^1H decoupled ^{13}C n.m.r spectrum of $[\text{NiL}^8]^{2+}$ in CD_3NO_2 (ref Me_4Si $\delta = 0$), run at 100.62MHz. (*) = 2nd symmetric species



Owing to the apparent ambiguities of the conformation of $[\text{Ni}(\text{L}^8)]^{2+}$, and the lack of success in growing suitable crystals for structural determination, the tetrafluoroborate anion was exchanged for a co-ordinating thiocyanate ligand. The complex obtained as a light blue solid, is formulated as $[\text{Ni}(\text{L}^8)(\text{NCS})_2]$. The I.r spectrum contains two absorbances at 2080cm^{-1} and 2060cm^{-1} corresponding to N bound thiocyanate. The two distinct absorbances clearly indicate two environmentally different thiocyanate groups, as observed in $[\text{Ni}(\text{TMC})(\text{NCS})_2]$ (Table 3.5); the latter assigned to a cis-octahedral geometry by Barefield.^{1 5 8} Conductivity experiments for $[\text{Ni}(\text{L}^8)(\text{NCS})_2]$ in nitromethane solution indicates a 1:1 electrolyte, suggesting a weakly bound thiocyanate group; this is in contrast to the non conducting behaviour of $[\text{Ni}(\text{TMC})(\text{NCS})_2]$. The weakly bound nature of one thiocyanate group is also evident in the U.V/visible spectrum in nitromethane, where absorbances are more consistent with five co-ordinate nickel(II). Therefore, there are apparent differences between the complexes $[\text{Ni}(\text{TMC})(\text{NCS})_2]$ and $[\text{Ni}(\text{L}^8)(\text{NCS})_2]$, possibly due to differently bound thiocyanate groups. To establish the conformation of the macrocyclic ring in $[\text{Ni}(\text{L}^8)(\text{NCS})_2]$, a single crystal X-ray structure was undertaken (Section 4.5).

Section 4.5

Crystal structure of $[\text{Ni}(\text{L}^8)(\text{NCS})_2]$

The structure of the complex $[\text{Ni}(\text{L}^8)(\text{NCS})_2]$ is shown in Figure 8.5(a). The complex is clearly six co-ordinate with the two thiocyanate ligands in trans positions, and the macrocycle adopts the Trans-I configuration (Figure 8.5(b)). The average Ni-N bond lengths in the macrocyclic ring are $2.183(5)\text{\AA}$, which is in good agreement with those found in five co-ordinate Trans-I $[\text{Ni}(\text{TMC})]^{2+}$ structures (Table 6.5)

	Nickel out of plane	Average bond lengths (Å)	ref
$[\text{Ni}(\text{L}^8)(\text{NCS})_2]$	0.0857	2.183(5)	this work
$[\text{Ni}(\text{TMC})(\text{CH}_3\text{CN})]^{2+}$	0.34	2.106(8)	(159)
$[\text{Ni}(\text{TMC})(\text{N}_3)]^+$	0.33	2.104(8)	(161)
$[\text{Ni}(\text{TMC})(\text{DMF})]^{2+}$	0.29	2.143(6)	(160)

Table 6.5

All the bond lengths are longer than the ideal strain free value for Ni-N (1.91Å) as predicted by molecular mechanics calculations.^{1 2} In the case of $[\text{Ni}(\text{TMC})(\text{X})]^{2+}$ this is attributed to the non-bonded repulsions between hydrogen atoms on the N-methyl groups with the co-ordinated ligands.

The Ni-NCS bond distance for the thiocyanate bound on the opposite side of the propyl groups is slightly longer than the corresponding bond distance for the other axial thiocyanate (Ni-N(5)-2.137(5)Å; Ni-N(6)-2.017(4)Å). This is consistent with the conductivity data presented above. The thiocyanate group is bent (C(01)-N(5)-Ni-168.5(5); Ni-N(6)-C(02)-167.9(4)), as shown in Figure 8.5(b). Allowing the six co-ordinate geometry means that the nickel(II) is pulled into the plane of the macrocyclic ring (nickel distance out of plane 0.0857Å), which is contrast to the Trans-I $[\text{Ni}(\text{TMC})(\text{X})]^{n+}$ structures where the nickel(II) is significantly out of the plane (Table 6.5). The inability to form six co-ordination complexes of Trans-I $[\text{Ni}(\text{TMC})(\text{X})]^{n+}$ complexes is attributed to the severe steric interactions between methyl groups and the axial donors, which occur if the nickel(II) is pulled into the plane. To observe this effect, non-bonded distances between opposite R-[CH₂]-N groups (Figure 9.5) are calculated to see how much the methylene groups are pulled in, and then compared to the opposite non-bonded distances of the CH₃-N groups in $[\text{Ni}(\text{TMC})(\text{DMF})]^{2+}$.

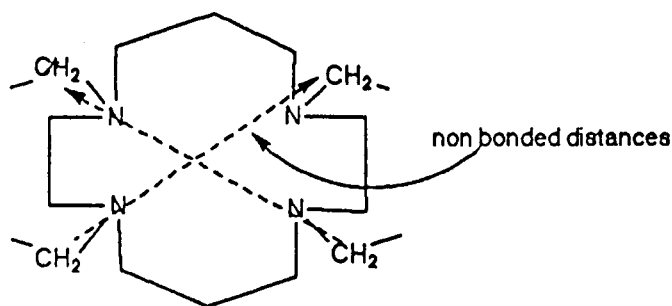


Figure 9.5

The average non-bonded distance for $[\text{Ni}(\text{L}^s)(\text{NCS})_2]$ is 5.69\AA which is reasonably shorter than for $[\text{Ni}(\text{TMC})(\text{DMF})]^{2+}$ (5.79\AA), and so supports the idea that allowing the nickel(II) ion into the plane pulls the R-N ($\text{R} = \text{CH}_2\text{-CH}_3$) groups closer together Figure 8.5(c). Therefore, there seems to be less unfavourable steric interactions between methylene groups and axial donors when compared to methyl groups, and so six co-ordination is possible in the former case.

Bond angles agree well with theoretical 90° and 180° angles for a perfect octahedral geometry (e.g. $\text{N}(1)\text{-Ni-N}(2)\text{-}85.3(2)^\circ$, $\text{N}(2)\text{-Ni-N}(4)\text{-}179.4(2)^\circ$). The macrocyclic ring bond angles are greater than the theoretical angle of 109.47° , which is attributed to the strain of complexation. Interestingly, the bond angles of $\text{N}(1)\text{-C}(1)\text{-C}(2)$ and $\text{C}(1)\text{-C}(2)\text{-N}(2)$ of $121.1(8)$ and $121.7(9)$ respectively, are large, and so most of the macrocyclic ring strain is centralised on this carbon backbone.

Figure 8.5(a)

Crystal structure of $[\text{NiL}^8(\text{NCS})_2]$ showing atomic numbering scheme. Hydrogens omitted for clarity.

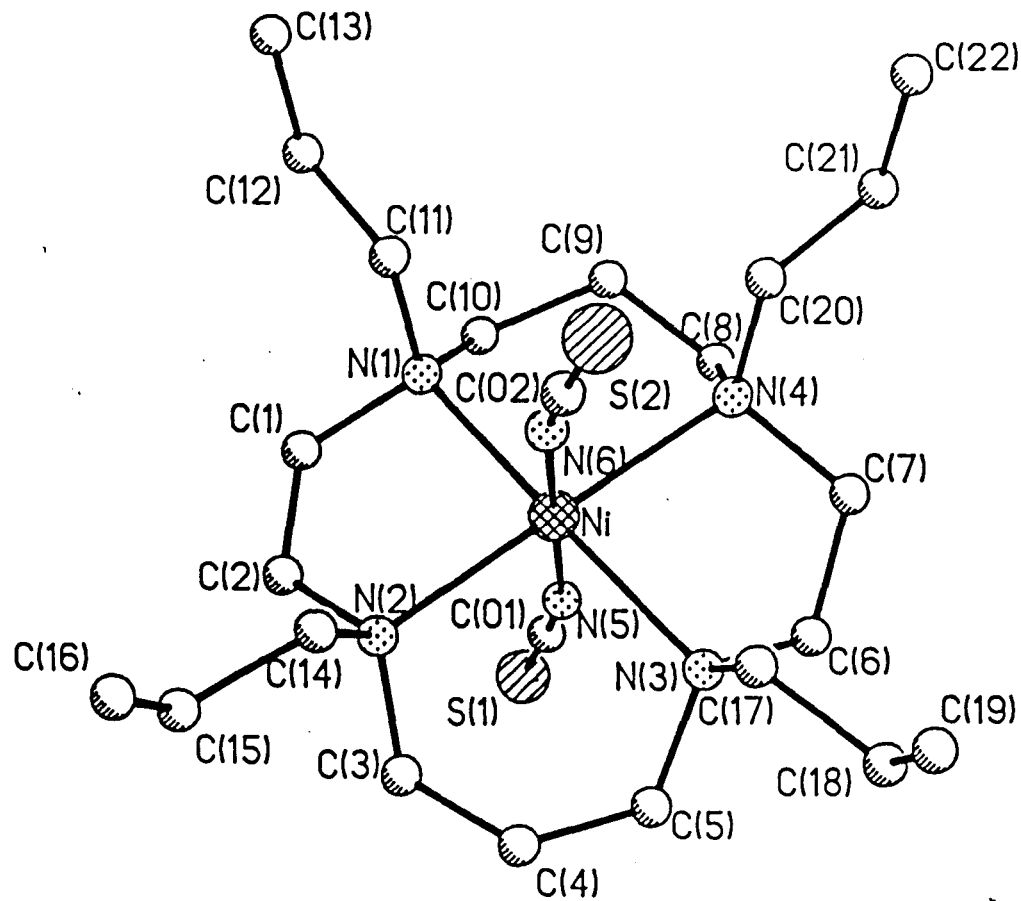


Figure 8.5(b)

Crystal structure of $[\text{NiL}^8(\text{NCS})_2]$ showing the Trans-I configuration and bent thiocyanate groups. Hydrogens omitted for clarity

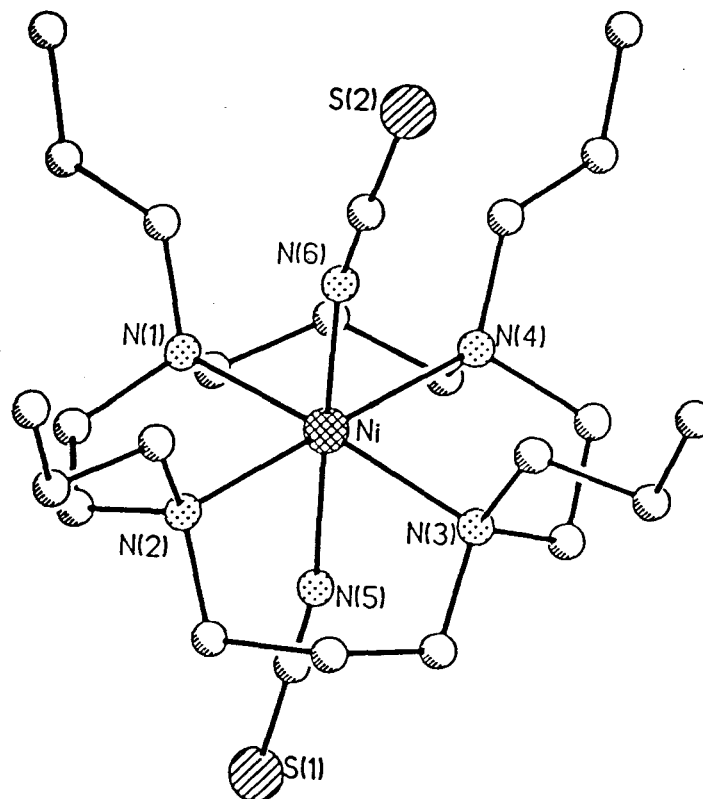


Figure 8.5(c)
Space filling models of Trans-I $[\text{NiL}^8(\text{NCS})_2]$ and Trans-I $[\text{NiTMC}(\text{DMF})]^{2+}$ (*) showing the different "crowding" caused by propyl groups over methyl groups. (*) space filling diagram generated from atomic co-ordinates of reference 160.

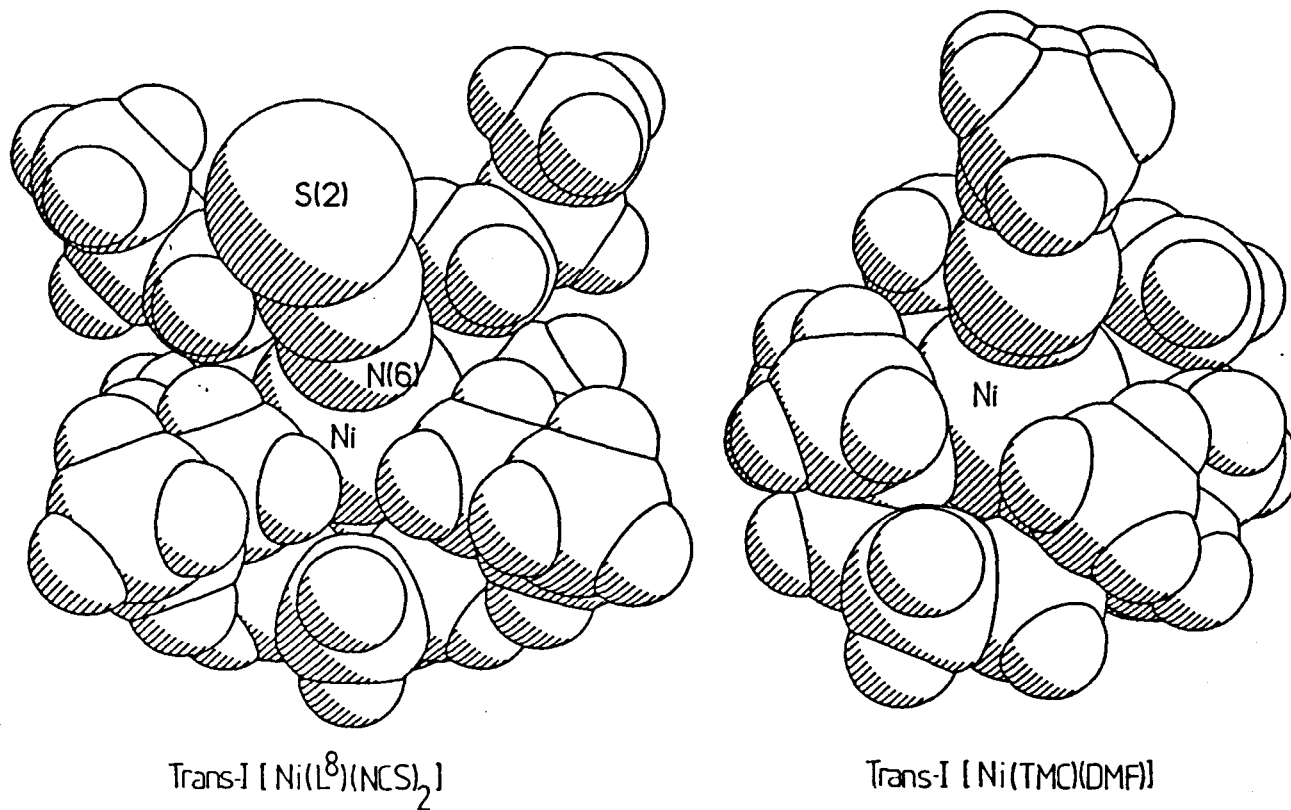


Table 8.5

Bond lengths and angles for $[\text{NiL}^8(\text{NCS})_2]$

Bond lengths (Å)

Ni-N(1)	2.183(5)	Ni-N(2)	2.170(6)
Ni-N(3)	2.170(4)	Ni-N(4)	2.210(5)
Ni-N(5)	2.137(5)	Ni-N(6)	2.017(4)
N(1)-C(1)	1.483(11)	N(1)-C(10)	1.483(10)
N(1)-C(11)	1.489(8)	N(2)-C(2)	1.498(12)
N(2)-C(3)	1.466(10)	N(2)-C(14)	1.494(9)
N(3)-C(5)	1.507(9)	N(3)-C(6)	1.492(8)
N(3)-C(17)	1.489(8)	N(4)-C(7)	1.553(7)
N(4)-C(8)	1.478(9)	N(4)-C(20)	1.491(6)
N(5)-C(01)	1.145(7)	N(6)-C(02)	1.136(7)
S(1)-C(01)	1.623(6)	S(2)-C(02)	1.613(6)
C(1)-C(2)	1.393(17)	C(3)-C(4)	1.520(12)
C(4)-C(5)	1.467(13)	C(6)-C(7)	1.499(9)
C(8)-C(9)	1.487(9)	C(9)-C(10)	1.496(11)
C(11)-C(12)	1.523(10)	C(12)-C(13)	1.492(12)
C(14)-C(15)	1.513(12)	C(15)-C(16)	1.479(14)
C(17)-C(18)	1.526(10)	C(18)-C(19)	1.473(13)
C(20)-C(21)	1.510(8)	C(21)-C(22)	1.490(9)

Bond angles (deg.)

N(1)-Ni-N(2)	85.3(2)	N(1)-Ni-N(3)	171.3(2)
N(2)-Ni-N(3)	96.5(2)	N(1)-Ni-N(4)	94.8(2)
N(2)-Ni-N(4)	179.4(2)	N(3)-Ni-N(4)	83.2(2)
N(1)-Ni-N(5)	87.4(2)	N(2)-Ni-N(5)	88.2(2)
N(3)-Ni-N(5)	84.2(2)	N(4)-Ni-N(5)	91.2(2)
N(1)-Ni-N(6)	93.7(2)	N(2)-Ni-N(6)	90.9(2)
N(3)-Ni-N(6)	94.7(2)	N(4)-Ni-N(6)	89.7(2)
N(5)-Ni-N(6)	178.5(2)	Ni-N(1)-C(1)	103.9(4)
Ni-N(1)-C(10)	107.5(4)	C(1)-N(1)-C(10)	111.3(6)
Ni-N(1)-C(11)	114.0(3)	C(1)-N(1)-C(11)	108.7(6)
C(10)-N(1)-C(11)	111.1(5)	Ni-N(2)-C(2)	102.6(6)
Ni-N(2)-C(3)	111.8(5)	C(2)-N(2)-C(3)	109.0(6)
Ni-N(2)-C(14)	114.3(4)	C(2)-N(2)-C(14)	109.5(7)
C(3)-N(2)-C(14)	109.3(6)	Ni-N(3)-C(5)	111.3(4)
Ni-N(3)-C(6)	102.9(3)	C(5)-N(3)-C(6)	107.9(5)
Ni-N(3)-C(17)	112.2(3)	C(5)-N(3)-C(17)	110.9(5)
C(6)-N(3)-C(17)	111.2(5)	Ni-N(4)-C(7)	105.2(4)
Ni-N(4)-C(8)	106.5(3)	C(7)-N(4)-C(8)	107.5(4)
Ni-N(4)-C(20)	115.8(3)	C(7)-N(4)-C(20)	107.8(4)
C(8)-N(4)-C(20)	113.5(5)	Ni-N(5)-C(01)	168.5(5)
Ni-N(6)-C(02)	167.9(4)	N(5)-C(01)-S(1)	178.6(5)
N(6)-C(02)-S(2)	176.8(5)	N(1)-C(1)-C(2)	121.1(8)
N(2)-C(2)-C(1)	121.7(9)	N(2)-C(3)-C(4)	113.3(6)
C(3)-C(4)-C(5)	115.0(8)	N(3)-C(5)-C(4)	115.3(6)
N(3)-C(6)-C(7)	111.1(5)	N(4)-C(7)-C(6)	114.0(5)
N(4)-C(8)-C(9)	112.7(5)	C(8)-C(9)-C(10)	118.1(6)
N(1)-C(10)-C(9)	117.4(6)	N(1)-C(11)-C(12)	117.9(6)
C(11)-C(12)-C(13)	112.5(7)	N(2)-C(14)-C(15)	118.5(6)
C(14)-C(15)-C(16)	113.6(9)	N(3)-C(17)-C(18)	118.5(5)
C(17)-C(18)-C(19)	110.8(7)	N(4)-C(20)-C(21)	118.2(4)
C(20)-C(21)-C(22)	112.0(5)		

Section 5.5

Thermodynamic and Kinetic studies of $[\text{Ni}(\text{L}^s)]^{2+}$ in acetonitrile

Thermodynamic and kinetic data were obtained by variable temperature studies of ^1H n.m.r chemical shifts, and ^{14}N n.m.r line broadening studies, respectively. The line broadening data were analysed using Swift-Connick plots¹⁶⁸ as shown in Figure 10.5. The data obtained, summarised in Table 7.5, confirm the Trans-I conformation of the complex.

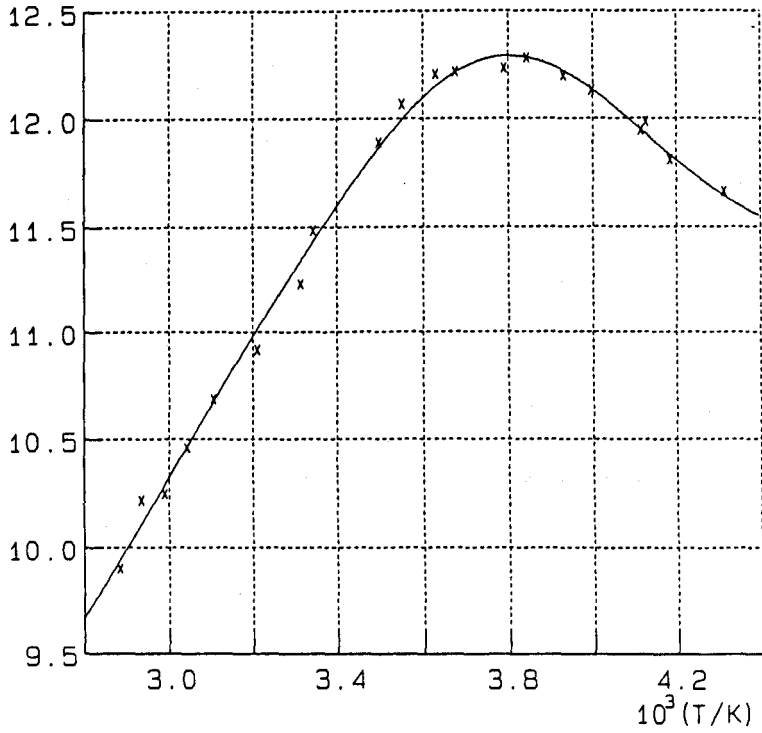
	K(298.2)	$-\Delta\text{H}^\ominus/$ kJ mol ⁻¹	$-\Delta\text{S}^\ominus/$ J K ⁻¹ mol ⁻¹	$k_{\text{ex}}/$ s ⁻¹ x 10 ⁶	ref
$[\text{Ni}(\text{L}^s)]^{2+}$ (a)	1.5	12.7±0.2	39.0±8.5	2.1±0.5	This work
Trans-I $[\text{Ni}(\text{TMC})]^{2+}$	0.977	16.8±0.8	32.0±2.0	5.6±0.4	(156)

(a) $[\text{Ni}] = 0.0260\text{M}$ in CH_3CN , $\Delta\text{H}^\ominus = 26 \pm 4$ kJ mol⁻¹, $\Delta\text{S}^\ominus = 35 \pm 14$ J K⁻¹ mol⁻¹

Table 7.5

The entropy value (-39.0 ± 8.5 J K⁻¹ mol⁻¹) is consistent with the four co-ordinate equilibrium, as expected with Trans-I conformations. The possibility of di-solvation is unlikely, as a value twice that observed would be expected. The only appreciable change is in the rate of solvent exchange, where acetonitrile exchange is slower for $[\text{Ni}(\text{L}^s)]^{2+}$. Again this slowing of solvent exchange is consistent with extra steric crowding of the propyl groups.

Swift-Connick plot of $\ln(1/T2r)$ versus $1/T$
 $\ln(1/T2r)$



Swift-Connick plot
 $10^{-3}(\Delta\omega(r))$

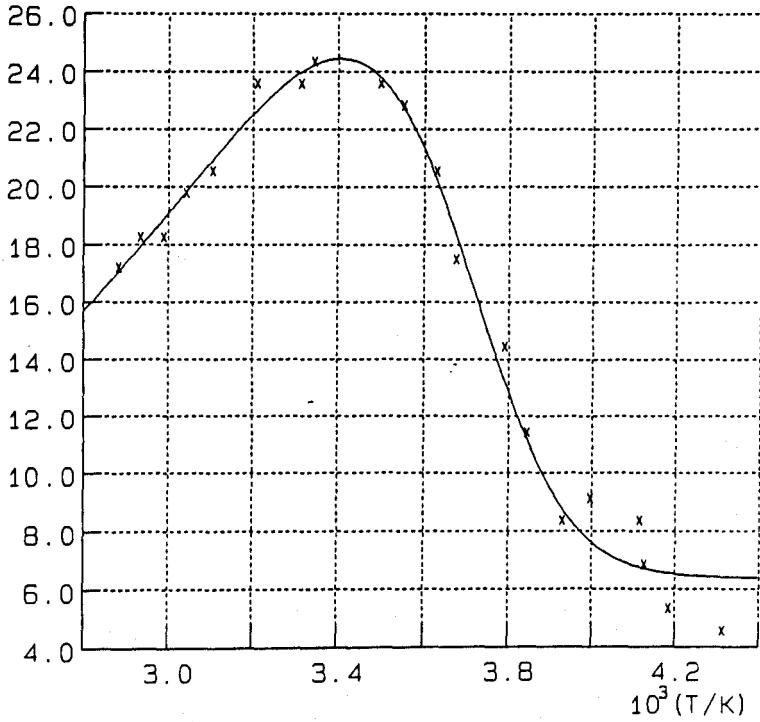


Figure 10.5

Swift-Connick plots for $[\text{NiL}^8]^{2+}$ (0.0260 mol dm^3) in acetonitrile/nitromethane (41:1) ratio.

Section 6.5

Nickel(II) complexes of L⁹

The poor solubility of L⁹ in ethanol makes this an unsuitable solvent for preparation of its metal complexes, and therefore hot solutions of L⁹ and [Ni(DMSO)₆](ClO₄)₂ were used instead. The solution takes several hours to turn purple, indicating slow metal complex formation. This is attributed to the long alkyl arms hindering entry of the nickel(II) into the macrocyclic ring. The dark purple complex formed is formulated as Trans-I [Ni(L⁹)(DMSO)](ClO₄)₂, by elemental analysis, and comparison with electronic spectra of Trans-I [Ni(TMC)]²⁺ (Table 3.5). The complex is soluble in most co-ordinating or polar solvents (*e.g.* CH₃CN, CH₃NO₂, CHCl₃). The infrared spectrum confirms the existence of a co-ordinated DMSO molecule (ν -958cm⁻¹).¹⁴⁷ In chloroform solution the purple complex dissociates to give a mixture of four co-ordinate (unsolvated λ_{\max} 557nm) and five co-ordinate (unsolvated λ_{\max} = 400nm) species, as shown in Figure 13.5. Addition of excess dry tetrabutylammonium perchlorate to the solution drives the equilibrium entirely to the four co-ordinate complex (Figure 13.5), and the extinction coefficient of this species is estimated from such solutions to be 137 dm³ mol⁻¹ cm⁻¹. In the absence of added perchlorate, and at a total nickel(II) concentration of 3.4mM the percentages of [Ni(L⁹)]²⁺ and [Ni(L⁹)(DMSO)]²⁺ present in chloroform solution are estimated from the U.V visible spectrum to be 86% and 14% respectively.

The ¹³C n.m.r in chloroform solution (Figure 11.5) is consistent with an equilibrium between a predominantly diamagnetic four co-ordinate complex and a small amount a paramagnetic five co-ordinate species in rapid equilibrium. There is also evidence for a small amount of a second species showing broad resonances at δ = 25.12, 35.32 and 36.62 p.p.m. The number of resonances observed for the dominant species is consistent with a symmetric structure of the Trans-I type. The nature of the minor species (presumably another isomer) is uncertain.

The ^1H n.m.r spectrum (Figure 12.5) confirms the presence of the paramagnetic five co-ordinate complex, with large shifted macrocyclic resonances at $\delta = 4.90, 5.65, 5.91, 8.23, 9.02, 19.61$ p.p.m. ($[\text{Ni}] = 1 \times 10^{-2} \text{ M}$, $T = 298\text{K}$).

Attempts were also made to prepare a complex in acetonitrile solution, but ingress of adventitious water led to an aquo rather than an acetonitrile solvate. Addition of a known concentration of nickel(II) cation, in acetonitrile, to an equimolar amount of L^9 in hot acetonitrile, gives after several hours reflux a dark purple solution. Again it is evident that the nickel(II) does not enter the macrocyclic cavity quickly. A dark purple solid is obtained, which after work up and even careful drying is formulated as $[\text{Ni}(\text{L}^9)(\text{OH}_2)](\text{BF}_4)_2 \cdot 2\text{H}_2\text{O}$ by elemental analysis (Table 2.5). The crystallised water comes from the nickel(II) solution (see experimental) used in the synthesis. The infrared spectrum confirmed the existence of water by absorbances at 3400cm^{-1} and 1620cm^{-1} . The U.V/visible spectrum in CHCl_3 again shows the same four co-ordinate to five co-ordinate equilibrium (Figure 14.5), but in this case there is an approximately 50:50 mixture. The paramagnetic moment of the complex is 1.75 B.M in accordance with a mixture of four co-ordinate (paramagnetic) and five co-ordinate (paramagnetic) species. The stability of the five co-ordinate complexes of the nickel(II) complexes of L^9 follows the trend $\text{H}_2\text{O} > \text{DMSO}$, which is in keeping with the extra steric bulkiness of the DMSO group.

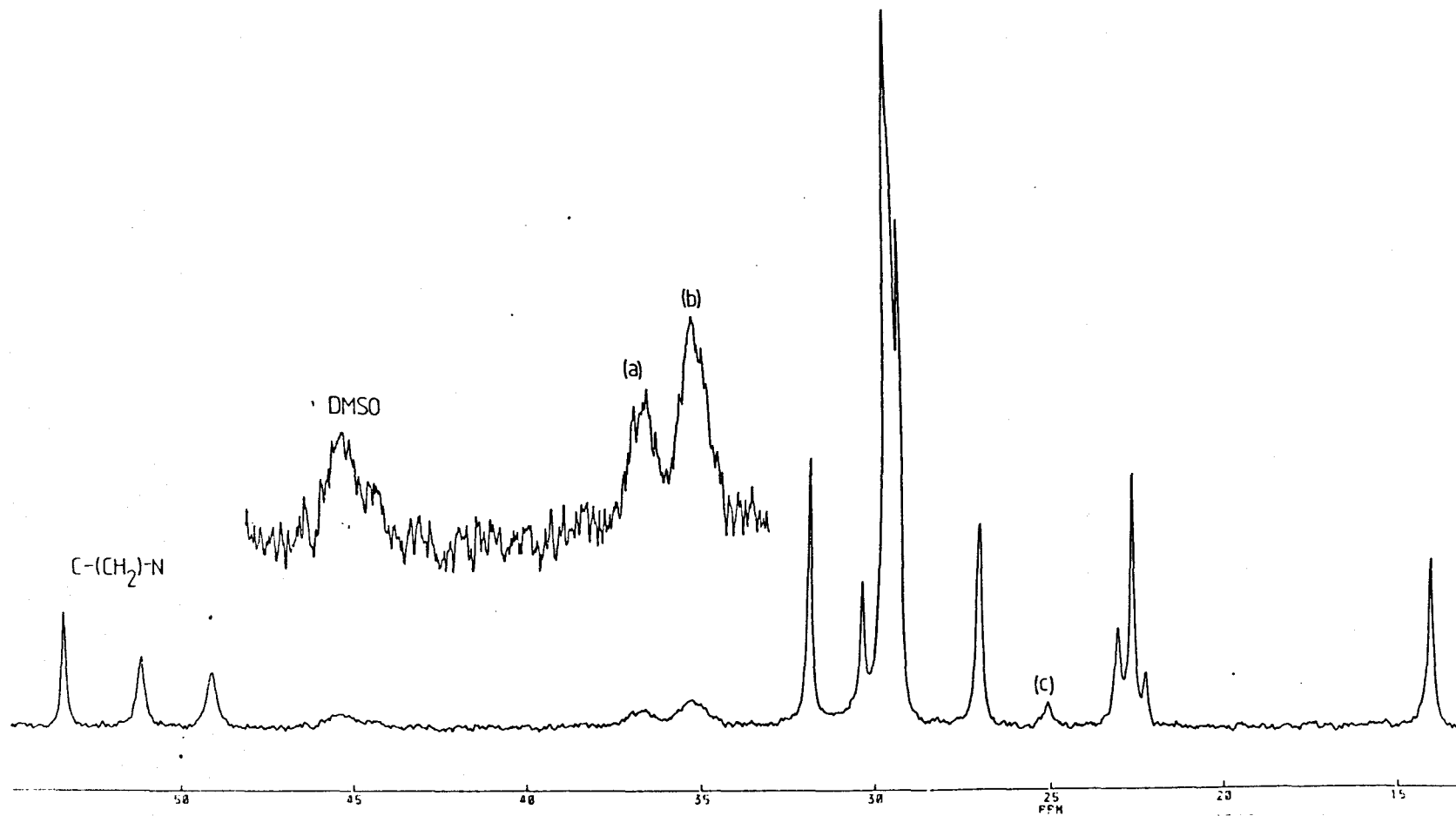


Figure 11.5

^1H decoupled ^{13}C n.m.r of $[\text{Ni}(\text{L}^9)(\text{DMSO})](\text{ClO}_4)_2$ in CDCl_3 (ref Me_4Si $\delta = 0$) at 100.63MHz. (a), (b), (c) are minor resonances.

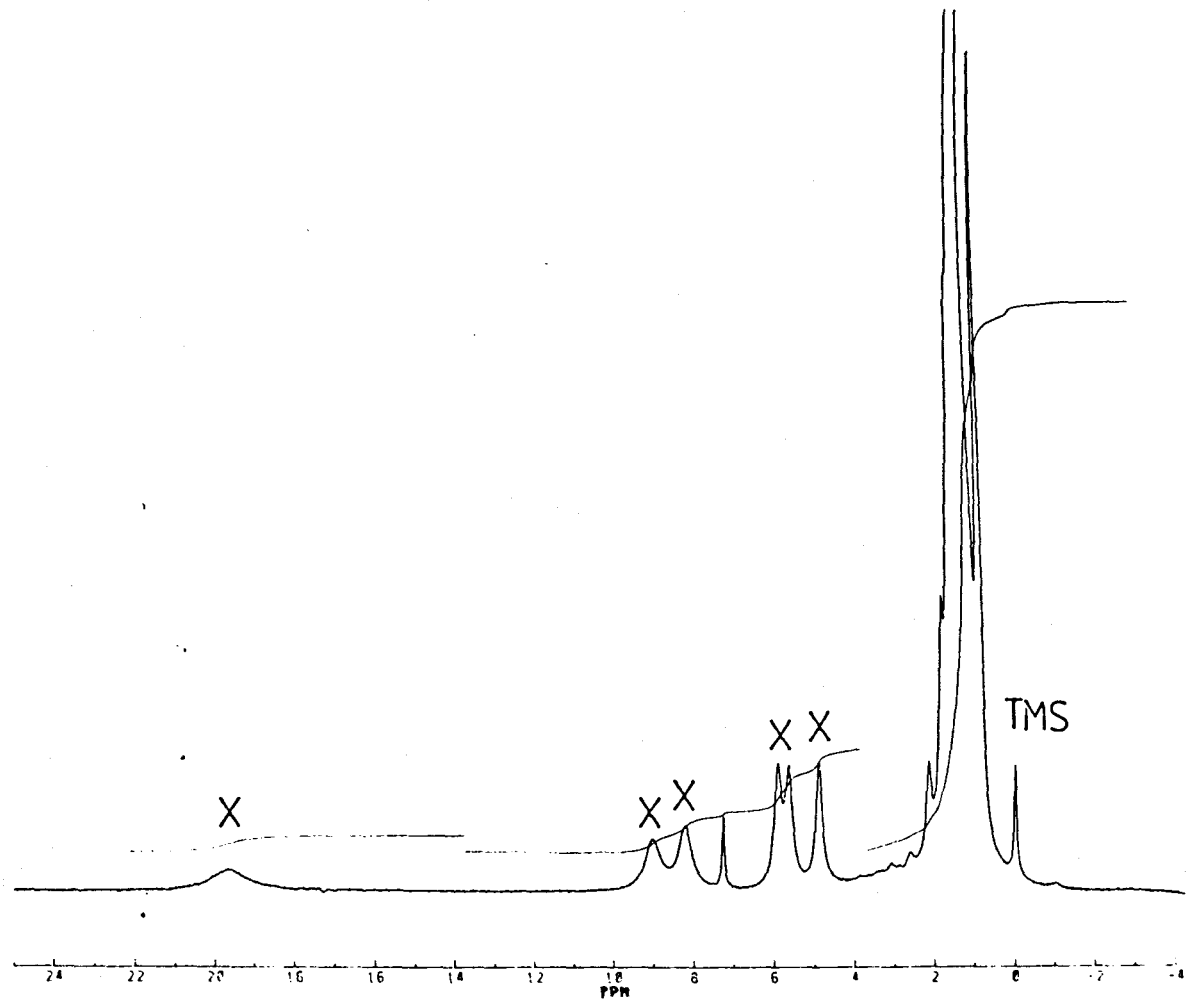


Figure 12.5

^1H n.m.r of $[\text{Ni}(\text{L}^9)\text{DMSO}](\text{ClO}_4)_2$ in CDCl_3 (ref Me_4Si $\delta = 0$) at 400MHz. X = resonances of five co-ordinate species.

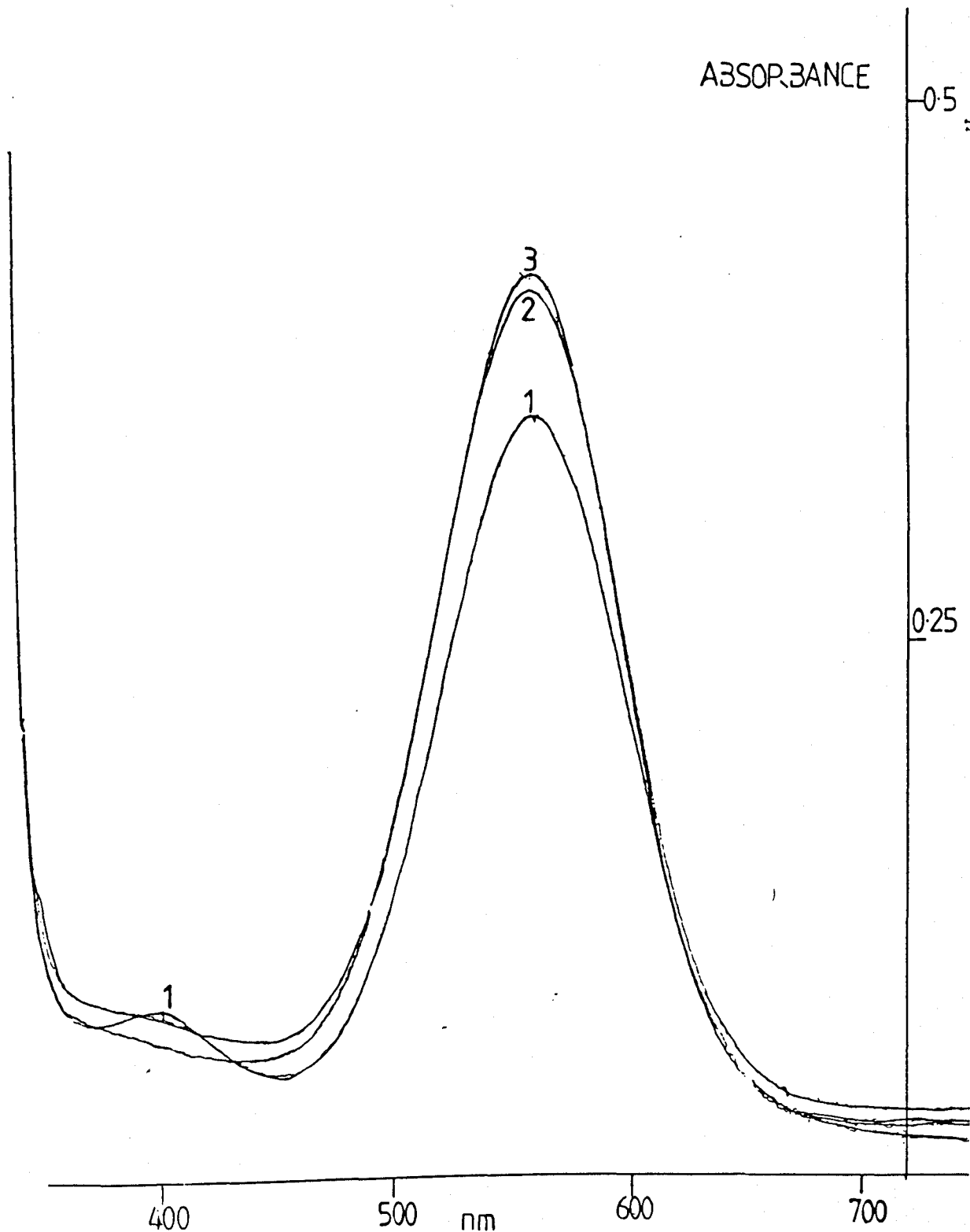


Figure 13.5

U.V/visible spectrum of $[\text{Ni}(\text{L}^9)(\text{DMSO})](\text{ClO}_4)_2$ (conc = 3.4mM) in CHCl_3 . (1) original sample (2) addition of slight excess of tetrabutylammonium perchlorate (TBAP) (3) Large excess of TBAP added.

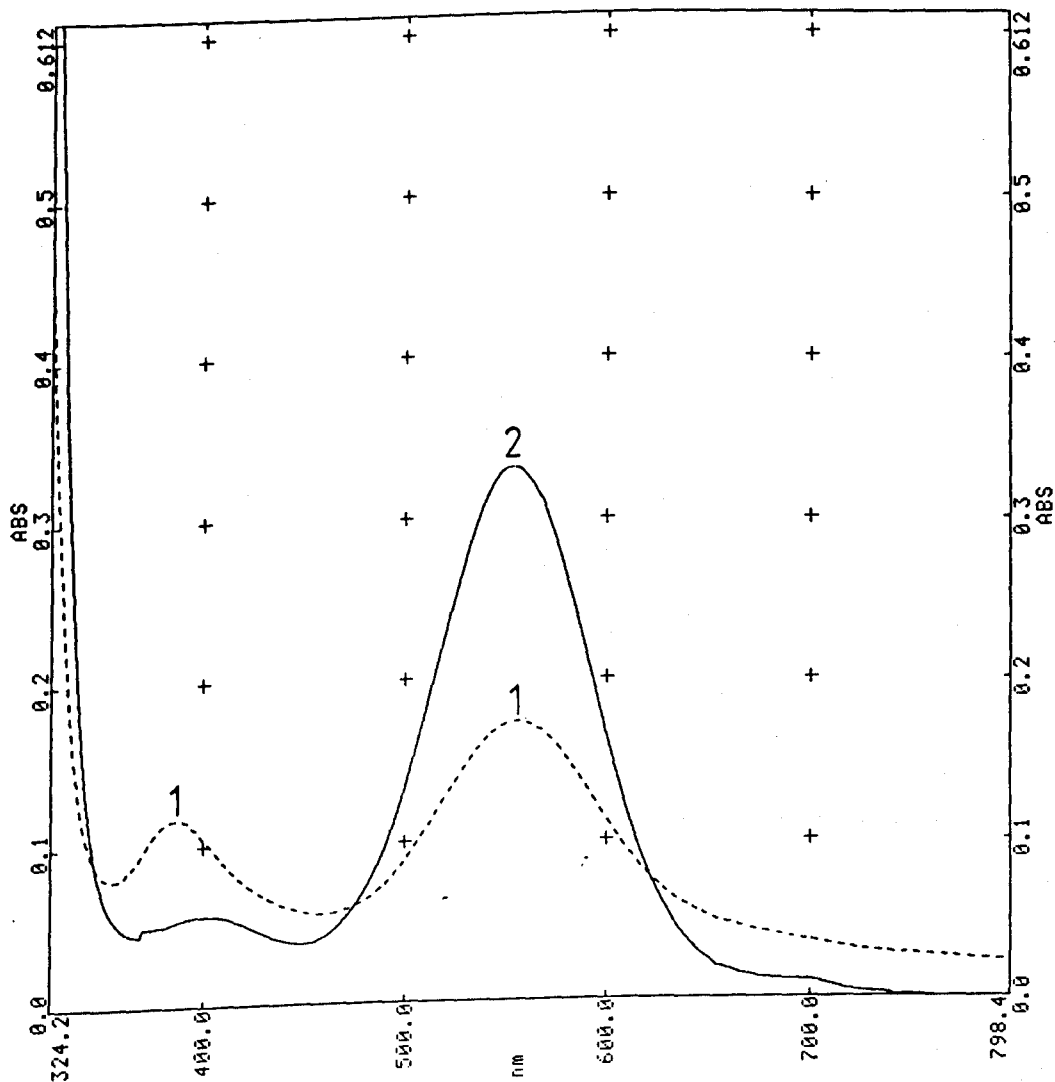


Figure 14.5

U.V/visible spectrum of $[\text{Ni}(\text{L}^9)(\text{OH}_2)](\text{BF}_4)_2 \cdot 2\text{H}_2\text{O}$ (conc = 1.7mM) in CHCl_3 . (1) original sample (2) addition of excess TBAP.

Conclusions

In the preparation of $[\text{Ni}(\text{L}^8)]^{2+}$ two isomers are produced in approximately equal amounts, which is in contrast to the single Trans-I isomer produced in direct $[\text{Ni}(\text{TMC})]^{2+}$ preparations. The crystal structure of $[\text{Ni}(\text{L}^8)(\text{NCS})_2]$ shows that the macrocycle adopts a Trans-I configuration. Since $[\text{Ni}(\text{L}^8)](\text{BF}_4)_2$ is a mixture of two isomers, addition of NCS^- appears to generate one isomer.

A further interesting point is the comparison of the two complexes $[\text{Ni}(\text{TMC})(\text{NCS})_2]$ and $[\text{Ni}(\text{L}^8)(\text{NCS})_2]$. From spectroscopic data they have different properties, and hence can be predicted to have different geometries. A crystal structure of $[\text{Ni}(\text{TMC})(\text{NCS})_2]$ is required to confirm this.

The nickel(II) complexes of the lipophilic ligand L^9 are interesting since they are soluble in non co-ordinating chlorohydrocarbon solvents like chloroform. The interest recently in such systems is in the transfer of metal ions across water/organic interfaces, where with certain ligands the problem of "leeching" of the metal complexes into the water phase is a problem. With L^9 this problem is overcome as the metal complexes are totally insoluble in water. However, there is a drawback in the use of L^9 for metal ion extraction, since the rate of complexation with the macrocycle is too slow for rapid extraction. Perhaps by shortening the alkyl chain lengths an "ideal" macrocycle could be produced for such purposes.

Compound	C-(CH ₂)-C + CH ₃ -C-C	C-N-(CH ₂)-C
L ⁸	11.90(4C), 19.23(4C), 23.15(2C)	50.59(4C), 51.55(4C), 57.82(4C)
L ⁹	14.10(4C), 22.72(4C), 23.18(2C) 27.49(4C), 27.65(4C), 29.39(4C) 29.69(20C), 31.96(4C)	50.73(4C), 51.68(4C), 55.82(4C)
[NiL ⁸](BF ₄) ₂ 0.25Et ₂ O two isomers(a)	11.45(4C), 11.55(4C), 16.71(4C) 18.25(4C), 22.21(2C), 22.69(2C)	51.36(4C), 54.33(4C), 56.24(4C) 56.66(4C), 57.17(4C), 58.06(4C)
[NiL ⁹ DMSO](ClO ₄) ₂	14.11(4C), {22.29, 22.69, 23.10}-(8C) 25.12(*), 27.05(4C) {29.38, 29.65, 30.38}-(24C) 31.93(4C), 35.32(*), 36.62(*)	45.32(2C dms), 49.14(4C), 51.19(4C) 53.4(4C)

Table 1.5

¹H decoupled ¹³C n.m.r data run in CDCl₃ (ref Me₄Si delta = 0) unless stated. (a) CD₃NO₂ (ref Me₄Si delta = 0). (*) = minor resonances

Compound	Colour	Yield	Formula	(C) (found in parentheses)	(H) (found in parentheses)	(N) (found in parentheses)
$[\text{NiL}^8](\text{BF}_4)_2 \cdot 0.25\text{Et}_2\text{O} (*)$	purple	89%	$\text{C}_{22}\text{H}_{48}\text{B}_2\text{F}_8\text{N}_4\text{Ni}1.0.25\text{Et}_2\text{O}$	44.55 (44.84)	8.15 (8.45)	9.04 (9.46)
$[\text{NiL}^8(\text{NCS})_2]$	light blue	83%	$\text{C}_{24}\text{H}_{48}\text{N}_6\text{Ni}1\text{S}_2$	53.04 (52.66)	8.90 (8.87)	15.46 (15.21)
$[\text{NiL}^9(\text{DMSO})](\text{ClO}_4)_2$	purple	61%	$\text{C}_{60}\text{H}_{126}\text{Cl}_2\text{N}_4\text{Ni}1\text{O}_9\text{S}_1$	59.59 (59.50)	10.50 (10.20)	4.63 (4.72)
$[\text{NiL}^9(\text{OH}_2)](\text{BF}_4)_2 \cdot 2\text{H}_2\text{O}$	purple	89%	$\text{C}_{58}\text{H}_{126}\text{B}_2\text{F}_8\text{N}_4\text{Ni}1\text{O}_3$	60.05 (60.22)	10.95 (10.77)	4.83 (4.88)

Table 2.5

Combustion analysis results for complexes of Chapter 5. (*) ^1H n.m.r confirmed existence of trace of Et_2O

Compound	Magnetic Moment(B.M)(a)	$\lambda_{\max}(\text{nm})$ $\epsilon_{\max}(\text{mol}^{-1}\text{dm}^3\text{cm}^{-1})$			Molar Conductivity ^g ($\Omega^{-1}\text{mol}^{-1}\text{cm}^2$)
		DMSO ^f	CH ₃ NO ₂ ^f	CH ₃ CN ^f	
[NiL ⁸](BF ₄) ₂ ·0.25Et ₂ O	diamagnetic	407(38) 551(98) 700(sh,7)	544(212)	386(45) 548(24)	203(1:2 electrolyte)
[NiL ⁸ (NCS) ₂]	2.5	676(39)	684(47)		68(1:1 electrolyte)
[NiL ⁹ (DMSO)](ClO ₄) ₂	diamagnetic		384(57)	400(18) ^d 552(100)	557(101)
[NiL ⁹ (OH ₂)](BF ₄) ₂ ·2H ₂ O	1.75(e)				556(77) 428(70)
[NiTMC(NCS) ₂](b)			975(10) 820(15) 610(13) 390(23)		
Trans-I[NiTMC](ClO ₄) ₂ (c)			519(185)		
Trans-III[NiTMC](ClO ₄) ₂ (c)			492(83)		

Table 3.5

(a) Evans method ~ 1x10⁻²M solutions at 25 C. (b) from reference .(c) from ref 158 .(d) minor peak. (e) solid sample. (f) solvents used. (g) CH₃NO₂ solution.

[NiL⁸-H]⁺

m/z(calc)	m/z(found)
425-(100%)	425-(100%)
426-(27%)	426-(38%)
427-(42%)	427-(9%)
428-(12%)	428-(19%)
429-(7%)	429-(/)
430-(2%)	430-(/)

[NiL⁸NCS]⁺

m/z(calc)	m/z(found)
484-(100%)	484-(100%)
485-(29%)	485-(25%)
486-(47%)	486-(49%)
487-(15%)	487-(13%)
488-(9%)	488-(12%)
489-(2.4%)	489-(2%)
490-(2.2%)	490-(4%)

[NiL⁹-H]⁺ (†)

m/z(calc)	m/z(found)
929-(100%)	929-(/)
930-(68%)	930-(23%)
931-(62%)	931-(100%)
932-(33%)	932-(71%)
933-(16%)	933-(42%)
934-(6%)	934-(25%)
935-(3%)	935-(/)
936-(1%)	936-(/)

Table 4.5

Mass spectral data for complexes of Chapter 5. Relative isotopic abundances in parentheses expressed as % of main isotopic peak.(†) Even though the calculated mass and observed mass are two units out, the isotopic patterns are similar. All

RMM	555.504
System	Monoclinic
Space Group	$P2_1/c$
Systematic Absences	$h,0,l:l=2n+1, 0,k,0:k=2n+1$
$a/\text{\AA}$	17.743(7)
$b/\text{\AA}$	9.605(5)
$c/\text{\AA}$	19.898(8)
$\alpha/^\circ$	/
$\beta/^\circ$	102.03(4)
$\gamma/^\circ$	/
$U/(\text{\AA}^3)$	2942(2)
D_c/gcm^{-3}	1.25
Z	4
$\mu(\text{Mo-K}\alpha)/\text{cm}^{-1}$	8.2
Unique Reflections	5754
Total Reflections	
$I/\sigma(I)\geq 2.0$	5408
2θ max	50
Range 2θ about	
$K\alpha_1$ - $K\alpha_2$	+ 0.50/-0.5
Speed $2\theta/^\circ \text{ min}^{-1}$	2-29
Dimensions(mm)	0.1x0.1x0.1
Max/Min Transmission	
Factors	+ 0.844/-0.799
Final R/(R ¹)	0.0668/0.0862
Weighting(g)	0.0102
Largest peak on ΔF map($e \text{\AA}^3$)	+ 0.6/-0.60

Table 5.5
Crystal data for $[\text{Ni}(\text{L}^8)(\text{NCS})_2]$

Experimental

For experimental techniques and instrumentation see Chapter 7. Chemicals and solvents are discussed in Chapter 2 (Section 14.2). Cyclam was prepared as discussed in Chapter 2. The nickel(II) salt $[\text{Ni}(\text{DMSO})_6]\text{X}$, where $\text{X} = \text{BF}_4$, ClO_4 were prepared by standard literature method.^{1 2 2} The nickel(II) salt $[\text{Ni}(\text{CH}_3\text{CN})_6](\text{BF}_4)_2$ was prepared by the same method as the DMSO solvate complexes, except that the blue solid obtained did not give a U.V/visible spectrum which was consistent with the literature.^{1 6 5} Therefore, known mass of solid was dissolved in CH_3CN (25cm^3), and a EDTA titration carried out to determine the percentage nickel(II) present. Complexes were obtained by syringing known volumes of the standardised solution into reaction mixtures.

Preparation of 1,4,8,11-Tetrapropylamido-1,4,8,11-tetraazacyclotetradecane →(1)

Cyclam (1g, 5mmol) and Et_3N (5g, 50mmol) in dry CH_2Cl_2 (50cm^3) were added slowly to a cooled solution of propanoyl chloride (4.6g, 50mmol) in CH_2Cl_2 (100cm^3) and stirred for 12 hours. The organic layer was washed with H_2O ($2 \times 20\text{cm}^3$), separated and dried over anhydrous MgSO_4 , and the solvent removed on a rotary evaporator, to give a brown solid. Column Chromatography on silica using CH_2Cl_2 removed unreacted propanoyl chloride, and MeOH gave after solvent removal a white solid (1.85g, 87% yield). I.r (Nujol Mull): 1600cm^{-1} (C=O). ^1H n.m.r (CDCl_3): 1.15(t, 12H), 1.90(m, 4H), 2.40(m, 8H), 3.50(m, 16H). C.I mass spectrum m/z calculated 425, m/z found 425 $[\text{M} + \text{H}]^+$.

Preparation of 1,4,8,11-Tetrapropyl-1,4,8,11-tetraazacyclotetradecane (L^8)

The tetraamide derivative (1) (1.77g, 2.2mmol) was dissolved in dry THF (200cm^3). $\text{BH}_3 \cdot \text{thf}$ (40cm^3 , 42mmol) was added and the mixture refluxed overnight under nitrogen. The excess $\text{BH}_3 \cdot \text{thf}$ was destroyed by addition of MeOH. The solvent was removed on a rotary evaporator, and the white solid remaining dissolved in Butan-1-ol (30cm^3), H_2O (30cm^3), concHCl (80cm^3) and refluxed for 12 hours. The solvent was basified to $\text{pH} \geq 12$ and extracted with

CH_2Cl_2 ($6 \times 50\text{cm}^3$), the combined organic layers were then dried over anhydrous MgSO_4 , and the solvent removed on a rotary evaporator to give a yellow oil. The oil was passed down an alumina column using CHCl_3 (95%)/ MeOH (5%), and after solvent removal gave a pale yellow oil (1.26g, 82% yield). I.r (Nujol Mull): loss of $\text{C}=\text{O}$. ^1H n.m.r (CDCl_3): 0.90(t, 12H), 1.50(m, 8H), 1.70(m, 4H), {2.45, 2.65}(m, 24H). C.I mass spectrum m/z calculated 369 m/z found 369 $[\text{M} + \text{H}]^+$.

Preparation of Dodecanoyl chloride

Dodecanecarboxylic acid (10g, 50mmol) was dissolved in excess thionyl chloride (100cm^3) and refluxed overnight. The excess thionyl chloride was distilled off, and the remaining thionyl chloride removed *in vacuo*. The remaining yellow oil was distilled on a Kugelöhr apparatus at 125°C (0.7mmHg) to give a colourless liquid (10g, 91% yield). I.r (thin film): 2940cm^{-1} (C-H), 1800cm^{-1} (C=O), 1470cm^{-1} , 1410cm^{-1} .

Preparation of 1,4,8,11-Tetradodecanamido-1,4,8,11-tetraazacyclotetradecane (2)

Cyclam (0.9g, 4.5mmol) and Et_3N (2.3g, 30mmol) in dry CH_2Cl_2 (50cm^3) were added to a stirring solution of dodecanoyl chloride (10g, 46mmol) in dry CH_2Cl_2 (100cm^3) and stirred for 12 hours. The organic layer was washed with H_2O ($2 \times 50\text{cm}^3$), separated and dried over anhydrous MgSO_4 . After solvent removal the crude product was passed down a silica column, eluting with CH_2Cl_2 to remove unreacted dodecanoyl chloride, and MeOH to remove the desired product. After solvent removal, the yellow oil produced was recrystallised from MeOH to give a white powdery solid (2.5g, 60% yield). I.r (Nujol Mull): 1600cm^{-1} (C=O). ^1H n.m.r (CDCl_3): 0.90(t, 12H), 1.30(br, 68H), 1.65(m, 9H), 1.90(m, 3H), 2.30(m, 4H), 3.50(m, 16H). F.A.B mass spectrum m/z calculated 929 m/z found 929 $[\text{M}]^+$.

Preparation of 1,4,8,11-Tetradodecanyl-1,4,8,11-tetraazacyclotetradecane (L^9)

The tetraamide derivative (2) (2.5g, 2.7mmol) was dissolved in dry THF (100cm^3) and $\text{BH}_3 \cdot \text{thf}$ (37cm^3 , 37mmol) added, and the mixture refluxed overnight under nitrogen. The excess $\text{BH}_3 \cdot \text{thf}$ was destroyed by adding excess

MeOH, and the solvent removed on a rotary evaporator to give a white solid. The solid was dissolved in Butan-1-ol (25cm³), H₂O (25cm³) and concHCl (75cm³), and refluxed overnight, cooled, and basified to pH≥12. The solution was extracted with CH₂Cl₂ (6x50cm³), combined, and dried over anhydrous MgSO₄, and removed on a rotary evaporator to give white solid. Recrystallisation from CH₂Cl₂/Et₂O (1:1) yielded a fine white powder (1.98g, 84% yield). I.r (Nujol Mull) loss of C=O, m.p 50-51° C, r.f (CHCl₃) = 0.46. ¹H n.m.r (CDCl₃) 0.90(t, 12H), 1.30(br, 96H), 2.40(m, 8H), 2.50(br, 16H). F.A.B mass spectrum m/z calculated 874, m/z found 874 [M]⁺.

Preparation of [Ni(L^s)](BF₄)₂.0.25Et₂O

The ligand L^s (0.30g, 0.82mmol) was dissolved in EtOH (10cm³), and added to stirred solution of [Ni(DMSO)₆](BF₄)₂ (0.57g, 0.82mmol) in EtOH (10cm³) under nitrogen. A purple solid precipitated was collected and purged *in vacuo* for several hours to remove any remaining DMSO, and recrystallised from CH₃NO₂/Et₂O (1:2) to give a dark purple solid (0.45g, 89% yield). I.r (KBr disc): 2940cm⁻¹ (C-H), 1070cm⁻¹ (br, BF₄), no signs of DMSO. Analytical data is in Tables 2.5/3.5/4.5.

Preparation of [Ni(L^s)(NCS)₂]

[NiL^s](BF₄)₂.0.25EtOH (0.20g, 0.32mmol) was slurried in EtOH (10cm³), and NaSCN (0.070g, 0.86mmol) added, and stirred for 12 hours under nitrogen. The resulting blue solid was filtered off and recrystallised from MeOH/DMSO (1:1) to give light blue crystals (0.145g, 83% yield). I.r (Nujol Mull): 2080cm⁻¹, 2060cm⁻¹ (NCS). Analytical data is in Tables 2.5/3.5/4.5

Preparation of [Ni(L^o)DMSO](ClO₄)₂

The ligand L^o (0.21g, 0.24mmol) was dissolved in hot butan-1-ol (20cm³), and added to a stirred solution of [Ni(DMSO)₆](ClO₄)₂ (0.17g, 0.24mmol) in hot butan-1-ol (10cm³), under nitrogen. A faint purple colour began to form which became darker with time. The mixture was stirred for a least 12 hours, and cooled to precipitate dark purple crystals (0.17g, 61% yield). I.r (KBr disc):

cooled to precipitate dark purple crystals (0.17g, 61% yield). I.r (KBr disc): 1100cm^{-1} (br, ClO_4), 958cm^{-1} (DMSO), m.p $101-104^\circ\text{C}$. Analytical data is in Tables 2.5/3.5/4.5

Preparation of $[\text{Ni}(\text{L}^9)(\text{OH}_2)](\text{BF}_4)_2 \cdot 2\text{H}_2\text{O} (*)$

The ligand L^9 (0.30g, 0.34mmol) was dissolved in hot CH_3CN (10cm^3), and a solution of $[\text{Ni}(\text{CH}_3\text{CN})_6](\text{BF}_4)_2 (**)$ (4.19cm^3 , 0.08M) was added, and the mixture refluxed for 12 hours. The mixture was cooled, filtered, and the solvent removed. The blue solid was heated at 60°C (0.05mmHg), and turned dark purple, due to solvent removal. The dark purple solid was recrystallised from $\text{CH}_3\text{NO}_2/\text{Et}_2\text{O}$ (1:2) to give a purple solid (0.35g, 89% yield). I.r (KBr disc): 2900cm^{-1} , 2840cm^{-1} (C-H), 1070cm^{-1} (BF_4), no CH_3CN present. Analytical data is in Tables 2.5/3.5/4.5. (*) The water comes from the impure starting material nickel(II) salt. (**) The salt is not a pure hexakis acetonitrile complex and is more probably $[\text{Ni}(\text{CH}_3\text{CN})_x(\text{OH}_2)_y](\text{BF}_4)_2$

Section 9.5

Crystallography

The data for $[\text{Ni}(\text{L}^8)(\text{NCS})_2]$ was collected and processed as described in Chapter 4 (Section 13.4) All data is given in Table 5.5. Bond lengths and angles are given in Table 8.5. Atomic co-ordinates are given in Appendix I.

Compound $[\text{Ni}(\text{L}^8)(\text{NCS})_2]$

Crystals suitable for X-ray crystallography were obtained as light blue diamond shaped crystals from a saturated DMSO/MeOH (1:1) mixture. Systematic absences defined the space group $\text{P2}_1/\text{c}$ uniquely, and the crystals behaved well during data collection.

CHAPTER 6

Future work and Conclusions

Section 1.6

Redox active macrocycles

The macrocycle L^3 shows promise for further functionalisation of the "free" secondary nitrogen, possibly with ferrocenemethyl chloride to produce the fully tetraalkylated macrocycle (L^c), or other donor groups (e.g bipyridyl) (Figure 1.6)

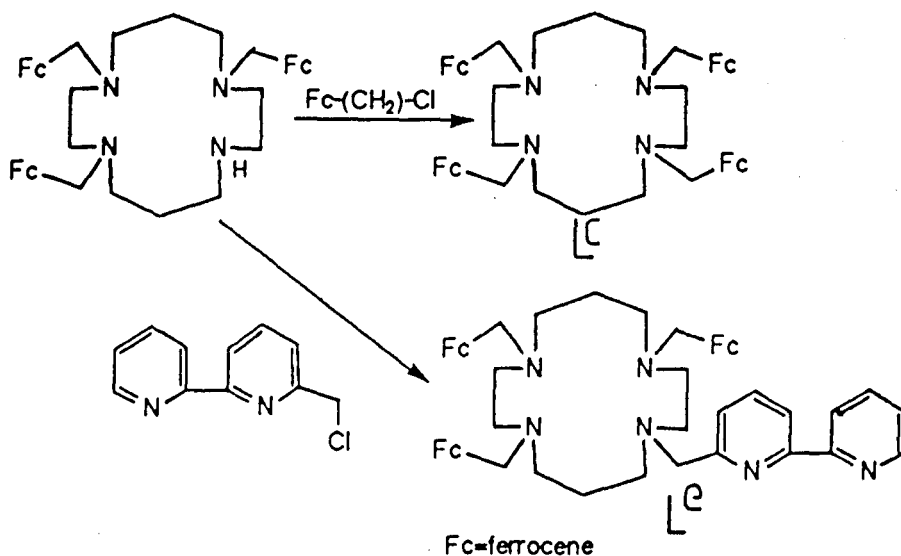


Figure 1.6

The electrochemistry of L^c could be examined to see whether larger shifts in the half wave potential occur on addition of metal ions. The macrocycle L^e could be reacted with $[Ru(bipy)_2]^{2+}$ to produce a system with two different redox centres (Figure 2.6), one of them a photoredox centre.

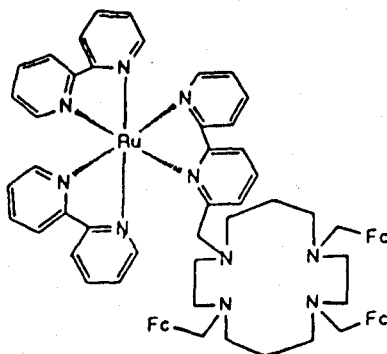


Figure 2.6

Instead of using cyclam as the "base" ligand other macrocycles could be functionalised, especially those which are structurally rigid, in the hope of making more specific macrocycles (Figure 3.6).

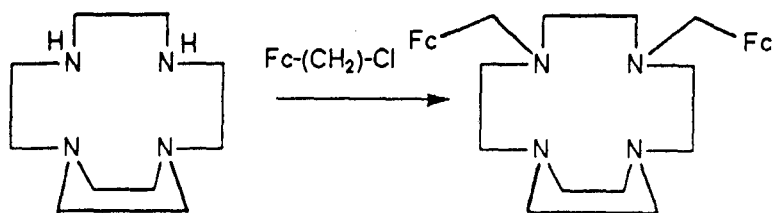


Figure 3.6

The main problem with all of these nitrogen alkylated macrocycles is the tertiary amine oxidation, and so the use of other redox centres could be used (*e.g.* cobalticenium). Some suggestions together with possible problems are shown in Figure 4.6

The cobalticenium macrocycle L^5 could also be used as a possible anion detector by the protonation of the tertiary amines (Figure 5.6) to make ideal anion binding sites.

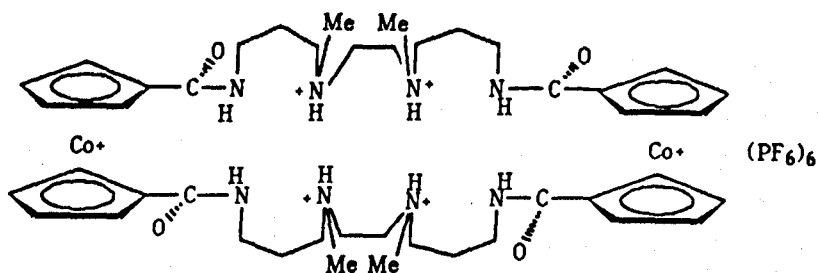


Figure 5.6

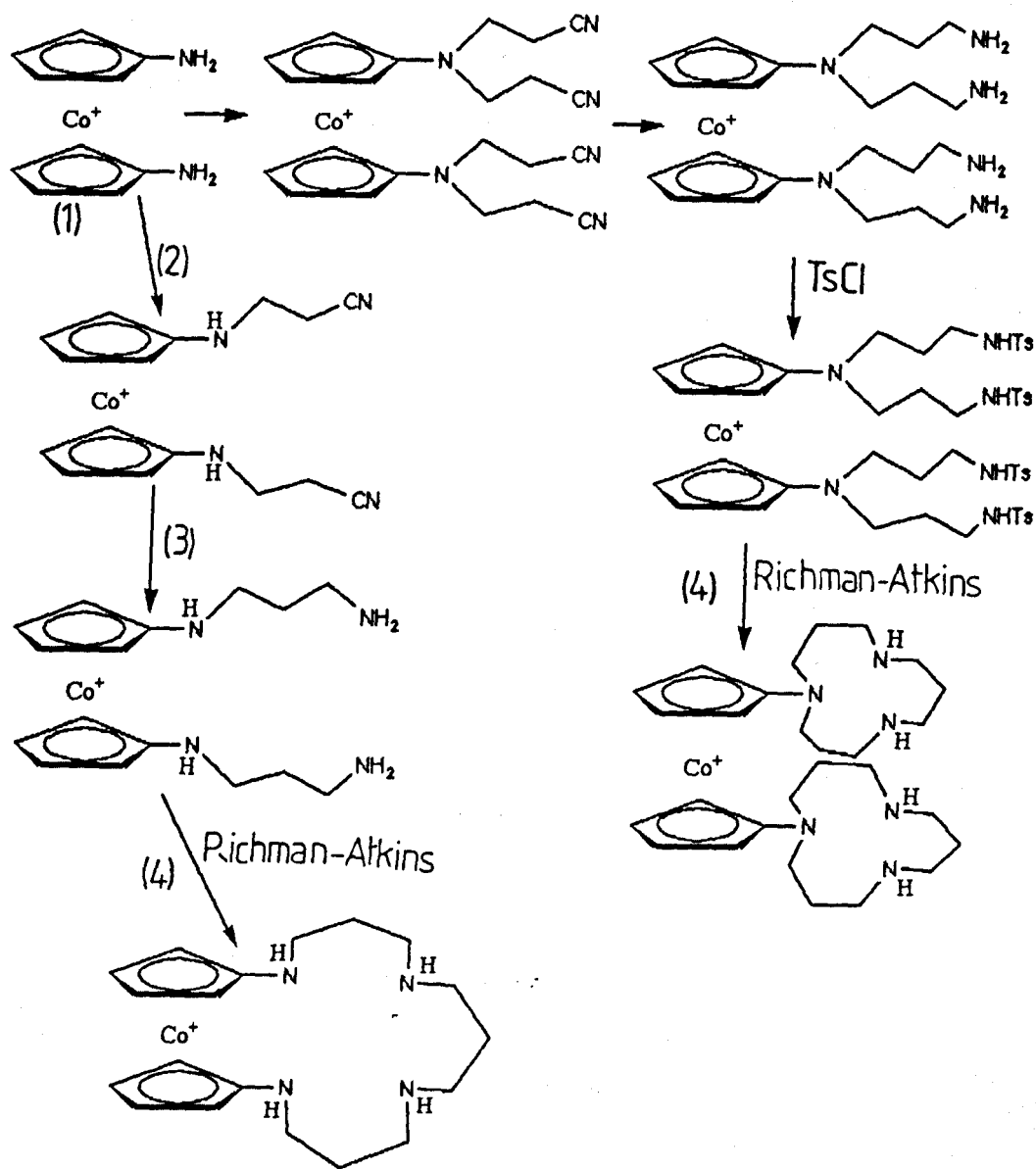


Figure 4.6

- (1) Synthesised from method given in *J. Organomet. Chem.*, 1976, **112**, 189.
- (2) The amino groups are not very basic and possibly only react with two moles of acrylonitrile.
- (3) Reduction may effect the cobalticene centre.
- (4) Removal of tosyl groups should be fine as cobalticene compounds are resistant to oxidation.

Section 2.6

Functionalised Macrocycles

The success of changing the geometry of the metal ions, by increasing the length of the pendant arm chain, could be furthered by functionalisation of the remaining secondary amine groups of L⁶ and L⁷. Two synthetic methods could be employed:-

- (1) Dequaternarisation of the pyrrolidinylium nitrogen (Figure 6.6(a))
- (2) Reaction with acid chlorides followed by reduction of the amide oxygens (Figure 6.6(b))

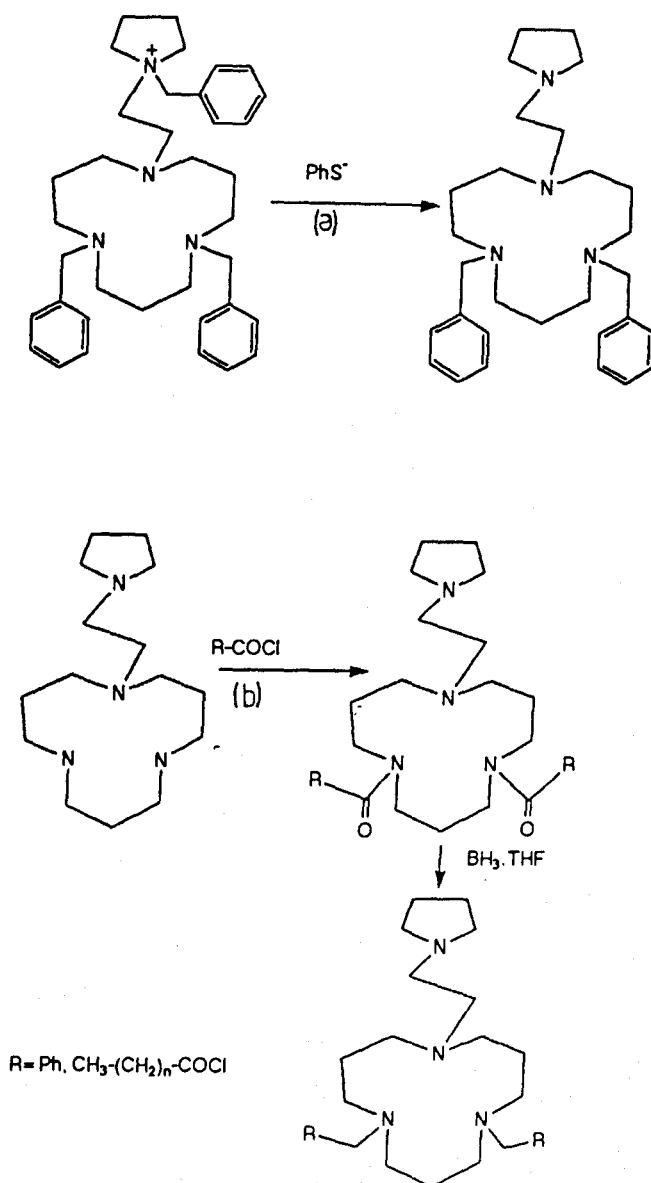


Figure 6.6

Section 3.6

Tetra-N-alkylated Macrocycles

The two isomers present in $[\text{Ni}(\text{L}^8)]^{2+}$ need to be separated by possibly using a sephadex column, and the two isomers identified. Also direct alkylation of $[\text{Ni}(\text{cyclam})]^{2+}$ could be tried to see if one or more isomers are produced (Figure 7.6). In the case of $[\text{Ni}(\text{TMC})]^{2+}$ only one isomer Trans-III, is produced by this route.^{1 5 8}

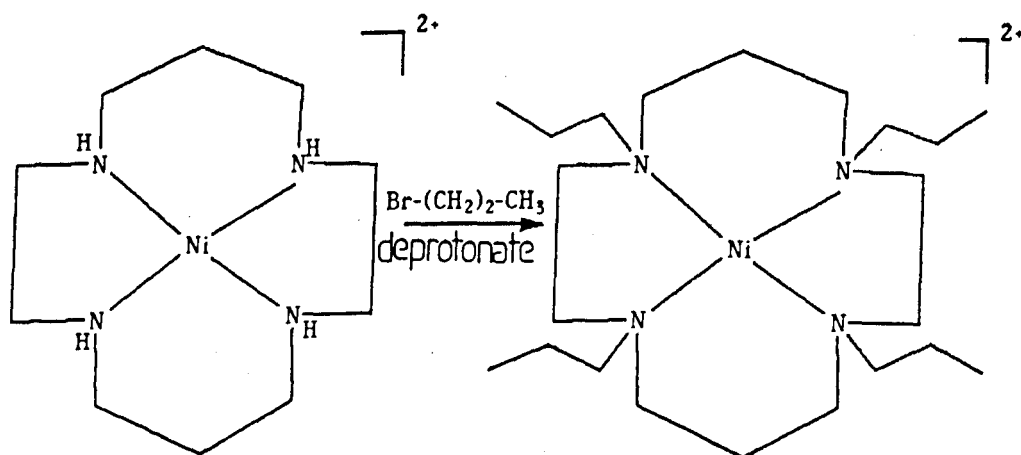


Figure 7.6

If "pure" Trans-I and Trans-III isomers of $[\text{Ni}(\text{L}^8)]^{2+}$ can be produced, then equilibrium and kinetic studies can be carried out in different solvents, and compared to the $[\text{Ni}(\text{TMC})]^{2+}$ studies.

CHAPTER 7

General experimental techniques and instrumentation

Section 1.7

^1H decoupled, natural abundance, ^{13}C n.m.r spectra were obtained at 45.28 MHz with a Bruker WH180 Fourier Transform spectrometer (10mm diameter tube, with teflon vortex suppression plug), or at 100.6 MHz using a Bruker WH400 Fourier Transform spectrometer (5mm diameter tube). ^1H n.m.r spectra were recorded with either a Perkin-Elmer (Model R34) 220 MHz continuous wave spectrometer, or a Bruker WH180/90 Fourier Transform n.m.r spectrometers. Infrared spectra were recorded with a Perkin-Elmer (Model 580B) infrared spectrometer, or a Perkin-Elmer 1720X FT.Ir spectrometer, using either nujol mulls, thin films on NaCl plates, or KBr (dried in a oven at 100°C) discs. Electronic spectra were recorded with a Shimadzu (Model 365) spectrometer in 1cm^3 path length quartz cells. Mass spectra were recorded using a Kratos (MS80) instrument fitted with a fast atom bombardment (F.A.B) attachment. Metal complex mass spectra were obtained using the F.A.B technique, as well as some of the heavier ligands. Mass spectra were simulated with a Hewlett-Packard 9845B minicomputer.

Section 2.7

Electrochemical Techniques

Experiments were carried out using an Oxford Electrode potentiostat, with voltage recorded on a Bryans series 60000 XY-t recorder. Platinum and glassy carbon electrodes were supplied by Oxford electrodes, and a cleaned surface was obtained by polishing with a slurry of 1.0μ and 3.0μ alumina (Banner Scientific), in water. Counter electrodes were made of platinum wire ($\sim 3\text{cm}$ long) and Bunsen flamed before use. All experiments were carried out in small volume (5cm^3), two compartment pyrex cells. In this cell the reference electrode is contacted to the bulk solution by means of a pin capillary hole (Diagram 1.7).

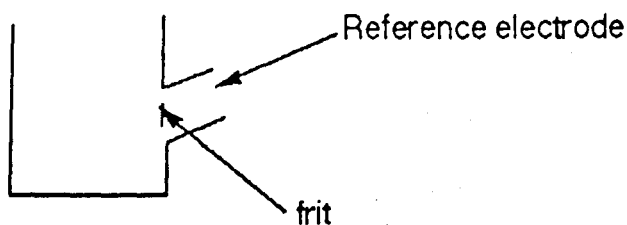


Diagram 1.7

Deoxygenation of solutions was achieved by purging with nitrogen which had traces of oxygen removed by passage through a train of Dreshel bottles containing a caustic solution of anthraquinone-2-sulphonate in contact with zinc/mercury amalgam. All solutions were degassed for at least twenty minutes before experiments.

Section 3.7

Conductivity Experiments

Conductivity was carried out using two platinum electrodes (cell constant = 0.727 cm^{-1}), connected to a Phillips PW9527 digital conductivity meter on approximately 10^{-3} M solutions thermostated at 25° C . Molar conductivity was calculated using equation (1), and assuming all solutions to be ideal.

$$\Lambda_m = \kappa/c \rightarrow (1)$$

Section 4.7

Magnetic susceptibility measurements

Magnetic moments of paramagnetic complexes were obtained in solution at room temperature by the Evans n.m.r method.¹⁶⁶ In the Evans n.m.r method the chemical shifts of the proton resonances of inert reference molecules caused by the presence of dissolved paramagnetic substances are given by:-

$$\Delta H/H = 2\pi \Delta K/3$$

ΔK = change in volume susceptibility.

For $^2[\text{H}]_3$ -nitromethane solutions of complexes discussed in chapters 3,4,5 about 2% t-butanol in $^2[\text{H}]_3$ -nitromethane was used as an external reference in a capillary (Wilmad) tube placed co-axially inside the 5mm diameter n.m.r tube. Two resonances were observed for the methyl protons of the t-butanol, because of the difference in volume susceptibilities of the two solutions; the resonance for the paramagnetic solution occurs at higher frequency. The corrected molar susceptibility of the dissolved substance χ_m is given by:-

$$\chi_m' = 3 \cdot \Delta H \cdot M / 2\pi \cdot H \cdot M + \chi_o + M \cdot \chi_o \cdot (d_o - d_s) / m + \text{DC}$$

$\Delta H/H$ = shift separation in ppm of the two resonances. M = molecular weight of complex. m = mass of sample in 1 cm^3 .

χ_o = mass susceptibility of solvent (-0.72×10^6 for dil t-butanol).

d_o = density of solvent, d_s = density of solution. D.C = diamagnetic correction for complex calculated using Pascals constants).

The density term ($d_0 - d_s$) is often neglected. The value of χ_m' is then related to the magnetic moment of the paramagnetic ion μ_{eff} by:-

$$\mu_{\text{eff}} = 2.828 (\chi_m' \cdot T)^{1/2} \text{ Bohr Magnetons (B.M.)}$$

T = Absolute temperature

Section 5.7

Atomic Absorption Spectrophotometry

Atomic absorption experiments were carried out by using a Varian Tech-tron Atomic Absorption Spectrophotometer AA6. In a usual experiment samples from a stock solution, made up in distilled water (e.g. $\text{Ni}^{2+} - 1001.2 \mu\text{g}/\text{cm}^3$, $\text{Cu}^{2+} - 1002.7 \mu\text{g}/\text{cm}^3$, $\text{K}^+ - 1010.8 \mu\text{g}/\text{cm}^3$) were diluted to make a series of calibration samples. A calibration curve was then obtained, from which the concentration of metal ions, of a known weighed amount of sample under study, in V cm^3 of distilled water, was calculated. The percentage of metal ion under study was calculated from:-

$$\%M = c \times V \times M/m \times 100$$

where c = concentration found ($\mu\text{g}/\text{cm}^3$), V = volume (cm^3), M = mass of metal ion (e.g. $\text{Ni}^{2+} - 58.71$, $\text{Cu}^{2+} - 63.54$, $\text{K}^+ - 39.10$), m = mass of sample in V cm^3 (g).

Section 6.7

Solvent exchange by ^{14}N n.m.r line broadening

The full theory of nuclear magnetic resonance for the study of ligand substitution processes is given by Stengle and Langford.¹⁶⁷ The ^{14}N n.m.r linewidths and shifts were fitted with modified Swift-Connick equations¹⁶⁸ (1)-(7).

$$1/T_{2p} = 1/T_2 - 1/T_{2A^0} = P_m/\tau_m \cdot (X)/(Y) + P_m/T_{2os} \text{-----(1)}$$

$$(X) = T_{2m}^{-2} + T_{2m}^{-1} \tau_m^{-1} + \Delta\omega_m^2, \quad (Y) = (T_{2m}^{-1} + \tau_m^{-1}) + \Delta\omega_m^2$$

$$1/T_{2m} = A_m(E_m/RT) \text{-----(2)}$$

$$1/T_{2os} = A_{os}(E_{os}/RT) \text{-----(3)}$$

$$\Delta\omega_m = B_1/T + B_0 \text{-----(4)}$$

$$\Delta\omega = P_m/\omega_m / [(\tau_m \cdot T_{2m}^{-1} + 1)^2 + \tau_m \Delta\omega_m^2] \text{-----(5)}$$

$$k_{\text{ex}} I_m \tau_m^{-1} = (k_B T/h) \exp(-\Delta H^\ddagger/RT + \Delta S^\ddagger/R) \text{-----(6)}$$

$$P_m = n.K[Ni_o]/[S](1 + K) \text{---(7)}$$

where n = number of bound solvent molecules, $[S]$ is the total solvent concentration, T_2 is the observed relaxation time, T_{2A^0} is the relaxation time of pure solvent, T_{2m} is the relaxation time of the bound solvent, T_{2os} is the outer sphere contribution, τ_m is the residue time of a bound solvent molecule, and is related to the pseudo first order rate constant for exchange of a single solvent molecule ($k_{ex}^I = \tau_m^{-1}$). P_m is the mole fraction of bound solvent. $\Delta\omega$ is the observed chemical shift relative to that of pure solvent, $\Delta\omega_m$ is the chemical shift between free and bound solvent molecules in the absence of exchange, and is assumed to have a normal $1/T$ temperature dependence. Data fitting was performed by non-linear least squares program with automatic weighting of each data set. The equilibrium constant K was calculated using 1H n.m.r shift studies. Data were fitted as $\ln(1/T_{2p})$ and $\Delta\omega$ as functions of inverse temperature, taking B_o , ΔH^\ddagger , ΔS^\ddagger , B_1 , A_m , A_{os} , ΔH^\ominus , ΔS^\ominus as unknowns to be optimised.

Equilibrium Studies

The enthalpy (ΔH^\ominus) and entropy (ΔS^\ominus), and hence the equilibrium constant K were calculated by observing the shift of resonances for the macrocycle at varying temperatures. The data were simultaneously fitted by non-linear least squares to equations (8)-(10):-

$$\nu_{obs} = \nu_p \alpha + \nu_d (1 - \alpha) \text{---(8)}$$

$$K = \alpha / (1 - \alpha) \text{---(9)}$$

$$\nu_p = C/T + \nu_d \text{---(10)}$$

where ν_{obs} is the measured shift and ν_p and ν_d are the shifts of the paramagnetic and diamagnetic species respectively, C is the Currie constant, α is the mole fraction of paramagnetic complex. Values of ν_{obs} as a function of T were fitted taking ν_p , ν_d , C and K as the unknown parameters.

REFERENCES

References

- 1: D.J.Cram, C.J.Pedersen, J.M.Lehn, *Angew. Chem. Int. Ed. Engl.*, 1988, pages 1009, 1021, 89.
- 2: G.A.Melson, *Co-ordination Chemistry of Macrocyclic Compounds*, Plenum Press, New York- and references therein.
- 3: N.F.Curtis, *J. Chem. Soc.*, 1960, 4409.
- 4: M.C.Thompson, D.C.Busch, *J. Am. Chem. Soc.*, 1964, **86**, 3651.
- 5: C.O.Dietrich-Buchecker, J.P.Sauvage, *Chem. Rev.*, 1987, **87**, 795.
- 6: F.C.Kohnke, A.M.Z.Slawin, J.F.Stoddardt, D.J.Williams, *Angew Chem. Int Ed. Engl.* 1987, **26**, 892.
- 7: M.W.Hosseini, J.M.Lehn, K.C.Jones, K.E.Plute, K.Bronan-Mertes, M.P.Mertes, *J. Am. Chem. Soc.*, 1989, **111**, 6330.
- 8: P.Beer, H.Sikanyika, C.Blackburn, J.F.McAleer, M.G.B.Drew, *J. Organomet. Chem.*, 1988, **356**, C19.
- 9: P.Beer, A.D.Keefe *J. Organomet. Chem.*, 1989, **375**, C40.
- 10: J.Morphy, D.Parker, R.Alexander, A.Bains, A.F.Carne, M.A.Eaton, A.Harrison, A.Millican, A.Phipps, S.K.Rhund, R.Titmus, D.Weatherby, *J. Chem. Soc. Chem. Commun.*, 1988, 156.
- 11: J.J.Christensen, D.J.Eatough, R.M.Izatt, *Chem. Rev.*, 1974, **74**, 351.
- 12: R.D.Hancock, *Prog. Inorg. Chem.*, 1989, **37** 187.
- 13: D.J.Cram, T.Kaneda, R.C.Helgeson, S.B.Brown, C.B.Knobler, E.Haverick, K.N.Trueblood, *J. Am. Chem. Soc.*, 1985, **107**, 3645.
- 14: Y.Hung, L.Y.Martin, S.C.Jackels, A.M.Tait, D.H.Busch, *J. Am. Chem. Soc.*, 1977, **99**, 4029.
- 15: V.J.Thöm, G.J.McDougall, J.C.A.Boeyens, R.D.Hancock, *J. Am. Chem. Soc.*, 1984, **106**, 3198.
- 16: V.J.Thöm, R.D.Hancock, *J. Chem. Soc. Dalton. Trans.*, 1985, 1877.
- 17: V.J.Thöm, C.C.Fox, J.C.A.Boeyens, R.D.Hancock, *J. Am. Chem. Soc.*, 1984, **106**, 5947.

- 18: V.J.Thöm, G.D.Hosken, R.D.Hancock, *Inorg. Chem.*, 1985, **24**, 3378.
- 19: V.J.Thöm, R.D.Hancock, *J. Chem. Soc. Dalton. Trans.*, 1985, 1877.
- 20: R.D.Hancock, *Pure. Appl. Chem*, 1986, **58**, 1445
- 21: R.D.Hancock, M.P.Ngwenya, A.Evers, P.W.Wade, J.C.A.Boeyens, S.M.Dobson, *Inorg. Chem*, 1990, **29**, 264.
- 22: L.Fabbrizzi, *J. Chem. Soc. Dalton. Trans.*, 1979, 1857.
- 23: M.Paiksoh, W.Shun, H.Kim, C.Hoe-Koo, *Inorg. Chem.*, 1987, **26**, 1846.
- 24: C.J.Pedersen, *J. Am. Chem. Soc.*, 1970, **92**, 391.
- 25: R.M.Izatt, D.P.Nelson, J.H.Rytting, B.L.Haymore, J.J.Christenson, *J. Am. Chem. Soc.*, 1971, **93**, 1619.
- 26: R.D.Hancock, R.Bhavan, P.W.Wade J.C.A.Boeyens, S.M.Dobson, *Inorg. Chem.*, 1989, **28**, 187.
- 27: M.J.Bovill, D.J.Chadwick, I.O.Sutherland, D.Walkin, *J. Chem. Soc. Perkin. Trans(I)*, 1980, 1529.
- 28: G.Wipff, P.Weiner, P.Kollman, *J. Am. Chem. Soc.*, 1982, **104**, 3249.
- 29: L.F.Lindoy, K.Henrick, P.Tasker, *J. Chem. Soc. Dalton. Trans.*, 1987, 2537.
- 30: D.Fenton, B.P.Murphy, A.L.Leong, L.F.Lindoy, A.Bashall, M.McPartlin, *J. Chem. Soc. Dalton. Trans.*, 1987, 2543.
- 31: For full theory see:- K.Henrick, P.A.Tasker, L.F.Lindoy, *Prog. Inorg. Chem.*, 1985, **33**, 1.
- 32: G.Anderegs, A.Ekstrom, L.F.Lindoy, R.J.Smith, *J. Am. Chem. Soc.*, 1980, **102**, 2670.
- 33: A.Ekstrom, L.F.Lindoy, R.J.Smith, *Inorg. Chem.*, 1980, **19**, 724.
- 34: K.R.Adam, K.P.Dancey, B.A.Harrison, A.J.Leong, L.F.Lindoy, M.McPartlin, P.A.Tasker, *J. Chem. Soc. Chem. Commun.*, 1983, 1351.
- 35: K.R.Adams, A.J.Leong, L.F.Lindoy, H.C.Lip, B.W.Skelton, A.H.White, *J. Am. Chem. Soc.*, 1983, **105**, 4645.
- 36: B.Bosnich, C.K.Poon, M.L.Tobe, *Inorg. Chem.*, 1965, **4**, 1102.

- 37: D.K.Cabbiness, D.W.Margerum, *J. Am. Chem. Soc.*, 1969, **91**, 6540.
- 38: M.Kodama, E.Kimura, *J. Chem. Soc. Chem. Commun.*, 1975, 326.
- 39: A.Anichini, L.Fabbrizzi, P.Paoletti, R.M.Clay, *Inorg. Chim. Acta.*, 1977, **22**, L25.
- 40: F.R.Hinz, D.W.Margerum, *Inorg. Chem.*, 1974, **12**, 2941.
- 41: G.Smith, D.W.Margerum, *J. Chem. Soc. Chem. Commun.*, 1975, 807.
- 42: A.Dei, R.Gori, *Inorg. Chim. Acta.*, 1975, **14**, 157.
- 43: P.Paoletti, L.Fabbrizzi, R.Barbucci, *Inorg. Chem.*, 1973, **12**, 1961.
- 44: M.Kodama, E.Kimura, *J. Chem. Soc. Dalton. Trans.*, 1976, 116.
- 45: L.Fabbrizzi, P.Paoletti, A.A.P.Lever, *Inorg. Chem.*, 1976, **15**, 1502.
- 46: H.F.Frensdorff, *J. Am. Chem. Soc.*, 1971, **93**, 600.
- 47: M.Kodama, E.Kimura, *Bull. Chem. Soc. Jpn.*, 1976,**49**, 2465.
- 48: B.L.Haymore, J.D.Lamb, R.M.Izatt, J.J.Christensen, *Inorg. Chem.*, 1982, **21**, 1598.
- 49: J.S.Bradshaw, G.E.Maas, R.M.Izatt, J.J.Christensen, *Chem. Rev*, 1979, **79**, 37.
- 50: L.F.Lindoy, *Chem. Soc. Rev.*, 1975, 4421.
- 51: N.F.Curtis, *Coord. Chem. Rev*, 1968, **3**, 3.
- 52: R.Bhula, P.Osvath, D.C.Weatherburn, *Coord. Chem. Rev.*, 1988, **91**, 89.
- 53: P.Chavadhuri, K.Weighardt, *Prog. Inorg. Chem.*, 1987, **35**, 329.
- 54: J.E.Richnman, T.J.Atkins, *J. Am. Chem. Soc.*, 1974, **96**, 2268.
- 55: C.J.Pedersen, *J. Am. Chem. Soc.*, 1967, **89**, 7017.
- 56: J.P.Behr, J.M.Lehn, P.Vierling, *J. Chem. Soc. Chem. Commun.*, 1976, 621.
- 57: D.J.Sam, H.E.Simmons, *J. Am. Chem. Soc.*, 1972, **94** 4024
- 58: G.W.Gokel, H.D.Dirst, *Synthesis*, 1976, **8**, 168.
- 59: C.J.Pedersen, *Organic Synthesis*, 1972, **52**, 66.
- 60: R.N.Greene, *Tetrahedron. Lett.*, 1972, 1793.
- 61: B.Dietrich, J.M.Lehn, J.P.Sauvage, *Tetrahedron. Lett.*, 1969, 2889.
- 62: J.M.Lehn, J.P.Sauvage, *J. Chem. Soc. Chem. Commun.*, 1971, 440.

- 63: B.K.Vriesema, J.Butler, R.M.Kellog, *J. Org. Chem.*, 1984, 49 110.
- 64: N.W.Alcock, K.P.Balakrishnan P.Moore, H.A.A.Omar, *J. Chem. Soc. Dalton. Trans.*, 1987, 545.
- 65: N.W.Alcock, P.Moore, H.A.A.Omar, *J. Chem. Soc. Dalton. Trans.*, 1986, 985.
- 66: M.Green, P.A.Tasker, *J. Chem. Soc. Chem. Commun.*, 1968, 518.
- 67: J.L.Love, H.K.J.Powell, *J. Chem. Soc. Chem. Commun.*, 1968, 39.
- 68: E.K.Barefield, *Inorg. Chem.*, 1972, 11 2273.
- 69: E.K.Barefield, F.Wagner, *Inorg. Chem.*, 1973, 12, 2435.
- 70: N.W.Alcock, P.Moore, C.J.Reader, S.M.Roe, *J. Chem. Soc. Dalton. Trans.*, 1988, 2959.
- 71: T.Kaden, D.Tschudin, A.Riesen, *Helv. Chim. Acta.*, 1989, 72 131.
- 72: D.Gerber, P.Chongsawangvirod, A.K.Leung, L.A.Ochrymowycz, *J. Org. Chem.*, 1974, 42, 2644.
- 73: D.Sellmann, L.Zapf, *Angew. Chem. Int. Ed. Engl.*, 1984, 23, 807.
- 74: J.R.Hartman, E.J.Hintsa, S.R.Cooper, *J. Chem. Soc. Chem. Commun.*, 1984, 386.
- 75: J.Riker-Napier, D.W.Meek, *J. Chem. Soc. Chem. Commun.*, 1974, 442.
- 76: E.D.Kyba, S.S.P.Chou, *J. Chem. Soc. Chem. Commun.*, 1980, 449.
- 77: T.Kauffmann, J.Ennen, *Chem. Ber.*, 1985, 118, 2692.
- 78: S.Tomoda, M.Iwaoka, *J. Chem. Soc. Chem. Commun.*, 1990, 231.
- 79: T.A.Kaden, *Top.Curr.Chem.*, 1984, 121, 157.
- 80: R.W.Hay, D.M.S.Clark, *Inorg. Chim. Acta.*, 1984, 83, L23.
- 81: B.A.Sayer, J.P.Michael, R.D.Hancock, *Inorg. Chim. Acta.*, 1983, 77, L63.
- 82: M.Takahashi, S.Takamoto, *Bull. Chem. Soc. Jpn.*, 1977, 50, 3413.
- 83: N.W.Alcock, R.G.Kingston, P.Moore, C.Pierpoint, *J. Chem. Soc. Dalton. Trans.*, 1984, 1937.
- 84: D.Tschudin, A.Basak, T.A.Kaden, *Helv. Chim. Acta.*, 1988, 71, 100.
- 85: M.Hediger, T.A.Kaden, *Helv. Chim. Acta.*, 1983, 66, 861.

- 86: A.E.Martin, T.M.Ford, J.E.Bulkowski, *J. Org. Chem.*, 1982, 47, 412.
- 87: M.P.Andrews, C.Blackburn, J.F.Mcleer, V.D.Patel, *J. Chem. Soc. Chem. Commun.*, 1987, 1122.
- 88: P.J.Hammond, A.P.Bell, C.D.Hall, *J. Chem. Soc. Perkin. Trans(I).*, 1983, 707.
- 89: L.Echegoyen, D.A.Gustowski, V.J.Gatto, G.W.Gokel, *J. Chem. Soc. Chem. Commun.*, 1986, 220.
- 90: A.Kaifer, D.A.Gustowski, L.Echegoyen, V.J.Gatto, R.A.Shultz, T.P.Cleary, C.R.Morgan, D.M.Goli, A.M.Rois, G.W.Gokel, *J. Am. Chem. Soc.*, 1985, 107, 1958.
- 91: G.Oepen, F.Vogtle, *Liebigs. Ann. Chem.*, 1979, 1094.
- 92: M.Sato, S.Tanaka, S.Ebine, S.Akabori, *Bull. Chem. Soc. Jpn.*, 1984, 57, 1929.
- 93: S.Akabori, S.Shibahara, Y.Habata, M.Sato, *Bull. Chem. Soc. Jpn.*, 1984, 57, 63.
- 94: M.Saji, *Chemistry Letters*, 1986, 275.
- 95: P.Beer, *J. Organomet. Chem.*, 1985, 297 313.
- 96: P.Beer, *J. Organomet. Chem.*, 1989, 375, C35.
- 97: "Instrumentational Methods in Electrochemistry" - Southampton. Ellis -Horwood, page 178.
- 98: R.M.Izatt, D.J.Eatough, J.J.Christensen, *Structure and Bonding*, 1973, 16, 161.
- 99: P.D.Beer, H.Sikanyika, C.Blackburn, J.F.McAleer, M.G.B.Drew, *J. Organomet, Chem.*, 1988, 356, C19.
- 100: P.D.Beer, C.G.Crane, *Polyhedron*, 1988, 7, 2649.
- 101: P.D.Beer, C.G.Crane, A.D.Keefe, A.R.Whyman, *J. Organomet, Chem.*, 1986, 314, C9.
- 102: P.C.Reeves, *Organic Synthesis*, 1977, 56, 28.
- 103: A.N.Nesmeyanov, E.G.Perevalova, L.P.Jaryeva, *Chem. Ber*, 1960, 93, 2729.

- 104: D.E.Bublitz, G.H.Harris, *J. Organomet, Chem.*, 1965, 4404.
- 105: S.J.Goldberg, *J. Org. Chem*, 1960, 25, 482.
- 106: H.Lau, H.Hart, *J. Org. Chem*, 1959, 24, 280.
- 107: Von.H.J.Lorkowski, R.Pannier, A.Wende, *J. Prakt. Chem*, 1967, 35, 149.
- 108: E.S.Schmidt, T.S.Calderwood, T.C.Bruce, *Inorg. Chem.*, 1986, 25, 3718.
- 109: A.Sonoda, I.Moritani, *J. Organomet, Chem.*, 1971, 26, 133.
- 110: K.Schlögl, *Monatsh.Chem*, 1957, 88, 601.
- 111: E.Fu, M.L.H.Green, V.J.Lower, S.R.Marder, *J. Organomet. Chem.*, 1988, 341, C39.
- 112: N.A.Obaidi, P.D.Beer, J.P.Bright, C.J.Jones, J.A.McCleverty, S.S.Salam
J. Chem. Soc. Chem. Commun., 1986, 239.
- 113: J.Granell, M.L.H.Green, V.J.Lowe, S.R.Marder, P.Mountfield,
G.C.Saunders, N.M.Walker, *J. Chem. Soc. Dalton. Trans.*, 1990, 605.
- 114: R.J.Gale, K.M.Motyl, R.Job, *Inorg. Chem.*, 1983, 22, 130.
- 115: G.J.Bullen, B.J.Howlin, J.Silver, B.W.Fitzsimmons, I.Sager,
L.F.Larkworthy, *J. Chem. Soc. Dalton. Trans.*, 1986, 1937.
- 116: W.M.Reiff, E.H.Witten, K.Mottle, T.F.Brennan, A.R.Garfalo,
Inorg. Chim. Acta, 1983, 77, L83.
- 117; M.G.B.Drew, V.Mckee, S.M.Nelson, *J. Chem. Soc. Dalton. Trans.*,
1978,80.
- 118: J.R.Linsay-Smith, D.Masheder, *J. Chem. Soc. Perkin. Trans (II).*, 1977,
1732.
- 119: R.L.Shaaf, *J. Org. Chem.*, 1962, 27, 107.
- 120: H.H.Lau, H.Hart, *J. Org. Chem.*, 1959, 24, 280.
- 121: D.D.Perrin, W.L.F.Armarego, D.R.Perrin, *Purification of Laboratory
Chemicals*, 2nd Edition, Pergamon Press.
- 122: J.Selbin, W.E.Bull, L.H.Holmes, *J. Inorg. Nucl. Chem.*, 1961, 16, 219.
- 123: G.M Sheldrick, *SHELXTL PLUS user manual*, Nicolet XRD Corpora-
tion, Madison, Wisconsin, 1983.

- 144: N.W.Alcock, F.Mclaren, P.Moore, G.A.Pike, S.M.Roe, *J. Chem. Soc. Chem. Commun.*, 1989, 629.
- 145: N.W.Alcock, K.P.Balakrishnan, P.Moore, H.A.A.Omar, *J.Chem. Soc Dalton. Trans.*, 1987, 545.
- 146: M.R.Rosenthal, *J. Chem. Educ.*, 1973, 331.
- 147: K.Nakamoto, *Infrared and Raman spectra of inorganic and co-ordination compounds*, 3rd Edition, Wiley interscience, page 228.
- 148: F.A.Cotton, G.Wilkinson, *Advanced Inorganic Chemistry*, 4th Edition, Wiley interscience, page 14.
- 149: M.Ciampolini, N.Nardi, *Inorg. Chem.*, 1966, 5, 41.
- 150: Dr.S.C.Rawle, postdoctoral work, Warwick University, 1989.
- 151: E.Kimura, T.Koike, K.Toriumi, *Inorg. Chem.*, 1988, 27, 3687.
- 152: P.M.Shaber, J.C.Fettinger, M.R.Churchill, D.Nalewajek, K.Fries, *Inorg. Chem.*, 1988, 27, 1641.
- 153: E.K.Barefield, F.Wagner, *Inorg. Chem.*, 1973, 12, 2435.
- 154: P.Moore, J.Sachinidis, G.R.Willey, *J. Chem. Soc. Chem. Commun.*, 1983, 523.
- 155: A.E.Merbach, P.Moore, K.E.Newman, *J. Mag. Res.*, 1980, 41, 30.
- 156: P.Moore, J.Sachinidis, G.R.Willey, *J. Chem. Soc. Dalton. Trans.*, 1984, 1323.
- 157: E.Iwamoto, T.Yokoyama, S.Yamasaki, T.Yabe, T.Kumamaru, Y.Yamamoto, *J. Chem. Soc. Dalton. Trans.*, 1988, 1935.
- 158: E.K.Barefield, F.Wagner, *Inorg. Chem.*, 1973, 12, 2435.
- 159: I.S.Crick, B.F.Hoskins, P.A.Treglon, *Inorg. Chem. Acta.*, 1986, 114, L33.
- 160: S.F.Lincoln, T.W.Hambley, D.L.Pisaniello, J.H.Coates, *Aust. J. Chem.*, 1984, 37, 713.
- 161: M.J.D'Aniello(Jr), M.T.Mocella, F.Wagner, E.K.Barefield, I.C.Paul, *J. Am. Chem. Soc.*, 1975, 97, 192.
- 162: S.Lincoln, D.Pisaniello, D.Coates, D.Hadi, *Inorg. Chim. Acta.*, 1984, 81, 19.

- 163: N.Herron, PhD Thesis, University of Warwick, 1978, page 164.
- 164: N.Herron, PhD Thesis, University of Warwick, 1978, page 210.
- 165: B.J.Hathaway, D.G.Holah, A.E.Underhill, **J. Chem. Soc.**, 1962, 2444.
- 166: D.F.Evans, **J. Chem. Soc.**, 1959, 2003.
- 167: T.R.Stengle, C.H.Langford, **Coord. Chem. Rev.**, 1967, **2**, 349.
- 168: C.H.McAteer, P.Moore, **J. Chem. Soc. Dalton. Trans.**, 1983, 353.

APPENDIX

Appendix I

Atomic co-ordinates and bond lengths of crystal structures undertaken in this thesis

L²

Atomic coordinates ($\times 10^4$) and equivalent isotropic displacement parameters ($\text{Å}^2 \times 10^3$)

	x	y	z	U(eq)
Fe(1)	6574(2)	8148(5)	-451(2)	51(2)
Fe(2)	9530(2)	1606(5)	2362(2)	45(2)
Cl(1)	2756(4)	7266(10)	2489(4)	90(4)
Cl(2)	1255(5)	6354(10)	1671(4)	94(4)
Cl(3)	2254(5)	8067(13)	1162(4)	119(5)
Cl(4)	5777(6)	3974(13)	638(5)	125(6)
Cl(5)	6563(7)	1747(12)	1609(5)	150(7)
Cl(6)	7169(6)	4970(14)	1594(5)	137(6)
O(1)	7651(8)	3972(20)	217(8)	49(8)
O(2)	10834(10)	730(20)	1474(7)	54(8)
N(1)	8552(11)	5844(24)	253(8)	33(6)
N(2)	10002(10)	2483(22)	774(8)	35(5)
C(1)	9394(13)	7997(32)	40(12)	43(7)
C(2)	8719(13)	7611(29)	250(11)	43(8)
C(3)	9110(13)	4791(29)	712(11)	49(8)
C(4)	9251(11)	3109(27)	445(9)	35(7)
C(5)	10604(13)	2929(28)	542(11)	33(7)
C(6)	7824(17)	5306(36)	41(13)	48(8)
C(7)	7220(16)	6090(33)	-526(13)	50(14)
C(8)	7242(15)	7367(33)	-963(12)	54(8)
C(9)	6470(15)	7767(36)	-1394(13)	66(9)
C(10)	5994(18)	6708(42)	-1200(13)	81(16)
C(11)	6422(19)	5723(35)	-683(15)	64(17)
C(12)	6948(18)	8841(41)	494(14)	78(18)
C(13)	7030(17)	10205(36)	95(14)	57(9)
C(14)	6347(20)	10621(37)	-356(15)	83(18)
C(15)	5741(20)	9601(44)	-296(18)	80(19)
C(16)	6155(23)	8602(37)	251(17)	70(19)
C(17)	10163(15)	1249(32)	1249(12)	39(8)
C(18)	9601(15)	709(30)	1524(11)	35(12)
C(19)	9801(14)	-560(30)	2013(11)	36(7)
C(20)	9190(17)	-870(34)	2224(12)	47(14)
C(21)	8615(18)	142(38)	1886(13)	60(15)
C(22)	8824(16)	1154(31)	1453(13)	50(14)
C(23)	10473(18)	2448(47)	3077(20)	86(21)
C(24)	9875(24)	2098(39)	3293(14)	72(17)
C(25)	9239(20)	3087(43)	2990(16)	79(18)
C(26)	9460(20)	4031(39)	2557(15)	62(10)
C(27)	10175(24)	3690(45)	2594(15)	77(21)
C(101)	6656(18)	3346(38)	1140(14)	80(17)
C(201)	1985(14)	7766(30)	1823(13)	61(14)

* Equivalent isotropic U defined as one third of the trace of the orthogonalized U_{ij} tensor

Bond lengths (Å)

Fe(1)-C(7)	2.090 (29)	Fe(1)-C(8)	2.053 (31)
Fe(1)-C(9)	2.060 (30)	Fe(1)-C(10)	2.012 (29)
Fe(1)-C(11)	2.016 (29)	Fe(1)-C(12)	2.051 (30)
Fe(1)-C(13)	2.058 (28)	Fe(1)-C(14)	2.063 (31)
Fe(1)-C(15)	2.066 (40)	Fe(1)-C(16)	2.003 (46)
Fe(2)-C(18)	2.044 (26)	Fe(2)-C(19)	2.043 (26)
Fe(2)-C(20)	2.084 (28)	Fe(2)-C(21)	2.046 (29)
Fe(2)-C(22)	2.030 (25)	Fe(2)-C(23)	2.040 (31)
Fe(2)-C(24)	1.985 (30)	Fe(2)-C(25)	2.045 (39)
Fe(2)-C(26)	2.015 (32)	Fe(2)-C(27)	2.026 (37)
Cl(1)-C(201)	1.720 (23)	Cl(2)-C(201)	1.716 (26)
Cl(3)-C(201)	1.724 (33)	Cl(4)-C(101)	1.713 (29)
Cl(5)-C(101)	1.703 (34)	Cl(6)-C(101)	1.728 (31)
O(1)-C(6)	1.225 (35)	O(2)-C(17)	1.249 (31)
N(1)-C(2)	1.458 (30)	N(1)-C(3)	1.455 (27)
N(1)-C(6)	1.346 (35)	N(2)-C(4)	1.431 (25)
N(2)-C(5)	1.431 (35)	N(2)-C(17)	1.407 (31)
C(1)-C(2)	1.518 (39)	C(1)-C(5A)	1.495 (37)
C(3)-C(4)	1.538 (33)	C(5)-C(1A)	1.495 (37)
C(6)-C(7)	1.511 (35)	C(7)-C(8)	1.425 (40)
C(7)-C(11)	1.438 (46)	C(8)-C(9)	1.466 (34)
C(9)-C(10)	1.401 (47)	C(10)-C(11)	1.400 (40)
C(12)-C(13)	1.453 (46)	C(12)-C(16)	1.403 (50)
C(13)-C(14)	1.365 (40)	C(14)-C(15)	1.440 (54)
C(15)-C(16)	1.440 (47)	C(17)-C(18)	1.449 (42)
C(18)-C(19)	1.444 (33)	C(18)-C(22)	1.446 (40)
C(19)-C(20)	1.396 (45)	C(20)-C(21)	1.351 (39)
C(21)-C(22)	1.414 (45)	C(23)-C(24)	1.388 (62)
C(23)-C(27)	1.434 (50)	C(24)-C(25)	1.395 (49)
C(25)-C(26)	1.395 (55)	C(26)-C(27)	1.335 (58)

Bond angles ($^{\circ}$)

C(7)-Fe(1)-C(8)	40.2(11)	C(7)-Fe(1)-C(9)	69.9(11)
C(8)-Fe(1)-C(9)	41.8(10)	C(7)-Fe(1)-C(10)	68.8(12)
C(8)-Fe(1)-C(10)	67.8(12)	C(9)-Fe(1)-C(10)	40.2(13)
C(7)-Fe(1)-C(11)	40.9(13)	C(8)-Fe(1)-C(11)	67.7(14)
C(9)-Fe(1)-C(11)	68.9(13)	C(10)-Fe(1)-C(11)	40.7(12)
C(7)-Fe(1)-C(12)	107.1(12)	C(8)-Fe(1)-C(12)	126.3(12)
C(9)-Fe(1)-C(12)	164.2(13)	C(10)-Fe(1)-C(12)	154.4(14)
C(11)-Fe(1)-C(12)	119.6(13)	C(7)-Fe(1)-C(13)	123.6(11)
C(8)-Fe(1)-C(13)	111.5(13)	C(9)-Fe(1)-C(13)	126.5(13)
C(10)-Fe(1)-C(13)	161.4(12)	C(11)-Fe(1)-C(13)	157.6(11)
C(12)-Fe(1)-C(13)	41.4(13)	C(7)-Fe(1)-C(14)	156.7(14)
C(8)-Fe(1)-C(14)	122.5(14)	C(9)-Fe(1)-C(14)	107.3(12)
C(10)-Fe(1)-C(14)	124.8(12)	C(11)-Fe(1)-C(14)	161.2(13)
C(12)-Fe(1)-C(14)	69.0(12)	C(13)-Fe(1)-C(14)	38.7(11)
C(7)-Fe(1)-C(15)	161.8(14)	C(8)-Fe(1)-C(15)	154.2(13)
C(9)-Fe(1)-C(15)	116.2(13)	C(10)-Fe(1)-C(15)	104.1(13)
C(11)-Fe(1)-C(15)	123.0(15)	C(12)-Fe(1)-C(15)	71.7(13)
C(13)-Fe(1)-C(15)	68.1(13)	C(14)-Fe(1)-C(15)	40.8(15)
C(7)-Fe(1)-C(16)	126.6(12)	C(8)-Fe(1)-C(16)	163.8(11)
C(9)-Fe(1)-C(16)	153.3(13)	C(10)-Fe(1)-C(16)	120.5(14)
C(11)-Fe(1)-C(16)	108.5(14)	C(12)-Fe(1)-C(16)	40.5(14)
C(13)-Fe(1)-C(16)	65.6(14)	C(14)-Fe(1)-C(16)	66.1(14)
C(15)-Fe(1)-C(16)	41.4(14)	C(18)-Fe(2)-C(19)	41.4(10)
C(18)-Fe(2)-C(20)	68.8(11)	C(19)-Fe(2)-C(20)	39.5(12)
C(18)-Fe(2)-C(21)	68.1(12)	C(19)-Fe(2)-C(21)	65.3(12)
C(20)-Fe(2)-C(21)	38.2(11)	C(18)-Fe(2)-C(22)	41.6(11)
C(19)-Fe(2)-C(22)	68.2(10)	C(20)-Fe(2)-C(22)	67.7(10)
C(21)-Fe(2)-C(22)	40.6(12)	C(18)-Fe(2)-C(23)	121.3(15)
C(19)-Fe(2)-C(23)	108.7(13)	C(20)-Fe(2)-C(23)	124.8(13)
C(21)-Fe(2)-C(23)	159.7(14)	C(22)-Fe(2)-C(23)	157.8(16)
C(18)-Fe(2)-C(24)	157.2(14)	C(19)-Fe(2)-C(24)	122.2(12)
C(20)-Fe(2)-C(24)	108.6(12)	C(21)-Fe(2)-C(24)	124.7(15)
C(22)-Fe(2)-C(24)	160.2(16)	C(23)-Fe(2)-C(24)	40.3(18)
C(18)-Fe(2)-C(25)	160.6(11)	C(19)-Fe(2)-C(25)	156.3(13)
C(20)-Fe(2)-C(25)	121.4(14)	C(21)-Fe(2)-C(25)	108.7(14)
C(22)-Fe(2)-C(25)	123.4(12)	C(23)-Fe(2)-C(25)	68.6(15)
C(24)-Fe(2)-C(25)	40.5(14)	C(18)-Fe(2)-C(26)	124.6(13)
C(19)-Fe(2)-C(26)	162.3(14)	C(20)-Fe(2)-C(26)	157.1(15)
C(21)-Fe(2)-C(26)	124.5(13)	C(22)-Fe(2)-C(26)	108.7(11)
C(23)-Fe(2)-C(26)	67.2(14)	C(24)-Fe(2)-C(26)	66.7(13)
C(25)-Fe(2)-C(26)	40.2(15)	C(18)-Fe(2)-C(27)	107.9(14)
C(19)-Fe(2)-C(27)	127.0(15)	C(20)-Fe(2)-C(27)	162.7(14)
C(21)-Fe(2)-C(27)	157.9(13)	C(22)-Fe(2)-C(27)	121.8(12)
C(23)-Fe(2)-C(27)	41.3(14)	C(24)-Fe(2)-C(27)	67.5(15)
C(25)-Fe(2)-C(27)	67.4(16)	C(26)-Fe(2)-C(27)	38.6(16)
C(2)-N(1)-C(3)	118.0(16)	C(2)-N(1)-C(6)	120.3(20)
C(3)-N(1)-C(6)	116.8(21)	C(4)-N(2)-C(5)	118.6(18)
C(4)-N(2)-C(17)	123.4(21)	C(5)-N(2)-C(17)	117.2(19)
C(2)-C(1)-C(5A)	114.4(19)	N(1)-C(2)-C(1)	113.7(21)
N(1)-C(3)-C(4)	114.8(17)	N(2)-C(4)-C(3)	112.4(16)
N(2)-C(5)-C(1A)	114.9(18)	O(1)-C(6)-N(1)	121.1(23)
O(1)-C(6)-C(7)	115.5(23)	N(1)-C(6)-C(7)	122.1(26)
Fe(1)-C(7)-C(6)	123.5(21)	Fe(1)-C(7)-C(8)	68.5(16)
C(6)-C(7)-C(8)	133.0(26)	Fe(1)-C(7)-C(11)	66.8(17)
C(6)-C(7)-C(11)	122.0(27)	C(8)-C(7)-C(11)	104.7(22)
Fe(1)-C(8)-C(7)	71.3(18)	Fe(1)-C(8)-C(9)	69.4(17)
C(7)-C(8)-C(9)	110.6(25)	Fe(1)-C(9)-C(8)	68.8(16)
Fe(1)-C(9)-C(10)	68.0(17)	C(8)-C(9)-C(10)	104.4(24)
Fe(1)-C(10)-C(9)	71.7(17)	Fe(1)-C(10)-C(11)	69.8(16)
C(9)-C(10)-C(11)	110.8(27)	Fe(1)-C(11)-C(7)	72.3(16)

Fe(1)-C(11)-C(10)	69.5(17)	C(7)-C(11)-C(10)	109.5(29)
Fe(1)-C(12)-C(13)	69.5(17)	Fe(1)-C(12)-C(16)	67.9(20)
C(13)-C(12)-C(16)	100.7(25)	Fe(1)-C(13)-C(12)	69.0(16)
Fe(1)-C(13)-C(14)	70.9(17)	C(12)-C(13)-C(14)	111.5(29)
Fe(1)-C(14)-C(13)	70.4(18)	Fe(1)-C(14)-C(15)	69.7(19)
C(13)-C(14)-C(15)	110.8(29)	Fe(1)-C(15)-C(14)	69.5(21)
Fe(1)-C(15)-C(16)	66.9(23)	C(14)-C(15)-C(16)	100.8(28)
Fe(1)-C(16)-C(12)	71.6(24)	Fe(1)-C(16)-C(15)	71.7(24)
C(12)-C(16)-C(15)	115.9(34)	O(2)-C(17)-N(2)	117.5(25)
O(2)-C(17)-C(18)	120.1(22)	N(2)-C(17)-C(18)	122.1(22)
Fe(2)-C(18)-C(17)	124.0(17)	Fe(2)-C(18)-C(19)	69.3(14)
C(17)-C(18)-C(19)	119.4(23)	Fe(2)-C(18)-C(22)	68.7(15)
C(17)-C(18)-C(22)	136.2(22)	C(19)-C(18)-C(22)	104.4(24)
Fe(2)-C(19)-C(18)	69.3(14)	Fe(2)-C(19)-C(20)	71.8(16)
C(18)-C(19)-C(20)	110.4(22)	Fe(2)-C(20)-C(19)	68.6(15)
Fe(2)-C(20)-C(21)	69.4(17)	C(19)-C(20)-C(21)	106.8(26)
Fe(2)-C(21)-C(20)	72.5(17)	Fe(2)-C(21)-C(22)	69.1(16)
C(20)-C(21)-C(22)	112.0(30)	Fe(2)-C(22)-C(18)	69.7(13)
Fe(2)-C(22)-C(21)	70.3(15)	C(18)-C(22)-C(21)	106.4(22)
Fe(2)-C(23)-C(24)	67.7(17)	Fe(2)-C(23)-C(27)	68.8(19)
C(24)-C(23)-C(27)	104.4(31)	Fe(2)-C(24)-C(23)	72.0(21)
Fe(2)-C(24)-C(25)	72.1(19)	C(23)-C(24)-C(25)	111.6(31)
Fe(2)-C(25)-C(24)	67.4(21)	Fe(2)-C(25)-C(26)	68.7(22)
C(24)-C(25)-C(26)	104.0(34)	Fe(2)-C(26)-C(25)	71.1(20)
Fe(2)-C(26)-C(27)	71.2(21)	C(25)-C(26)-C(27)	111.8(29)
Fe(2)-C(27)-C(23)	69.9(20)	Fe(2)-C(27)-C(26)	70.3(22)
C(23)-C(27)-C(26)	108.2(36)	Cl(4)-C(101)-Cl(5)	110.2(20)
Cl(4)-C(101)-Cl(6)	111.8(18)	Cl(5)-C(101)-Cl(6)	111.6(17)
Cl(1)-C(201)-Cl(2)	112.7(15)	Cl(1)-C(201)-Cl(3)	111.4(16)
Cl(2)-C(201)-Cl(3)	111.6(14)		

L³.HCl

. Atomic coordinates ($\times 10^4$) and equivalent isotropic displacement parameters ($\text{\AA}^2 \times 10^3$)

	x	y	z	U(eq)
Fe(1)	2008(2)	492(1)	5557(1)	43(1)
Fe(2)	6975(2)	-2916(2)	9278(1)	68(1)
Fe(3)	5844(2)	4449(1)	6093(1)	53(1)
Cl(11)	5801(5)	3548(4)	1926(2)	134(3)
Cl(12)	8299(6)	2189(6)	2266(4)	245(6)
Cl(21)	11108(8)	4909(9)	2922(3)	265(7)
Cl(13)	8201(10)	2949(12)	1079(3)	373(11)
Cl(22)	8801(9)	5832(6)	3783(4)	283(7)
Cl(23)	9886(8)	3358(5)	3608(4)	239(6)
Cl(31)	-274(6)	7707(6)	310(3)	185(5)
Cl(32)	2366(6)	7838(9)	244(3)	225(6)
Cl(33)	188(8)	9216(9)	1049(4)	264(7)
Cl(4)	2030(5)	4243(4)	7850(3)	128(3)
N(1)	3956(10)	509(8)	7108(4)	45(4)
N(2)	6951(10)	-486(8)	7676(4)	46(4)
N(3)	6564(10)	2147(8)	7695(4)	46(4)
N(4)	3976(10)	1778(9)	8098(4)	50(5)
C(1)	4626(13)	-779(10)	7209(5)	53(6)
C(2)	6105(13)	-1234(10)	6891(5)	50(6)
C(3)	7007(13)	-588(10)	7031(5)	56(6)
C(4)	8036(13)	14(10)	7739(5)	56(6)
C(5)	7886(12)	1258(10)	7481(5)	50(5)
C(6)	6449(14)	2416(11)	8319(5)	60(6)
C(7)	5002(14)	2851(11)	8635(5)	60(6)
C(8)	4240(14)	1959(12)	8688(5)	64(7)
C(9)	3104(13)	993(11)	8151(5)	58(6)
C(10)	2741(13)	944(10)	7554(5)	57(6)
C(101)	3674(12)	807(10)	6513(5)	47(5)
C(102)	2709(12)	263(9)	6335(5)	40(5)
C(103)	3086(14)	-835(10)	6065(5)	52(6)
C(104)	1922(17)	-1060(11)	5994(6)	65(7)
C(105)	766(16)	-117(14)	6226(5)	69(7)
C(106)	1253(14)	747(11)	6434(5)	56(6)
C(107)	3189(20)	578(21)	4771(7)	100(11)
C(108)	2771(26)	1653(22)	5026(8)	99(12)
C(109)	1392(26)	2064(14)	5105(7)	94(10)
C(110)	965(16)	1246(16)	4891(6)	70(8)
C(111)	2104(21)	323(14)	4680(5)	74(8)
C(201)	7261(13)	-1687(10)	7992(5)	55(6)
C(202)	6823(15)	-1553(10)	8649(5)	57(6)
C(203)	5518(16)	-1519(11)	8969(6)	70(7)
C(204)	5504(20)	-1387(13)	9567(7)	90(9)
C(205)	6749(21)	-1329(14)	9623(6)	87(9)
C(206)	7593(16)	-1455(11)	9062(6)	72(7)
C(207)	7793(37)	-4302(16)	9805(13)	138(16)
C(208)	8595(26)	-4370(19)	9303(19)	200(18)
C(209)	7921(52)	-4445(19)	8851(10)	235(28)
C(210)	6623(31)	-4443(15)	9196(14)	138(17)
C(211)	6628(25)	-4362(14)	9751(11)	101(11)
C(301)	6397(13)	3266(9)	7336(5)	52(6)
C(302)	6328(14)	3123(9)	6719(5)	47(6)
C(303)	5215(15)	3089(10)	6488(6)	64(7)
C(304)	5561(21)	2943(11)	5886(7)	70(8)
C(305)	6908(22)	2876(12)	5716(6)	90(9)
C(306)	7416(15)	2977(11)	6214(6)	74(7)
C(307)	4298(23)	5987(12)	6336(11)	101(11)
C(308)	4563(32)	5868(16)	5737(13)	121(15)
C(309)	5851(35)	5803(16)	5478(9)	122(15)
C(310)	6470(24)	5897(14)	5942(12)	117(12)
C(311)	5563(29)	5999(12)	6449(9)	101(12)
C(11)	7524(5)	3297(7)	1798(3)	116(11)
C(21)	9581(7)	4755(5)	3273(3)	114(11)
C(31)	853(6)	7890(8)	698(3)	215(18)

* Equivalent isotropic U defined as one third of the trace of the orthogonalized U_{ij} tensor

Bond lengths (Å)

Fe(1)-C(102)	2.047	(12)	Fe(1)-C(103)	2.031	(12)
Fe(1)-C(104)	2.024	(14)	Fe(1)-C(105)	2.052	(15)
Fe(1)-C(106)	2.042	(11)	Fe(1)-C(107)	2.002	(16)
Fe(1)-C(108)	2.010	(26)	Fe(1)-C(109)	2.015	(15)
Fe(1)-C(110)	2.039	(16)	Fe(1)-C(111)	2.046	(14)
Fe(2)-C(202)	2.048	(12)	Fe(2)-C(203)	2.031	(13)
Fe(2)-C(204)	2.024	(14)	Fe(2)-C(205)	2.043	(18)
Fe(2)-C(206)	2.028	(16)	Fe(2)-C(207)	2.002	(24)
Fe(2)-C(208)	1.988	(21)	Fe(2)-C(209)	2.007	(22)
Fe(2)-C(210)	1.999	(25)	Fe(2)-C(211)	2.033	(20)
Fe(3)-C(302)	2.033	(11)	Fe(3)-C(303)	2.007	(14)
Fe(3)-C(304)	2.023	(17)	Fe(3)-C(305)	2.010	(13)
Fe(3)-C(306)	2.009	(12)	Fe(3)-C(307)	2.040	(16)
Fe(3)-C(308)	1.998	(24)	Fe(3)-C(309)	2.034	(20)
Fe(3)-C(310)	2.010	(22)	Fe(3)-C(311)	2.000	(17)
Cl(11)-C(11)	1.710	(8)	Cl(12)-C(11)	1.710	(10)
Cl(21)-C(21)	1.710	(11)	Cl(13)-C(11)	1.710	(10)
Cl(22)-C(21)	1.710	(10)	Cl(23)-C(21)	1.710	(8)
Cl(31)-C(31)	1.710	(12)	Cl(32)-C(31)	1.710	(9)
Cl(33)-C(31)	1.710	(13)	N(1)-C(1)	1.469	(13)
N(1)-C(10)	1.452	(14)	N(1)-C(101)	1.456	(15)
N(2)-C(3)	1.503	(14)	N(2)-C(4)	1.491	(19)
N(2)-C(201)	1.496	(13)	N(3)-C(5)	1.466	(13)
N(3)-C(6)	1.488	(15)	N(3)-C(301)	1.468	(13)
N(4)-H(4C)	0.960		N(4)-H(4)	1.082	(105)
N(4)-C(8)	1.503	(16)	N(4)-C(9)	1.492	(20)
C(1)-H(1A)	0.960		C(1)-H(1B)	0.960	
C(1)-C(2)	1.525	(16)	C(2)-H(2A)	0.960	
C(2)-H(2B)	0.960		C(2)-C(3)	1.505	(21)
C(3)-H(3A)	0.960		C(3)-H(3B)	0.960	
C(4)-H(4A)	0.960		C(4)-H(4B)	0.960	
C(4)-C(5)	1.502	(16)	C(5)-H(5A)	0.960	
C(5)-H(5B)	0.960		C(6)-H(6A)	0.960	
C(6)-H(6B)	0.960		C(6)-C(7)	1.494	(17)
C(7)-H(7A)	0.960		C(7)-H(7B)	0.960	
C(7)-C(8)	1.509	(23)	C(8)-H(8A)	0.960	
C(8)-H(8B)	0.960		C(9)-H(9A)	0.960	
C(9)-H(9B)	0.960		C(9)-C(10)	1.524	(18)
C(10)-H(10A)	0.960		C(10)-H(10B)	0.960	
C(101)-H(10C)	0.960		C(101)-H(10D)	0.960	
C(101)-C(102)	1.514	(20)	C(102)-C(103)	1.403	(17)
C(102)-C(106)	1.429	(18)	C(103)-H(10E)	0.960	
C(103)-C(104)	1.385	(25)	C(104)-H(10F)	0.960	
C(104)-C(105)	1.406	(18)	C(105)-H(10G)	0.960	
C(105)-C(106)	1.448	(24)	C(106)-H(10H)	0.960	
C(107)-H(10I)	0.960		C(107)-C(108)	1.357	(34)
C(107)-C(111)	1.339	(34)	C(108)-H(10J)	0.960	
C(108)-C(109)	1.353	(36)	C(109)-H(10K)	0.960	
C(109)-C(110)	1.369	(31)	C(110)-H(11A)	0.960	
C(110)-C(111)	1.370	(21)	C(111)-H(11B)	0.960	
C(201)-H(20A)	0.960		C(201)-H(20B)	0.960	
C(201)-C(202)	1.508	(16)	C(202)-C(203)	1.415	(22)
C(202)-C(206)	1.415	(24)	C(203)-H(20C)	0.960	
C(203)-C(204)	1.408	(23)	C(204)-H(20D)	0.960	
C(204)-C(205)	1.371	(32)	C(205)-H(20E)	0.960	
C(205)-C(206)	1.411	(20)	C(206)-H(20F)	0.960	
C(207)-H(20G)	0.960		C(207)-C(208)	1.287	(47)
C(207)-C(211)	1.288	(49)	C(208)-H(20H)	0.960	
C(208)-C(209)	1.409	(60)	C(209)-H(20I)	0.960	
C(209)-C(210)	1.439	(56)	C(210)-H(21A)	0.960	
C(210)-C(211)	1.302	(42)	C(211)-H(21B)	0.960	
C(301)-H(30A)	0.960		C(301)-H(30B)	0.960	
C(301)-C(302)	1.479	(17)	C(302)-C(303)	1.401	(23)
C(302)-C(306)	1.443	(18)	C(303)-H(30C)	0.960	
C(303)-C(304)	1.385	(21)	C(304)-H(30D)	0.960	
C(304)-C(305)	1.374	(31)	C(305)-H(30E)	0.960	
C(305)-C(306)	1.401	(26)	C(306)-H(30F)	0.960	
C(307)-H(30G)	0.960		C(307)-C(308)	1.374	(38)
C(307)-C(311)	1.419	(41)	C(308)-H(30H)	0.960	
C(308)-C(309)	1.351	(46)	C(309)-H(30I)	0.960	
C(309)-C(310)	1.402	(42)	C(310)-H(31A)	0.960	
C(310)-C(311)	1.344	(32)	C(311)-H(31B)	0.960	
C(11)-H(11C)	0.960		C(21)-H(21C)	0.960	
C(31)-H(31C)	0.960				

Bond angles ($^{\circ}$)

C(102)-Fe(1)-C(103)	40.2(5)	C(102)-Fe(1)-C(104)	67.9(6)
C(103)-Fe(1)-C(104)	39.9(7)	C(102)-Fe(1)-C(105)	68.5(6)
C(103)-Fe(1)-C(105)	67.7(5)	C(104)-Fe(1)-C(105)	40.4(5)
C(102)-Fe(1)-C(106)	40.9(5)	C(103)-Fe(1)-C(106)	68.4(4)
C(104)-Fe(1)-C(106)	68.8(5)	C(105)-Fe(1)-C(106)	41.4(7)
C(102)-Fe(1)-C(107)	123.0(7)	C(103)-Fe(1)-C(107)	108.9(6)
C(104)-Fe(1)-C(107)	123.9(8)	C(105)-Fe(1)-C(107)	159.4(9)
C(106)-Fe(1)-C(107)	158.2(9)	C(102)-Fe(1)-C(108)	108.9(8)
C(103)-Fe(1)-C(108)	124.6(8)	C(104)-Fe(1)-C(108)	159.6(8)
C(105)-Fe(1)-C(108)	159.1(7)	C(106)-Fe(1)-C(108)	122.9(8)
C(107)-Fe(1)-C(108)	39.5(9)	C(102)-Fe(1)-C(109)	125.3(7)
C(103)-Fe(1)-C(109)	160.6(9)	C(104)-Fe(1)-C(109)	158.8(10)
C(105)-Fe(1)-C(109)	124.1(8)	C(106)-Fe(1)-C(109)	109.2(5)
C(107)-Fe(1)-C(109)	65.8(8)	C(108)-Fe(1)-C(109)	39.3(10)
C(102)-Fe(1)-C(110)	161.5(5)	C(103)-Fe(1)-C(110)	157.5(7)
C(104)-Fe(1)-C(110)	123.4(8)	C(105)-Fe(1)-C(110)	109.5(6)
C(106)-Fe(1)-C(110)	125.4(5)	C(107)-Fe(1)-C(110)	65.3(7)
C(108)-Fe(1)-C(110)	66.0(9)	C(109)-Fe(1)-C(110)	39.5(9)
C(102)-Fe(1)-C(111)	157.1(6)	C(103)-Fe(1)-C(111)	122.6(5)
C(104)-Fe(1)-C(111)	108.7(6)	C(105)-Fe(1)-C(111)	124.6(8)
C(106)-Fe(1)-C(111)	161.1(8)	C(107)-Fe(1)-C(111)	38.6(9)
C(108)-Fe(1)-C(111)	65.9(9)	C(109)-Fe(1)-C(111)	65.9(6)
C(110)-Fe(1)-C(111)	39.2(6)	C(202)-Fe(2)-C(203)	40.6(6)
C(202)-Fe(2)-C(204)	68.1(5)	C(203)-Fe(2)-C(204)	40.6(6)
C(202)-Fe(2)-C(205)	68.0(6)	C(203)-Fe(2)-C(205)	67.5(7)
C(204)-Fe(2)-C(205)	39.4(9)	C(202)-Fe(2)-C(206)	40.6(7)
C(203)-Fe(2)-C(206)	68.1(7)	C(204)-Fe(2)-C(206)	67.6(7)
C(205)-Fe(2)-C(206)	40.6(6)	C(202)-Fe(2)-C(207)	160.5(11)
C(203)-Fe(2)-C(207)	158.5(11)	C(204)-Fe(2)-C(207)	124.2(9)
C(205)-Fe(2)-C(207)	110.8(10)	C(206)-Fe(2)-C(207)	125.6(12)
C(202)-Fe(2)-C(208)	125.5(11)	C(203)-Fe(2)-C(208)	161.4(13)
C(204)-Fe(2)-C(208)	157.1(14)	C(205)-Fe(2)-C(208)	123.6(12)
C(206)-Fe(2)-C(208)	109.5(9)	C(207)-Fe(2)-C(208)	37.6(14)
C(202)-Fe(2)-C(209)	106.4(7)	C(203)-Fe(2)-C(209)	122.9(12)
C(204)-Fe(2)-C(209)	160.2(16)	C(205)-Fe(2)-C(209)	158.1(17)
C(206)-Fe(2)-C(209)	121.4(13)	C(207)-Fe(2)-C(209)	67.0(10)
C(208)-Fe(2)-C(209)	41.3(18)	C(202)-Fe(2)-C(210)	124.6(10)
C(203)-Fe(2)-C(210)	109.4(10)	C(204)-Fe(2)-C(210)	124.1(10)
C(205)-Fe(2)-C(210)	158.3(10)	C(206)-Fe(2)-C(210)	160.2(9)
C(207)-Fe(2)-C(210)	63.7(14)	C(208)-Fe(2)-C(210)	66.2(12)
C(209)-Fe(2)-C(210)	42.1(16)	C(202)-Fe(2)-C(211)	159.3(10)
C(203)-Fe(2)-C(211)	124.8(9)	C(204)-Fe(2)-C(211)	110.6(7)
C(205)-Fe(2)-C(211)	125.1(8)	C(206)-Fe(2)-C(211)	159.7(9)
C(207)-Fe(2)-C(211)	37.2(14)	C(208)-Fe(2)-C(211)	63.7(11)
C(209)-Fe(2)-C(211)	67.4(10)	C(210)-Fe(2)-C(211)	37.7(12)
C(302)-Fe(3)-C(303)	40.6(6)	C(302)-Fe(3)-C(304)	69.1(6)
C(303)-Fe(3)-C(304)	40.2(6)	C(302)-Fe(3)-C(305)	69.6(5)
C(303)-Fe(3)-C(305)	67.3(6)	C(304)-Fe(3)-C(305)	39.8(9)
C(302)-Fe(3)-C(306)	41.8(5)	C(303)-Fe(3)-C(306)	67.9(6)
C(304)-Fe(3)-C(306)	68.0(7)	C(305)-Fe(3)-C(306)	40.8(7)
C(302)-Fe(3)-C(307)	118.1(7)	C(303)-Fe(3)-C(307)	106.5(7)
C(304)-Fe(3)-C(307)	124.1(9)	C(305)-Fe(3)-C(307)	161.2(10)
C(306)-Fe(3)-C(307)	155.4(9)	C(302)-Fe(3)-C(308)	153.6(9)
C(303)-Fe(3)-C(308)	120.8(10)	C(304)-Fe(3)-C(308)	108.9(10)
C(305)-Fe(3)-C(308)	126.7(10)	C(306)-Fe(3)-C(308)	163.7(9)
C(307)-Fe(3)-C(308)	39.8(10)	C(302)-Fe(3)-C(309)	164.8(11)
C(303)-Fe(3)-C(309)	153.9(11)	C(304)-Fe(3)-C(309)	120.2(9)
C(305)-Fe(3)-C(309)	109.1(7)	C(306)-Fe(3)-C(309)	127.4(9)
C(307)-Fe(3)-C(309)	68.2(9)	C(308)-Fe(3)-C(309)	39.1(13)
C(302)-Fe(3)-C(310)	126.6(9)	C(303)-Fe(3)-C(310)	163.1(9)

C(304)-Fe(3)-C(310)	156.1(8)	C(305)-Fe(3)-C(310)	123.0(8)
C(306)-Fe(3)-C(310)	110.2(8)	C(307)-Fe(3)-C(310)	67.8(9)
C(308)-Fe(3)-C(310)	65.7(12)	C(309)-Fe(3)-C(310)	40.6(12)
C(302)-Fe(3)-C(311)	107.5(7)	C(303)-Fe(3)-C(311)	126.3(7)
C(304)-Fe(3)-C(311)	162.5(9)	C(305)-Fe(3)-C(311)	156.6(11)
C(306)-Fe(3)-C(311)	121.6(9)	C(307)-Fe(3)-C(311)	41.1(11)
C(308)-Fe(3)-C(311)	66.1(11)	C(309)-Fe(3)-C(311)	67.4(8)
C(310)-Fe(3)-C(311)	39.2(9)	C(1)-N(1)-C(10)	110.3(9)
C(1)-N(1)-C(101)	112.6(9)	C(10)-N(1)-C(101)	112.3(9)
C(3)-N(2)-C(4)	108.3(9)	C(3)-N(2)-C(201)	111.6(9)
C(4)-N(2)-C(201)	106.5(9)	C(5)-N(3)-C(6)	111.1(9)
C(5)-N(3)-C(301)	110.3(8)	C(6)-N(3)-C(301)	108.5(9)
H(4C)-N(4)-H(4)	114.5(52)	H(4C)-N(4)-C(8)	111.1(6)
H(4)-N(4)-C(8)	104.6(65)	H(4C)-N(4)-C(9)	107.3(5)
H(4)-N(4)-C(9)	107.9(74)	C(8)-N(4)-C(9)	111.5(9)
N(1)-C(1)-H(1A)	108.4(6)	N(1)-C(1)-H(1B)	108.4(7)
H(1A)-C(1)-H(1B)	109.5(1)	N(1)-C(1)-C(2)	113.9(10)
H(1A)-C(1)-C(2)	108.4(6)	H(1B)-C(1)-C(2)	108.4(7)
C(1)-C(2)-H(2A)	108.2(7)	C(1)-C(2)-H(2B)	108.2(6)
H(2A)-C(2)-H(2B)	109.5(1)	C(1)-C(2)-C(3)	114.4(10)
H(2A)-C(2)-C(3)	108.2(6)	H(2B)-C(2)-C(3)	108.2(6)
N(2)-C(3)-C(3)	115.0(10)	N(2)-C(3)-H(3A)	108.1(5)
C(2)-C(3)-H(3A)	108.1(6)	N(2)-C(3)-H(3B)	108.1(6)
C(2)-C(3)-H(3B)	108.1(5)	H(3A)-C(3)-H(3B)	109.5(1)
N(2)-C(4)-H(4A)	107.9(5)	N(2)-C(4)-H(4B)	107.9(5)
H(4A)-C(4)-H(4B)	109.5(1)	N(2)-C(4)-C(5)	115.8(10)
H(4A)-C(4)-C(5)	107.9(7)	H(4B)-C(4)-C(5)	107.9(6)
N(3)-C(5)-C(4)	114.1(10)	N(3)-C(5)-H(5A)	108.3(6)
C(4)-C(5)-H(5A)	108.3(7)	N(3)-C(5)-H(5B)	108.3(7)
C(4)-C(5)-H(5B)	108.3(8)	H(5A)-C(5)-H(5B)	109.5(1)
N(3)-C(6)-H(6A)	108.6(5)	N(3)-C(6)-H(6B)	108.6(7)
H(6A)-C(6)-H(6B)	109.5(1)	N(3)-C(6)-C(7)	112.8(12)
H(6A)-C(6)-C(7)	108.6(6)	H(6B)-C(6)-C(7)	108.6(8)
C(6)-C(7)-H(7A)	108.2(8)	C(6)-C(7)-H(7B)	108.2(6)
H(7A)-C(7)-H(7B)	109.5(1)	C(6)-C(7)-C(8)	114.6(11)
H(7A)-C(7)-C(8)	108.2(6)	H(7B)-C(7)-C(8)	108.1(7)
N(4)-C(8)-C(7)	110.8(10)	N(4)-C(8)-H(8A)	109.2(6)
C(7)-C(8)-H(8A)	109.2(6)	N(4)-C(8)-H(8B)	109.1(6)
C(7)-C(8)-H(8B)	109.1(7)	H(8A)-C(8)-H(8B)	109.5(1)
N(4)-C(9)-H(9A)	109.5(6)	N(4)-C(9)-H(9B)	109.5(5)
H(9A)-C(9)-H(9B)	109.5(1)	N(4)-C(9)-C(10)	109.5(9)
H(9A)-C(9)-C(10)	109.4(6)	H(9B)-C(9)-C(10)	109.5(6)
N(1)-C(10)-C(9)	111.5(11)	N(1)-C(10)-H(10A)	109.0(6)
C(9)-C(10)-H(10A)	109.0(6)	N(1)-C(10)-H(10B)	109.0(7)
C(9)-C(10)-H(10B)	109.0(7)	H(10A)-C(10)-H(10B)	109.5(1)
N(1)-C(101)-H(10C)	107.7(5)	N(1)-C(101)-H(10D)	107.7(6)
H(10C)-C(101)-H(10D)	109.5(1)	N(1)-C(101)-C(102)	116.5(10)
H(10C)-C(101)-C(102)	107.7(5)	H(10D)-C(101)-C(102)	107.7(5)
Fe(1)-C(102)-C(101)	128.8(8)	Fe(1)-C(102)-C(103)	69.3(7)
C(101)-C(102)-C(103)	125.9(10)	Fe(1)-C(102)-C(106)	69.3(7)
C(101)-C(102)-C(106)	126.3(10)	C(103)-C(102)-C(106)	107.8(12)
Fe(1)-C(103)-C(102)	70.5(6)	Fe(1)-C(103)-H(10E)	126.0(3)
C(102)-C(103)-H(10E)	125.4(8)	Fe(1)-C(103)-C(104)	69.7(7)
C(102)-C(103)-C(104)	109.3(11)	H(10E)-C(103)-C(104)	125.4(7)
Fe(1)-C(104)-C(103)	70.3(8)	Fe(1)-C(104)-H(10F)	124.9(4)
C(103)-C(104)-H(10F)	125.5(7)	Fe(1)-C(104)-C(105)	70.9(8)
C(103)-C(104)-C(105)	109.1(14)	H(10F)-C(104)-C(105)	125.5(11)
Fe(1)-C(105)-C(104)	68.7(8)	Fe(1)-C(105)-H(10G)	127.5(4)
C(104)-C(105)-H(10G)	126.4(11)	Fe(1)-C(105)-C(106)	68.9(8)
C(104)-C(105)-C(106)	107.2(14)	H(10G)-C(105)-C(106)	126.4(7)
Fe(1)-C(106)-C(102)	69.8(6)	Fe(1)-C(106)-C(105)	69.7(7)
C(102)-C(106)-C(105)	106.6(10)	Fe(1)-C(106)-H(10H)	125.5(3)
C(102)-C(106)-H(10H)	126.7(8)	C(105)-C(106)-H(10H)	126.7(7)

Fe(1)-C(107)-H(10I)	123.5(5)	Fe(1)-C(107)-C(108)	70.5(12)
H(10I)-C(107)-C(108)	125.1(15)	Fe(1)-C(107)-C(111)	72.4(10)
H(10I)-C(107)-C(111)	125.2(11)	C(108)-C(107)-C(111)	109.7(18)
Fe(1)-C(108)-C(107)	69.9(14)	Fe(1)-C(108)-H(10J)	124.7(7)
C(107)-C(108)-H(10J)	126.4(15)	Fe(1)-C(108)-C(109)	70.6(13)
C(107)-C(108)-C(109)	107.2(25)	H(10J)-C(108)-C(109)	126.4(14)
Fe(1)-C(109)-C(108)	70.2(12)	Fe(1)-C(109)-H(10K)	124.3(4)
C(108)-C(109)-H(10K)	125.9(14)	Fe(1)-C(109)-C(110)	71.2(9)
C(108)-C(109)-C(110)	108.2(17)	H(10K)-C(109)-C(110)	125.9(11)
Fe(1)-C(110)-C(109)	69.3(10)	Fe(1)-C(110)-H(11A)	125.4(5)
C(109)-C(110)-H(11A)	126.2(11)	Fe(1)-C(110)-C(111)	70.7(9)
C(109)-C(110)-C(111)	107.6(18)	H(11A)-C(110)-C(111)	126.2(13)
Fe(1)-C(111)-C(107)	68.9(10)	Fe(1)-C(111)-C(110)	70.1(8)
C(107)-C(111)-C(110)	107.3(17)	Fe(1)-C(111)-H(11B)	126.1(5)
C(107)-C(111)-H(11B)	126.4(11)	C(110)-C(111)-H(11B)	126.4(13)
N(2)-C(201)-H(20A)	109.2(7)	N(2)-C(201)-H(20B)	109.2(6)
H(20A)-C(201)-H(20B)	109.5(1)	N(2)-C(201)-C(202)	110.7(9)
H(20A)-C(201)-C(202)	109.2(8)	H(20B)-C(201)-C(202)	109.2(7)
Fe(2)-C(202)-C(201)	126.3(8)	Fe(2)-C(202)-C(203)	69.0(7)
C(201)-C(202)-C(203)	124.8(15)	Fe(2)-C(202)-C(206)	68.9(8)
C(201)-C(202)-C(206)	128.4(14)	C(203)-C(202)-C(206)	106.8(12)
Fe(2)-C(203)-C(202)	70.4(7)	Fe(2)-C(203)-H(20C)	125.7(5)
C(202)-C(203)-H(20C)	126.1(9)	Fe(2)-C(203)-C(204)	69.4(8)
C(202)-C(203)-C(204)	107.8(16)	H(20C)-C(203)-C(204)	126.1(11)
Fe(2)-C(204)-C(203)	69.9(8)	Fe(2)-C(204)-H(20D)	125.1(5)
C(203)-C(204)-H(20D)	125.5(11)	Fe(2)-C(204)-C(205)	71.0(9)
C(203)-C(204)-C(205)	108.9(15)	H(20D)-C(204)-C(205)	125.5(9)
Fe(2)-C(205)-C(204)	69.6(10)	Fe(2)-C(205)-H(20E)	127.0(5)
C(204)-C(205)-H(20E)	125.9(9)	Fe(2)-C(205)-C(206)	69.1(9)
C(204)-C(205)-C(206)	108.3(16)	H(20E)-C(205)-C(206)	125.8(12)
Fe(2)-C(206)-C(202)	70.5(9)	Fe(2)-C(206)-C(205)	70.3(10)
C(202)-C(206)-C(205)	108.1(15)	Fe(2)-C(206)-H(20F)	124.8(4)
C(202)-C(206)-H(20F)	126.0(8)	C(205)-C(206)-H(20F)	126.0(12)
Fe(2)-C(207)-H(20G)	123.8(9)	Fe(2)-C(207)-C(208)	70.6(16)
H(20G)-C(207)-C(208)	124.6(24)	Fe(2)-C(207)-C(211)	72.7(16)
H(20G)-C(207)-C(211)	124.5(17)	C(208)-C(207)-C(211)	110.9(32)
Fe(2)-C(208)-C(207)	71.8(15)	Fe(2)-C(208)-H(20H)	124.9(8)
C(207)-C(208)-H(20H)	124.8(24)	Fe(2)-C(208)-C(209)	70.1(16)
C(207)-C(208)-C(209)	110.4(32)	H(20H)-C(208)-C(209)	124.9(21)
Fe(2)-C(209)-C(208)	68.7(13)	Fe(2)-C(209)-H(20I)	124.4(6)
C(208)-C(209)-H(20I)	130.1(21)	Fe(2)-C(209)-C(210)	68.6(14)
C(208)-C(209)-C(210)	99.8(23)	H(20I)-C(209)-C(210)	130.1(20)
Fe(2)-C(210)-C(209)	69.2(15)	Fe(2)-C(210)-H(21A)	124.5(9)
C(209)-C(210)-H(21A)	125.2(20)	Fe(2)-C(210)-C(211)	72.6(15)
C(209)-C(210)-C(211)	109.6(31)	H(21A)-C(210)-C(211)	125.2(18)
Fe(2)-C(211)-C(207)	70.1(14)	Fe(2)-C(211)-C(210)	69.7(13)
C(207)-C(211)-C(210)	109.3(25)	Fe(2)-C(211)-H(21B)	126.4(6)
C(207)-C(211)-H(21B)	125.4(17)	C(210)-C(211)-H(21B)	125.3(18)
N(3)-C(301)-H(30A)	108.7(5)	N(3)-C(301)-H(30B)	108.6(7)
H(30A)-C(301)-H(30B)	109.5(1)	N(3)-C(301)-C(302)	112.7(10)
H(30A)-C(301)-C(302)	108.6(6)	H(30B)-C(301)-C(302)	108.6(8)
Fe(3)-C(302)-C(301)	126.9(8)	Fe(3)-C(302)-C(303)	68.7(7)
C(301)-C(302)-C(303)	128.7(12)	Fe(3)-C(302)-C(306)	68.2(7)
C(301)-C(302)-C(306)	127.2(14)	C(303)-C(302)-C(306)	104.1(12)
Fe(3)-C(303)-C(302)	70.7(8)	Fe(3)-C(303)-H(30C)	126.0(3)
C(302)-C(303)-H(30C)	124.4(7)	Fe(3)-C(303)-C(304)	70.5(9)
C(302)-C(303)-C(304)	111.2(14)	H(30C)-C(303)-C(304)	124.4(12)
Fe(3)-C(304)-C(303)	69.3(9)	Fe(3)-C(304)-H(30D)	126.5(5)
C(303)-C(304)-H(30D)	126.2(11)	Fe(3)-C(304)-C(305)	69.6(10)
C(303)-C(304)-C(305)	107.6(17)	H(30D)-C(304)-C(305)	126.2(10)
Fe(3)-C(305)-C(304)	70.6(9)	Fe(3)-C(305)-H(30E)	125.8(4)
C(304)-C(305)-H(30E)	125.6(10)	Fe(3)-C(305)-C(306)	69.5(8)
C(304)-C(305)-C(306)	108.8(13)	H(30E)-C(305)-C(306)	125.6(10)

Fe(3)-C(306)-C(302)	70.0(7)
C(302)-C(306)-C(305)	108.4(15)
C(302)-C(306)-H(30F)	125.8(9)
Fe(3)-C(307)-H(30G)	126.5(6)
H(30G)-C(307)-C(308)	128.7(18)
H(30G)-C(307)-C(311)	128.7(12)
Fe(3)-C(308)-C(307)	71.8(13)
C(307)-C(308)-H(30H)	123.0(18)
C(307)-C(308)-C(309)	114.0(30)
Fe(3)-C(309)-C(308)	69.0(13)
C(308)-C(309)-H(30I)	127.8(18)
C(308)-C(309)-C(310)	104.4(22)
Fe(3)-C(310)-C(309)	70.7(14)
C(309)-C(310)-H(31A)	125.4(15)
C(309)-C(310)-C(311)	109.3(25)
Fe(3)-C(311)-C(307)	70.9(12)
C(307)-C(311)-C(310)	109.7(22)
C(307)-C(311)-H(31B)	125.2(12)
Cl(11)-C(11)-Cl(12)	110.9(5)
Cl(12)-C(11)-Cl(13)	111.1(5)
Cl(12)-C(11)-H(11C)	107.6(4)
Cl(21)-C(21)-Cl(22)	109.7(6)
Cl(22)-C(21)-Cl(23)	110.4(5)
Cl(22)-C(21)-H(21C)	108.4(4)
Cl(31)-C(31)-Cl(32)	110.8(5)
Cl(32)-C(31)-Cl(33)	109.7(7)
Cl(32)-C(31)-H(31C)	108.9(4)

Fe(3)-C(306)-C(305)	69.7(8)
Fe(3)-C(306)-H(30F)	126.1(5)
C(305)-C(306)-H(30F)	125.8(10)
Fe(3)-C(307)-C(308)	68.5(11)
Fe(3)-C(307)-C(311)	68.0(9)
C(308)-C(307)-C(311)	102.7(22)
Fe(3)-C(308)-H(30H)	125.0(9)
Fe(3)-C(308)-C(309)	71.9(14)
H(30H)-C(308)-C(309)	123.0(18)
Fe(3)-C(309)-H(30I)	126.0(6)
Fe(3)-C(309)-C(310)	68.8(12)
H(30I)-C(309)-C(310)	127.8(15)
Fe(3)-C(310)-H(31A)	125.5(6)
Fe(3)-C(310)-C(311)	70.0(13)
H(31A)-C(310)-C(311)	125.4(18)
Fe(3)-C(311)-C(310)	70.8(11)
Fe(3)-C(311)-H(31B)	124.7(6)
C(310)-C(311)-H(31B)	125.2(18)
Cl(11)-C(11)-Cl(13)	109.9(6)
Cl(11)-C(11)-H(11C)	108.8(3)
Cl(13)-C(11)-H(11C)	108.6(6)
Cl(21)-C(21)-Cl(23)	108.5(5)
Cl(21)-C(21)-H(21C)	110.3(4)
Cl(23)-C(21)-H(21C)	109.6(4)
Cl(31)-C(31)-Cl(33)	110.9(5)
Cl(31)-C(31)-H(31C)	107.6(4)
Cl(33)-C(31)-H(31C)	108.8(4)

$2L^b Fe_2 OCl_6$ Atom coordinates ($\times 10^4$) and temperature factors ($\text{\AA}^2 \times 10^3$)

Atom	x	y	z	U
Fe(1)	8646.4(8)	1475.6(10)	3667.5(5)	61(1)*
Fe(2)	4436.7(8)	636.6(10)	4084.9(5)	59(1)*
Cl(1)	2810.5(17)	966.3(20)	4052.1(13)	87(1)*
Cl(2)	5146.3(16)	2698.8(21)	3840.9(11)	86(1)*
Cl(3)	4605.3(20)	-915.3(23)	3147.8(12)	106(1)*
O(1)	5072	0	4927	101(4)*
N(1)	7708(5)	3857(5)	5683(3)	47(2)*
C(101)	8775(8)	3(15)	2825(8)	104(6)*
C(102)	8098(12)	1042(13)	2525(5)	107(6)*
C(103)	7339(8)	1007(13)	2954(8)	101(6)*
C(104)	7532(11)	1(13)	3519(6)	93(6)*
C(105)	8424(11)	-672(9)	3470(7)	101(6)*
C(106)	8557(7)	2754(7)	4611(3)	48(3)*
C(107)	8638(7)	3587(8)	3933(4)	74(4)*
C(108)	9546(11)	3225(12)	3696(6)	116(6)*
C(109)	10010(7)	2166(13)	4214(7)	107(6)*
C(110)	9407(7)	1875(9)	4771(4)	68(4)*
C(1)	7688(5)	2718(5)	5032(3)	45(3)*
C(2)	8666(6)	3744(7)	6279(3)	67(3)*
C(3)	8772(6)	2374(8)	6747(4)	93(4)*
C(4)	6790(6)	3609(8)	6049(4)	68(4)*
C(5)	6698(6)	4580(8)	6751(4)	91(4)*
C(6)	7700(6)	5361(6)	5325(3)	74(3)*
C(7)	6777(7)	5757(7)	4742(4)	105(4)*

* Equivalent isotropic U defined as one third of the trace of the orthogonalised $U(ij)$ tensor

[Zn(L⁶)(OCIO₃)](ClO₄)

TABLE 1. Atom coordinates (x10⁴) and temperature factors (A²x10³)

Atom	x	y	z	U
Zn	-2560.8(8)	2500.0	-5561.4(6)	43(1)*
Cl(1)	2307(2)	2534(10)	-5494(2)	65(1)*
O(11)	2976(11)	1415(23)	-5505(12)	151(9)*
O(12)	1674(6)	2527(36)	-6183(5)	136(6)*
O(13)	1773(8)	2413(33)	-4797(6)	167(7)*
O(14)	2835(16)	3671(14)	-5577(10)	125(8)*
Cl(2)	-3981(2)	2455(7)	-3434(2)	74(1)*
O(21)	-3418(2)	2969(7)	-4105(2)	171(12)*
O(22)	-4941(2)	2980(7)	-3490(2)	215(11)*
O(23)	-3559(2)	2873(7)	-2669(2)	170(8)*
O(24)	-4007(2)	1000(7)	-3472(2)	143(8)*
N(1)	-1637(6)	2652(22)	-6575(6)	61(4)*
N(2)	-3414(8)	906(13)	-5680(7)	78(5)*
N(3)	-3402(7)	4204(13)	-5754(5)	66(4)*
N(4)	-1370(5)	2496(23)	-4827(5)	57(3)*
C(1)	-1690(14)	1352(22)	-7116(13)	67(5)
C(2a)	-2706(14)	722(23)	-7190(13)	41(6)
C(2b)	-2038(33)	-110(46)	-6659(29)	62(12)
C(3)	-3262(23)	68(29)	-6407(19)	126(10)
C(4)	-4362(10)	1155(18)	-5698(8)	84(7)*
C(5)	-4706(10)	2594(43)	-6170(10)	112(9)*
C(6)	-4494(11)	3666(27)	-5766(13)	119(11)*
C(7)	-3030(20)	4963(18)	-6499(13)	107(9)*
C(8)	-2259(19)	4836(23)	-6776(14)	163(12)*
C(9)	-1887(20)	3799(22)	-7135(11)	151(12)*
C(10)	-699(8)	2285(37)	-6164(7)	116(11)*
C(11)	-583(8)	1993(18)	-5419(8)	92(8)*
C(12)	-1220(24)	1435(25)	-4293(17)	130(15)*
C(13)	-528(12)	1728(21)	-3634(10)	65(5)*
C(14)	-772(25)	3132(40)	-3526(23)	218(20)
C(15)	-1299(16)	3703(29)	-4262(13)	92(9)*

* Equivalent isotropic U defined as one third of the trace of the orthogonalised U_{ij} tensor

[Zn(L⁷)](ClO₄)₂

Atomic coordinates ($\times 10^4$) and equivalent isotropic displacement parameters ($\text{\AA}^2 \times 10^3$)

	x	y	z	U(eq)
Zn(1)	4363(1)	712(2)	2186(2)	63(1)
Zn(2)	3165(1)	9170(2)	6633(2)	59(1)
Cl(1)	715(2)	9162(6)	1433(6)	103(5)
Cl(2)	1823(4)	4098(7)	2773(8)	151(7)
Cl(3)	2030(3)	7228(7)	-271(7)	115(6)
Cl(4)	419(3)	1975(7)	4809(7)	134(6)
O(11)	995(4)	9003(14)	934(11)	182(17)
O(12)	489(6)	8537(12)	1439(20)	254(25)
O(13)	835(6)	9297(17)	2205(9)	253(25)
O(14)	542(6)	9812(13)	1156(13)	226(21)
O(21)	1515(6)	3703(21)	2909(20)	261(27)
O(22)	1811(11)	4808(12)	3157(18)	414(46)
O(23)	1867(10)	4210(19)	1956(10)	318(32)
O(24)	2099(7)	3670(20)	3071(22)	349(37)
O(31)	2021(7)	6430(8)	-341(16)	227(23)
O(32)	1858(7)	7451(16)	423(12)	251(25)
O(33)	2374(4)	7473(17)	-236(17)	260(24)
O(34)	1869(7)	7559(16)	-931(14)	344(33)
O(41)	518(7)	2344(15)	4106(12)	247(23)
O(42)	69(4)	1791(15)	4771(13)	149(14)
O(43)	478(6)	2461(18)	5456(13)	365(32)
O(44)	613(6)	1305(13)	4901(20)	337(35)
N(11)	4414(10)	1354(21)	3370(23)	167(13)
N(12)	4275(7)	-521(22)	2577(17)	163(19)
N(13)	4840(8)	856(28)	1766(24)	451(55)
N(14)	3950(6)	1210(14)	1508(15)	71(11)
C(101)	4557(11)	826(25)	3923(29)	191(20)
C(102)	4267(12)	93(27)	3956(31)	233(24)
C(103)	4423(10)	-624(21)	3500(21)	134(14)
C(104)	4513(11)	-894(29)	1929(27)	214(24)
C(105)	4861(10)	-759(24)	1912(24)	155(16)
C(106)	4951(21)	47(34)	1452(42)	389(52)
C(107)	5114(10)	847(19)	2231(21)	129(13)
C(108)	5048(10)	1657(19)	2706(25)	157(18)
C(109)	4719(8)	1933(20)	3248(23)	146(15)
C(110)	4021(12)	1601(27)	3452(26)	203(21)
C(111)	3853(13)	2059(29)	2789(30)	221(23)
C(112)	3741(11)	1639(26)	2091(27)	173(20)
C(113)	4107(10)	1711(22)	751(22)	143(15)
C(114)	4111(12)	1065(26)	126(26)	192(21)
C(115)	3885(11)	433(26)	383(26)	177(19)
C(116)	3724(10)	587(23)	1161(22)	135(15)
N(21)	3158(10)	9198(21)	7828(22)	174(20)
N(22)	2677(9)	8760(26)	6220(19)	295(35)
N(23)	3127(9)	10309(16)	6176(17)	154(18)
N(24)	3633(11)	8547(20)	6382(22)	156(20)
C(201)	2870(11)	8605(27)	8168(28)	181(24)
C(202)	2508(11)	8536(25)	7681(23)	155(16)
C(203)	2521(12)	8223(23)	6913(24)	155(16)
C(204)	2507(19)	9565(30)	6084(39)	481(62)
C(205)	2625(8)	10201(26)	5418(25)	197(20)
C(206)	3042(8)	10295(25)	5265(17)	150(16)
C(207)	3055(9)	10922(20)	6795(22)	114(12)
C(208)	3197(10)	10798(22)	7610(22)	133(14)
C(209)	3050(13)	10070(25)	8126(27)	192(20)
C(210)	3471(11)	9019(27)	8303(27)	172(18)
C(211)	3700(11)	8448(24)	7993(26)	177(20)
C(212)	3857(12)	8490(29)	7175(31)	188(22)
C(213)	3768(11)	8611(26)	5557(26)	171(19)
C(214)	3492(15)	8208(35)	5079(35)	305(36)
C(215)	3347(14)	7523(29)	5402(28)	232(24)
C(216)	3536(12)	7611(29)	6266(28)	211(22)

* Equivalent isotropic U defined as one third of the trace of the orthogonalized U_{ij} tensor

[Ni(L^s)(NCS)₂]

TABLE 1. Atom coordinates (x10⁴) and temperature factors (A²x10³)

Atom	x	y	z	U
Ni	2337.4(4)	1698.1(6)	1661.4(3)	49(1)*
N(1)	2823(3)	556(4)	2612(3)	67(2)*
N(2)	3268(3)	483(5)	1244(3)	73(2)*
N(3)	1687(3)	2624(5)	697(2)	61(2)*
N(4)	1378(3)	2920(4)	2081(3)	57(2)*
N(5)	1424(3)	47(5)	1373(3)	72(2)*
N(6)	3203(3)	3258(4)	1908(2)	54(2)*
S(1)	513.7(12)	-2434.8(17)	1172.2(10)	80(1)*
S(2)	4127(2)	5703(2)	1993(2)	144(1)*
C(01)	1041(4)	-973(6)	1283(3)	58(2)*
C(02)	3605(3)	4249(6)	1949(3)	53(2)*
C(1)	3280(7)	-655(9)	2390(5)	122(4)*
C(2)	3445(9)	-724(10)	1729(7)	163(7)*
C(3)	2894(6)	-37(8)	553(5)	106(4)*
C(4)	2538(6)	1110(10)	45(4)	107(4)*
C(5)	1685(5)	1651(8)	102(4)	86(3)*
C(6)	773(4)	2772(7)	785(3)	69(2)*
C(7)	737(4)	3507(6)	1443(3)	71(2)*
C(8)	893(4)	1916(7)	2420(3)	72(2)*
C(9)	1450(5)	1219(7)	3021(3)	76(3)*
C(10)	2061(5)	110(7)	2888(4)	87(3)*
C(11)	3450(4)	1356(6)	3134(3)	69(2)*
C(12)	3798(6)	668(9)	3827(4)	106(4)*
C(13)	4419(6)	1576(11)	4301(5)	122(5)*
C(14)	4098(4)	1227(7)	1232(4)	79(3)*
C(15)	4809(5)	448(12)	982(5)	135(5)*
C(16)	5608(6)	1277(13)	1014(5)	152(6)*
C(17)	2063(4)	4000(6)	573(3)	66(2)*
C(18)	1605(7)	4868(9)	-37(4)	112(4)*
C(19)	2065(7)	6193(8)	-73(4)	113(4)*
C(20)	1733(3)	4121(5)	2527(3)	50(2)*
C(21)	1120(4)	4928(6)	2873(3)	66(2)*
C(22)	1545(5)	6175(7)	3243(4)	83(3)*

* Equivalent isotropic U defined as one third of the trace of the orthogonalised U(ij) tensor

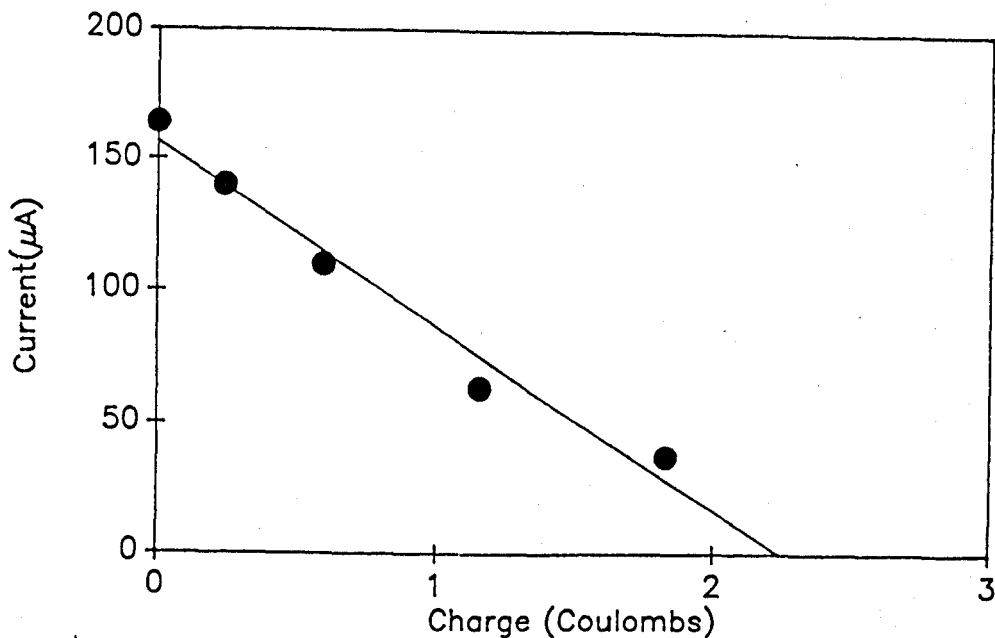
Appendix II

Coulometric Titration Results for L^2

The ligand L^2 in acetonitrile (0.40mmol) is placed in a cell containing a platinum rotating disc electrode, and a very large platinum gauze electrode. The potential of the gauze is stepped to 800mV vs S.C.E, and a known charge (Q mC) passed. Polarograms are recorded at each stage, and the peak current ($i_{ox} \mu A$) recorded. A plot of current against charge gives a intercept on the x axis from which the number of electrons can be calculated according to equation (1)

$$n = \text{intercept}/c \times V \times F \text{ ---1}$$

where c = concentration (mol dm^3), V = volume of sample (dm^3), F = Faradays constant (96480 C mol^{-1}). Using this equation a value of n was calculated to be 3.9 ± 0.2 , which is in good agreement with the expected four electron process of L^2 .



A plot of current (i_{ox}) against charge passed for L^2